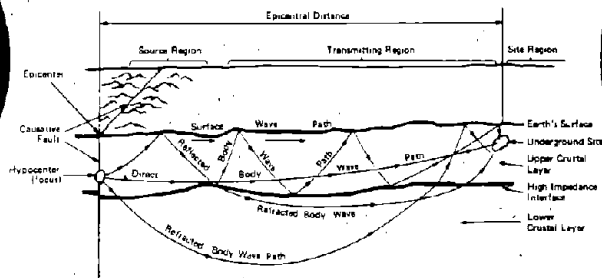


Report No. FHWA/RD-80/195

PB81-247918

EARTHQUAKE ENGINEERING OF LARGE UNDERGROUND STRUCTURES

January 1981
Final Report



Document is available to the public through
the National Technical Information Service,
Springfield, Virginia 22161



Prepared for
FEDERAL HIGHWAY ADMINISTRATION
Offices of Research & Development
Structures and Applied Mechanics Division
Washington, D.C. 20590

REPRODUCED BY
**NATIONAL TECHNICAL
INFORMATION SERVICE**
U.S. DEPARTMENT OF COMMERCE
SPRINGFIELD, VA. 22161

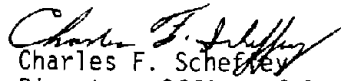


NATIONAL SCIENCE FOUNDATION
1800 G Street, N.W.
Washington, D.C. 20550

FOREWORD

This report is the result of research conducted by URS/John A. Blume Associates, Engineers, for the Federal Highway Administration (FHWA), Office of Research, under FHWA agreement 7-1-0514 and the National Science Foundation (NSF) under NSF PFR-7706505. The report will be of interest to those researchers and engineers concerned with assessing the vulnerability of underground tunnels to strong ground motion. Specifically, the current state-of-the-art of earthquake engineering of transportation tunnels and other large underground structures is evaluated.

Copies of the report are being distributed by FHWA transmittal memorandum. Additional copies may be obtained from the National Technical Information Service, 5285 Port Royal Road, Springfield, Virginia 22161.


Charles F. Scheffey
Director, Office of Research
Federal Highway Administration

NOTICE

This document is disseminated under the sponsorship of the Department of Transportation in the interest of information exchange. The United States Government assumes no liability for its contents or use thereof. The contents of this report reflect the views of the contractor, who is responsible for the accuracy of the data presented herein. The contents do not necessarily reflect the official views or policy of the Department of Transportation. This report does not constitute a standard, specification, or regulation.

The United States Government does not endorse products or manufacturers. Trade or manufacturers' names appear herein only because they are considered essential to the object of this document.

Technical Report Documentation Page

1. Report No. FHWA/RD-80/195		2. Government Accession No.		3. Recipient's Catalog No.	
4. Title and Subtitle Earthquake Engineering of Large Underground Structures			5. Report Date January 1981		
			6. Performing Organization Code		
7. Author(s) G. Norman Owen and Roger E. Scholl			8. Performing Organization Report No. JAB-7821		
9. Performing Organization Name and Address URS/John A. Blume & Associates, Engineers 130 Jessie Street San Francisco, California 94105			10. Work Unit No. (TRAIS) 35B3-412		
			11. Contract or Grant No. NSF PFR-7706505		
12. Sponsoring Agency Name and Address National Science Foundation Washington, D.C. 20550 and Federal Highway Administration Department of Transportation Washington, D.C. 20590			13. Type of Report and Period Covered April 1978 - September 1980 Final Report		
			14. Sponsoring Agency Code SO 1138		
15. Supplementary Notes National Science Foundation Program Manager: Dr. William W. Hakala (202) 357-7737 Federal Highway Administration Contract Manager: Mr. James D. Cooper (703) 557-5272					
16. Abstract This study identifies and evaluates the current state of the art of earthquake engineering of transportation tunnels and other large underground structures. A review of the past performance of 127 underground openings during earthquakes indicates that underground structures in general are less severely affected than surface structures at the same geographic location. However, some severe damage, including collapse, has been reported. Stability of tunnels during seismic motion is affected by peak ground motion parameters, earthquake duration, type of support, ground conditions, and in situ stresses. The literature on the nature of underground seismic motion is reviewed in detail. Although recorded underground motions tend to substantiate the idea that motion does reduce with depth, amplification at depth has been observed. The current procedures used in the seismic design of underground structures vary greatly depending upon the type of structure and the ground conditions. Procedures for subaqueous tunnels are fairly well formulated; however, procedures for structures in soil and rock are not as well formulated. Numerical procedures to predict dynamic stresses are not completely compatible with current static design procedures, which are more strongly affected by empirical methods than by stress-prediction models. Recommended research activities include the systematic reconnaissance of underground structures following major earthquakes, the placement of instrumentation for recording seismic motion in tunnels, analytical studies of underground motion, and the further development of seismic design procedures for structures in soil and rock.					
17. Key Words Earthquake Engineering, Underground Structures, Earthquake Effects, Seismic Response, Submerged Tunnels, Tunnels in Soil, Tunnels in Rock, Seismic Design			18. Distribution Statement Document is available to public through the National Technical Information Service, Springfield, VA 22161		
19. Security Classif. (of this report) Unclassified		20. Security Classif. (of this page) Unclassified		21. No. of Pages	22. Price

Contents

	<u>page</u>
ACKNOWLEDGEMENTS	ix
SUMMARY	xi
Effects of Earthquakes on Underground Structures	xi
Variation of Seismic Motion with Depth	xii
Seismic Wave Study of a Circular Cavity	xiii
Analytical and Design Procedures for Underground Structures	xiv
Critique of the State of the Art	xv
Research Recommendations	xvi
1. INTRODUCTION	1
2. BACKGROUND INFORMATION	3
Underground Structures	3
Seismic Activity and Earthquake Hazard	5
Earthquake Magnitude and Intensity	11
3. OBSERVED EFFECTS OF EARTHQUAKES AND UNDERGROUND EXPLOSIONS	13
Effects of Earthquakes	13
Response Parameters	14
Summary of Available Data	16
Effects of Underground Explosions	22
Conventional Blasting	23
High-Explosive Tests	23
Underground Nuclear Explosions	27
Summary and Conclusions	35
4. SEISMIC ANALYSIS	38
Current Techniques Used in Seismic Analysis	38
Available Numerical Models	38
Analysis of Free-Field Stresses and Strains	39
Seismic Analysis of Underground Structures	49
Properties Required for Seismic Analysis	64
Techniques for Measuring Soil and Rock Properties	64
Problems in Synthesizing Measured Properties	70

CONTENTS (Continued)

	<u>page</u>
5. SEISMIC WAVE PROPAGATION	74
The Nature of Underground Motion	74
Factors Affecting Underground Motion	74
Prediction of Underground Motion	80
Depth-Dependence of Underground Motion	82
Literature Review	82
Theoretical Formulation of Depth Dependence	86
Parametric Studies of Depth Dependence	92
Dynamic Response of Underground Cavities	105
Literature Review	107
Theoretical Formulation of Cavity Response	108
Numerical Study of Cavity Response	113
6. CURRENT PRACTICE IN SEISMIC DESIGN	123
Submerged Tunnels	125
SFBART Approach to Submerged Tunnels	128
Japanese Approach to Submerged Tunnels	139
Dynamic Analysis of Submerged Tunnels	145
Special Design Consideration: Seismic Joint	148
Underground Structures in Soil	150
SFBART Approach to Structures in Soil	151
Mononobe-Okabe Theory of Dynamic Soil Pressure	154
Computer Methods for Structures in Soil	155
Special Considerations in Design	156
Underground Structures in Rock	158
Design Based on Geologic Engineering Principles	162
Design Based on Stress Calculations	166
Special Design Considerations	170
Underground Structures Intersecting Active Faults	171
Case Studies of Special Design Features	171
Recommendations for Special Design Features of Box Conduits	174
7. CRITIQUE OF THE STATE OF THE ART	177
Effects of Earthquakes on Underground Structures	177
Underground Seismic Motion	178
Current Practice in Seismic Design of Underground Structures	179

CONTENTS (Continued)

	<u>page</u>
Seismic Design of Subaqueous Tunnels	179
Seismic Design of Underground Structures in Rock	180
Seismic Design of Underground Structures in Soil	184
8. RECOMMENDED RESEARCH ACTIVITIES	186
Observed Effects of Earthquakes on Underground Structures	186
Research Activity 1: Comprehensive Survey of Earthquake Effects on Underground Structures	187
Research Activity 2: Postearthquake Reconnaissance of Underground Structures	188
Research Activity 3: Observations of Selected Tunnels Before and After Earthquakes	188
Underground Seismic Motion	189
Research Activity 4: Recording of Seismic Motion in Deep Boreholes	192
Research Activity 5: Recording of Seismic Motion in Underground Openings	192
Research Activity 6: Development of Analytical Models for Predicting Seismic Motion at Depth	195
Seismic Analysis and Design of Underground Structures	197
Research Activity 7: Development of Computer Codes for Stability Evaluation of Openings in Rock	198
Research Activity 8: Development of Empirical Procedures for Seismic Design	199
Research Activity 9: Analytical Parametric Study of Seismic Stability of Openings in Rock	199
REFERENCES	256

APPENDICES

A Persons Contacted About Seismic Design of Underground Structures	200
B Abridged Modified Mercalli Intensity Scale	204
C Summary of Damage to Underground Structures from Earthquake Shaking	206
D A Short Review of Seismological Terms	242
E Derivation of the Green's Function for Two-Dimensional SH Motion in a Half-Space	251

CONTENTS (Continued)

page

TABLES

1	Possible damage modes due to shaking for openings in rock	15
2	Test section schedule	30
3	Summary of damage in Drift C, Shot Hard Hat	34
4	Approximate peak values of measured free-field quantities versus range, Shot Hard Hat	36
5	Compatibility of earthquake design methods with static design methods for openings in rock	181

FIGURES

1	Relation between the major tectonic plates and recent earthquakes and volcanoes	6
2	Seismic zone map of the United States	9
3	Contour map for effective peak acceleration	10
4	Calculated peak surface accelerations and associated damage observations for earthquakes	19
5	Calculated peak particle velocities and associated damage observations for earthquakes	20
6	Correlation of damage criteria for earthquakes and explosions	24
7	Damage zones from UET program	26
8	Vertical section, Project Hard Hat	28
9	Plan view of test sections, Project Hard Hat	29
10	Analytical versus empirical method for estimating tunnel response	32
11	Reflections and refractions of SH-waves in a horizontally stratified soil mass	44
12	Typical example of the amplification function for a soil layer over bedrock	44
13	Lumped-mass and spring idealization of a semi-infinite layered soil mass	46
14	Axial deformation along tunnel	50
15	Curvature deformation along tunnel	50

CONTENTS (Continued)

	<u>page</u>
16 Hoop deformation of cross section	50
17 Circular cylindrical cavity and incident wave	52
18 Biaxial stress field created by a horizontal pressure	52
19 Dynamic stress concentration factors for P-wave	53
20 Maximum dynamic stress concentration factor K_1 for P-wave incident upon a cylindrical cavity	55
21 Maximum dynamic stress concentration factor K_2 for SV-wave incident upon a cylindrical cavity	55
22 Circular cylindrical liner and incident wave	57
23 Maximum medium dynamic stress concentration factor K_m versus liner thickness parameter \tilde{r} for various $\tilde{\mu}$ and $\tilde{\alpha}$ ($\nu_m = \nu_l = 0.25$)	58
24 Maximum liner dynamic stress concentration factor K_l versus liner thickness parameter \tilde{r} for various $\tilde{\mu}$ and $\tilde{\alpha}$ ($\nu_m = \nu_l = 0.25$)	58
25 Some wave paths between source and site regions	75
26 Amplitude ratio versus dimensionless depth for Rayleigh wave	79
27 Schematic of coordinate axis, incident and reflected wave fronts at arbitrary angle of incidence, and surface control point	87
28 Critical depth for interference of incident and reflected wave trains	91
29 Displacement time histories at depth for vertically incident wave ($\theta = 0^\circ$)	94
30 Strain component, ϵ_{32} , time histories at depth for vertically incident wave ($\theta = 0^\circ$)	95
31 Displacement time histories at depth for wave incident at $\theta = 30^\circ$	97
32 Strain components, ϵ_{31} and ϵ_{32} , time histories for angle of incidence $\theta = 30^\circ$	98
33 Displacement time histories at the same monitoring point for variable angle of incidence of incoming wave	99
34 Strain components, ϵ_{31} and ϵ_{32} , time histories at the same monitoring point for variable angle of incidence of incoming wave	100
35 Displacement record of the 1966 Parkfield (California) earthquake monitored to below the critical depth	102

CONTENTS (Continued)

	<u>page</u>
36 Variation of peak displacement and peak acceleration with depth for the 1966 Parkfield (California) earthquake	104
37 The cavity, coordinates, and excitation	106
38 Relation between Cartesian coordinates and cylindrical polar coordinates	110
39 Discretization scheme for eight points	115
40 Effect of angle of incidence on cavity response ratio around the circumference	116
41 Ratio of steady-state cavity bottom response to free- surface response versus frequency for various depths and various angles of inclination	117
42 Motion at cavity bottom and incident wave field in absence of cavity	119
43 The overall design process for underground structures	124
44 Identification of sectional and circumferential forces	127
45 Geometry of sinusoidal shear wave oblique to axis of tunnel	129
46 Interaction between tube and soil due to difference between free-field and tube displacements in SFBART approach	131
47 Assumed geometry for determination of K_g in SFBART approach	133
48 Simple model for the analysis of circumferential bending due to dynamic soil pressure in SFBART approach	138
49 Simple model for the analysis of circumferential bending due to inertial forces in SFBART approach	138
50 Relative response velocity per unit acceleration	143
51 Distribution of sectional forces by seismic deformation analysis and dynamic analysis	146
52 Distribution of sectional forces by dynamic analysis using four different earthquake waves	147
53 Details of seismic joint for the SFBART subaqueous tube	149
54 Racking due to shear distortion of the soil	153
55 Corner details for seismic design	157
56 Seismic joint for North Point tunnel	159
57 Cross-sectional details of drain for Marina Boulevard box	160
58 Detail of vertical drain for Marina Boulevard box	161
59 Tunnel stabilization system using steel sets	164
60 Tunnel stabilization system using rock bolts	165

CONTENTS (Continued)

	<u>page</u>
61 Profile for Beartrap access structure	172
62 Typical section of Beartrap access structure	173
63 Proposed seismic joint for reinforced concrete conduit	176
64 Comparison of current level of development between the various design methods	182
65 Proposed locations of triaxial accelerometers for a tunnel	194
66 Proposed location of triaxial accelerometers for a large cavern	196
67 Representation of half-space model and associated coordinate system	243
68 Deformation due to body waves	245
69 Motion due to Rayleigh waves	246
70 Plane layer over a half-space	248
71 Reflection and refraction of body waves	250
72 Image source location	254

Acknowledgments

The authors gratefully acknowledge the interest and active participation of many persons during this investigation. Special recognition is given to those who conducted certain portions of the investigation under the sponsorship of the National Science Foundation: Arthur Carriveau for the study of dynamic response of underground cavities (in Chapter 5), Robert Edwards for the discussion of the nature of underground motion (in Chapter 5), Fred Kintzer for the section on dynamic properties of earth material (in Chapter 4), Bruce Redpath for the discussion of motion transducers (in Chapter 8), Peter Yanev for his collection of data on earthquake effects on underground structures in Japan and Italy, and Jack Zanetti for the parametric study of variation of motion with depth (in Chapter 5).

Our consultants under sponsorship of the National Science Foundation were Tor Brekke of the University of California, Berkeley, and Donovan Jacobs and A. M. (Pete) Petrofsky of Jacobs Associates. They have made very valuable contributions during the course of the work and during the review of the final report. Don Ross of Tudor Engineering Company reviewed the final report and offered many useful suggestions.

In the course of this study, a number of individuals in many different private firms and government agencies have been contacted to obtain both specific and general information on their concerns and approaches to seismic design of underground structures. During our visit to Japan, the Japanese engineers were particularly helpful and informative. We wish to thank E. Kuribayashi and T. Iwasaki of the Public Works Research Institute, Ministry of Construction; K. Muto and K. Uchida of the Muto Institute of Structural Mechanics; K. Yamahara of The Research Laboratory, Shimizu Construction Company; and T. Ohira and T. Tottori of the Japan Railway Construction Public Corporation. The contributions that these people have made to our understanding of the current state of the art are gratefully acknowledged.

This report will be the primary element in the future activities of the International Tunneling Association's Working Group on Seismic Effects on Underground

Structures. We acknowledge the interest of the group in conducting this study.

Any opinions, findings, and conclusions or recommendations expressed in this publication are those of the authors and do not necessarily reflect the views of the National Science Foundation or the Federal Highway Administration.

Summary

The objective of this study is to identify and evaluate the current state of the art of earthquake engineering of underground structures and to determine those areas in which additional research is most needed. Transportation tunnels are emphasized in the study, but other large underground structures are also included.

In recent years, new environmental requirements and population density factors have led to an increased interest in the exploitation of underground space for such diverse uses as transportation, liquid and gas storage, manufacturing, and disposal of hazardous materials. Simultaneously, there has been an increase in awareness that potentially destructive earthquakes are possible throughout most of the United States. Given this increased awareness of seismic hazard, it follows that seismic vulnerability should be considered in planning underground structures.

The general view is that underground structures are much less severely affected by strong seismic motion than surface structures. This view is substantiated by the limited observations of earthquake damage to tunnels and other underground structures; however, some severe damage, including collapse, has been reported. While the seismic environment is not expected to pose a design problem, seismic evaluations should be conducted for most proposed critical structures such as nuclear power plants, liquefied petroleum gas storage facilities, and nuclear waste repositories for nearly all locations in the United States. In areas of particularly high seismic hazard, all underground projects of public importance should probably be investigated and engineered for seismic motion.

EFFECTS OF EARTHQUAKES ON UNDERGROUND STRUCTURES

A review of the past performance of 127 underground openings during earthquakes, including recent (1978) earthquakes, was conducted for this study. The review indicated that underground structures in general are less severely affected than surface structures at the same geographic location. While a surface structure responds as a resonating cantilevered beam, amplifying the ground motion,

an underground structure responds essentially with the ground. However, the review showed that severe damage is often associated with tunnels in soil and poor rock, whereas damage to tunnels in competent rock is usually (but not always) minor.

Peak ground motion parameters, such as acceleration and particle velocity, seem to correlate with the extent of damage. Duration of the earthquake motion also has an effect on the extent of damage. Besides geology and earthquake parameters, other important parameters that affect tunnel stability are tunnel support and in situ stresses.

A thorough evaluation of the relation between these parameters and the performance of the underground structures was not possible because a complete suite of data could not be compiled. Many of the documents citing the earthquake performance of underground structures do not provide details on all the parameters. Furthermore, many of the events occurred many years ago, and it is no longer possible to obtain complete information on all the relevant factors. Consequently, at this time empirical relations between various parameters (for example, peak acceleration) and tunnel damage are approximate and tentative. A more detailed definition of the relationship requires more comprehensive studies than are currently available.

VARIATION OF SEISMIC MOTION WITH DEPTH

As an alternative to using empirical relationships to evaluate the stability of underground structures during earthquakes, quantitative, or numerical, analyses of stresses and strains can be conducted. This alternative method requires the characterization of seismic motion beneath the ground surface. Because motion is generally recorded at the surface, the question is raised as to whether the motion decreases with depth in some predictable manner in comparison with ground surface motion. Although studies of motion recorded underground tend to substantiate the idea that motion does reduce with depth, amplification at depth has been observed.

There are few instances of motion recorded underground in the United States; however, the Japanese have approximately 200 instruments placed underground at

this time. About 75% of these instruments have been placed at depths less than 131 ft (40 m) for the purpose of studying soil-structure interaction and would be of little value for studying deep structures. While the data base being developed from these records is very useful, it is not yet sufficient to facilitate a quantitative prediction of motion at depth.

In an attempt to obtain a better theoretical understanding of the variation of motion with depth below the ground surface, a parametric study was conducted of a horizontally polarized shear wave train propagating in an elastic half-space. The study revealed that the incident (upward-traveling) wave and the reflective (downward-traveling) wave interfere to a considerable depth, which depends upon the duration of the wave train. In addition, the study showed that variation of the peak amplitudes with depth depends on the characteristics of the wave train. For example, using a surface record from the 1966 Parkfield earthquake, the study showed that the value of the peak acceleration was reduced to one-half the surface value at a depth of 200 ft (61 m), while at a greater depth of 400 ft (122 m) the value was approximately three-quarters of the surface value. Consequently, peak accelerations do not necessarily reduce uniformly with increasing depth. Because the displacement time history is a much smoother curve than the acceleration time history, the values of the peak displacements reduce very slowly with depth. Using the record of the 1966 Parkfield earthquake, it was found that peak displacements reduced only about 5% at a depth of 1,000 ft (305 m). Substantial reductions (on the order of 40%) were not apparent until very great depths of about 5,000 ft (1,524 m) were reached.

SEISMIC WAVE STUDY OF A CIRCULAR CAVITY

To obtain a better understanding of the seismic response of a cavity, the response of a circular cavity in a half-space was compared with the incident wave field in the half-space. For simplicity, the incident wave field was a horizontally polarized shear wave with an angle of incidence to the free surface of the half-space of 0° , 30° , 60° , and 90° . The depth of the cavity was taken at a shallow, intermediate, and great depth by considering depths of 6, 20, and 100 times the cavity radius, respectively. In general, for cavities in hard rock or for cavities at great depth, it was found that the diffraction effects are small for the normal frequency range (say 0.1 to 15.0 Hz) of an earthquake and

that the cavity response can be estimated by the incident, unscattered motion. However, for shallow cavities in stiff soil, it was found that there is a strong interaction between the cavity and the free surface and that the cavity response is significantly different from the incident field.

ANALYTICAL AND DESIGN PROCEDURES FOR UNDERGROUND STRUCTURES

Analytical procedures for predicting the response of structures to earthquake shaking are not as well developed for underground structures as they are for surface structures. The current procedures used in the seismic design of underground structures vary greatly depending upon the type of structure and the ground condition.

Analytical procedures for subaqueous tunnels have been developed in both the United States and Japan. Procedures for submerged tunnels employ classical theory from the mechanics of solids and modern methods of dynamic analysis. Consequently, the procedures for subaqueous tunnels are fairly well formulated.

The procedures for seismic design of structures in soil and rock are not as well formulated. The sophistication of stress analysis procedures ranges from simple calculations based upon peak ground velocity and plane wave mechanics to the more detailed modeling of finite-element analysis. Current static design practice for underground openings in rock is more strongly affected by empirical methods and engineering judgment during the construction phase than by stress-prediction models. For this reason, procedures to predict dynamic response are not completely compatible with current static design procedures.

The principal concept currently in use for enhancing the seismic stability of underground openings is to improve the construction details so as to achieve better ground-support interaction. For openings in rock, this may include additional rock bolting and reinforced shotcrete and continuous blocking of steel sets. Continuous blocking is automatically provided in structures that have a cast-in-place concrete liner.

CRITIQUE OF THE STATE OF THE ART

From the available information on earthquake engineering of underground structures and from the wave propagation studies conducted for this report, certain conclusions were drawn regarding the current state of the art:

- The data on the effects of earthquakes on underground structures are not sufficient to determine the relative importance of various parameters for predicting damage or lack of damage. The historical data base compiled for this study, although significantly larger than that compiled for other studies, is too small a base from which to draw hard and definite conclusions. The most important reason for the small data base is the apparent lack of systematic surveys of underground facilities following major earthquakes.
- Data on seismic motion recorded at depth indicate a general trend in the reduction of peak acceleration with depth, although records exist of peak amplitudes that are greater at depth than at the surface. Many more records will have to be obtained at depth before better descriptions can emerge showing variation of motion amplitudes and frequency content with depth. The development of earthquake engineering technologies for underground structures will only make significant advances when our understanding of the underground motion and its effects on underground structures is adequately founded on observations.
- Seismic design methodologies for subaqueous tunnels have been drawn from contemporary analytical technologies and up-to-date procedures for the design of steel and reinforced concrete surface structures. Therefore, the state of the art for the seismic design of subaqueous tunnels appears adequate.
- Technologies for analyzing the seismic stability of an opening in rock and for specifying mitigating action are poorly developed. The principal approaches for the static design of openings in rock place a great deal of emphasis on empirical methods and very little emphasis on analytical calculations for stresses. There has been very little effort directed toward developing empirical seismic analysis and design methods that would be compatible with the existing empirical static analysis and design methods. A method is proposed based upon a qualitative assessment of rock-support interaction and upon preliminary relationships between damage to rock tunnels and peak ground motion parameters of earthquakes.

- Static design methodologies for soil tunnels are very similar to those for rock tunnels. In this respect, the relationship between static and seismic design methods for soil tunnels is in much the same state as it is for rock tunnels -- that is, the seismic methods are not entirely compatible with the static methods and are poorly developed at this time.

RESEARCH RECOMMENDATIONS

A number of research recommendations have been derived from this study. Briefly the principal recommendations are as follows:

- Systematic reconnaissance of underground structures needs to be undertaken in the epicentral regions of recent and future major earthquakes in order to define empirical relationships between tunnel and geologic parameters and expected damage.
- More instrumentation for recording seismic motions needs to be placed in tunnels and drill holes.
- Further research is needed to better quantify underground seismic motions and to relate details of support enhancement to specific ground motion parameters.
- Procedures need to be further developed for the analysis and design of important openings in soil and rock.

1. Introduction

The objective of this study is to advance the state of the art of earthquake engineering of transportation tunnels and other large underground structures by evaluating the current practice in underground earthquake engineering and determining those areas in which additional research is most needed.

In the past, facilities that have been successfully constructed underground have included water supply and distribution systems, sanitary sewers, box conduits, underground passageways, tunnels, mass transit systems (including stations), and subaqueous tunnels. In recent years, there has been a growing interest in the exploitation of underground space for such uses as transportation, liquid and gas storage, manufacturing, and disposal of hazardous materials. With continuing improvements in construction techniques and capabilities, construction of underground facilities is rapidly expanding. Because of new environmental and population density factors, the underground construction of major industrial installations is becoming more economically feasible and environmentally desirable. Current United States policy on the terminal disposal of nuclear waste is strongly directed toward burial within a repository mined at great depth, approximately 3,000 ft (1 km).

At the same time that construction of underground facilities is expanding, an awareness that potentially destructive earthquakes are possible throughout much of the United States is increasing. It is becoming clear that the design problem posed by earthquakes is not confined to California. Although underground structures are regarded as being safer than surface structures during strong seismic motion (a view that is, in general, supported by observed damage to tunnels from earthquakes), some severe damage, including collapse, has been reported. Verification of seismic stability will therefore be required for nearly all locations proposed for underground construction of sensitive structures such as nuclear power plants, liquefied petroleum gas storage facilities, and nuclear waste repositories. Moreover, all underground projects of public importance located in areas of particularly high seismic activity should probably be investigated and engineered for seismic motion

The work performed to achieve the objective of the present study includes seismic wave propagation analyses; a summary of observed effects of earthquakes on underground structures; an assessment of contemporary seismic-resistive analysis, design, and construction procedures; and an identification of future research needs. The seismic wave propagation studies consist of a review of theory and current approaches to inferring subsurface ground motion amplitudes and of numerical studies of the seismic response of an underground cavity. Information on the observed effects of earthquakes (and, to a limited extent, of blasts) on underground structures was obtained through a rigorous literature search and is used to determine the performance of various types of underground structures subjected to seismic motions. Contemporary seismic analysis and design was assessed through a literature search, discussions with professionals in the field of underground design (see Appendix A), and an engineering evaluation of the information obtained. The report concludes with recommendations that identify fruitful areas of research involving both analytical studies and field (experimental) studies.

2. Background Information

This report documents a study that deals with large underground structures and with earthquake engineering. Because these subjects are not commonly associated with each other in the engineering design literature (except as it relates to those particular structures that are part of lifelines), this chapter begins with a brief description of the various types of underground structures considered in the study and the particular features of these structures that might be important to earthquake engineering.

Most readers of this report are likely to be engineers who are professionally active in the design of tunnels and other large underground structures but who may have had little or no prior experience with earthquake design or earthquake terminology. Therefore, this chapter also includes brief discussions of seismic activity and earthquake hazard and of earthquake magnitude and intensity.

UNDERGROUND STRUCTURES

This report divides large underground structures into two major categories: linear structures, which are used to convey people, materials, or objects from one geographic point to another, and volume structures, which provide open spaces below ground for production facilities or storage. Linear structures consist of subaqueous (or immersed) tunnels, soil tunnels, rock tunnels, cut-and-cover conduits, and culverts. They constitute portions of transportation systems for motor vehicles, railroads, and mass and rapid transit. Linear structures also are used in the conveyance systems for liquids, primarily fresh water and wastewater. Underground structures that provide volume for storage or production facilities are usually either reinforced concrete structures with a shallow burial in soil (cut-and-cover construction) or caverns excavated from rock. Some are constructed for facilities associated with human activity; for example, convention halls, communication centers, recreational facilities, and defense installations. Other volume facilities are used as water reservoirs and petroleum product reservoirs and for the storage of hazardous wastes, while still others serve as manufacturing facilities and power plant houses. Some structures function as both linear and volume structures. For example, the

main collectors of wastewater systems that collect both sanitary sewer and storm water may be greatly oversized for normal daily sanitary sewer runoff in order to provide for temporary storage of storm-water runoff.

The subaqueous tunnel is a unique underground structure, being quite different from other tunnels both in form and in construction procedures. The principal portion of the tunnel consists of concrete-lined steel segments (sometimes reinforced concrete only) that are floated into position and then sunk into trenches prepared in the floor of the river or bay being crossed. The segments are joined together, the trench backfilled, and bulkheads between the segments removed, forming a tubular tunnel submerged in the bottom muds. Thus, the subaqueous tunnel is usually modeled as an elastic beam on an elastic foundation.

Structures within rock and soil can be quite different from each other depending on the strength and quality of the ground, as well as on the size of the opening. The rock mass can vary from very competent rock with massive blocks to very weak and highly fractured rock. Thus the support requirements can vary from no support at all to fairly heavy steel sets. Similarly, the soil mass can vary from a very stiff soil requiring very light steel sets to a wet, soft soil requiring the installation of a closed circular lining behind a shield.

Regardless of the differences in the type of supports required for soil and rock openings, it is important to design a support that is flexible in comparison with the ground. This concept is generally accepted practice in the design of tunnel liners for static loads. It also applies equally well to design for earthquake loads. The flexible support will have a good capacity for sustaining dynamic loads, providing its integrity is maintained during motion.

The concept of flexibility is developed in liner design for soft-ground tunnels.¹ It is represented by the flexibility ratio, which is the flexural stiffness of the soil medium divided by that of the liner. Thus a flexibility ratio greater than 1 means that the liner is more flexible than the ground. An important parameter in the determination of stiffness is the modulus of elasticity.

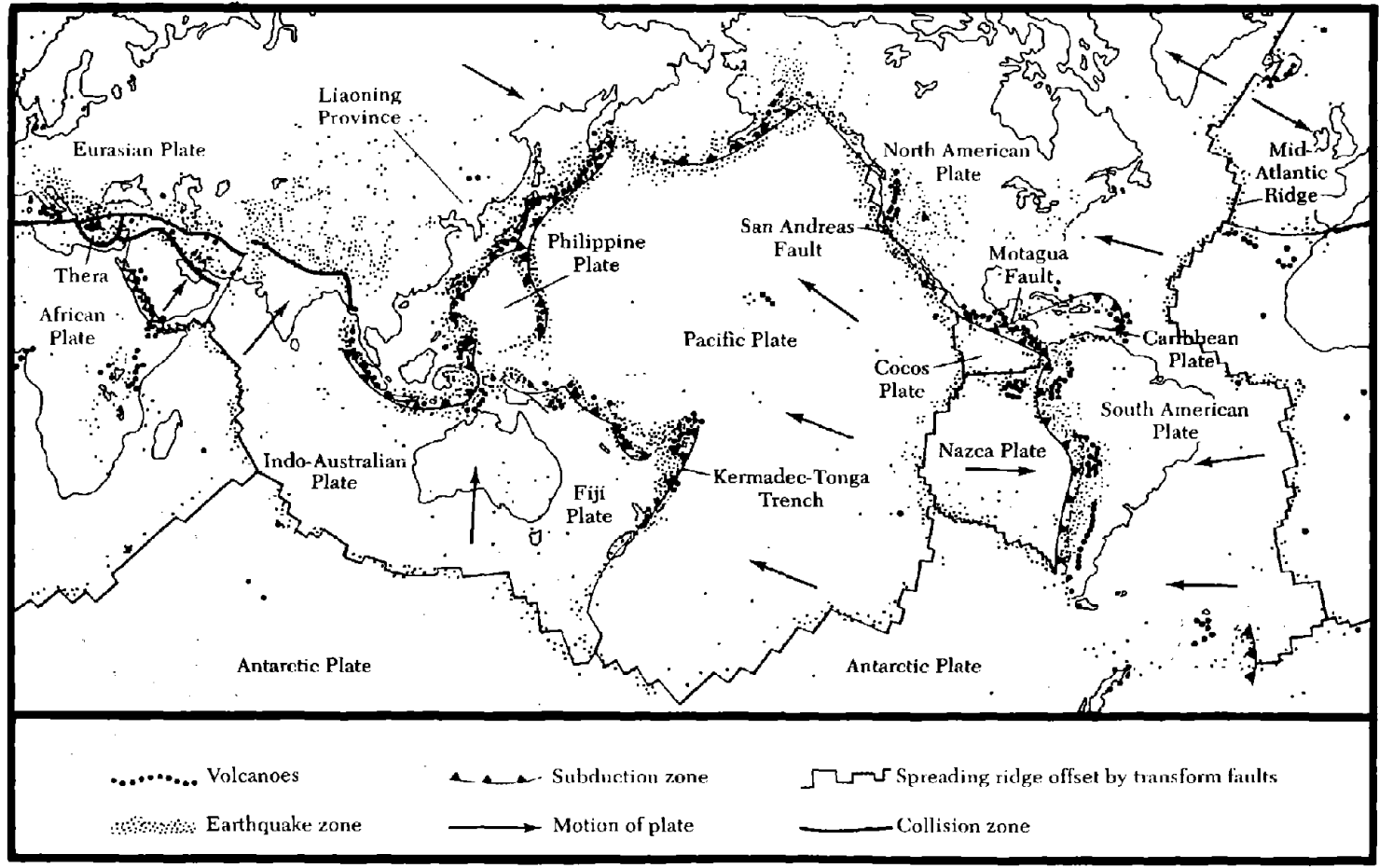
The stiffness of the soil varies directly with its modulus of elasticity, as does the stiffness of the liner. In addition, the stiffness of the liner varies directly with its moment of inertia and inversely with the cube of the radius of the opening. In general, bending moments in the liner under static loads increase rapidly as the flexibility ratio reduces below the value of 10. Thus it is desirable to design liners with flexibility ratios significantly greater than 1.

In practice, flexible support conditions are easily achieved in good rock, where support might consist of rock bolts or a layer of shotcrete. In less competent rock or soil, where thick liners are required, it is both possible and desirable to achieve a flexible liner.

SEISMIC ACTIVITY AND EARTHQUAKE HAZARD

The following brief discussion is intended to provide the newcomer to the field of earthquake engineering with some of the basic concepts associated with seismic hazards. It is not intended to be complete or thorough. For more detailed information on the relevant aspects of seismology, the reader is referred to the general literature.^{2,3,4,5}

The subject of seismicity addresses the spatial distribution of earthquakes as well as their frequency of occurrence. Most earthquakes occur at the boundaries of the major tectonic plates, as shown in Figure 1, and are due to the relative motion between these plates. The San Andreas fault in California delineates part of the boundary between the North American Plate and the Pacific Plate. Earthquakes generated along this fault result from the northwesterly movement of the Pacific Plate relative to the North American Plate as these two plates slide past each other. At some boundaries, two plates have a relative motion toward each other. If one plate is an oceanic plate and the other is a continental plate, the oceanic plate slides underneath the continental plate in a process referred to as subduction. This phenomenon is typical of the plate boundaries along Japan, south of Alaska, and along the western coast of South America. If the two plates in relative motion toward each other are both continental masses, neither plate is subducted. Instead, the two plates collide, and mountain ranges are pushed up along the boundary. The most active boundaries



Reprinted by permission of the publisher: From *Earthquakes: A Primer* by Bruce A Bolt. W. H. Freeman and Company. Copyright © 1978.

Figure 1. Relation between the major tectonic plates and recent earthquakes and volcanoes. (Source: Reference 2.)

are those between converging plates, as described above. Boundaries between diverging plates, marked by spreading ridges, are relatively inactive.

In the interior of tectonic plates, the frequency at which earthquakes occur is much less than along the plate boundaries, although, even in these areas, major destructive earthquakes do sometimes occur. The central and eastern portions of the United States are not as seismically active as the western portions, particularly California; however, several major earthquakes have occurred in these midplate regions of the North American Plate in the recent past. Two moderately large earthquakes occurred off Cape Ann, Massachusetts, in 1638 and 1755. A series of three extremely large earthquakes occurred near New Madrid, Missouri, in 1811-12 and were felt as far away as Washington, D.C. Another major eastern event was the destructive earthquake at Charleston, South Carolina, in 1886. Neither of these large earthquakes nor the many shocks of moderate size in the eastern and central regions of the United States can be explained by interaction between tectonic plates.

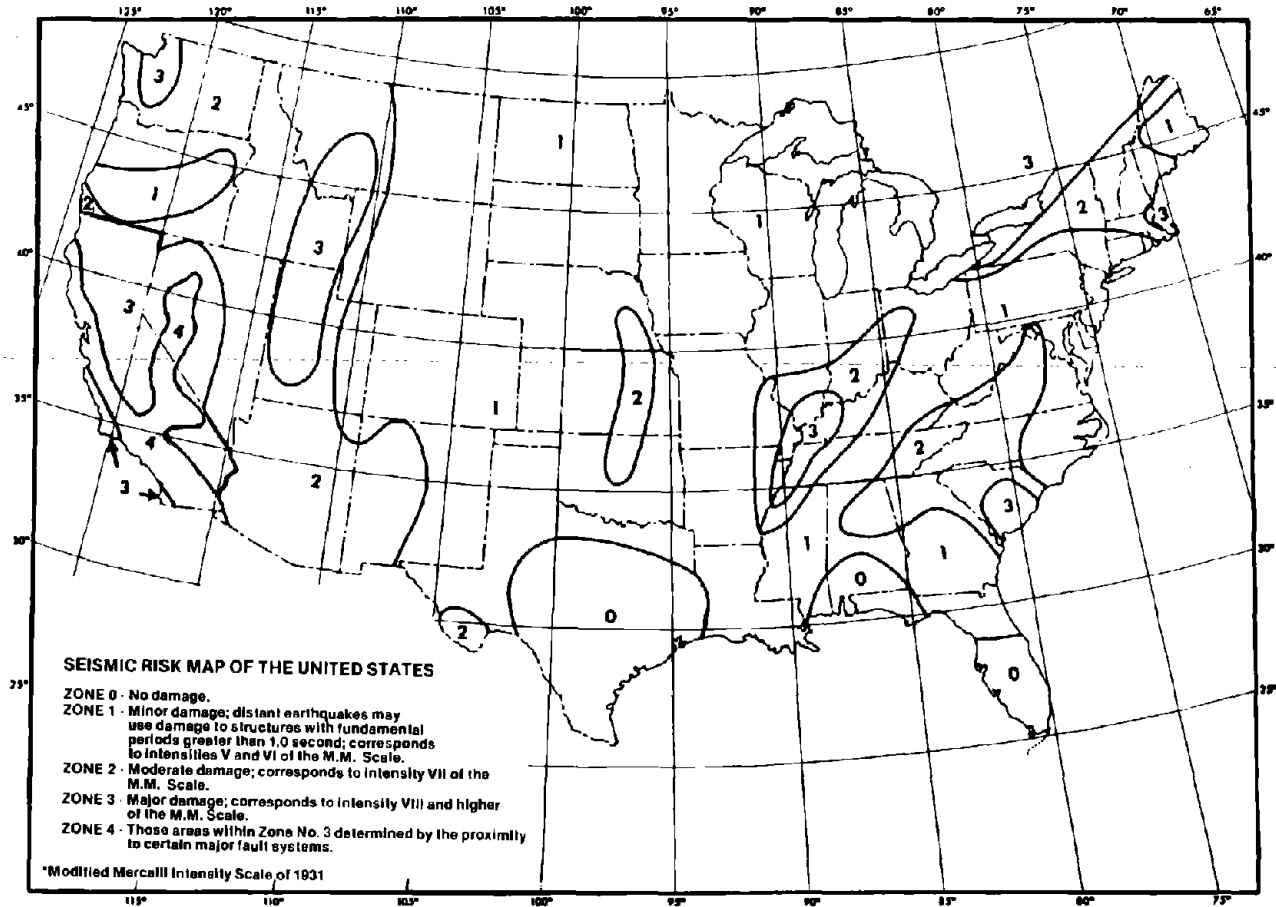
In assessing earthquake hazards, one of the main distinctions between the eastern and western regions of the United States is the degree of difficulty encountered in identifying and mapping active faults. In the western United States, earthquakes can usually be associated with active faults, which in general have been readily identified and mapped. However, in the eastern and central United States, it has not yet been possible to associate earthquakes in general with known faults. Geologic history seems to have obscured the faults in these regions so that it is much more difficult to identify and map active faults. Furthermore, relatively few earthquakes have occurred in the eastern United States, making prediction of both spatial distribution and frequency of occurrence much more difficult there than in the western region.

Although major earthquakes in the eastern United States appear to be infrequent and are more widely dispersed than those in the western United States, the question remains: can damaging earthquakes such as those of 1755, 1811-12, and 1886 occur anywhere in the eastern North American continent? The importance of intraplate earthquakes has only recently begun to receive attention, and many valuable studies, such as those by Sykes⁶ and Bollinger,⁷ are being conducted. The historic record of earthquakes in the eastern United States spans

less than 300 years, and Bollinger suggests that that is not a long enough period from which to deduce the presence or absence of a cyclical behavior of earthquakes in the region. In support of this view, Bollinger points to the work of Ambraseys⁸ on damaging earthquakes over a period of 2,000 years for the Istanbul region in northeastern Turkey and for the Anatolian fault zone in northern Turkey. Both of these regions have experienced quiescent periods of up to several hundred years followed by long periods of intense earthquake activity.

By studying regional seismicity, the comparative earthquake hazard for various locations can be determined. Qualitatively, this is expressed in the form of a seismic zone map in the *Uniform Building Code*,⁹ as illustrated in Figure 2. A better indication of seismic hazard would be gained by expressing it in the form of the odds that an earthquake that produces peak ground acceleration exceeding a given value within a given period of time will occur at a certain site. Such a probabilistic expression of seismic hazard was used to prepare a new seismic hazard map of the United States for the Applied Technology Council.¹⁰ This map, shown in Figure 3, indicates the effective peak acceleration (EPA) that might be expected to be exceeded during a 50-year period with a probability of 1 in 10. Although, at present, EPA does not have a precise physical definition, it is related to the smoothed elastic response spectrum in this way: the 5%-damped spectrum for the actual motion is drawn and fitted with a straight line between the periods of 0.1 and 0.5 sec; then the ordinate of this straight line is divided by 2.5 to obtain EPA.¹⁰ Bolt suggests that EPA "can be thought of as the maximum acceleration in earthquakes on firm ground after high frequencies that do not affect sizeable structures (large houses, factories, bridges, dams, and so on) have been discounted."¹²

It is extremely important to note that both these seismic hazard maps are based upon seismic history only. This may be inadequate because the distribution of active faults has not been considered and because some of these active faults have not produced activity during the relatively short historical observation period.



Reproduced from the 1979 edition of the *Uniform Building Code*, copyright 1979, with permission of the publisher, the International Conference of Building Officials.

Figure 2. Seismic zone map of the United States. (Source: Reference 9.)

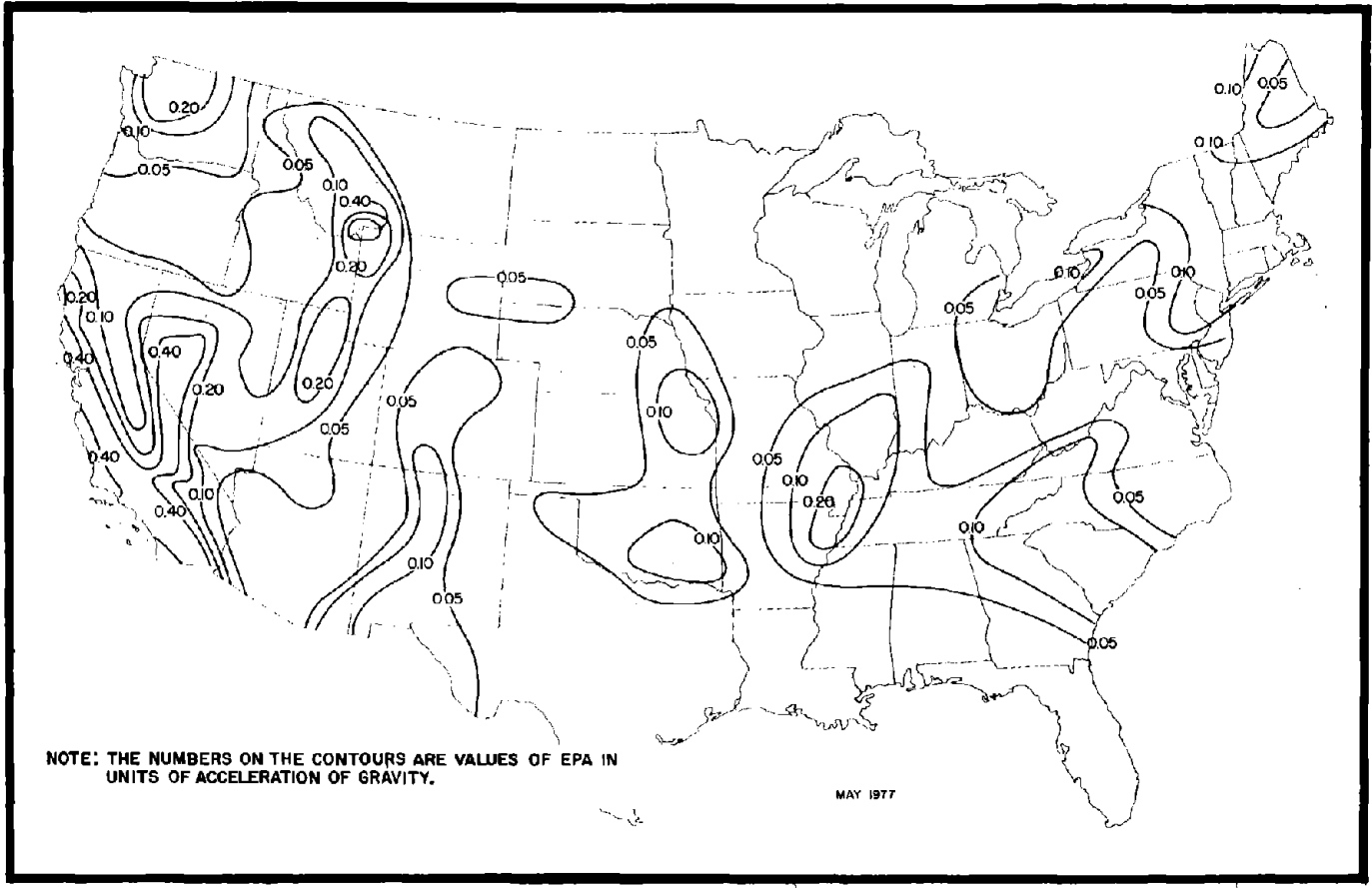


Figure 3. Contour map for effective peak acceleration. (Source: Reference 10.)

EARTHQUAKE MAGNITUDE AND INTENSITY

Because the Richter scale is widely used to describe the size of earthquakes, a few brief comments about the significance of the scale and its general relationship to the severity of ground motion are given here for the benefit of those outside the earthquake engineering field. Basically, a value on the Richter scale logarithmically represents the amount of energy released by the event. An increase of one unit on the scale represents approximately a 30-fold increase in the energy released. An earthquake is generated by the rupture of rock and slip along a fault in the earth's crust. Sometimes surface rupture occurs and delineates the fault. Generally, the larger the magnitude (M), the greater the length of rupture. This means that usually a greater length of a fault will slip during a large-magnitude event than during a small one; conversely, a longer fault can produce a larger magnitude earthquake.

The experience of strong ground motion at a particular site is of course related to the Richter magnitude; however, distance from the source and the local site conditions are also factors that affect the ground motion at the site. As earthquake waves propagate from the source, they attenuate with distance. This relationship has been investigated and presented in the form of attenuation curves, such as those given by Schnabel and Seed,¹¹ Idriss,¹² and Blume.¹³ Because the source of motion is not a point but rather is distributed along a long section of a fault, the severity of ground shaking at a site close to a fault may not change greatly as a function of magnitude. As an example, consider the transbay tube of the San Francisco Bay Area Rapid Transit District, located in San Francisco Bay between the cities of San Francisco and Oakland, California. The following rather interesting discussion of the earthquake considerations for the design of the tube is given by Housner:¹⁴

A great earthquake . . . is very likely to occur on the San Andreas fault as it did in 1906. That earthquake is estimated to have had a Richter magnitude of 8.25 and slipping occurred along a length of fault of some 200 miles with the maximum relative offset of the two sides of the fault reaching approximately 20 feet in the neighborhood of Tomales Bay. The ground motion produced in the general bay area by the 1906 shock is judged to be equal to the most intense motion likely to be produced by any future earthquakes. If an earthquake larger than the 1906 shock were to occur, say one having magnitude 8.6, this would mean that the length

of the fault along which slipping had occurred was somewhat greater than in the 1906 shock and these increments of extra slipping would be at distances of one hundred miles or more from the tube location and hence would have a negligible effect upon the intensity of ground motion at the proposed site of the tube. In fact, the length of slipping associated with a magnitude 7 shock (approximately fifty miles) is sufficiently great so that the intensity of ground motion at the tube site can be expected to be almost as severe as during an earthquake of 8.25 magnitude. This point is emphasized to call attention to the fact that it is not necessary to wait for an extreme earthquake (magnitude 8 or greater) in order to experience extreme ground motion.

Another way of describing the size of an earthquake is by means of intensity scales that are related to the amount of damage to buildings and other man-made structures, to the extent of the reactions of animals and people, and to the degree of disturbance to the ground. Intensity is not always directly related to magnitude because it is a function of other parameters as well -- in particular, local soil conditions and the distance from the epicenter.

The Rossi-Forel scale, the first intensity scale of modern times, ranges in value from I to X. It dates back to the 1880s and was used to describe the intensities of the 1906 San Francisco earthquake in the published reports immediately following that event. The Rossi-Forel scale has been largely replaced by the Modified Mercalli Intensity (MMI) scale, which ranges in value from I to XII. The original Mercalli Intensity scale was modified by Richter in 1956,⁴ but a newer version has been developed by Wood and Newmann to represent more contemporary construction practices.² This newer version, called the abridged Modified Mercalli Intensity scale, is given in Appendix B. Note that all structural references in the appendix are for surface structures and that there are no references to underground structures.

3. Observed Effects of Earthquakes and Underground Explosions

This chapter summarizes the effects of earthquakes and subsurface blasts on large underground structures. Much of the information presented here was obtained from published reports. Primary attention is given to the effects of earthquakes; however, the effects of underground conventional and nuclear explosions are also included.

The term *large underground structure* denotes transportation tunnels, mines,* underground power plants, aqueducts, and utility tunnels. Although submerged-tube transportation tunnels are large underground structures, they are usually fairly rigid compared with the surrounding medium and behave much differently than tunneled or mined structures in rock and firm soils. Consequently, submerged tunnels are excluded from this review. Because information regarding cut-and-cover structures is sparse, only a brief discussion of those structures is possible in this report.

EFFECTS OF EARTHQUAKES

The effects of earthquakes on tunnels, mines, and other large underground structures have been summarized in several reports.¹⁵⁻¹⁸ Duke and Leeds presented one of the early evaluations of earthquake damage to tunnels.¹⁵ Stevens reviewed the effects of earthquakes on mines and other underground openings.¹⁶ Dowding and Rozen studied the response of rock tunnels to earthquakes and correlated the damage to peak ground motion.¹⁷ Additional information was obtained from other sources.¹⁹⁻³³

Earthquake damage to underground structures may be attributed to three factors:

- fault slip
- ground failure
- shaking

*It is recognized that mines are different from underground, civil-engineered structures; however, mines yield useful information on seismic response.

Damage due to sudden fault slip has been reported in tunnels where the opening passes through a fault zone. The damage varied from minor cracking of the tunnel lining to collapse and closure of the opening. Usually damage was restricted to the fault zone. Clearly, fault slip cannot be prevented; therefore, the only way to avoid this damage is to avoid intersecting an active fault. When this is not possible, fault slip damage is to be expected, and postearthquake repairs should be planned in advance.

Ground failures, such as rock slides, landslides, squeezing, soil liquefaction, and soil subsidence, have damaged portals and shallow structures. Sometimes slides from slopes adjacent to tunnel portals have closed tunnels while doing little or no damage to the portal. More often, slides have caused severe damage to the portals when the rock and soil around the portal have been involved in the slides. Shallow structures in steep terrain may also be affected by slides. For example, a major section of a highway tunnel in the Izu Peninsula, Japan, was removed by a landslide during the Near Izu-Oshima earthquake of January 14, 1978. Damage due to ground failure may be avoided by careful siting and attention to slope stability.

Effects of shaking deserve special attention. It should be noted that ground failure induced by shaking can cause damage to the structure indirectly, without the shaking itself causing damage. This discussion is centered on damage to underground openings caused directly by shaking. Possible modes of damage due to shaking are listed in Table 1. Possible secondary consequences of these damage modes are also indicated.

Response Parameters

Information about the underground structure and about the earthquake is needed to evaluate damage due to earthquake shaking. The parameters that influence the earthquake response of underground structures are:

- Cross-sectional dimensions (shape and size)
- Depth of structure below the ground surface
- Type, strength, and deformability of rock or soil
- Support and lining systems
- Shaking severity (intensity, peak ground motion)

Table 1. Possible damage modes due to shaking for openings in rock.

Possible Damage Mode	Possible Consequence
Rock fall	Injure personnel Block transportation Block ventilation Disrupt water management and other services Damage equipment Damage shaft wall
Rock slabbing	Same as for rock fall
Existing rock fractures and seams open up, rock blocks shift	Increase permeability along the opening Weaken rock structure
Cracking of concrete liners	Increase permeability Weaken liner
Spalling of shotcrete or other surfacing material	Lead to rock fall if extensive
Unraveling of rock-bolted system	Same as for rock fall
Steel set collapse	Same as for rock fall

The values of the in situ stresses at the depth of the underground structure are very important for the seismic evaluation of the structure. Unfortunately, it is extremely difficult to obtain reliable data on in situ stresses; however, the stresses can be estimated using empirical relations that associate with depth. Therefore, the depth of the structure below the ground surface is the desired parameter from a practical point of view.

The types of support that are found include rock bolts (sometimes with wire mesh), steel sets, shotcrete, and concrete (or even brick) lining, alone or in combination; in some cases, no support at all is used. Ground conditions may be characterized mainly by the type, strength, and deformability of the rock or soil.

The severity of the earthquake shaking at the site of the underground structure may be represented simply by an intensity scale or by peak ground motion parameters. It would be most appropriate to have information on shaking at the depth of the opening; however, data are usually available only for shaking at the ground surface or not at all.

Summary of Available Data

Information concerning damage to tunnels, mines, and other underground openings from earthquake shaking is summarized in the table that makes up Appendix C. The table was constructed using data obtained from Stevens,¹⁶ Dowding and Rozen,¹⁷ and many other sources.¹⁹⁻³³ Of the 127 cases cited, cases 1 through 71 coincide with the cases studied by Dowding and Rozen.^{17,24}

Appendix C identifies each case by the name of the earthquake and the name of the tunnel, mine, or underground opening. General information about the earthquake, such as date of occurrence, magnitude (M), and duration (D), may be provided along with the earthquake name. The table summarizes available data concerning the opening, the shaking at the ground surface, and the shaking underground. The important factors influencing the earthquake behavior of underground structures are represented by individual columns in the table. Completion of all columns for each case was not possible because of data limitations and time constraints; however, the columns do present the data

on the opening and the shaking that are needed to properly evaluate possible underground structural damage and to correlate that damage with ground motion. It is hoped that, following future destructive earthquakes, all such information on openings in the epicentral regions can be assembled by reconnaissance teams.

It should be noted that the reporting of portal damage in Appendix C differs somewhat from the method used by Dowding and Rozen,^{17,24} who reported all portal damage under the heading "damage due to ground failure and other reasons" as separate from damage due to shaking and fault movement. Inspection of some of the data sources revealed that some portal damage could not be directly attributed to landslides or to other types of ground failure. It is quite likely that, unless ground failure or faulting was indicated, portal damage was probably due to shaking alone. Therefore, if the actual cause of the portal damage was not reported, that damage is reported in Appendix C as having been due to shaking.

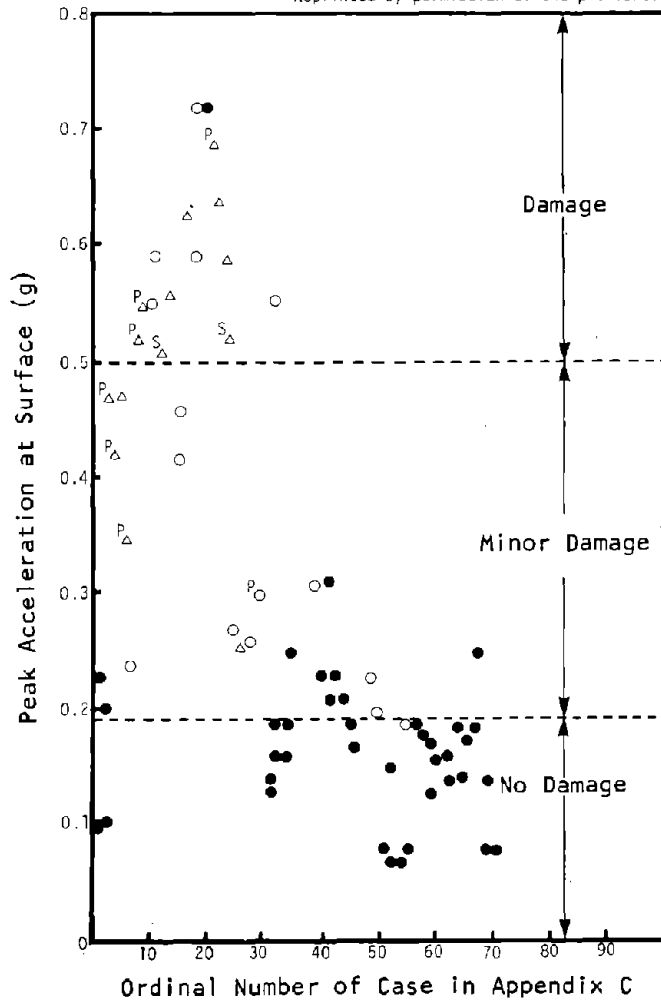
Peak Ground Motion Parameters. Peak ground motion parameters reported in Appendix C for cases 1 through 71 were obtained from Rozen, who calculated them for a ground surface location above each tunnel using an empirical prediction procedure.²⁴ The reader should be careful in regarding these values as accurate, or even approximate, representations of ground motions at the sites. The procedure employed by Rozen required using the distance from the epicenter to the site. Values calculated in this manner may be misleading when the site is adjacent to the ruptured fault. For example, Wright Tunnel No. 1 and No. 2 were approximately 84 miles (135 km) from the epicenter of the 1906 San Francisco earthquake, and Rozen predicted a peak acceleration of 0.13g* at these sites (cases 1 and 2). However, the actual peak acceleration must have been significantly higher because the San Andreas fault intersected Wright Tunnel No. 1 and created an offset in that tunnel of 4.5 ft (1.4 m). Therefore, it appears that Rozen simply used the distance from the site to the epicenter rather than the shortest distance to the ruptured fault, the latter being the more appropriate procedure.

*g is a constant representing acceleration of gravity equal to 32.2 ft/sec (981 cm/sec² or 981 Gal)

Another reason for regarding Rozen's predictions of the peak ground motions as approximate values is that a given attenuation relation cannot be applied to all earthquakes or to all site conditions. The selection of an appropriate attenuation relation for a given earthquake and a given site requires careful consideration of seismological data. Relations other than the one used by Rozen may result in very different predicted values. To illustrate this point, let us consider specific tunnels for two different earthquakes -- the 1964 Alaska earthquake and the 1971 San Fernando earthquake. For Whittier Tunnel No. 1 and No. 2 (cases 39 and 40), located 47 miles (75 km) from the epicenter of the Alaska earthquake, Rozen predicted a peak acceleration of 0.26g. However, an attenuation relation from the *Offshore Alaska Seismic Exposure Study*, which should be a much more appropriate reference, yields a much lower value of 0.14g.³⁴ A relation by McGuire predicts a much higher value of 0.35g.³⁵ The relation is based upon western United States data and may not be appropriate for the Alaska setting. In the example of the San Fernando earthquake, consider first the Tehachapi Tunnels (cases 53 and 54), which are located 45 miles (73 km) from the epicenter. The McGuire relation happens to yield a value of 0.07g.³⁵ The value was predicted by Rozen; however, the SAM V relation by Blume yields a lower estimate of 0.04g.¹³ Tunnels closer to the epicenter are even more interesting with regard to the diversity of predicted values. Consider several tunnels (cases 47, 48, and 49) located 10 miles (16 km) from the epicenter. For these tunnels, the Blume relation agrees with the 0.23g predicted by Rozen, while an attenuation relation developed specifically from the San Fernando earthquake by Duke et al. estimates a much larger value of 0.36g.³⁶ Clearly, the use of attenuation relations to estimate peak ground motion parameters requires careful consideration of the location of the earthquake, the type of earthquake source, and the characteristics of the ground at the site.

Figures 4 and 5 summarize the correlations of observed damage to peak accelerations and to peak particle velocities at the surface as prepared by Dowding and Rozen.¹⁷ Three damage levels due to shaking were identified. The classification *no damage* means no new cracks or fall of rocks, *minor damage* includes new cracking and minor rockfalls; and *damage* includes severe cracking, major rockfalls, and closure.

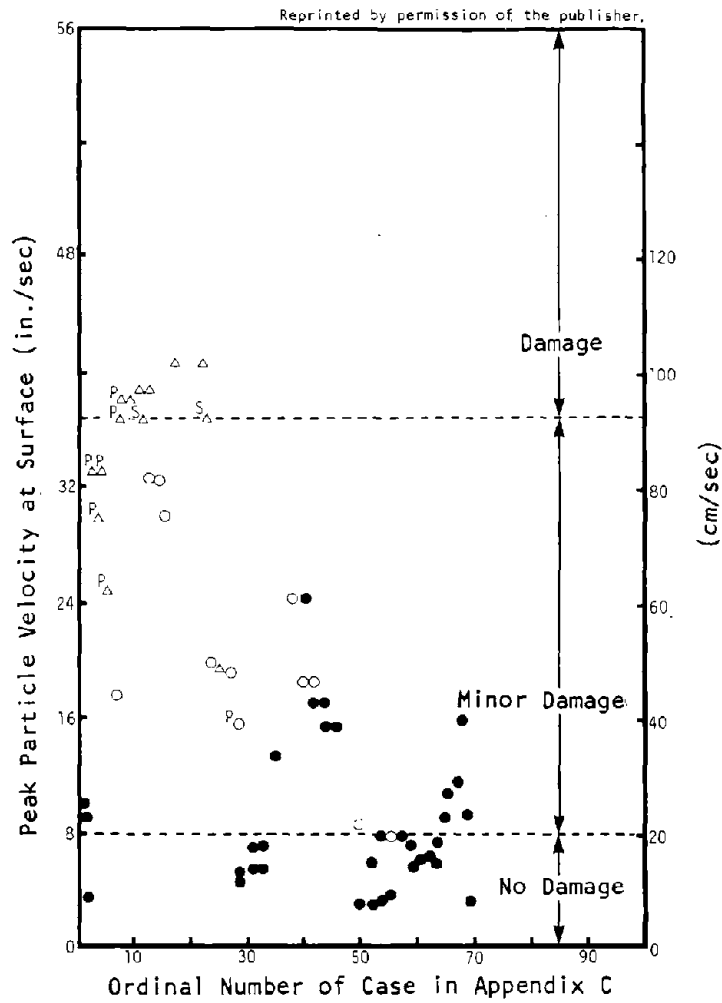
Reprinted by permission of the publisher.



LEGEND

- No damage
- Minor damage, due to shaking
- △ Damage from shaking
- P_{Δ} Near portal
- S_{Δ} Shallow cover

Figure 4. Calculated peak surface accelerations and associated damage observations for earthquakes. (Adapted from Reference 17.)



LEGEND

- No damage
- Minor damage, due to shaking
- △ Damage from shaking
- P_A Near portal
- S_A Shallow cover

Figure 5. Calculated peak particle velocities and associated damage observations for earthquakes.
(Adapted from Reference 17.)

Cut-and-Cover Structures. Shallow structures constructed in soil (or soft rock) by cut-and-cover procedures form a unique class of underground structures that deserves special attention. Previous studies of the effects of earthquakes on underground structures have emphasized openings mined from rock. Dowding and Rozen emphasized rock tunnels in their studies but included a few soil tunnels,^{17,24} while Stevens discussed only mines.¹⁶ A few reports of damage to cut-and-cover structures were documented from other reports, however. Case 115 in Appendix C involves a cut-and-cover railroad tunnel destroyed by the 1906 San Francisco earthquake. Cases 121 through 126 report damage to cut-and-cover conduits and culverts during the 1971 San Fernando earthquake, and case 127 reports damage from the same earthquake to a large buried reservoir. Although there may be many more such structures, both damaged and undamaged by strong earthquake motion, their documentation would be time consuming and was not possible for this study.

The sample of cut-and-cover structures available for this report is too small to provide firm conclusions; however, some observations are possible. Much of the damage may be attributed to large increases in the lateral forces on buried structures from the soil backfill during seismic motion. This would account for racking of structures and damage to walls, including failure of longitudinal construction joints, development of midheight longitudinal cracks, and formation of plastic hinges at the top, midheight, and bottom of walls. Structures with no moment resistance, such as the unreinforced brick arch of case 115, are susceptible to collapse under the dynamic action of the soil backfill. As with surface structures, the extent of the damage in shallow buried structures may depend greatly upon the duration of the strong shaking. Damage initially inflicted by earth movements, such as faulting and landslides, may be greatly increased by continued reversal of stresses on already damaged sections.

Conclusions. The following conclusions may be drawn from the data presented in Appendix C:

- Little damage occurred in rock tunnels for ground surface accelerations below 0.4g. Dowding and Rozen found that there was no damage in either lined or unlined tunnels for ground surface accelerations up to 0.19g. They found a few cases of minor damage, such as falling of loose stones and cracking of brick

or concrete linings, for ground surface accelerations above 0.19g and below 0.4g. (For reasons noted above, these values of accelerations must be regarded as approximate and tentative.)

- Severe damage and collapse of tunnels from shaking occurred only under extreme conditions. Dowding and Rozen observed that no collapse occurred for ground surface accelerations up to 0.5g. Severe damage to the lining or portals from strong shaking was usually associated with marginal construction, such as brick or plain concrete liners and the lack of grout between wood lagging and the overbreak. Poor soil or incompetent rock also seemed to contribute to the susceptibility of tunnels to damage.
- Severe damage was inevitable when the underground structure was intersected by a fault that slipped during the earthquake.
- Instances of complete tunnel closure appeared to be associated with movement of an intersecting fault and with other major ground movements, such as landslides and liquefaction, but not with shaking alone.
- Dowding and Rozen concluded that tunnels were much safer than aboveground structures for a given intensity of shaking. Only minor damage to tunnels was observed in areas subjected to MMI VIII to IX, although damage to surface structures at these intensities is usually extensive.
- There was some evidence that tunnels deep in rock were safer than shallow tunnels, although the data providing this evidence were incomplete.
- Damage to cut-and-cover structures appeared to be caused mainly by large increases in the lateral forces from the surrounding soil backfill.
- Duration of strong seismic motion appeared to be an important factor contributing to the severity of damage to underground structures

EFFECTS OF UNDERGROUND EXPLOSIONS

The effects of explosion-induced ground vibrations on underground openings are reported in several different contexts. Conventional blasting, as used in mining and underground excavation, constitutes the most common source of explosion-induced vibration. Other sources are high explosives and underground nuclear explosions (UNEs) used in connection with national defense studies. The ground motions from these three sources differ from earthquake ground motions

(and to a certain extent from each other) in frequency content, values of peak ground motion parameters, and duration. For example, low-cycle fatigue failure of rock may be an important causative influence in some ground motion effects; but fatigue failure is dependent on the number of stress cycles, which, in turn, depends upon the frequency content and duration of the blast- or earthquake-induced waves. Valuable insights are obtained by studying the effects of underground explosions.

Conventional Blasting

Langefors and Kihlstrom suggest particle velocity criteria for damage to unlined rock tunnels during blasting operations.³⁷ A particle velocity of 12 in./sec (30.5 cm/sec) causes rock to fall in unlined tunnels, and that of 24 in./sec (61 cm/sec) results in the formation of new cracks in the rock. Bauer and Calder relate damage from blasting vibrations to particle velocity as follows:³⁸

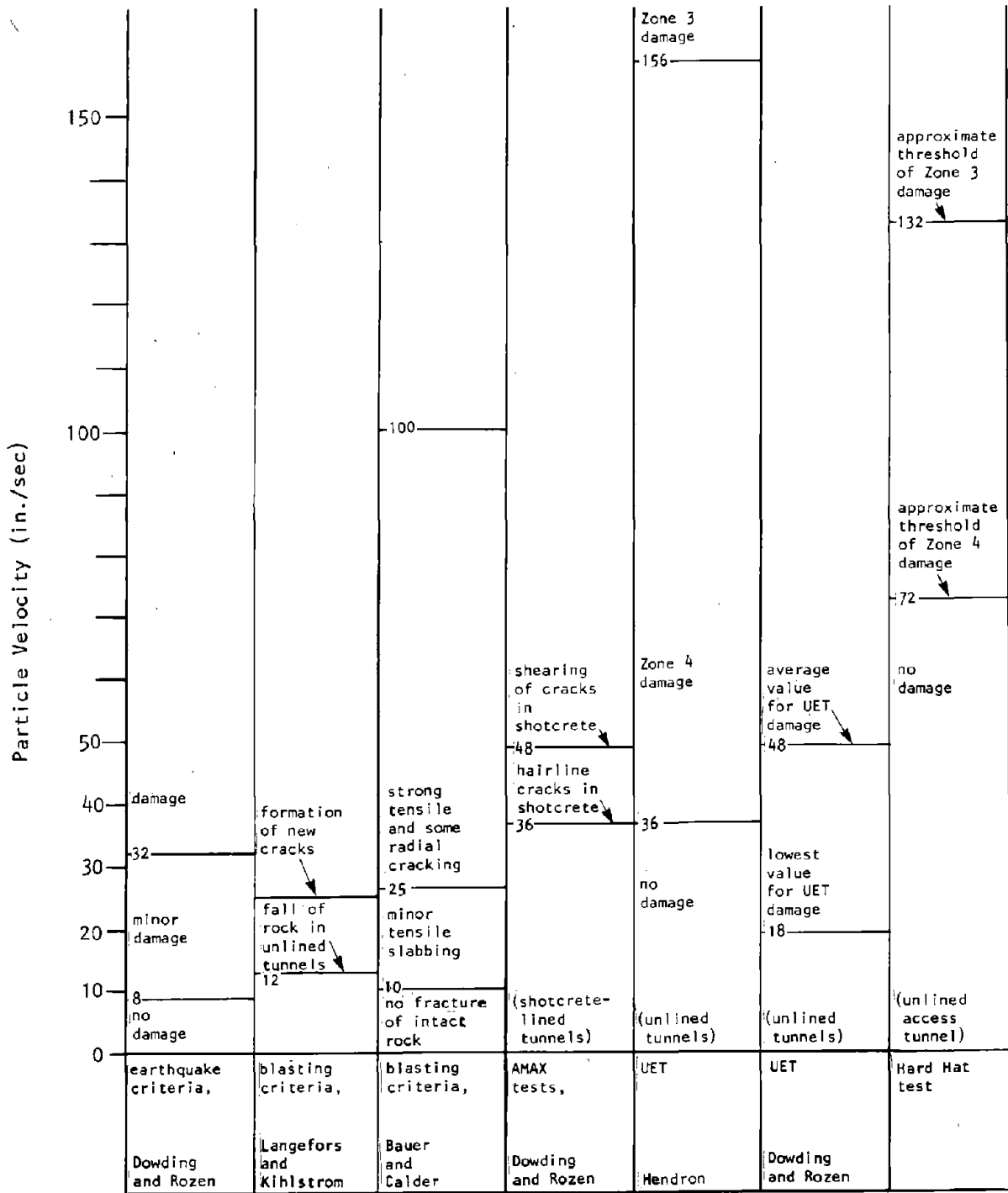
- less than 10 in./sec (25 cm/sec) - no fracturing of intact rock
- 10 to 25 in./sec (25 to 64 cm/sec) - minor tensile slabbing
- 25 to 100 in./sec (64 to 254 cm/sec) - strong tensile cracking, some radial cracking
- over 100 in./sec (254 cm/sec) - complete breakup of rock mass

These criteria correlate well with the peak particle velocity thresholds for earthquakes suggested by Dowding and Rozen that are illustrated in Figure 6.

Dowding and Rozen reviewed an experiment conducted at the Climax, Colorado, mine of AMAX to investigate cracking of shotcrete liners caused by explosion-induced vibrations.¹⁷ The tunnels were rock bolted and lined with 2 to 11 in. (5 to 28 cm) of shotcrete. Dowding and Rozen reported that formation of hair-line cracks in the shotcrete liner occurred at peak particle velocities of approximately 36 in./sec (91 cm/sec), and faulting of cracks, which evidently means shearing of existing cracks, at approximately 48 in./sec (122 cm/sec).

High-Explosive Tests

Similar results were obtained for rock tunnels in the underground explosion tests (UET) conducted by Engineering Research Associates for the U.S. Army



NOTE: 1 in./sec = 2.54 cm/sec.

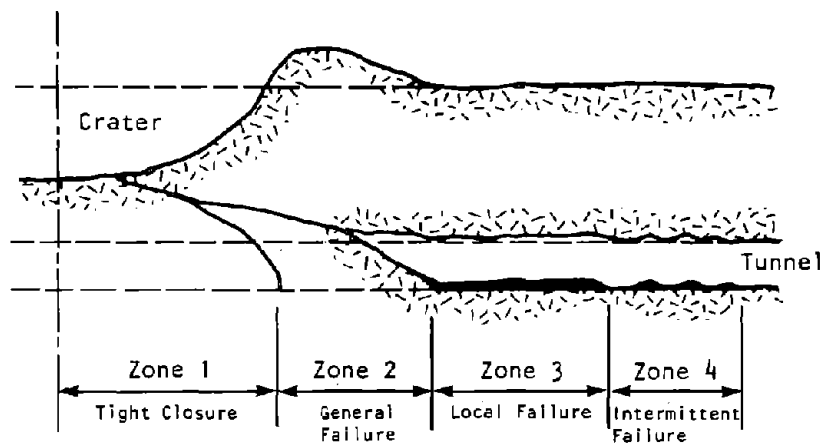
Figure 6. Correlation of damage criteria for earthquakes and explosions.

Corps of Engineers.³⁹ These tests studied the damage to unlined tunnels in sandstone, granite, and limestone due to TNT explosions. Diameters of the tunnels varied from 6 to 30 ft (1.8 to 9 m), and the charge varied from 320 to 320,000 lb (145 to 145,000 kg). Four zones of failure were identified in the UET program, as illustrated in Figure 7. Zone 1 represents heavy damage with tight closure of the tunnel. Damage in Zone 2 is also very heavy, but it decreases with distance from the explosion. Zone 3 represents a length of continuous damage to the tunnel surface toward the charge and intermittent spalling around the rest of the tunnel. Damage in Zone 4 consists of intermittent spalling of rock that may have been loosened by the excavation process. Beyond Zone 4, there is no damage. The peak particle velocities associated with the boundaries of Zone 4 are of particular interest because they indicate thresholds for minor damage (such as falling of loose rock) as well as for major damage. Hendron analyzed the UET results and found that the outer limit of Zone 4 corresponded to a particle velocity (radial with respect to the explosion) of 36 to 72 in./sec (91 to 183 cm/sec) and that the outer limit of Zone 3 corresponded to a particle velocity of 156 in./sec (396 cm/sec).⁴⁰ Hendron also noted that the free-field radial strains corresponding to the outer limits of these two zones were 0.0004 for Zone 4 and 0.0012 for Zone 3. Dowding and Rozen further investigated Hendron's data on the outer limit of Zone 4 and found that, although the particle velocity of one of the 14 tests may have been as low as 18 in./sec (46 cm/sec), the average particle velocity was 48 in./sec (122 cm/sec).¹⁷ These values for particle velocity from the UET program are shown in Figure 6 for comparison with results from other studies.

The final report³⁹ on the UET program makes the following comments regarding protection against damage:

There is some evidence from these tests regarding the type of structure which would protect a tunnel installation against damage to tunnels. While this evidence is meager, it does indicate that reflecting surfaces could be used to turn back much of the energy. In a few cases geological conditions provided such surfaces, and the damage beyond them was considerably reduced. This could well afford the basis for protective design by tunnel liners with reflecting surfaces. The following comments represent rough estimates which should be tested experimentally.

The damage which occurs in Zone 4 and some of that in Zone 3 is inferred to consist of the dislodgement of rock fragments



Hendron, "Engineering of Rock Blasting on Civil Projects",
 in *Structural and Geotechnical Mechanics*, edited by W. J. Hall,
 © 1977, p. 256. Reprinted by permission of Prentice-Hall, Inc.,
 Englewood Cliffs, New Jersey.

Figure 7. Damage zones from UET program.
 (Adapted from Reference 40.)

which have been partially separated from the main body of the rock by blasting or by weathering. . . . A simple concrete lining placed in contact with the rock might prove effective in protecting against this kind of damage.

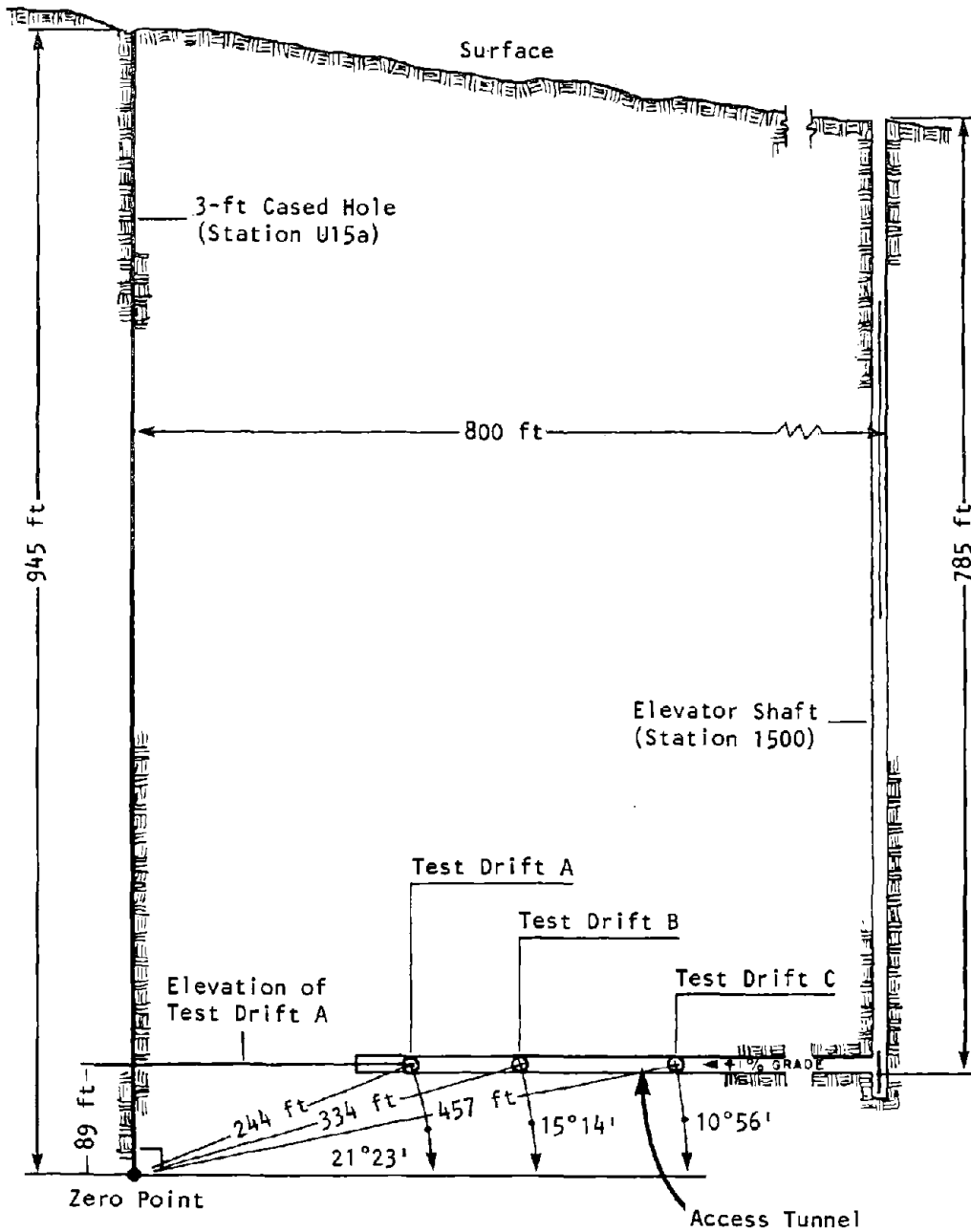
In Zone 3 damage, solid rock is cracked and slabs fall off. . . . A substantial lining is required which should not make contact with the rock. The space between the lining and the tunnel surface should be filled with a material of low density that will absorb the energy of the flying rock, distribute the pressure from fallen rock, and provide a mismatch of acoustic impedance so that reflection will take place at the tunnel surface rather than at the surface of the lining.

Underground Nuclear Explosions

Tests on tunnel damage have also been conducted in conjunction with UNEs. Various tunnel cross sections and liners were tested during the shot Hard Hat (February 1962) in the Climax granite at the U.S. Department of Energy's Nevada Test Site.⁴¹ Extensive tunnel tests were also performed in connection with Project Piledriver, but those reports are not declassified as yet and cannot be summarized here.

Tunnel Test Sections. The Hard Hat tunnel experiments consisted of 43 tunnel sections with varying cross sections, liners, and backpacking. These test sections were distributed among three test drifts (A, B, and C) with increasing distance from the zero point of the explosion. The layout for the tunnel tests is illustrated in the vertical section of Figure 8 and the plan view of Figure 9. The elevator shaft, access tunnel, and test drifts were excavated through reasonably competent quartz monzonite.

The variations in cross section, liner, and backpacking are presented in Table 2. Test sections with circular cross sections and others with square cross sections, some unlined (unsupported) and some lined simply with rock bolts and wire mesh, were located in Drifts B and C. Horseshoe-shaped sections supported by steel sets with wood lagging, familiar in civil and mining projects, were also located in Drifts B and C. Circular sections lined with reinforced concrete cast against the rock were constructed in all three drifts. The remaining 30 sections were all circular, with backpacking between the liners and the rock. The various combinations of liners and backpacking can be summarized in several general categories as follows:



NOTE: 1 ft = 0.3048 m.

Figure 8. Vertical section, Project Hard Hat.
(Adapted from Reference 41.)

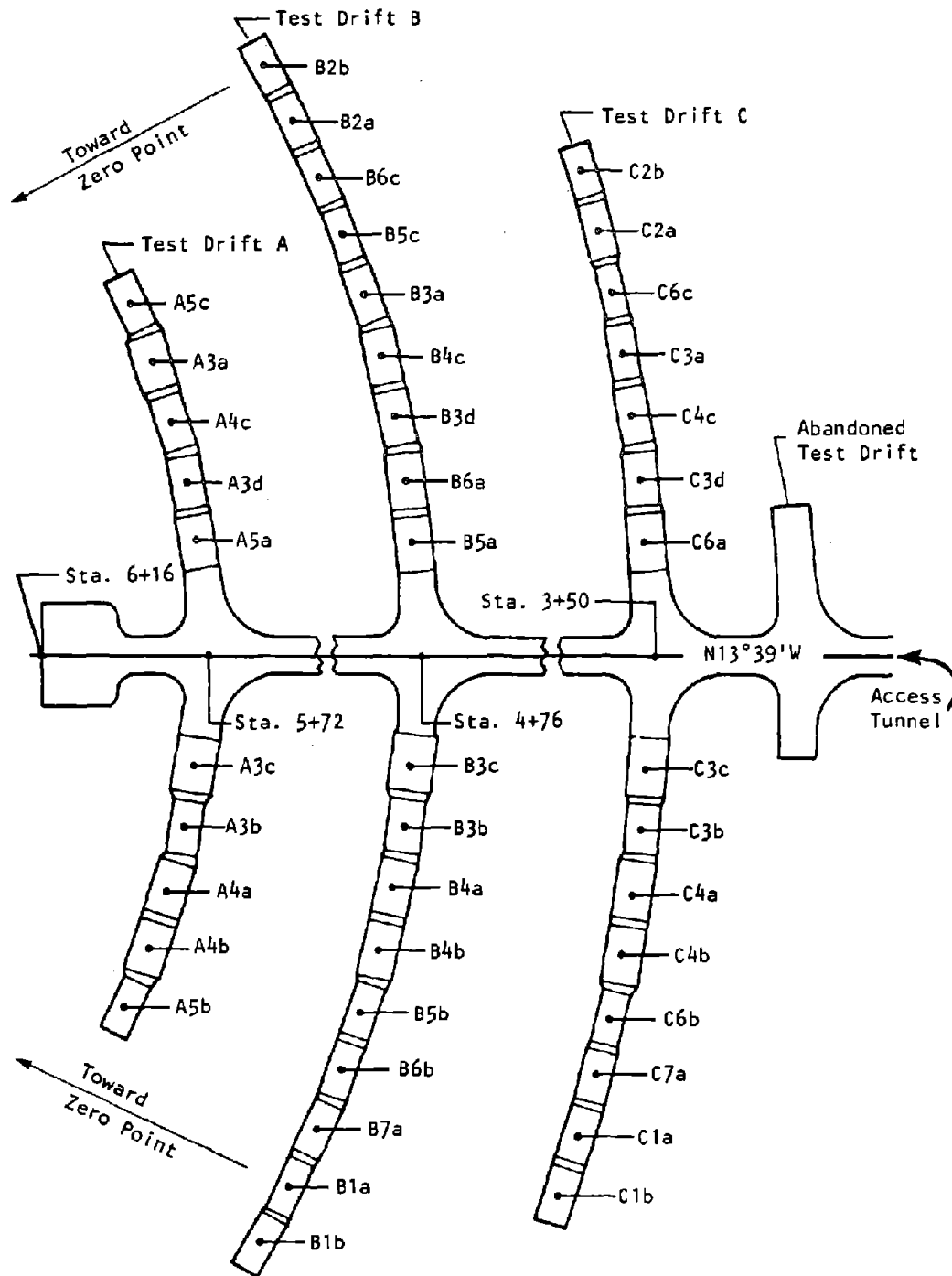


Figure 9. Plan view of test sections, Project Hard Hat.
 (Adapted from Reference 41.)

Table 2. Test section schedule. (Source: Reference 41.)

Test Section			Shape	Liner Type	Backpacking	
Drift	Number					
B	C	1a	□	Unlined	None	
B	C	1b	□	Lined with rock bolts and wire mesh	None	
B	C	2a	○	Unlined	None	
B	C	2b	○	Lined with rock bolts and wire mesh	None	
A	B	C	3a	○	Reinforced concrete	None
A	B	C	3b	○	Reinforced concrete	Foam
A	B	C	3c	○	Reinforced concrete	Foam
A	B	C	3d	○	Reinforced concrete	Cinder
A	B	C	4a	○	Steel set with steel lagging	Cinder
A	B	C	4b	○	Steel set with steel lagging	Foam
A	B	C	4c	○	Steel set with wood lagging	Foam
A	B		5a	○	3-gage steel	Foam
A	B		5b	○	3-gage steel	Foam
A	B		5c	○	3-gage steel	Cinder
	B	C	6a	○	8-gage steel	Foam
	B	C	6b	○	8-gage steel	Foam
	B	C	6c	○	8-gage steel	Cinder
	B	C	7a	∩	Steel set and wood lagging	None

- Categories of liners with backpacking
 - Flexible - 8-gage or 3-gage corrugated steel
 - Rigid - 8-in. (20-cm) or 12-in. (30-cm) reinforced concrete
 - Intermediate - steel rings or horseshoe-shaped sets with wood or steel lagging
- Categories of backpacking
 - Thick filler - 20 in. (51 cm) or 24 in. (61 cm) of polyurethane foam
 - Thin filler - 5 in. (13 cm) or 9 in. (23 cm) of polyurethane foam or 9 in. (23 cm) of volcanic cinder

Preshot estimates of tunnel response were made assuming a 5.0-kiloton (4.5-kt) device. A simple analytical procedure based on wave theory was used to estimate limits of compression failure, tensile splitting, and spalling (or scabbing). In addition, an empirical approach derived from the UET program and previous UNE tests was employed to estimate damage zones. These estimates are illustrated in Figure 10.

The actual yield of the Hard Hat device was 5.9 kiloton (5.4 kt). Postshot determinations of the actual point of closure and the actual limits of Zones 2, 3, and 4 were made along the unlined access tunnel as indicated in Figure 10. Drift A was tightly closed, and most of the data were unrecoverable. Drift B was well within the closure zone, although preshot estimates placed it beyond closure at the limit of Zone 2. Many of the intended results of Drift B were lost, but some observations were possible. Drift C also sustained heavier damage than planned; however, the test sections there provided some interesting results.

Damage Data. Some damage to the elevator shaft was observed at all depths, but damage was heavier in the upper half than in the lower half. Damage consisted of permanent misalignment of the shaft, permanent distortion of sets, sheared bolts at the hanger connections, and some rockfall. The elevator shaft was located just beyond the limit of Zone 4, where no damage was observed in the access tunnel. Damage to the shaft may be attributed to the different orientation of the shaft with respect to the expanding shock wave as compared with the

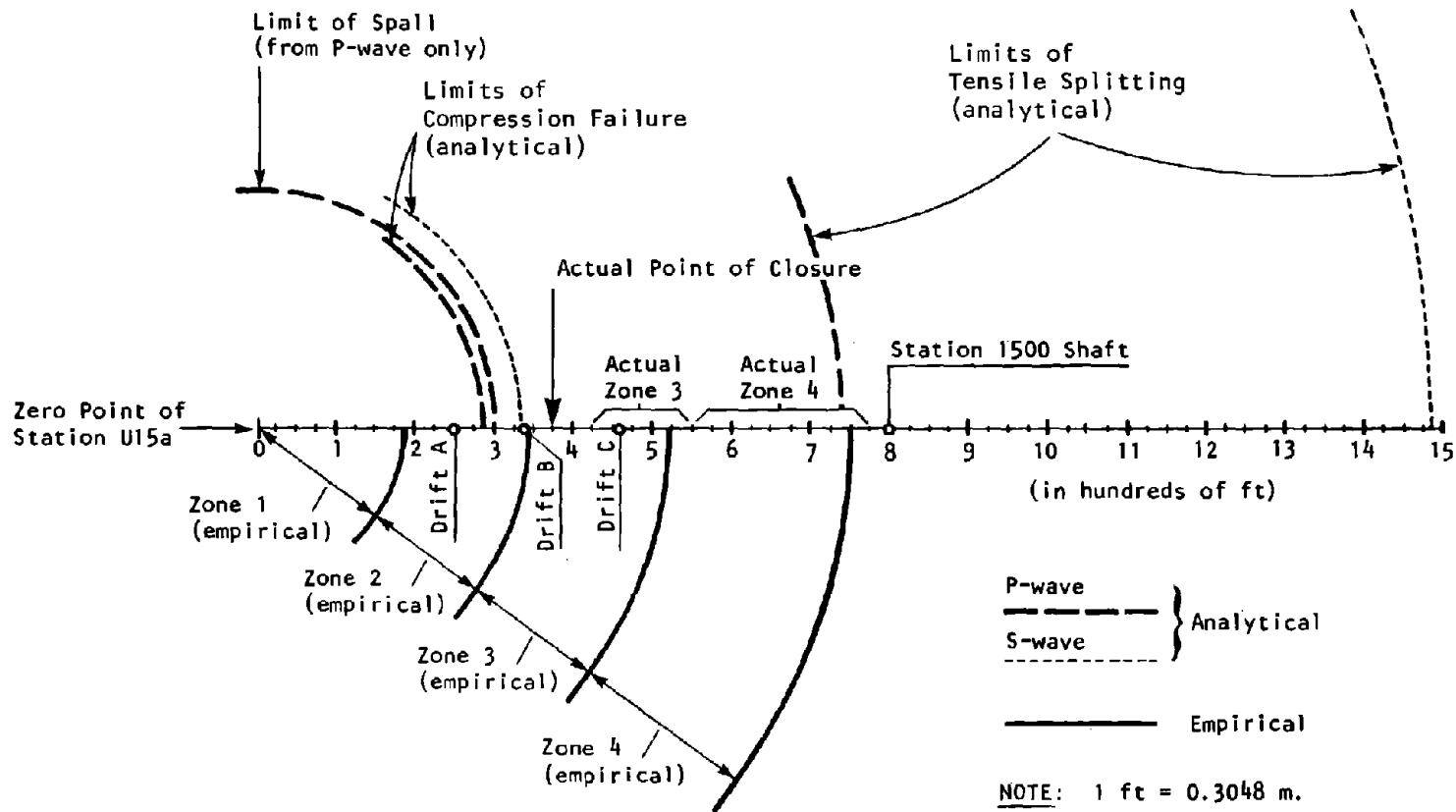


Figure 10. Analytical versus empirical method for estimating tunnel response.
(Adapted from Reference 41.)

tunnel's orientation. In addition, the response of the shaft was probably affected by the looser deposits and more weathered rock near the ground surface.

Damage to the 15 test sections in Drift C is detailed in Table 3. The severe damage of the unlined circular section (C2a) is consistent with a location well within Zone 3. The rock bolts and wire mesh of an adjacent circular section (C2b) reduced the damage somewhat by preventing large rocks from dropping. On the other hand, the square sections (C1a and C1b) that were unlined or were supported with rock bolts and wire mesh were completely closed. Heavier damage to square sections as compared with circular sections is to be expected because square sections are inherently the weaker of the two. Moreover, the square sections were excavated through a highly fractured zone, which probably contributed to their destruction. The horseshoe-shaped sections supported by steel sets and wood lagging experienced moderate to severe damage. The main mechanism of failure seems to have been the heaving of the floor, which dislodged the invert timber struts. This, in turn, permitted the bottom of the sets toward the zero point to be kicked inward. The rigid (concrete) liner without backpacking received moderate to light damage. The remaining 9 sections, all with backpacking of some kind, were negligibly damaged. Little difference between the type of liner, the type of backpacking, and the thickness of the backpacking was noted, indicating that the important factor for these sections was the mere presence of the backpacking.

All sections in Drift B were either closed or severely damaged, with one notable exception. A rigid liner with a thick backpacking had negligible damage. The similar section in Drift A remained open but suffered severe damage, while all other sections in Drift A were completely closed.

Response Data. Response measurements in test sections are not particularly useful for this review: the few mechanical gages that were recovered were badly damaged and electronic gages provided only a limited amount of data about strains and particle velocities for liners in Drifts A and B. However, the free-field data obtained from stations along the access tunnel are useful. Experimentally determined relationships were plotted for peak acceleration, particle velocity, strain, and stress parallel to the direction of the shock. Values of these quantities

Table 3. Summary of damage in Drift C, Shot Hard Hat.

Section Number	Cross Section Shape and Size	Liner and Backpacking	Geology	Damage
C2b	circular 8.00-ft diameter	rock bolts and wire mesh	granite -- competent, but degree not described	severe to moderate damage, maximum breakage 1-1/2 ft thick, pieces 2 in. to 6 in. or larger, mesh torn loose from bolts at one place
C2a	circular 8.00-ft diameter	unlined	"	severe to moderate damage, maximum breakage 2-1/2 ft. thick
C6c	circular 7.50-ft diameter	8-gauge steel 9-in. cinder back- packing	"	negligible damage
C3a	circular 8.00-ft diameter	12-in. reinforced concrete cast against rock	"	moderate to light damage, liner crushed at one place exposing buckled reinforcing bars, maximum rock breakage 1 ft
C4c	circular 9.67-ft diameter	steel set/wood lag- ging, 5-in. foam backpacking	"	negligible damage
C3d	circular 9.50-ft diameter	12-in. reinforced concrete 9-in. cinder back- packing	"	"
C6a	circular 10.00-ft diameter	8-gauge steel 20-in. foam back- packing	"	"
C3c	circular 11.33-ft diameter	8-in. reinforced concrete 20-in. foam back- packing	"	"
C3b	circular 9.50-ft diameter	12-in. reinforced concrete 5-in. foam back- packing	"	"
C4a	circular 9.92-ft diameter	steel set/steel lag- ging, 9-in. cinder backpacking	"	"
C4b	circular 9.92-ft diameter	steel set/steel lag- ging, 5-in. foam backpacking	"	"
C6b	circular 7.50-ft diameter	8-gauge steel 5-in. foam back- packing	granite -- not as compe- tent as in C3c through C4b	"
C7a	horseshoe 8.67-ft width 9.33-ft height	steel set/wood lagging no backpacking	granite -- blocky, close to fault zone	severe to moderate damage, floor heaved 5 ft, struts dislodged, crown bearing plate bolts failed
C1a	square 8.00-ft	unlined	granite -- intensely faulted	completely closed
C1b	square 8.00-ft	rock bolts and wire mesh	"	assumed completely closed

NOTE: 1 ft = 0.3048 m; 1 in. = 2.54 cm.

for various ranges were determined from these plots and are shown in Table 4. Values for peak particle velocity and strain at the limits of Zones 3 and 4 are of the same order of magnitude as the values obtained from the UET program. However, it should be noted that accelerations experienced in Zones 3 and 4 greatly exceed accelerations for earthquakes by several orders of magnitude.

Observations. Some important observations that may have implications for earthquake motion can be drawn from the results of the Hard Hat tunnel tests:

- Horseshoe-shaped steel sets were vulnerable at the invert where heaving of the floor dislodged invert timber struts.
- The damage sustained in highly fractured rock was more severe than in the more competent rock.
- Thick concrete liners cast against the rock did not perform as well as thick concrete liners with back-packing, indicating that backpacking protects the liner in a shock loading.

SUMMARY AND CONCLUSIONS

The literature regarding the effects on tunnels, mines, and other large underground structures from shaking caused by earthquakes and underground explosions has been reviewed. Specific conclusions can be drawn from the studies on earthquake damage to tunnels in rock. Data from conventional mine blasting provide upper limits to the peak ground motion parameters that are associated with various kinds of tunnel damage. The colossal explosions of the UET program and the UNE tests create ground motions far more severe than those from earthquakes; however, these extreme situations provide insight into the dynamic behavior of tunnels that may be useful in understanding earthquake performance of underground structures.

The following conclusions represent the major findings of this review:

1. Little damage occurred in rock tunnels due to earthquake shaking when accelerations at the ground surface were below 0.4g. Studies found that there was no damage in lined or unlined tunnels for ground surface accelerations below 0.19g and that there were few cases of even minor damage, such as fall of loose rock and new cracks in concrete linings, for surface

Table 4. Approximate peak values of measured free-field quantities versus range, Shot Hard Hat.

Point of Interest	Slant Range (ft)	Acceleration (g)	Particle Velocity (fps)	Strain (in./in.)	Stress (psi)
Limit of Zone 1	NA	NA	NA	NA	NA
Drift A	244	6,000	90	.0022	45,000
Drift B	334	1,100	40	.0011	19,000
Point of Closure	375	700	30	.0010	15,000
Limit of Zone 2	425	330	20	.0008	11,000
Drift C	457	260	18	.0007	10,000
Limit of Zone 3	550	100	11	.0004	6,000
Limit of Zone 4	775	20	6	.0002	3,000

NOTE: 1 ft = 0.3048 m; 1 fps = 0.3048 m/sec; 1,000 psi = 6.895 MPa.

accelerations between 0.19g and 0.4g.^{17,24} As previously discussed, these values of acceleration must be regarded as approximate and tentative for the present time because of the limitations of the studies from which they were derived.

2. Severe damage and collapse of rock tunnels from earthquake shaking occurred only under extreme conditions, such as ground surface accelerations exceeding 0.5g, marginal construction, and poor rock.^{17,24} Furthermore, complete tunnel closure was not due to shaking alone but appeared to be associated with movement of an intersecting fault or other major ground movement.
3. Damage to cut-and-cover structures may be primarily attributed to large increases in lateral earth pressure during seismic motion and to inadequate design for such seismic loads.
4. The peak particle velocity threshold of 12 in./sec (30 cm/sec) for minor damage to unlined rock tunnels from conventional mine blasting correlates well with the threshold of 8 in./sec (20 cm/sec) found for earthquakes.
5. The colossal underground explosion tests (UET and UNE) indicate that minor damage to unlined rock tunnels, such as fall of rocks partially loosened by excavation and weathering, may be effectively prevented by thin concrete lining or by rock bolts and wire mesh.
6. In the UNE tests, tunnels in highly fractured rock were more severely damaged than tunnels in more competent rock. A similar comparison of damage to tunnels in these types of media is to be expected from the much less severe ground motion of an earthquake.
7. Okamoto found that thicker liners suffered more damage than thinner (and more flexible) liners.³³ The same findings were obtained from the UNE tests.
8. The collapse of horseshoe-shaped steel sets during the UNE tests was partly due to the dislodgement of timber invert struts. This would indicate that, if they are to be functional during ground motion, the invert struts should be securely fastened to the base of the sets.

4. Seismic Analysis

It is appropriate to review the theory and current approaches used in the analysis of underground seismic stresses before discussing the wave propagation study and the state-of-the-art review of current techniques in seismic design of underground structures that were conducted for this investigation. The first section of this chapter focuses on present techniques for estimating subsurface stresses and strains in the free field (that is, away from the underground structure). The discussion includes an assessment of current methods of determining subsurface ground motion amplitudes by inverting surface observations and an evaluation and review of various methods used for calculating stresses and strains around underground structures. The second section discusses earth material properties that must be considered in the analytical procedures and reviews the methods for measuring or estimating the properties.

CURRENT TECHNIQUES USED IN SEISMIC ANALYSIS

Available Numerical Models

Numerical techniques employed in geomechanics have been extensively presented in the literature and are adequately reviewed in several publications.^{42,43} For this discussion of dynamic problems in geomechanics, the principal methods of analysis are briefly described. The three main approaches reported in the literature are: (1) the *lumped-parameter* method, (2) the *finite-difference* method, and (3) the *finite-element* method. In each of these approaches, the geological structure and the spatial variables are uniquely discretized. In lumped-parameter models, the masses are physically lumped and are connected by springs and dashpots. Discretization is achieved for finite-difference models by replacing the continuous derivatives with respect to the spatial variables by ratios of changes in the unknown variables over a small but finite spatial increment. Finite-element models are generated by dividing the body into an equivalent system of finite elements (or small continua), a process that discretizes the mass and stiffness of the body.

The system of equations governing motion for each of the three models can be solved directly in the time domain by one of a variety of methods available

for step-by-step integration. The solution of the equations of motion can also be obtained indirectly in the frequency domain and then transformed into the time domain by using the inverse Fourier transformation. A third solution procedure is the use of modal analysis, a method that is used in the field of structural dynamics. Because a discussion of the working details and limitations of each of these solution techniques is beyond the scope of this report, the interested reader is referred to the literature on the subject.^{42,43}

Two other numerical formulations deserve attention. The method of *characteristics* is uniquely suited to solving the problem of wave propagation because the procedure simulates the physical process of propagation. The set of partial differential equations governing the propagation of waves in a medium is converted into a set of ordinary differential equations, in time only, using characteristic lines or paths of propagation. This method has proven to be very economical for certain applications; however, it can be difficult to use when the material is nonhomogeneous or nonlinear.⁴³

Boundary integral methods form a class of numerical procedures that may have great potential for the solution of subsurface dynamic problems. There are currently three different formulations of these methods: the boundary element method, the displacement discontinuity method, and the boundary integral equation method. The advantage of these methods over the finite-element and finite-difference methods is that only the boundaries of the underground cavity (and perhaps the ground surface) are represented by a finite number of segments. Otherwise, the region would extend to infinity in all directions, and there is no need to discretize a large region or to establish fictitious boundaries, as is the case in finite-element and finite-difference models. Most applications of the boundary integral methods have been to mining and other static load problems; so far, there have been very few applications to dynamic geotechnical problems. These methods are still under development; however, they show promise for the future.

Analysis of Free-Field Stresses and Strains

Simple Free-Field Analysis. The simplest analysis for seismic stresses within a soil or rock mass is derived from the principles of plane wave mechanics.

Two types of plane waves can propagate through an elastic, isotropic body of infinite extent: compressional (P) waves and shear (S) waves. (For more details, see Appendix D.) Assuming the propagation of a P-wave, the axial strain, ϵ , is given by⁴⁴

$$\epsilon = -\frac{1}{V_p} v \quad (1)$$

where v is the particle velocity, and V_p is the velocity of the P-wave in the medium. The axial strain and the particle velocity are both in the direction of the propagation. By this approach, the maximum axial strain at any given point is due to the peak particle velocity that occurs at that point:

$$\epsilon_{\max} = \pm \frac{|v_{\text{peak}}|}{V_p} \quad (2)$$

Assuming a linear elastic, isotropic material in plane strain, the normal stress is

$$\sigma = \frac{E(1-\nu)}{(1+\nu)(1-2\nu)} \epsilon \quad (3)$$

where E is the Young's modulus, and ν is Poisson's ratio. Thus, the maximum normal stress is

$$\sigma_{\max} = \pm \frac{E(1-\nu)}{(1+\nu)(1-2\nu)} \frac{|v_{\text{peak}}|}{V_p} \quad (4)$$

Using the relation

$$V_p = \sqrt{\frac{E(1-\nu)}{\rho(1+\nu)(1-2\nu)}} \quad (5)$$

where ρ is the density of the material, we can rewrite Equation (4) as

$$\sigma_{\max} = \pm \rho V_p |v_{\text{peak}}| \quad (6)$$

A similar expression can be determined for the shear stress due to the propagation of an S-wave. In this case, the maximum shear strain is

$$\gamma_{\max} = \pm \frac{|v_{n,\text{peak}}|}{V_s} \quad (7)$$

where v_n is the particle velocity normal to the direction of propagation and V_s is the velocity of an S-wave in the medium. The maximum shear stress is

$$\tau_{\max} = \pm G \frac{|v_{n,\text{peak}}|}{V_s} \quad (8)$$

where G is the shear modulus.

Since

$$V_s = \sqrt{\frac{G}{\rho}} \quad (9)$$

then

$$\tau_{\max} = \pm \rho V_s |v_{n,\text{peak}}| \quad (10)$$

The above approach is based upon an obviously oversimplified characterization of motion within the soil or rock mass. The material is assumed to be linear elastic and isotropic. Maximum stresses at a point are estimated assuming that the peak particle velocities are known or can be estimated at that point. The approach does not address the effects of multiple reflections within soil layers, free-surface reflections, nonlinear soil behavior, or time characteristics of the wave motion. The one virtue of this approach is that it offers a simple, albeit very approximate, method for calculating stresses below the surface of the ground.

More Refined Free-Field Analysis. The analysis of seismic stresses in the free field (that is, in the ground away from a structure) should appropriately account for the complexities in both the geologic medium and the wave form. Details on the form of the wave motion and the influence of geology on wave propagation are considered at length elsewhere in this report. It is sufficient for the discussion that follows to point out that the underground wave motion consists largely of body waves (compressional and shear waves) and surface waves (Rayleigh and Love waves). It is not possible in the current state of the art of seismology to break down a given time history of seismic motion into components of body waves and surface waves, although it is possible to recognize

their signatures in the wave form. Thus, it is not currently possible to use a time history of motion recorded at some point in a soil or rock mass to determine with reasonable accuracy the motion at some other point.

Theoretical approaches to determining underground seismic motion at some desired point on the basis of observations at another point are of necessity simplified in terms of both geology and the wave form. Conventionally, seismic motion is assumed to consist of a train of shear waves propagating vertically upward from bedrock. These models assume one or more layers of homogeneous soil over bedrock, the latter often taken as a rigid base. These assumptions severely restrict the representation of the real problem. The assumption of vertically propagating shear waves has its origin in the early development of seismic analysis of surface structures. Because all surface structures are designed to resist gravity or vertical loads, it was rightly felt that the primary concern for seismic resistance should be lateral or horizontal loads. This view, in turn, led to characterization of only the horizontal components of ground motion as inputs to the surface structure. Moreover, as seismic motion radiates from the source, it is continually refracted by the layering of surface material so that the body waves arrive with a nearly vertical incidence to the ground surface and not in a straight line from the source to the site. If the body waves are propagating vertically to the surface, then the compressional waves would contribute only to the vertical motion. Because it was assumed that only the horizontal motions need be considered for seismic analysis of surface structures, it became conventional to assume that the motion of interest consists only of vertically propagating shear waves. Clearly, the conventional approach has severe limitations in representing the actual motion within the free field. More rigorous models that represent more of the complexities of the problem are only now being developed.

In the conventional approach, the amplification characteristics of a horizontally stratified soil mass are established using the theory of propagation of plane waves.⁴³ As previously noted, plane waves in an infinite medium consist of compressional (P) and shear (S) waves. When these waves propagate through a horizontally layered soil mass, they are reflected by the free ground surface and refracted as well as reflected by the horizontal interfaces between the layers. In order to discuss this phenomenon, it is necessary to resolve the

S-wave motion into two components: one in a horizontal plane and the other in a vertical plane (both components being normal to the direction of propagation of the S-wave). The horizontal shear component is referred to as the horizontally polarized shear wave (SH-wave), and the vertical shear component as the vertically polarized shear wave (SV-wave). (For additional description, see Appendix D.)

Consider, first, horizontally polarized shear waves propagating through a horizontally stratified soil mass. A train of SH-waves traveling upward through such a medium will be reflected and refracted at the interfaces between the layers and finally reflected at the free surface, which will result in trains of SH-waves traveling both upward and downward. Figure 11 illustrates the reflection and refraction of SH-waves, assuming some arbitrary angle of incidence. Satisfying the continuity of displacements and equilibrium of shear stresses at each interface, an amplification function can be developed that gives the ratio of the amplitude of the surface motion to the amplitude of the bedrock motion as a function of frequency. An example of such an amplification function is illustrated in Figure 12. For multiple strata over bedrock, the SH-wave is usually assumed to be propagating vertically. The explicit forms for amplification functions for multiple strata are quite involved and do not lend themselves to hand calculation; however, numerical computations can very easily be performed on a digital computer using a computer code such as SHAKE.⁴⁵

P-waves and SV-waves propagating vertically can be easily handled in the same fashion because vertically propagating P and SV effects are uncoupled. The solution for the SV-waves is identical to that for the SH-waves, while the solution for the P-waves is identical in form to an appropriate change in the elastic modulus.* If either P- or SV-waves are not propagating vertically, both P- and SV-waves are created during reflections, which results in coupling between them. This situation is quite complicated and requires further analysis;⁴⁶ however, the conventional approach considers only vertically propagating waves.

* G in the solution for the SH-wave is replaced by $E(1 - \nu)/(1 + \nu)(1 - 2\nu)$ to obtain the solution for the P-wave.

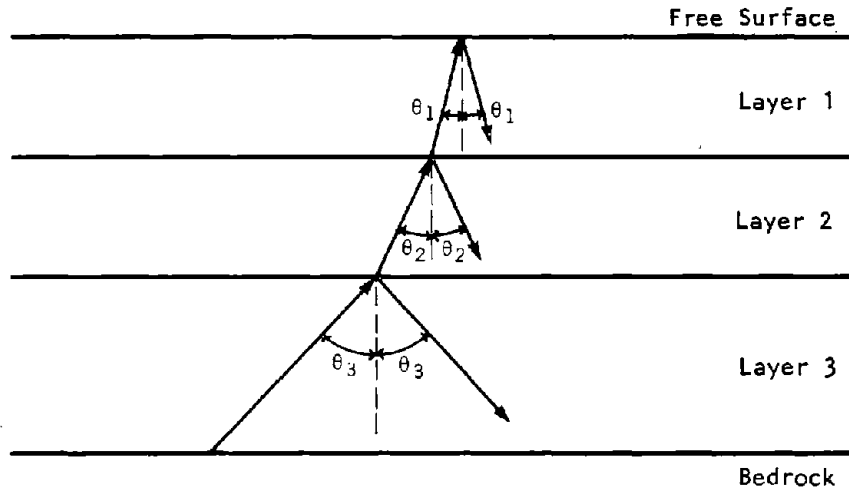


Figure 11. Reflections and refractions of SH-waves in a horizontally stratified soil mass.

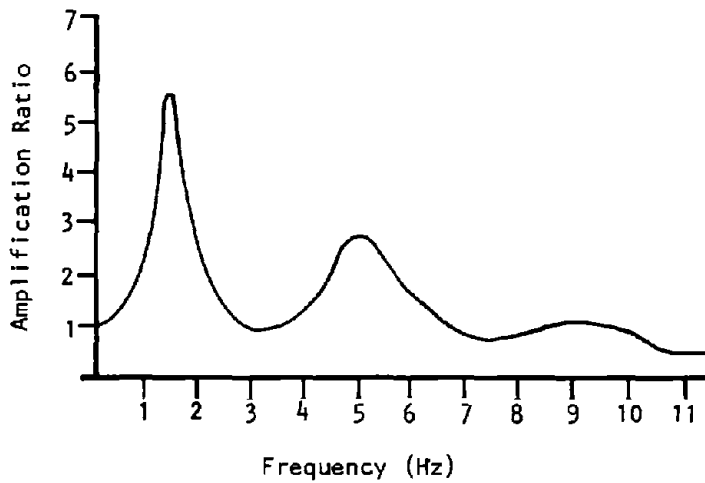


Figure 12. Typical example of the amplification function for a soil layer over bedrock.

The amplification function of the soil can be used to determine a time history at the surface of the free soil. Given a specific accelerogram assumed to represent the earthquake motion at bedrock, the corresponding time history can be determined at the free surface of the soil by (1) obtaining the Fourier transform of the input time history at bedrock, (2) multiplying the Fourier transform time history by the amplification function of the soil, and (3) applying the inverse Fourier transform back to the time domain. This procedure, assumes that the recorded time history is the result of waves of a specific type, usually vertically propagating shear waves. Because this discussion omits the details and intricacies of the procedure, the interested reader may wish to refer to the literature on the subject.⁴³

An earthquake time history can be constructed at the ground surface from a given time history at bedrock using the above procedure. In many situations, however, the inverse procedure is required. Often ground motions are specified at the soil surface (or very close to the soil surface), and the motion at some point within the soil column or at the bedrock is desired. This inverse, or deconvolution, process requires the application of the transfer function from the top of the soil column to the bottom, which is just the inverse of the transfer function from the bottom to the top.

The lumped-parameter approach has been particularly popular among practicing engineers for the determination of one-dimensional amplification and deconvolution. The discrete model suggested by Seed and Idriss^{47,48} assumes vertically propagating waves and horizontal soil layers as illustrated in Figure 13. Most studies using this method assume linear elastic soils and, in some cases, viscoelastic soils. However, during strong shaking, the soil behaves nonlinearly, and a linear model is not representative of actual behavior. The inclusion of nonlinear models in the deconvolution process greatly complicates the computational task for the lumped-parameter model.

A method that accounts for the nonlinear effects in soils during strong earthquakes was proposed by Seed and Idriss⁴⁷ through the introduction of the equivalent linear method.⁴⁹ Curves of the soil moduli and damping characteristics with respect to strain level are needed, first and are determined experimentally. The nonlinear behavior of the soil is simulated by an iterative

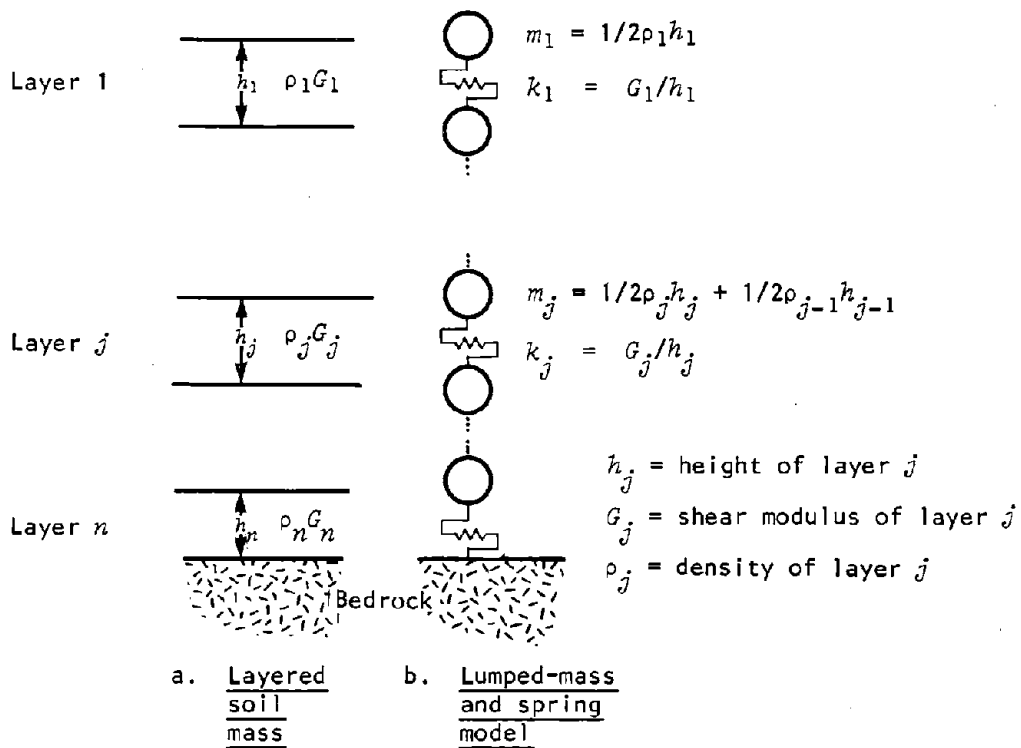


Figure 13. Lumped-mass and spring idealization of a semi-infinite layered soil mass.

procedure that assumes a linear soil response in each time step and matches the moduli to the level of strain from experimentally determined curves. Convergence cannot be guaranteed for this trial-and-error procedure, and problems often arise for deep or soft soil strata, particularly for strata containing very thin layers of soil with material properties that contrast highly with the adjacent soil layers.

The finite-element approach is currently enjoying widespread use for the determination of strains and stresses within a soil mass. The inclusion of nonlinear soil behavior usually does not pose any serious problem for the finite-element method. The most common approach is the equivalent linear method described above. One of the most widely used finite-element programs at this time is the FLUSH program, which assumes vertically propagating shear or compressional waves.⁵⁰

Boundary conditions often pose problems in the finite-element method. The discretization of a continuum by finite elements results in a finite domain with well-defined boundaries. If these boundaries do not correspond to the natural boundaries within the soil structure, then artificial reflections of wave energy will take place, leading to erroneous results. One method for overcoming this difficulty is to locate the boundaries sufficiently far away from the point of interest in the soil mass so that undesirable reflections will not arrive at that point during the time of observation. Such an approach can lead to extremely high computational cost. The second approach employs transmitting or viscous boundaries. For example, viscous dashpots, first suggested by Lysmer and Kuhlemeyer,⁵¹ are used in the FLUSH code.

Selected Computer Codes for Free-Field Analysis. To conclude this section on the analysis of free-field seismic motion, a few of the computer programs available for the computation of motion at depth are discussed:

- The SHAKE⁴⁵ program computes the response in a horizontally layered soil and rock system subjected to transient vertically propagating shear waves. The method does not rely upon a discretization scheme but rather uses transfer (amplification) functions. Nonlinear soil behavior during severe seismic motion is represented by the equivalent linear model described above. This program can determine subsurface ground motions by deconvolution from a surface record as well as surface

motions by direct computation with an input record at bedrock.

- The computer program MASH⁵² has capabilities similar to those of SHAKE in that it is designed to solve the dynamic response of a horizontally layered soil deposit to vertically propagating shear waves. However, with MASH the soil mass is discretized into a string of one-dimensional constant strain finite elements with masses lumped at the nodes. The characterization of the soil in the program MASH may be either viscoelastic or nonlinear with rate-independent damping.
- Another computer program for calculating the one-dimensional behavior of soils is the code CHARSOIL,⁵³ which employs the method of characteristics. Input motions may be introduced only at the rock-soil interface; therefore, CHARSOIL cannot handle the deconvolution problem. The response of the soil can be evaluated on the basis of elastic, viscoelastic, or nonlinear (Ramberg-Osgood) soil behavior.
- QUAKE⁵⁴ is a one-dimensional, explicit, finite-difference code for the propagation of shear waves through nonlinear soil layers. Its capabilities are very similar to those of SHAKE; however, instead of the equivalent linear soil model used in SHAKE, QUAKE is able to follow arbitrary stress-strain curves in very small time steps.
- Banister et al.⁵⁵ developed a program to study the stresses and strains due to reflection of seismic body waves (SH-, SV-, and P-waves) from the ground surface, the incident wave propagating with an arbitrary angle of incidence rather than propagating only vertically. However, this program was written for a homogeneous elastic half-space and is not applicable to a layered soil site. Furthermore, the program was not written to consider the deconvolution problem.
- Nair and Emery⁵⁶ included the propagation of both surface and inclined shear waves in a linear, homogeneous, horizontally stratified soil structure. Their program does not consider the deconvolution problem.
- The FLUSH⁵⁰ program, developed for the analysis of the interaction of surface structures with the soil mass, solves both the direct computational and deconvolution problems, assuming vertically propagating shear or compressional waves. FLUSH is a finite-element program that makes use of transmitting and viscous boundaries. Nonlinear soil behavior can be approximated by the equivalent linear model. This code was developed for near-surface applications of soil-structure interaction; therefore, it is not appropriate to use the FLUSH code for the determination of motion at great depths.

- STEALTH 2D is a finite-difference program specifically written to solve two-dimensional elastic wave propagation problems.⁵⁷ The parent program, STEALTH,⁵⁸ was written to solve nonlinear, large-deformation transient problems, and it is assumed that STEALTH 2D will eventually incorporate the same nonlinear features. STEALTH 2D has been used to study the direct computation of wave motion in a soil mass due to both vertically and obliquely propagating SH-waves.

Seismic Analysis of Underground Structures

The following discussion focuses primarily on linear structures, such as tunnels of all kinds. Underground chambers and reservoirs will be discussed briefly. The response of tunnels (lined or unlined) to seismic motion may be understood in terms of three principal types of deformation: axial, curvature, and hoop. Axial and curvature deformations develop when waves propagate either parallel or obliquely to a tunnel. Axial deformations are represented by alternating regions of compressive and tensile strain that travel as a wave train along the axis, as shown in Figure 14. Curvature deformations create alternate regions of negative and positive curvature propagating along the tunnel, as shown in Figure 15. A tunnel liner that is very stiff compared with the surrounding soil responds as an elastic beam. For positive curvature, the liner will be in compression on the top and in tension on the bottom. This situation is correctly assumed in the literature on seismic design of subaqueous tubes and subway tunnels.^{59,60} For the rock tunnel with a flexible lining or with no lining at all, the tunnel in positive curvature experiences tensile strains on the top and compressive strains on the bottom.

Hoop deformations result when waves propagate normal or nearly normal to the tunnel axis. Two effects of these deformations might be observed. One is a distortion of the cross-sectional shape that creates stress concentrations in the hoop stresses, as shown in Figure 16. The other effect is that of ringing -- the entrapment and circulation of seismic wave energy around the tunnel -- which is possible only when wavelengths are less than the tunnel's radius.⁶¹

The simplest approach to analyzing stresses around underground structures is to use the simple expressions for free-field stresses that were previously presented as Equations (6) and (10):

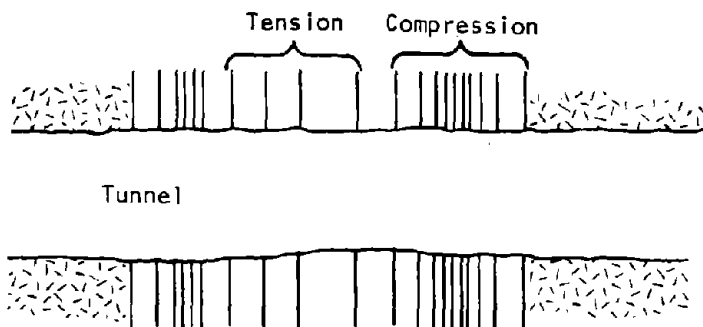


Figure 14. Axial deformation along tunnel.

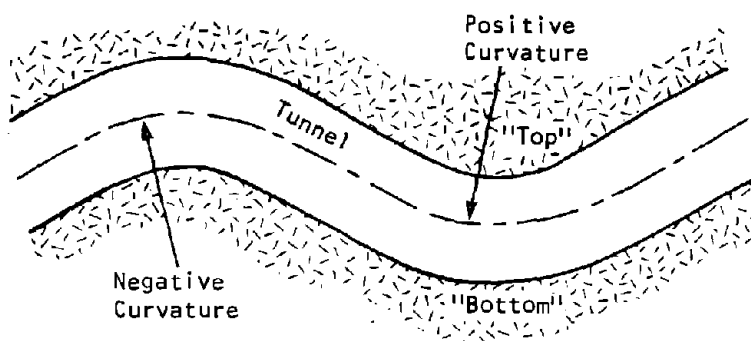


Figure 15. Curvature deformation along tunnel.

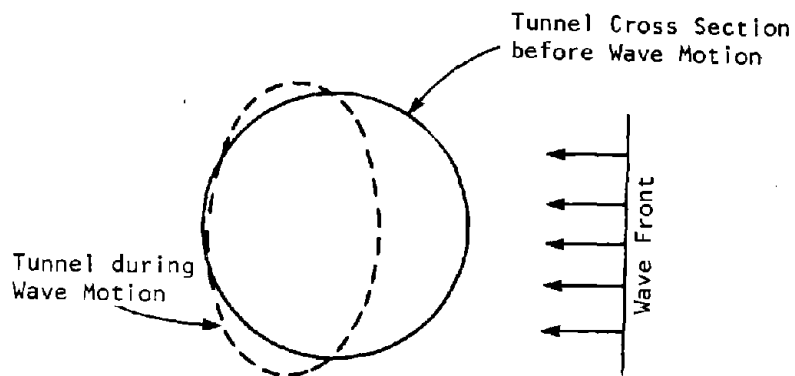


Figure 16. Hoop deformation of cross section.

$$\sigma_{\max} = \pm \rho V_p |v_{\text{peak}}|$$

$$\tau_{\max} = \pm \rho V_s |v_{n,\text{peak}}|$$

These expressions do not account for the presence of the structure and can be useful only in a qualitative evaluation of the stability of an opening in rock. This simple approach was taken in the evaluations of a cavern for an underground powerhouse⁶² and of tunnels for a nuclear waste repository.⁶³

Hoop Deformations by Classical Methods (Circular Sections Only). The concentration in the circumferential stresses due to hoop deformation may be estimated from simple expressions for free-field stresses as outlined by Chen et al.⁶⁴ Mow and Pao⁶⁵ have studied the interaction of steady-state waves with cylindrical cavities in cases where the propagation direction is normal to the longitudinal axis, as illustrated in Figure 17.

Consider first the stress concentration for the P-wave. The analogous static solution is Kirsch's solution for biaxial loading. When a static compressive stress of value σ_0 is applied in one direction and the lateral directions are constrained, the lateral compressive stress is $\sigma_0 \nu / (1 - \nu)$, as illustrated in Figure 18. The stress concentration factor for this static loading, which occurs at the cavity wall for $\psi = \pi/2$, is given by

$$\frac{\sigma_{\theta}}{\sigma_0} = 3.0 - \frac{\nu}{1 - \nu} \quad (11)$$

The dynamic stress concentration for a P-wave was determined by Mow and Pao for an isotropic, elastic medium and found to depend upon Poisson's ratio (as does the static analogy) and the dimensionless frequency of the wave, Ω , as shown in Figure 19. The dimensionless frequency is defined by

$$\Omega = \frac{\omega a}{V_p} \quad (12)$$

where ω is the circular frequency of the wave and a is the radius of the circular cavity. Note that $\Omega = 0$ corresponds to an infinitely long wavelength, which is the static solution given by Equation (11). The peaks in dynamic stress concentrations are approximately 10% to 15% greater than the static

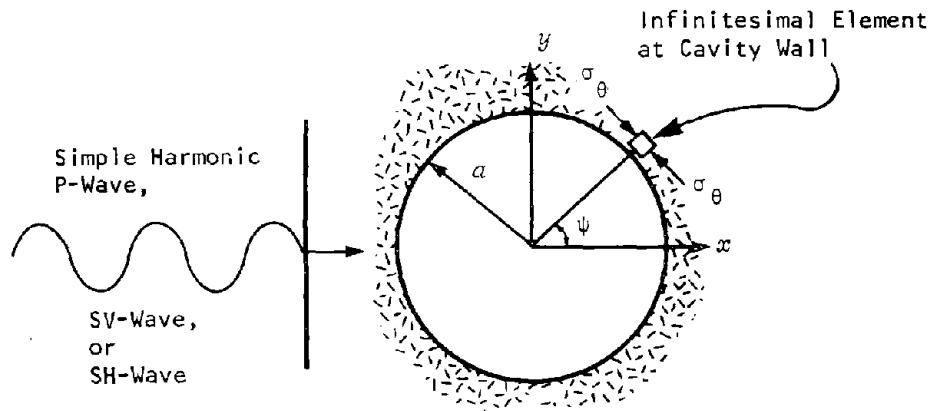


Figure 17. Circular cylindrical cavity and incident wave.

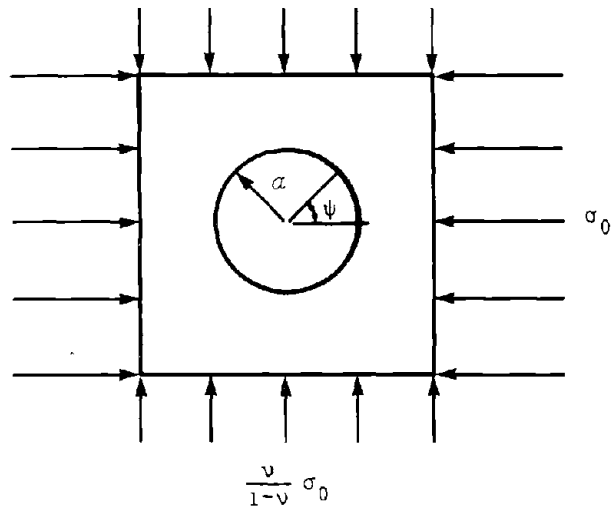
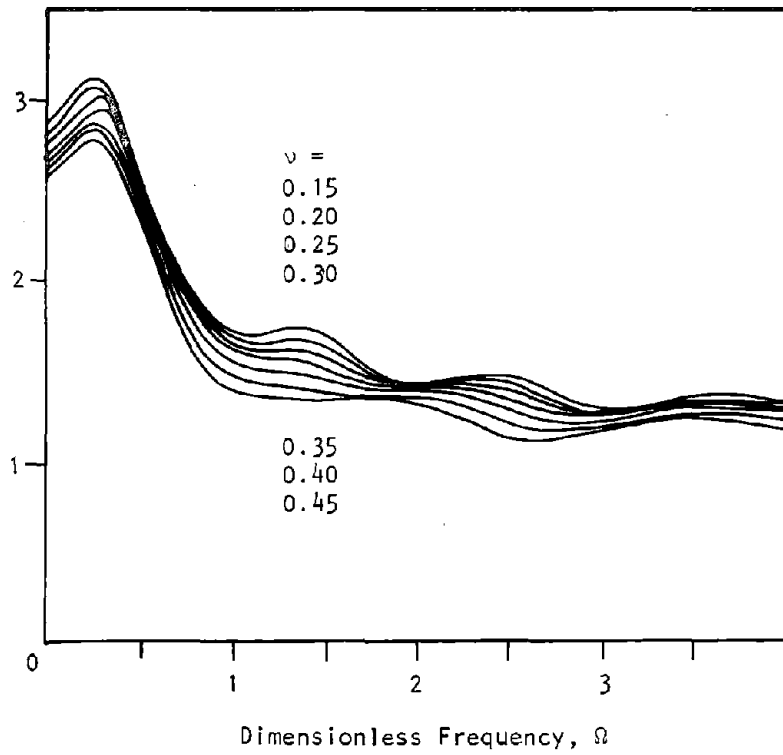


Figure 18. Biaxial stress field created by a horizontal pressure.



Reprinted by permission of the publisher.

Figure 19. Dynamic stress concentration factors for P-wave.
(Adapted from Reference 65.)

stress concentration values and occur at $\Omega \approx 0.25$, or at wavelengths approximately equal to 25 times the cavity radius. By selecting the largest value of the stress concentration factor over the entire range of frequencies for a given value of Poisson's ratio, Mow and Pao constructed a plot of the dynamic stress concentration versus Poisson's ratio for P-waves (Figure 20).

The dynamic stress concentration for an in-plane SV-wave was also determined by Mow and Pao. Because the propagation direction is normal to the longitudinal axis of the cylindrical cavity, which is oriented horizontally, the particle motion of the SV-wave is in the plane of the cross section. The equivalent static stress concentration factor is equal to 4, regardless of the value of Poisson's ratio. The dynamic value, however, depends on Poisson's ratio, as well as on frequency. Again, by selecting the largest value over the entire range of frequencies for a given value of Poisson's ratio, a plot of the dynamic stress concentration versus Poisson's ratio for SV-waves was obtained (Figure 21).

Mow and Pao⁶⁵ also studied the interaction of a steady-state SH-wave with a cylindrical cavity, in which the particle motion is normal to the plane of the cross section. The equivalent static stress concentration factor is equal to 2 regardless of the value of Poisson's ratio. The dynamic value does not depend upon Poisson's ratio either, although it does vary with frequency. The maximum dynamic stress concentration is about 2.1 (5% larger than static) and corresponds to a value of $\omega a/V_s$ equal to approximately 0.4.

Peak stresses around a circular cavity can be estimated by using the dynamic stress concentration factors and the simple formulas for free-field stresses given by Equations (6) and (10)

$$\sigma_{\max} = \pm K_1 \rho V_p |v_{\text{peak}}| \quad (13)$$

$$\tau_{\max} = \pm K_2 \rho V_s |v_{n,\text{peak}}| \quad (14)$$

where:

K_1 = the dynamic stress concentration factor for a P-wave (Figure 20)

K_2 = the dynamic stress concentration factor for an SV-wave (Figure 21)

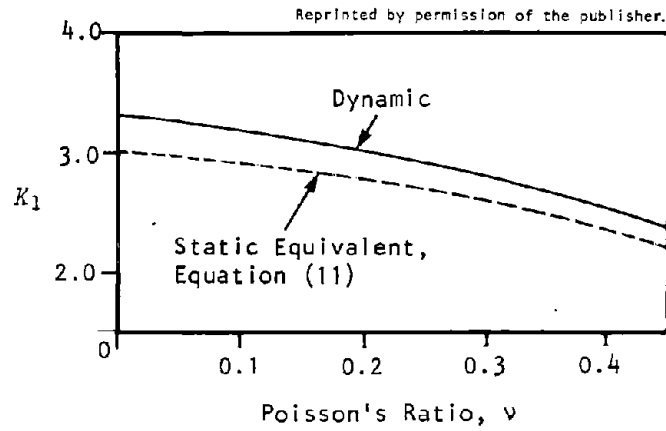


Figure 20. Maximum dynamic stress concentration factor K_1 for P-wave incident upon a cylindrical cavity. (Adapted from Reference 65.)

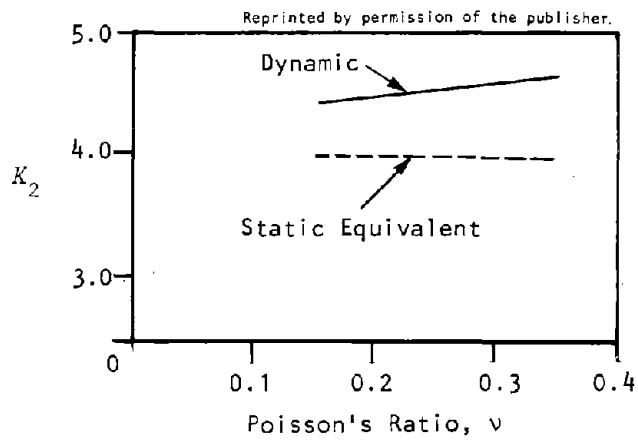


Figure 21. Maximum dynamic stress concentration factor K_2 for SV-wave incident upon a cylindrical cavity. (Adapted from Reference 65.)

$$|v_{\text{peak}}| = \text{the absolute maximum value of the particle velocity in the direction of propagation}$$

$$|v_{n,\text{peak}}| = \text{the absolute maximum value of the particle velocity normal to the direction of propagation}$$

In practice it may be impossible to determine v_{peak} and $v_{n,\text{peak}}$ separately, in which case the maximum particle velocity expected at the site, regardless of orientation, should be used.

This simple approach to estimating peak dynamic stresses around an unlined cylindrical cavity can be extended to lined cavities; however, the mathematics is considerably more involved. Mow and Pao⁶⁵ investigated the case of a P-wave incident upon an elastic liner of arbitrary thickness embedded in an elastic medium (see Figure 22). The solution depends upon ratios of the shear moduli, the P-wave velocities, and the Poisson's ratio of the two materials, as well as on the ratio of the outer and inner radii of the liner. Mow and Pao plot values for the maximum dynamic stress concentration factor for the medium, K_m , and for the liner, K_l , shown in Figures 23 and 24, respectively. Poisson's ratios for both the medium and the liner are set to 0.25, while dimensionless parameters are defined by

$$\bar{\mu} = \frac{G_m}{G_l} \quad (15)$$

$$\bar{\alpha} = \frac{V_{pm}}{V_{pl}} \quad (16)$$

$$\bar{r} = b/a \quad (17)$$

Note that the stress concentration in the medium is less than that in an unlined cavity and can be further reduced by using a thicker liner (larger value of \bar{r}) or a stiffer liner material (larger value of G_l). The stress concentration in the liner for a given \bar{r} will, conversely, increase with increasing liner modulus.

Note also that if the liner modulus is greater than the medium modulus ($\bar{\mu} < 1.0$), Figure 24 predicts that a thin liner will increase the stress concentration in the liner. This does not imply that a thicker (hence a stiffer) liner is preferable in soft ground, however. The desirability of a flexible liner has been established for soft-ground tunnels under static loads.¹ Peck et al.¹ show that

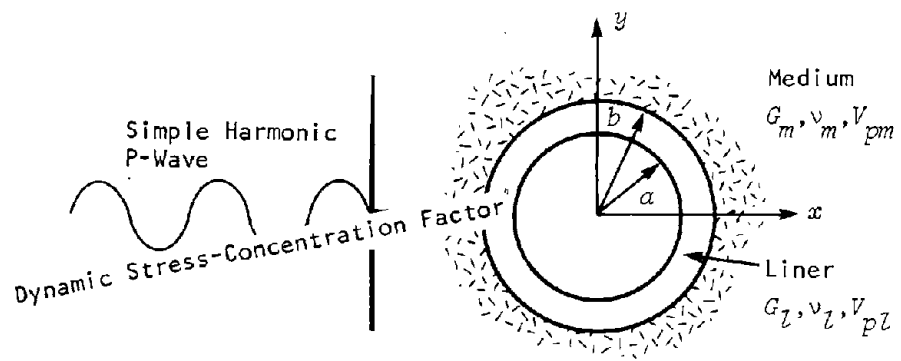


Figure 22. Circular cylindrical liner and incident wave.

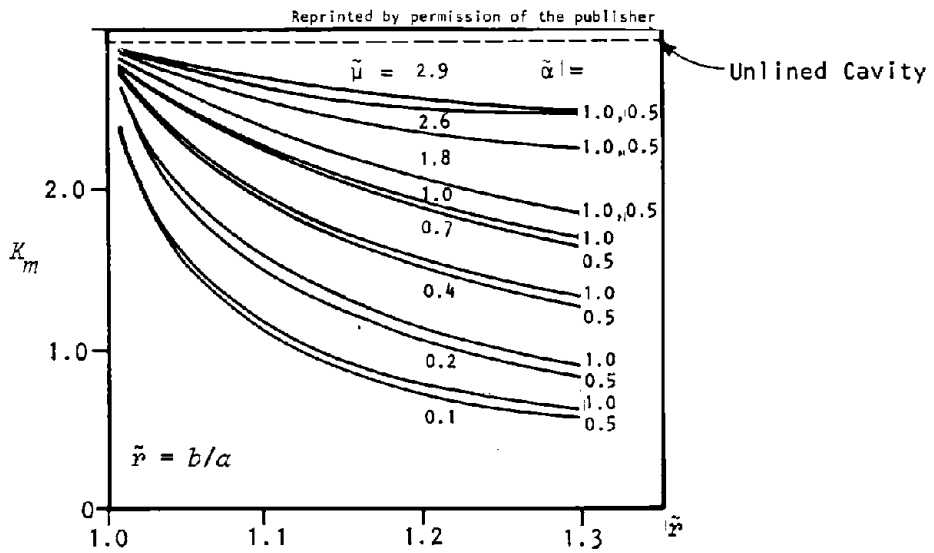


Figure 23. Maximum medium dynamic stress concentration factor K_m versus liner thickness parameter \tilde{x} for various $\tilde{\mu}$ and $\tilde{\alpha}$ ($\nu_m = \nu_z = 0.25$). (Adapted from Reference 65.)

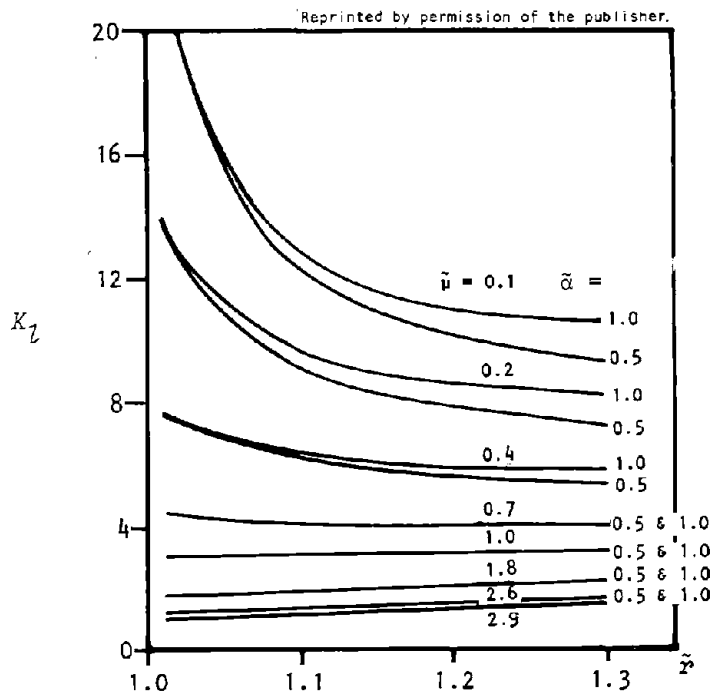


Figure 24. Maximum liner dynamic stress concentration factor K_z versus liner thickness parameter \tilde{x} for various $\tilde{\mu}$ and $\tilde{\alpha}$ ($\nu_m = \nu_z = 0.25$). (Adapted from Reference 65.)

flexural moments in a liner decrease as the thickness of the liner is reduced. However, the maximum stress may increase because stress varies not only with the moment but also with the inverse of the thickness squared. Therefore, caution should be exercised when applying these curves.

Although Mow and Pao consider only the P-wave incident on an elastic liner, Mente and French⁶⁶ present similar results for an SV-wave incident on an elastic liner.

The procedures based upon Mow and Pao assume that no slip occurs between the liner and the medium. Slip at this interface is probably not likely during an earthquake, except possibly for tunnels in soft soils. Slip is a possibility under large dynamic loads, such as those created by a nuclear explosion, and it has received attention in literature on protective structures for defense applications. Solutions for springline thrusts and moments in liners have been obtained by Lew,^{67,68} assuming full slip. The solutions are based upon small-displacement theory, which assumes that liner deflection from transverse shear stresses (perpendicular to the midsurface of the liner) are negligible. Lew's solution does not consider dynamic loading; instead, the equivalent static pressure is used with the assumption that the dynamic solution will be only 10% to 15% greater than the static solution.

Hoop Deformation by Computer Methods. Discrete models, such as finite-element and finite-difference models, provide excellent procedures for analyzing dynamic hoop deformations of a cavity. These modeling procedures permit consideration of a variety of practical aspects: lined as well as unlined cavities, arbitrary cross-sectional shape, rock joints, nonhomogeneous material properties, and rock bolts, among others. The models can be used to investigate the response of a structure in close proximity to the free ground surface.

Several computer programs are available for two-dimensional analysis of underground structures. SAP IV,⁶⁹ a finite-element structural analysis program, can be used to analyze linear systems. NONSAP⁷⁰ is a finite-element structural analysis program that permits consideration of geometric nonlinearities and several different material nonlinearities for two-dimensional plane stress and plane strain elements. Unfortunately, NONSAP is not able to directly accept

acceleration time-history inputs; the forcing function must be prescribed as a load history at any particular node. ANSYS⁷¹ is another general-purpose analysis program that has capabilities similar to those of NONSAP when applied to two-dimensional plane problems. Significantly, these general-purpose structural analysis programs do not contain nonreflecting boundaries. Thus, unwanted waves may reflect from the boundaries of the finite-element mesh back to the underground structure during the observation time. The FLUSH⁵⁰ program does contain nonreflecting boundaries and could be used to investigate near-surface openings for vertically propagating shear or compression waves. However, FLUSH was intended for analyzing the interaction between surface structures and the soil mass, and its use to model any other situation (such as underground structures) is not advised. Its use for deep structures would be both costly and inappropriate. Finite-difference codes such as STEALTH⁵⁸ are also available for modeling the dynamic response of two-dimensional underground structures. A nonreflecting boundary has been formulated for a finite-difference code by Cundall et al.⁷²

Finite-element codes have been applied to the dynamic analysis of underground structures. A few are cited here for perspective. John A. Blume & Associates, Engineers, investigated the seismic stability of a railroad tunnel through Franciscan Shale, a relatively weak and highly fractured rock.⁷³ The vertical cover above the tunnel varied in thickness from 23 to 37 ft (7 to 11.3 m). The finite-element model was subjected to an acceleration time history from the Golden Gate Park (San Francisco) earthquake of 1957. Yamahara et al. studied the earthquake safety of a rock cavern at a depth of approximately 250 ft (76.2 m).⁷⁴ The investigators used two acceleration time histories, one from the 1940 El Centro earthquake and the other from the 1968 Hachinohe earthquake. Glass determined stress concentrations around unlined rectangular cavities using a finite-element model subject to triangular stress pulses.⁶¹ Murtha employed a nonlinear finite-element code to study the dynamic response of a horizontally buried cylinder to very high shock loadings, such as those that might occur from the explosion of a nuclear weapon at the ground surface.⁷⁵ Wahi et al. investigated the stability of rectangular openings with the finite-difference code STEALTH using several different material models and several different earthquake time histories.⁷⁶ This investigation seems to be the first reported wave propagation study of an underground opening with two-component motion, one component being P-wave motion and the other SV-wave motion.

Large underground tanks (for the storage of liquefied natural gas, petroleum, or liquid nuclear wastes) also have been analyzed for seismic stresses using finite-element codes.^{77,78} Such tanks are steel or concrete cylinders with their axes of symmetry in a vertical position. They are usually buried at a shallow depth and are constructed by cut-and-cover operations.

Developments are still under way on means to include many important rock mass properties, such as joint behavior, strain softening, dilatancy, tensile cracking, and plasticity, in the application of discrete models to static problems. The inclusion of such properties continues to be the subject of much discussion. For example, rock discontinuities in finite-element models for static analysis were discussed by Goodman et al.⁷⁹ and by Roberds and Einstein.⁸⁰ Slip joints have been included in the finite-element code BMINES, a three-dimensional computer code developed to analyze mining problems.^{81,82}

In dynamic analysis, similar developments are under way. For example, the study performed by Wahi et al. employed an isotropic plastic model, a joint-slip model, and a tensile-cracking model.⁷⁶ The isotropic plastic model used the von Mises yield criterion and the Prantl-Reuss nonassociated flow rule. The joint-slip model simulated slip along the joints and accounted for dilation effects. The tensile-cracking model allowed new cracks to open up parallel to predefined joint sets and monitored the opening and closing of these cracks.

An interesting approach, currently under development, to analyzing the response of caverns in rock is the discrete-element method (DEM), first devised by Cundall.^{83,84} The original method assumed that deformations occur only at element boundaries and that the elements themselves are rigid. That assumption corresponds to low-stress rock situations -- those in which displacement of joints far exceeds displacement of the intact rock blocks. Maini et al.⁸⁵ undertook some major revisions of Cundall's original work, among them:

- Translating the original code written in machine language into standard FORTRAN
- Developing a method for allowing blocks to crack and break into separate elements
- Permitting fully deformable blocks
- Proposing constitutive laws for rock joints

Dowding and Belytschko of Northwestern University are currently engaged in a project to develop a computer code, based upon Cundall's DEM, that will be able to account both for rock mass inhomogeneities in the form of continuous joints or shear zones and for irregular geometry of the opening and the intact rock blocks.⁸⁶

Boundary integral methods, introduced briefly in the beginning of this chapter, may provide very powerful numerical approaches in the future for the dynamic analysis of underground structures. The boundary element method (BEM), one formulation of the boundary integral method, has already been applied to the analysis of static stresses around underground openings.^{87,88,89} We are not aware of applications of BEM to dynamic analysis of underground structures as yet. The boundary integral equation method (BIEM) has also been applied to static geomechanics problems, including the three-dimensional stress analysis of tunnel intersections.^{90,91} BIEM has been used for the dynamic analysis of soil-structure interaction of large rigid structures on, or embedded in, the ground surface.⁹² Alarcon et al. believe that the dynamic analysis of a lined tunnel can be easily treated with BIEM.⁹²

Physical models may also be employed in the analysis of underground openings for ground motion. Barton and Hansteen⁹³ studied the dynamic stability of large underground openings at shallow depth using jointed physical models at a scale of 1:300. The model material consisted of a mixture of red lead, sand, ballotini, plaster, and water. Joint sets were produced in cured slabs of the model material by a double-bladed guillotine-like device. Displacements of the simulated rock blocks in the model were measured by means of photogrammetry. Another experimental procedure that might be used is dynamic photoelasticity. Daniel⁹⁴ has used such a technique to study the effects on underground structures of blast waves moving over the ground surface.

Axial and Curvature Deformations. Having discussed the various methods for analyzing seismic stresses around a tunnel due to hoop deformation, we now direct our attention toward the analysis for axial and curvature deformations. Axial or curvature deformation created by the passage of seismic waves results in cycles of alternating compressive and tensile stresses in the tunnel wall. These dynamic stresses are superimposed upon the existing static state of stress

in the rock and in the tunnel liner (if a liner is present). There are several failure modes that might result. Compressive seismic stresses add to the compressive static stresses and may cause spalling along the tunnel perimeter due to local buckling. Tensile seismic stresses subtract from the compressive static stresses, and the resulting stresses may be tensile. This implies that rock seams or joints will open, permitting a momentary loosening of rock blocks and a potential fall of rock from the tunnel roof and walls.

The response of the medium and liner for axial and curvature deformation is most appropriately represented by a three-dimensional model. However, a one-dimensional model can be used for submerged transportation tubes, subway tunnels in soils, and steel or concrete pipes. Such structures can be treated as beams, permitting the application of standard structural analysis concepts. The only issues are the form of the ground motion input to the structure and the amount of interaction between the soil and the structure. Kuesel devised a deformation response spectrum method that prescribes a design curvature for the beam analysis.⁵⁹ Kuesel's method, which was a first attempt at dealing with this problem, was later expanded by Kuribayashi.⁶⁰ The revised method, referred to as seismic deformation analysis, utilizes a velocity response spectrum for base rock, evaluated from observed strong-motion accelerations. It provides a very simple analytical tool for the determination of axial force, shear force, and bending moment on a tunnel section. The method has very practical applications for design and, therefore, is described in detail in the chapter on current practice in design (Chapter 6).

A more refined model of the submerged tunnel has been proposed by Okamoto and fellow researchers.^{33,95,96} For this model, the subaqueous tunnel is assumed to be an elastic beam that can deform axially and in bending. It is further assumed that the natural period of the soil is not influenced by the existence of the tunnel and that the ground motions are only shearing vibrations. The soil layer above bedrock (or an appropriately stiff sublayer) is lumped into masses at discrete points along the tunnel. The mass points are connected in the longitudinal direction of the tunnel by springs that represent the relative axial stiffness and shearing stiffness of the layer between adjacent mass points. The soil masses are connected to the base by springs that

represent the shearing stiffness of the soil layer and are determined from the natural period of the soil and the lumped masses.

Three-dimensional models are needed to analyze rock tunnels and caverns for axial or curvature deformation. Free-field stresses estimated by Equations (6) and (10) have been used to make a qualitative evaluation of stability in several studies.^{62,63} However, more realistic models would include the tunnel or cavern itself. If the cavity is a circular cylinder, then two-dimensional axisymmetric models could be used to study axial deformations, but not curvature deformations. Regardless of the geometric shape of the cross section, the curvature deformations of a rock tunnel should be analyzed by a three-dimensional model. Computer codes such as SAP IV, NONSAP, and ANSYS currently provide the basic tools for such analyses. Unfortunately, the computer costs associated with three-dimensional models prevent studying anything more than the simplest configurations and input motions (or loads).

PROPERTIES REQUIRED FOR SEISMIC ANALYSIS

The properties of soil and rock currently required for seismic analysis include:

- density (ρ)
- seismic wave velocities (V_p and V_s)
- dynamic moduli (E and G)
- Poisson's ratio (ν)
- elastic damping (Q)

Advanced methods of analysis that are still in the process of development will eventually be capable of incorporating joint and fracture properties and anisotropy.

Techniques for Measuring Soil and Rock Properties

Density. Density, ρ , is readily measured on soil samples or rock cores in the laboratory. Errors in measurement can be reduced by careful use of undisturbed sampling techniques, such as a Pitcher tube sampling of soils and triple tube core barrel sampling of rocks.

Characterization of the earth or the rock mass at a site remains a problem whose solution requires judgment and care because of the natural inhomogeneity of these materials. Density, like all other material properties, is statistically distributed, and the sampling technique employed may not lead to a true representation of the mean value even though the accuracy appears to be high. For example, even the most careful coring techniques will tend to underrepresent soft layers or shear zones within hard rock. This difficulty can be overcome by the use of a nuclear density probe that can take continuous measurements as it is lowered down a borehole. This is a standard approach in the petroleum industry. Because of high costs, borehole logging probes are cost effective only for critical facilities or in deep boreholes.

Seismic Wave Velocities. Seismic wave velocities, V_p and V_s , are conventionally measured in situ using geophysical techniques. A well-planned site investigation will employ a variety of these techniques in order to obtain a good three-dimensional characterization of the site. In situ geophysical techniques provide more realistic values than do laboratory methods because properties are measured across a large volume of the subsurface and include the effects of fractures and inhomogeneities. However, seismic wave travel paths must be assumed, which can lead to inaccuracies for highly anisotropic and inhomogeneous site materials. A current description of seismic site investigation techniques is given by Wilson et al.⁹⁷

Surface refraction is the most commonly used method. The travel time is measured between the source of excitation, either an impact or an explosive charge, and a pattern of geophones spread across the ground surface. This method is used to measure nearly horizontally propagating compressional wave and shear wave travel times. However, relatively thin, soft layers are masked out wherever they are overlain by harder materials.

Crosshole seismic techniques also yield velocities of horizontally propagating waves. The seismic source is placed in one borehole, and the receivers are placed at the same depth in other boreholes. A depth profile may be made by lowering the entire array and repeating measurements at intervals. Difficulties arise in knowing, with sufficient precision, the distance between points in two closely spaced boreholes. Crosshole seismic techniques afford better resolution of low-velocity layers than do refraction techniques.

Uphole and downhole techniques measure velocities of seismic waves propagating in nearly vertical directions. Uphole measurements are made with seismic sources in the borehole and the geophone array spread across the ground, whereas downhole measurements are made with the geophones in the borehole and the seismic sources on the ground. These techniques are favored for earthquake engineering because they employ vertically propagating waves, which are thought to account for most of the damaging seismic energy input to a surface site. In addition, these techniques, especially the downhole technique, are best for distinguishing low-velocity layers overlain by high-velocity layers.

Velocity profiles can also be obtained by downhole probes that measure the travel time of impulses through the borehole wall from a transmitting source to a receiver. This technique has the advantage of continuous logging ability; but the effects of the casing, borehole wall, and short travel path make the results more useful for correlation of layers than for derivation of site properties. According to unpublished data gathered by URS/John A. Blume & Associates, Engineers (URS/Blume), borehole logging has yielded velocities some 20% to 25% higher than those obtained by downhole seismic surveys at the same locations. The work of Kanamori and Anderson⁹⁸ suggests at least a partial explanation; seismic velocities may be frequency dependent, with high-frequency signals traveling faster than low-frequency ones.

Compressional and shear impulse velocities are commonly obtained in the laboratory on intact specimens. Travel time of impulses is measured from one end of the sample to the other. Because this type of test involves short travel paths and small samples of the intact material, the results tend to under-represent joints and fractures. Therefore, seismic velocities obtained by this method may be biased toward higher velocities and should always be compared with field measurements.

Dynamic Moduli. Dynamic values of the Young's modulus, E , and the shear modulus, G , are most commonly calculated from seismic wave velocities using the well-known formulas:

$$E_{\text{seis}} = \rho V_p^2 \frac{(1 + \nu)(1 - 2\nu)}{(1 - \nu)} \quad (18)$$

$$G_{\text{seis}} = \rho V_s^2 \quad (19)$$

The uncertainties in E_{seis} and G_{seis} arise primarily from uncertainties in the seismic velocities used. Dynamic moduli are also obtained in the laboratory on soil or rock specimens by two main methods: dynamic triaxial compression tests and resonant column tests, the results of which are E_{dynamic} and G_{dynamic} , respectively.

A typical dynamic triaxial compression test involves jacketing the specimen with a rubber sleeve and placing it in a pressure cell. A confining pressure is introduced to approximate the stress conditions at depth, and a consolidation piston load is applied. The piston load is then cycled; for cohesionless soils and rock, difficulties are encountered unless the piston load remains compressive to prevent tensile failure of the specimen. The modulus E_{dynamic} is the slope of the axial stress-strain curve after a specified number of cycles. E_{dynamic} will tend to decrease with repeated cycling and with increasing strain level. Cycling frequencies on the order of 1 to 10 Hz are commonly used, depending on the stiffness of the specimen and on machine capabilities. Cyclic triaxial testing has become a standard test for determining the dynamic properties of soils.^{99,100} (For example, it has been used in the assessment of liquefaction potential of sands.) Cyclic triaxial testing of rock, however, has only recently received attention. Haimson suggests standards for dynamic triaxial rock testing and describes methods of overcoming the special problems of testing rock materials that have high compressional strength, low tensional strength, and brittle behavior.¹⁰¹

The test cell configuration for resonant column testing is similar to that for triaxial tests; however, the dynamic load applied to the piston is torsional. Various frequencies are applied until a resonance is found at which significant strains are achieved. The modulus thus calculated is a torsional shear modulus (G_{dynamic}). Specifications for testing and methods of data reduction are described by Drnevich, Hardin, and Shippy.¹⁰²

Hendron published correlations between dynamic moduli determined for rock masses by in situ seismic tests and static deformation moduli determined by laboratory compression tests and by jacking and pressure chamber tests in dam abutments.¹⁰³ These correlations also include a rock quality designation, a measure of fracture frequency, as a parameter. Silver et al. showed that

for clay shales good correlations could be found between static moduli determined with borehole pressure meters and dynamic moduli obtained from laboratory cyclic triaxial tests.¹⁰⁴ Empirical correlations such as these indicate that, at least for certain foundation materials and selected sites, static tests conventionally used for design purposes may also provide a means of estimating dynamic properties, given sufficient site-specific data.

Poisson's Ratio. Poisson's ratio, ν , for dynamic analysis is typically calculated from field geophysical measurements of seismic velocities using a variation of the following relation, which is correct for an elastic medium:

$$\nu = \frac{1}{2} \cdot \frac{(V_p/V_s)^2 - 2}{(V_p/V_s)^2 - 1} \quad (20)$$

It is apparent that Poisson's ratio is sensitive to uncertainties in the values of either of the elastic wave velocities. Field experience confirms this contention; therefore, Poisson's ratio must be assessed within the context of other exploration data and experience.

Laboratory measurements of Poisson's ratio are accomplished by monitoring the lateral strain of a sample subjected to triaxial compression. However, the results of such tests do not represent the behavior (including discontinuities) of the site materials, nor do the boundary conditions placed on the test sample correctly model subsurface confinement.

Damping. Although site damping, Q , is a property of great importance in soil-structure interaction calculations, developments in engineering geophysics have not kept pace with computational approaches to solving earthquake response problems.

Site damping factors are typically specified on the basis of results of dynamic laboratory tests, such as those described above. Seed and Idriss showed that damping increases with strain amplitude in laboratory tests, and they derived empirical curves for estimation of damping for soils.⁹⁹

In situ measurements of damping have not yet become commonplace; however, a limited body of experimental data indicates that site damping, at least in the

case of rock sites, is significantly greater than the damping found from laboratory tests. Damping (or attenuation) has been measured for near-surface geologic formations using explosives^{105,106} and on a crustal scale using spectral ratios of blast signals received at various distances.¹⁰⁷ These investigations have been primarily directed toward petroleum exploration and crustal seismology; virtually no applied work has been done in this area for earthquake engineering purposes.

A simple methodology for derivation of in situ material damping factors is needed. Such a methodology is currently being investigated at URS/Blume by Bruce B. Redpath under a research grant from the National Science Foundation (Grant No. PFR-7900192). Practical field techniques are being developed using downhole and crosshole surveys of seismic velocities and attenuation rates in holes 200 ft (61 m) deep at two different sites. The observed attenuation characteristics, corrected for geometrical spreading and changes of acoustic impedance in the ray paths, are being used to determine values of Q for the near-surface materials. Two methods of data analysis are being applied to impulsive signal sources: one determines Q indirectly by calculating the spectral ratios of both compressional and shear pulses to determine the magnitude and frequency dependence of the attenuation coefficient in the exponential term of the propagation equation; the other method tests a relationship in which the rise time of a seismic pulse is proportional to its travel time and in which the constant of proportionality is Q^{-1} . A third approach to measuring Q uses an electronically controlled hydraulic vibration generator to generate monofrequency signals over a range of 10 to 300 Hz; the attenuation of these signals with distance should provide values of Q without requiring the spectral analysis of complex pulses. The research will result in practical recommendations for field procedures and data analysis to measure Q -values in near-surface materials.

Joint and Fracture Properties. It has long been recognized that the discontinuities in jointed or fractured rock can increase the deformability and decrease the strength of the rock mass as a whole. Finite-element programs that include separate elements for intact rock and deformable joints have been developed and are undergoing improvements to make use of static properties such as joint friction, joint normal stiffness, and shear stiffness.⁷⁹ These properties can be derived by jacking tests on rock blocks that include a dis-

continuity or by plate or radial jacking tests on larger in situ rock masses. Numerous test methods are described by Stagg.¹⁰⁸

Dynamic testing of joints and fractures is a topic for research that has received little attention. Preliminary research indicates that joints fail by cumulative cyclic fatigue; therefore, confining pressure (depth of burial) is a critical factor in determining the residual strength of the failed joint.¹⁰⁹ As confining pressure increases, rocks and joints demonstrate increasing ductility with a wide range of behavior, depending on rock type. The number of test cycles and the amplitude of deformation are both important in determining whether or not failure has been reached.

Anisotropy. Typically, site conditions can be modeled as transversely isotropic or, in other words, as horizontally layered. This vertical variation in properties may arise from natural layering, the tendency of density to increase with depth due to overburden pressure, downward penetration of weathering effects, or presence of a water table. However, directional or horizontal anisotropy, a condition that is not usually considered, exists at some sites. Directional anisotropy can be pronounced at sites underlain by dipping rock strata. For example, seismic waves traveling perpendicular to bedding planes will travel at a velocity that is the net effect of multiple layers and interfaces. This velocity is likely to be lower than the velocity measured parallel to bedding. Likewise, a preferred orientation of fractures might produce a directional variation in velocity. A thorough site investigation should include an effort to discern any significant anisotropy in dynamic properties throughout the site materials.

Problems in Synthesizing Measured Properties

When all the field and laboratory data for a site have been collected and reduced, representative site properties must be synthesized from results obtained from tests that are not directly comparable. For example, dynamic moduli calculated from resonant column tests are different from the results of laboratory cyclic triaxial tests or field seismic refraction surveys. Some standard procedures have been adopted for reconciling different results; however, they are not without difficulties. The chief factors accounting for these

differences are strain dependence of the properties and the stochastic nature of the data.

Reconciliation of Site Properties. Laboratory tests offer advantages of close control of test conditions and ability to achieve high strains. However, it should be remembered that tests conducted on soil and rock samples do not perfectly model the behavior of soil or rock layers at a real site. Factors that place limitations on predictions of field behavior derived from laboratory tests are problems of sample disturbance and possible changes in sample structure, boundary effects inherent in the testing apparatus, difficulties in reproducing the in situ state of stress, and representativeness of samples.

Site properties are usually modeled using a combination of laboratory and field test data. Modulus values obtained from field geophysical surveys are taken to be maximum values (G_{\max}); laboratory test data are normalized to the low-strain maximum moduli. However, as pointed out by Richart et al.,¹¹⁰ this procedure for determining moduli in situ has not been verified. It is not yet clear that linking field data and laboratory tests in this fashion yields accurate predictions of site response to earthquake shaking. Richart suggested that moduli in the field may, with increasing strain, undergo reduction less dramatic than the reductions observed in the laboratory.

Strain Dependence. Seed and Idriss,⁹⁹ Hardin and Drnevich,¹¹¹ and others have studied strain dependence of dynamic modulus and damping in laboratory soil tests. Shear modulus has been shown to decrease significantly with increasing strain in the range of 10^{-5} to 10^{-2} . Conversely, damping increases from several percent to 25% or 30% over the same range of strain. The studies cited above were carried out on cohesionless sands of standardized gradation and on several types of clays. Derivation of modulus reduction curves and damping curves for additional soil and rock materials is an important topic for future research.

For laboratory dynamic testing of rock, strain-dependent properties cannot readily be generalized to in situ conditions because rock includes a wide range of materials in which the condition of the fractures and joints is frequently more influential in determining rock strength than are hardness, cementation,

etc., of the intact material. Extensive tests have been conducted on selected hard, fresh, rock cores.¹⁰¹ Typically, these have been laboratory tests on cores of crystalline plutonic rocks, sandstones, and limestones. However, the results are of limited interest in earthquake engineering of underground structures because failure in hard, strong rock is much more likely to occur at preexisting joints or fractures. More investigations are needed on the dynamic behavior of common sedimentary rocks such as shales, weak sandstones, and claystones; the influence of fractures should be included in such studies.

The advantage of seismic geophysical methods is that they are capable of measuring properties throughout the entire soil or rock mass, including its discontinuities and inhomogeneities. However, conventional field techniques usually permit evaluation of dynamic properties such as shear modulus only at strain levels well below 10^{-5} ; the results, then, are minimum or threshold values. A recently developed technique, a modified version of the crosshole seismic technique, has succeeded in obtaining higher strains, on the order of 10^{-5} to 10^{-3} .^{97,112} This method has not yet been applied to rock sites, and high setup costs are a severe limitation.

Dynamic Properties as Stochastic Functions. In the future, site analysis may be called upon to address the statistical nature of the data synthesized to make the model as well as the implications for cost and safety calculations. The following is a simple illustration of the usefulness of probabilistic consideration of geotechnical data.

Static tunnel stability is often presented in terms of a factor of safety that equals the ratio of driving forces to the forces resisting collapse. Both of these forces are estimated from test results and field observations and then viewed as deterministic values. If we calculate a factor of safety greater than 1.0, we say that on the basis of experience the hypothetical failure should not occur. In reality, a factor of safety slightly greater than 1.0 may or may not be a safe condition because our best estimates of joint orientations, joint plane friction angles, and in situ stress may err either on the conservative side or on the nonconservative side. Therefore, what is needed for analysis of critical facilities is a probabilistic estimate of safety.

A stochastic function is a mathematical model of a physical system that allows the variable of interest to take random values according to a prescribed probabilistic distribution. Baecher et al., for example, analyzed joint measurements from many excavations in rock and showed that joint length is best fitted by a lognormal distribution and that joint spacing is exponential.¹¹³ Similarly, density, modulus, and every other parameter that enters into the stability calculation could be modeled with a statistical distribution of values. From this information, a probability of occurrence and incurred costs could be calculated for every outcome or mode of failure. Underground seismic motion inputs needed for such a calculation could be derived with methods similar to those currently used to give probabilities of recurrence for accelerations at surface sites.

Site dynamic properties are not usually viewed as stochastic functions, despite known biases and variations due to the measurement techniques employed and the frequent occurrence of natural inhomogeneities in soil and rock materials. However, seismic safety criteria for critical structures are becoming increasingly stringent, and future site investigations are likely to place increased emphasis on probability and risk calculations.

5. Seismic Wave Propagation

The response of underground structures to seismic waves can be better understood by studying the theoretical and practical aspects of the propagation of the waves through the earth materials and the interaction of those waves with the structures. In this chapter, the general nature of underground motion is reviewed; particular attention is given to those factors that change the motion along the transmission path between the source and the site and at the site itself. Because the variation of motion amplitudes with depth is an important consideration at the site of underground structures, this subject is explored by a thorough literature review and some numerical studies. The chapter concludes with a detailed investigation of the interaction of seismic waves with a circular cavity in a half-space.

THE NATURE OF UNDERGROUND MOTION

Factors Affecting Underground Motion

A number of factors contribute to the ground motion arriving at the location of an underground structure. A discussion of these factors can be facilitated by referring to Figure 25. The three basic components that determine the characteristics of ground motion to be expected at a given site are the source region, the transmitting region, and the site region.

Source Region. The source region consists of that part of the earth's crust immediately surrounding the earthquake source. This volume of the crust serves as the region of energy release from which seismic waves emanate in all directions. Only a fraction of this energy will arrive at the site and contribute to the ground motion there.

The factor that approximately defines the amount of energy injected into the crust by the earthquake is the magnitude of the earthquake. The magnitude is in turn affected by the extent (area) of faulting, the amount of strain energy stored in the earth prior to the earthquake, and the particular manner in which the stress is released (i.e., the faulting mechanism).

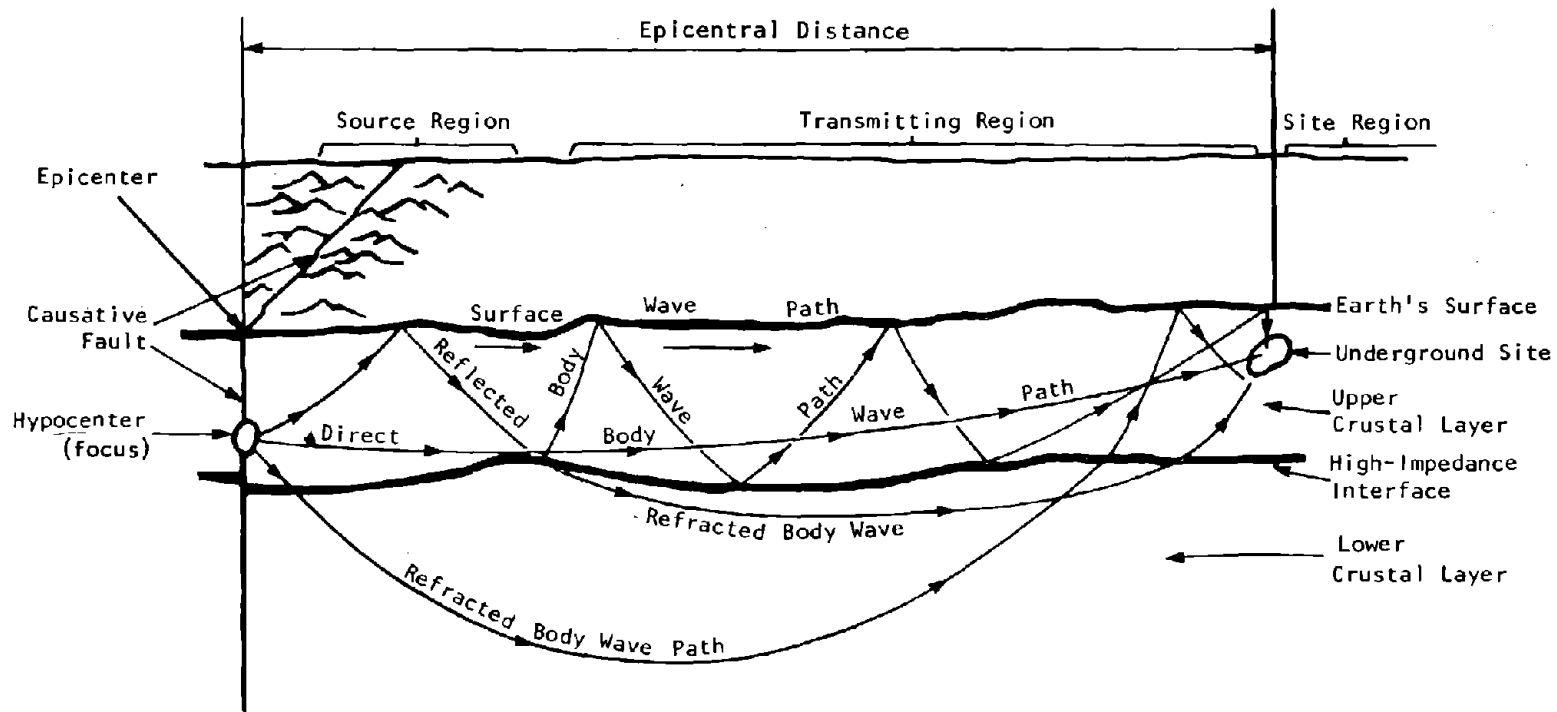


Figure 25. Some wave paths between source and site regions.

The energy that is released is distributed among various types of seismic waves. There are surface waves, such as Rayleigh and Love waves*, whose amplitudes are largest near the earth's surface and diminish with increasing depth below the surface. There are also body waves, which consist of compression (P) and shear (S) waves. The amplitudes of body waves diminish as they spread out in all directions from the source of the earthquake. Body waves can be reflected by or refracted through boundaries between adjacent layers of material within the earth. Thus, seismic energy released by the earthquake source may travel by a number of wave types (or modes) and along a number of paths (see Figure 25).

Faulting mechanisms and focal depth strongly affect the distribution of energy among the different types of seismic waves. For example, deep earthquakes tend to produce less surface wave energy than body wave energy. Furthermore, the wavelengths of the predominant surface waves tend to be somewhat greater for deep earthquakes than for shallow earthquakes.

Transmitting Region. The transmitting region is that part of the earth's crust through which the seismic waves travel from source to site. This region modifies transmitted seismic energy by attenuating the amplitude of seismic motion through the process of geometrical spreading. This simply reflects the fact that the same amount of energy must pass through larger and larger volumes of material as it proceeds away from the source. For surface waves, the geometrical spreading factor is approximately proportional to $1/\sqrt{R_s}$, where R_s is the distance measured from the source to the site along the path followed by the seismic waves. For body waves, this factor is proportional to $1/R_s$. Thus, as the seismic waves proceed outward from the source, geometrical spreading reduces body wave amplitudes more quickly than surface wave amplitudes.

The transmitting region also reduces the amplitude of seismic motion through absorption (anelastic attenuation). Because no medium is truly elastic, some energy is converted irreversibly to heat during each cycle of motion as the seismic wave proceeds through the medium. In general, except in the immediate vicinity of the source and in soil layers very close to the earth's surface,

*See Appendix D for an explanation of these and other seismological terms.

e.g., less than 300 ft (100 m), this absorption mechanism is usually not significant.

Finally, the distribution of seismic energy in the transmitting region may be modified through the presence of inhomogeneities in the earth's crust. As waves spread out from the source in a spherically symmetric way, they are reflected and refracted by discontinuities in the crust. Thus, the waves travel in many different directions, not just radially from the source. Depending upon the geometry of these structural discontinuities, there may be relative enhancement or diminution of motion amplitudes at a given point, relative to what would exist in a homogeneous medium. Given the right shapes, a given portion of the earth's crust could behave exactly like an optical lens, producing a considerable focusing of energy.

Elastic moduli and density generally increase with depth. Concomitantly, seismic wave velocities also increase with depth because increases in elastic moduli are usually greater than increases in density. Therefore, the earthquake waves that propagate away from the source with downward inclination pass from layer to layer of material with increasing wave speed. This results in a refraction of the waves in such a manner that the wave paths appear curved and concaved upward as illustrated in Figure 25.

In summary, the three factors that influence redistribution of seismic energy in the transmitting medium are distance traveled along the ray path by each wave type (geometrical spreading), anelastic attenuation, and spatial variations in the properties of the earth material.

Site Region. The site region consists of that portion of the earth's crust immediately adjacent to the underground structure. The response of the site to incoming seismic waves depends, in part, on the presence of soil layers overlying bedrock. In general, the seismic velocity in soil or similar products of weathering is lower than that in the parent rock below. Thus, as the incoming energy slows down, it must "pile up," that is, generate higher amplitude seismic motion, in a manner analogous to that in which ocean wave amplitudes increase upon approaching a beach. An additional property of near-surface soil layers is that they may trap energy in certain frequency inter-

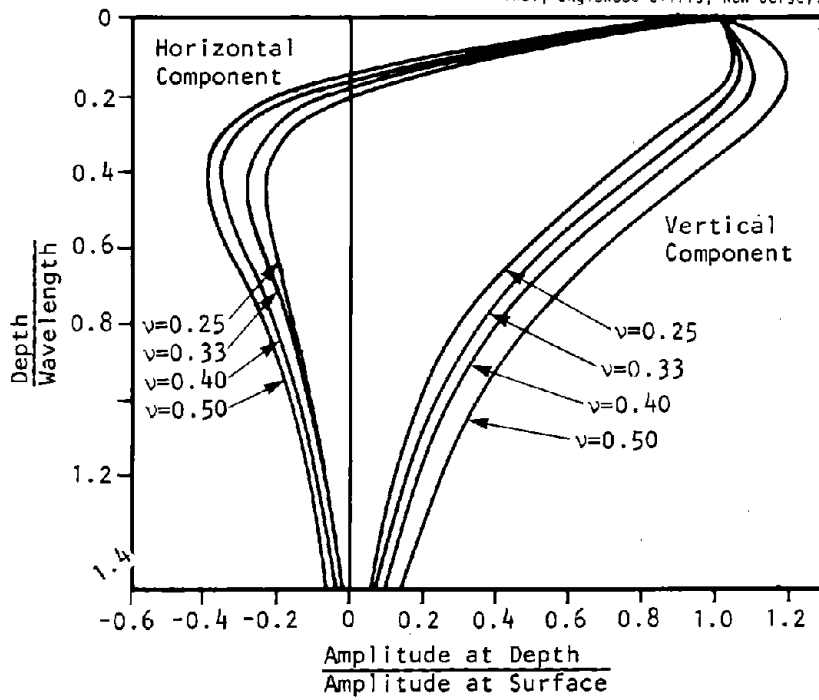
vals through a resonance process so that motion amplitudes at select frequencies are enhanced, while amplitudes at nonresonant frequencies are diminished. The layers thus act as if they have a resonant frequency. This effect can occur in layers of significant thickness; for example, the alluvial layer underlying Mexico City has a resonant period of approximately 2.5 sec.

The dependence of amplitude on depth is also a characteristic of the site region. The general amplification of seismic waves propagating from rock into soil as they approach the earth's surface is part of the physical explanation underlying the popular notion that seismic motion diminishes with increasing depth. The amplitude of surface waves generally diminishes with depth as well, also accounting in part for this popular observation. The predominant surface wave is the Rayleigh wave, whose amplitude varies with depth in an elastic half-space as shown in Figure 26. The Rayleigh wave motion in a real layered geology is much more complex, but the shape of the principal modes is fairly well represented by these curves. Considering a Rayleigh wave with a period of 0.5 to 1.0 sec and a velocity of 2,000 fps (610 m/sec) an underground opening at a depth of 100 ft (30 m) corresponds to a depth-to-wavelength ratio of 0.05 to 0.10 (wave length = period x velocity). The curves in Figure 26 indicate that the horizontal amplitude of the Rayleigh wave may be significantly smaller at that depth but that the vertical amplitude may actually be larger.

Another important factor in the depth-dependent phenomenon involves the reflection of body waves off the free surface of the earth. Because the earth's surface is stress-free, the amplitude of the motion associated with a body wave reflected there is larger than (up to twice) that of the incident wave. Below the surface, both the incident and reflected waves are present, and their amplitudes and phase relationships combine to produce a complex interference pattern that varies both with time and with depth. Theoretically, for a homogeneous medium, there is a critical depth below which the amplitudes of vertically propagating body waves will be one-half of the surface amplitudes. From the surface down to the critical depth, peak amplitudes are less than the surface values but do not necessarily decrease monotonically with depth.

The exact behavior of motion amplitude with depth depends upon the time duration of the wave train, its velocity in the medium, the angle at which the wave

Richart, Hall, Wood, *Vibrations of Soils and Foundations*,
© 1970, p. 89. Reprinted by permission of Prentice-Hall,
Inc., Englewood Cliffs, New Jersey.



NOTE: ν is Poisson's ratio.

Figure 26. Amplitude ratio versus dimensionless depth for Rayleigh wave. (Adapted from Reference 114.)

1.0

train approaches the surface, and the characteristics of the time history of the approaching seismic wave. This effect is treated in detail later in this chapter.

Finally, the response of the underground structure itself must be considered, as described in Chapter 4. The response will be a function of the manner in which the immediate vicinity of the opening is excited or shaken, along with such factors as the size and shape of the opening, type of rock support, conditions of the surrounding rock or soil, damping, and depth below ground.

Prediction of Underground Motion

Problems Created by Lack of Recorded Motion. Very few records of strong motion in mines and tunnels are available due to a lack of adequate instrumental coverage. Without the actual recorded motion in underground structures where damage has been reported, there is no basis for empirical estimates of the relations between structural damage, associated ground shaking, and such common earthquake parameters as magnitude and epicentral distance.

The absence of well-documented empirical correlations forces the engineer and seismologist to use some type of modeling technique to predict the response of an idealized form of the underground structure. However, the theoretical models representing underground structural response have not been verified by recorded ground motion, and the validity of the predicted response is very much in doubt. One solution to these problems is to substantially increase ground motion recordings in and around underground structures so that both the empirical and theoretical approaches are effective predictors of potential damage and can be used to make recommendations for remedial action.

General Descriptions of Prediction Approaches. Predicting the response of an underground structure located at some particular epicentral distance from a hypothetical earthquake begins at the source region by postulating a certain magnitude event. The most sophisticated way to proceed is to model the earthquake source mathematically using such parameters as fault length, focal depth, and rupture velocity. The outcome of such a model study would be a fairly complete description of the radiation pattern of seismic energy emanating from the fault region. This radiation pattern would contain information about the

amount of seismic energy of each wave type (P, S, Rayleigh, Love) and its directional distribution relative to the source. The accuracy of such a description would be dependent on the accuracy of the faulting model and on knowledge of the surrounding crustal structure. Next, the wave paths to the site could be traced, using known laws of reflection, refraction, and attenuation, with a model of the crustal structure between the source and site regions. The outcome of such a calculation would be a fairly complete description of the seismic wave field at the location of the underground structure. A mathematical model of the underground structure and the surrounding rock mass would be required to complete the problem. The response of the model of the structure and rock mass to the seismic wave field would be the subject of interest to the engineer concerned with design.

A far more simplified approach avoids sophisticated mathematical modeling of the source, transmitting, and site regions; however, this ground motion characterization is almost devoid of detail. The simplified approach would use an assumed earthquake magnitude and an epicentral distance in conjunction with the large number of empirical distance-attenuation relations that have been derived from numerous ground motion recordings to arrive at an estimate of peak ground motion parameters (such as acceleration, particle velocity, and displacement) at the site of the underground structure. Peak ground motion parameters can then be used with empirical correlations to predict cavity response (such as the use of damage correlations developed by Dowding and Rozen^{17,25} to predict tunnel damage).

This latter approach to underground motion prediction is in extreme opposition to the former approach. The former approach provides a virtually complete mathematical description of the theoretical motion of the structure, while the latter approach provides only estimated values (those based on empirical relations) of peak acceleration, particle velocity, or displacement associated with the free-field motion in the vicinity of the structure.

Other approaches to estimating or predicting underground motion at the site might involve use of a "typical" seismogram corresponding to the epicentral distance under question. This seismogram would describe the time history at a point on the earth's surface directly above the underground site. Then, using

techniques described later in this chapter, the seismic wave field for all points below the surface could be estimated and used to excite the response of the underground structure.

DEPTH-DEPENDENCE OF UNDERGROUND MOTION

The nature of subsurface seismic motion in comparison with surface motions and with respect to its variation with depth has been discussed in general terms. To further clarify the manner in which depth influences underground motion, the literature of observational research and theoretical studies is reviewed in this section. In addition, numerical studies are conducted to explore the influence of the duration and characteristics of the time history and the effect of varying the angle of incidence to the ground surface.

Literature Review

Considerable work has been done on selective amplification of seismic waves in near-surface soil layers by Japanese researchers.¹¹⁵⁻¹²² In general, their efforts have been directed toward understanding the effects of near-surface soil conditions upon surface ground motion. Their reports have been largely observational and descriptive, although mathematical studies were presented in some. Shima¹²¹ compared earthquake records at the surface with those in two boreholes at depths of approximately 66 ft (20 m). The site geology consisted of sand and clay layers over gravel. Shima found that the predominant frequencies in the surface records were explained by the multiple reflections of the waves that occurred in the strata above the gravel bed. Kanai et al.¹²² compared records obtained with surface geophones with those obtained with near-surface geophones and attempted to model the data in terms of the multiple reflections in the alluvial soil layers. They considered four sites of various subsoil conditions, generally consisting of layers of sand, clay, and silt over rock. The deepest geophone at each site was at 72.8 ft (22.2 m), 120.7 ft (36.8 m), 122.4 ft (37.3 m), and 171.9 ft (52.4 m). The results indicate that in certain frequency intervals (corresponding to the natural frequencies of the soil system) there is selective amplification of seismic waves and that the high-frequency components, in general, attenuate more rapidly with depth than do the low-frequency components.

Similar studies have been conducted in the United States. Data from a 102-ft (31-m) downhole array in Union Bay (Seattle), Washington, were analyzed by Seed and Idriss¹²³ and others.^{124,125} Joyner et al.¹²⁶ collected data from a downhole array on the shore of San Francisco Bay in California, the deepest monitoring point being 6.6 ft (2 m) below the top of the bedrock at a depth of 610 ft (186 m). Recorded surface motions were compared with surface motions predicted by a simple plane-layered model. They found that simple plane-layered models are capable of giving reasonably good approximations of the effects of local soil conditions for low-amplitude ground motion.

The amplification of seismic waves by near-surface soil layers and the explanation offered by multiple reflection theory were reviewed by Blume¹²⁷ and Okamoto.³³ The general acceptance of this phenomenon is reflected by the current technology for predicting the dynamic response of soil systems as reviewed in Chapter 4.

Researchers have given some attention to earthquake motion at depth, specifically in rock. A series of papers by Kanai et al.^{117-119,122} utilized low-intensity motions recorded in the Hitachi copper mine at depths of 492 ft (150 m), 984 ft (300 m), and 1,476 ft (450 m). It should be noted that the principal intent of these papers was to obtain an understanding of the nature of surface motion that was recorded at an alluvial site approximately 1,000 ft (300 m) away. However, for this discussion, the motions recorded at depth are of interest. The horizontal displacement at the 1,476-ft (450-m) monitoring point was larger than the displacements above it at some instances of time. Furthermore, the peak amplitude at 1,476 ft (450 m) for the entire time history was often of the same order of magnitude as the peak amplitudes above. These records reveal a complexity in the nature of the motion at depth in rock and do not support a definitive statement on the attenuation of seismic amplitudes with depth.

Okamoto³³ reported on a study for which motions were recorded at the surface and at depths of 56.4 ft (17.2 m), 112.2 ft (34.2 m), 168.0 ft (51.2 m), and 220.5 ft (67.2 m) in a vertical shaft at the Kjnugawa Power Station. The geology of the site consisted mainly of hard, coarse-grained tuff. There was almost no difference in displacement between the ground surface and the bottom

of the shaft; however, accelerations in the upper stratum were 1.5 to 2.5 times those of the lower stratum.

Similar results were obtained in a study of accelerograms recorded at a rock site during the 1976 Friuli earthquake sequence.¹²⁸ That study also found that peak accelerations recorded at the surface are normally much higher than those recorded simultaneously at depth. The Fourier spectra of the deeper recordings appear smoother and flatter than those of the surface recordings. An important finding of that study is that significant amplifications of bedrock accelerations may be recorded on the outcrop of a rock mass if the outcrop is heavily weathered at the surface.

It should be noted that some of the underground motions discussed above were recorded in tunnels or power plant caverns; however, this was apparently done for the convenience of obtaining an underground recording site rather than in an attempt to observe behavior specific to an underground opening. Some recent observations have been conducted in three power plant caverns by Ichikawa.¹²⁹ The purpose of those observations was to not only clarify the characteristics of motion with depth but also to determine the behavior of an underground cavity during seismic motion. The observations revealed that the horizontal motions of the two sidewalls were in phase for some earthquakes and out of phase for others and that the vertical motions were always in phase.

The results of ongoing work by Iwasaki on underground seismic motion at four sites around Tokyo Bay¹²⁰ may begin to clarify the differences between earthquake motion recorded in rock as opposed to that recorded in alluvium. Three of the sites -- Futtsu Cape, Ukishima Park, and Ohgishima -- are typical alluvial deposits of sands, silts, and clays, while the fourth site, Kannonzaki, may be characterized as soft rock, consisting of layers of sandstones and siltstones. The deepest borehole accelerometer at each of these four sites is at 361 ft (110 m), 417 ft (127 m), 492 ft (150 m), and 394 ft (120 m). Iwasaki has recorded a sufficient number of earthquakes at these sites to begin to describe statistical trends.¹³⁰

For Ukishima Park (one of the alluvial sites), the mean value of the two horizontal components of acceleration recorded at 417 ft (127 m) is approximately

one-third of the mean value for the surface. Individual records do not vary greatly from this mean; the mean value plus and minus one standard deviation is between one-half and one-quarter of the surface mean. Thus, it would appear that at Ukishima Park peak horizontal accelerations at the surface are amplified approximately two to four times those at depth. This observation is consistent with both theoretical and observational studies of alluvial sites.

The data obtained at Kannonzaki (the soft rock site) are very different from those obtained at Ukishima Park. The mean value of the two horizontal components of acceleration recorded at 394 ft (120 m) at Kannonzaki is 80% of the mean value for the surface. Furthermore, individual records vary rather markedly from this mean, with peak accelerations at depth greatly exceeding peak surface accelerations for some earthquakes. This is reflected by a very large standard deviation, and the mean value plus and minus one standard deviation varies between 132% and 28% of the surface mean. This suggests that, for fairly uniform rock sites, peak accelerations are not, in general, significantly reduced at depth as compared with peak accelerations at the surface. However, individual earthquakes may result in accelerations at depth that are either significantly larger or smaller than the surface accelerations.

A recent paper by Nakano and Kitagawa indicates that there are approximately 200 instruments for recording underground motion in Japan at this time.¹³¹ About 5% of these are actually at the ground surface, 57% are between the surface and a depth of 66 ft (20 m), and 28% are at depths between 66 ft (20 m) and 197 ft (60 m). Thus, 90% are within 197 ft (60 m) of the ground surface. The shallow depth of most of the seismometers and the fact that many are located near buildings indicate that the purpose of this instrumentation is primarily for the analysis of soil-structure interaction. At this time, only two seismometers are located below 660 ft (200 m) -- one at about 1,000 ft (300 m) and the other at about 11,500 ft (3.5 km).

These studies of recorded motion, as well as observations by miners underground during earthquakes,^{16,32} tend to substantiate the notion that motion does reduce with depth. Unfortunately, the data are not sufficient to provide quantitative predictions of the reduction. Furthermore, in some cases the data reveal an increase in motion with depth.

Underground motion predictions by mathematical models have been compared with actual recordings, but the extent of agreement has depended upon the sophistication of the model and the complexity of the site geology. As previously noted, the models that assume shear waves propagating vertically through horizontal layers have provided good agreement with records from sites with horizontally layered soil deposits.^{120,122-126} A very simple model has sometimes been suggested in which a vertically propagating body wave is represented by a single sinusoidal pulse of length equal to the wavelength. Such a model predicts that underground motion (in a half-space) reduces to one-half of surface value at depths greater than one-fourth the wavelength. However, such results are meaningless because the pulse is an oversimplified model of typical earthquake motion. O'Brien and Saunier¹³² have developed a fairly sophisticated model that includes P-, SV-, and SH-waves propagating upward at various angles of incidence in a medium consisting of a single horizontal layer over a half-space. Their model should be more representative of horizontally layered sites than previous models. Unfortunately, their comparison of predicted motion with recorded motion was not very satisfactory because the model did not represent the actual site geology.

Theoretical Formulation of Depth Dependence

The depth dependence of seismic motion due to incident horizontally polarized shear (SH) waves in a homogeneous, isotropic, perfectly elastic half-space is considered below. There is a loss in generalization by considering only SH waves and ignoring vertically polarized shear (SV) waves and compressional waves. However, it is justified for this study because it permits the easy evaluation of underground motion without the complications introduced by coupled waves.

We begin with a brief discussion of the mathematical model to be used in this study. Consider a point located at a depth z_2 below the free surface of a homogeneous, isotropic half-space with S-wave velocity β (see Figure 27).

The general equation governing the displacement in a homogeneous, elastic medium is

$$\rho \frac{\partial^2 \vec{u}}{\partial t^2} = (\lambda + \mu) \nabla(\nabla \cdot \vec{u}) + \mu \nabla^2 \vec{u} \quad (21)$$

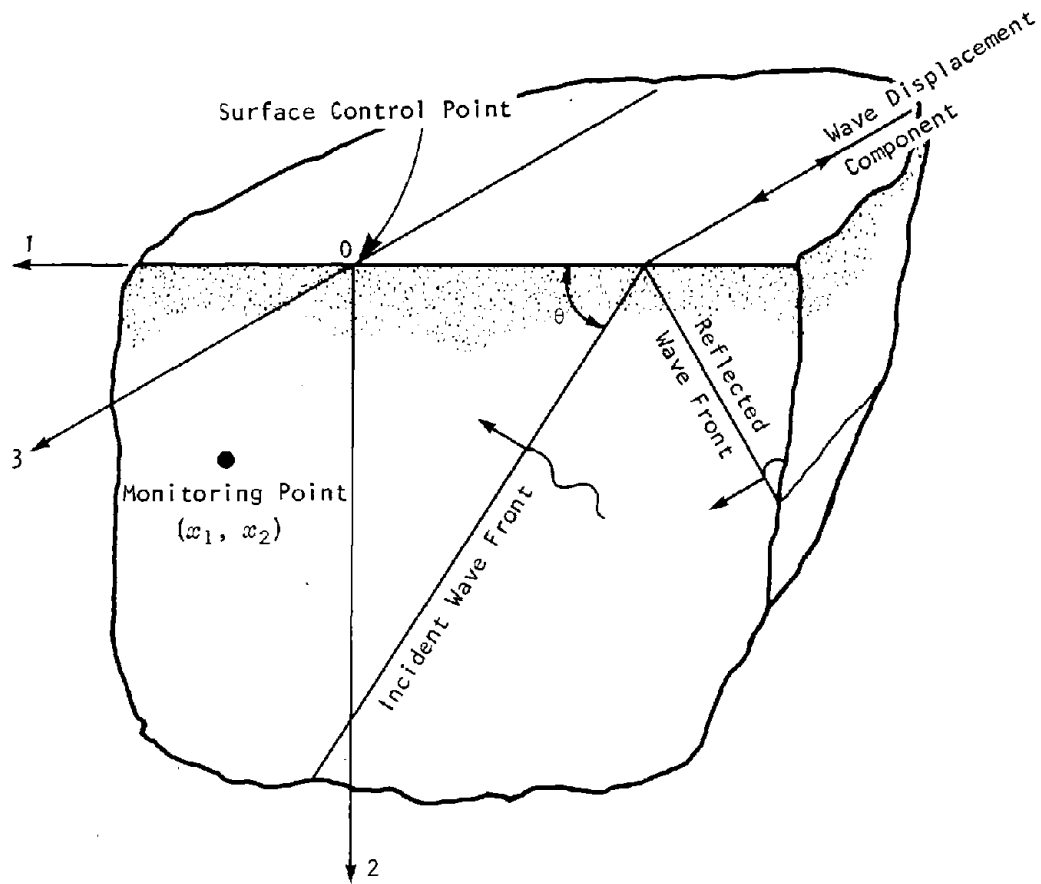


Figure 27. Schematic of coordinate axis, incident and reflected wave fronts at arbitrary angle of incidence, and surface control point.

where ρ is the density of the medium, \vec{u} is the displacement vector, and λ and μ are the Lamé constants of the medium.

For SH motion, Equation (21) reduces to the simple scalar form:

$$\frac{\partial^2 u_3}{\partial t^2} = \frac{\mu}{\rho} \nabla^2 u_3 \quad (22)$$

where $\beta^2 = \frac{\mu}{\rho}$.

The displacement component u_3 describes the antiplane component of the motion defined in the plane of x_1 and x_2 as shown in Figure 27. Consider SH body waves incident at angle θ to the free surface ($x_2 = 0$). This assumes that the source of the motion is sufficiently removed from this region to allow wave front curvature to be neglected. Using the Fourier transform of u_3 defined as

$$U_3(x_1, x_2, \omega) = \int_{-\infty}^{\infty} u_3(x_1, x_2, t) e^{-i\omega t} dt \quad (23)$$

A solution for the displacement field at point (x_1, x_2) may be written in the form

$$U_3 = \left[A_1 e^{-i\frac{\omega}{\beta}x_1 \sin\theta + i\frac{\omega}{\beta}x_2 \cos\theta} + A_2 e^{-i\frac{\omega}{\beta}x_1 \sin\theta - i\frac{\omega}{\beta}x_2 \cos\theta} \right] e^{i\omega t} \quad (24)$$

where ω is the angular frequency of the motion, β is the shear wave velocity (V_s) in the medium, and $i = \sqrt{-1}$. The angle θ is the angle of incidence of the impinging wave measured counterclockwise between the outward normal to the free surface and the normal to the incident wave front. The factors A_1 and A_2 are amplitudes of the waves impinging on and reflected from the free surface, respectively. Application of the stress-free condition at $x_2 = 0$ implies that $A_1 = A_2$. Thus, with the help of trigonometric identities, we may write

$$\begin{aligned} \frac{U_3(x_1, x_2, \omega)}{U_3(0, 0, \omega)} &= \frac{1}{2} \left[e^{i\frac{\omega}{\beta}x_2 \cos\theta} + e^{-i\frac{\omega}{\beta}x_2 \cos\theta} \right] e^{-i\frac{\omega}{\beta}x_1 \sin\theta} \\ &= \cos\left(\frac{\omega}{\beta}x_2 \cos\theta\right) e^{-i\frac{\omega}{\beta}x_1 \sin\theta} \end{aligned} \quad (25)$$

Alternatively, we can take the ratio of $U_3(x_1, x_2, \omega)$ to $U_3^i(\omega)$, the part of the incident displacement that is independent of the spatial variable, namely

$$U_3^i(\omega) = A_1 e^{i\omega t} \quad (26)$$

Since $U_3(0, 0, \omega) = 2U_3^i(\omega)$, Equation (25) becomes

$$\frac{U_3(x_1, x_2, \omega)}{U_3^i(\omega)} = 2 \cos\left(\frac{\omega}{\beta} x_2 \cos \theta\right) e^{-i \frac{\omega}{\beta} x_1 \sin \theta} \quad (27)$$

Equation (27) gives the displacement of the SH component in terms of the incident SH motion as a function of frequency, depth, wave velocity, and angle of incidence. This ratio applies to the case for which the incident wave consists of a harmonic wave of infinite duration, and thus is a frequency-domain transfer function, relating the motion at depth to that of the incident wave field for a frequency ω . Note that substitution of $x_2 = 0$ in Equation (27) gives the familiar effect of amplitude doubling of the incident motion due to reflection at a free surface of SH-waves.

The literature has sometimes reported that amplitudes at depth are one-half those at the surface; that statement, however, is oversimplified and misleading. Equation (25) shows that the amplitude at depth is not half that at the surface. There are an infinite number of depths at which the motion is reduced to one-half its surface value because the incident wave field is assumed to be of infinite duration. Thus, the interference pattern described by Equation (25) is stationary.

Consider now the general problem in which the wave field consists of a displacement time history of arbitrary time dependence. In general, this wave motion will be composed of all frequencies, each with its appropriate amplitude and phase. Let $u_3^0(0, 0, t)$ be the displacement time history of this wave train at the free surface. Then, to find $u_3(x_1, x_2, t)$ at point (x_1, x_2) , we first compute $U_3(0, 0, \omega)$, the Fourier transform of u_3^0 , by Equation (23).

Then, $U_3(0,0,\omega)$ is multiplied by the frequency transfer function given by Equation (25) to obtain $U_3(x_1,x_2,\omega)$. Finally, $u_3(x_1,x_2,t)$ is obtained by the inverse Fourier transform of $U_3(x_1,x_2,\omega)$, given by:

$$u_3(x_1,x_2,t) = \frac{1}{2\pi} \int_{-\infty}^{\infty} U_3(x_1,x_2,\omega) e^{i\omega t} d\omega \quad (28)$$

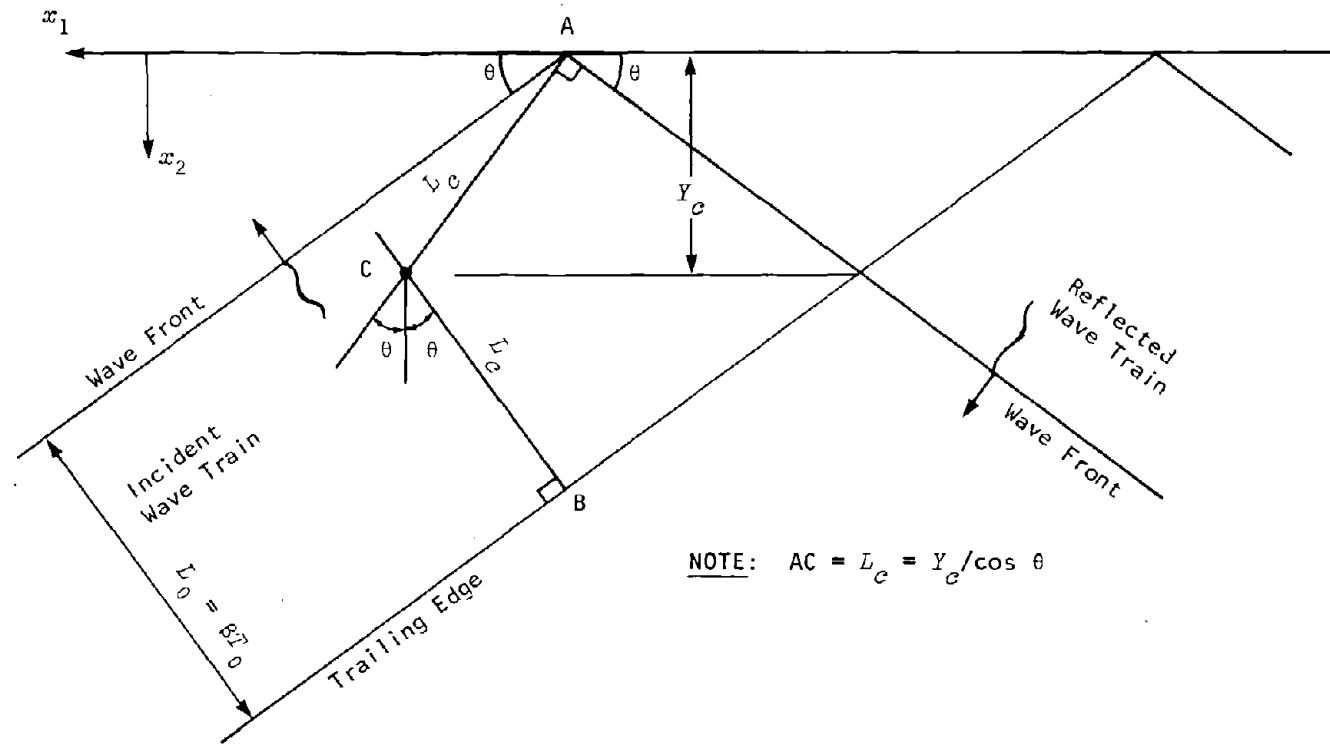
The same general procedure would be followed for the x_1 and x_2 components of the motion (i.e., P and SV), though the details would be somewhat more complicated because these motions are coupled upon reflection from the free surface.

So far, we have discussed the depth dependence as a function of the frequency content of the incident wave field, which relates the amplitude at depth to that at the surface for each frequency. The amplitude of the incident wave field is, of course, a function of magnitude, epicentral distance, etc. The effect of duration is not resolved by the transfer function represented by Equation (25).

Referring to Figure 28, consider now the case where the leading edge of a wave train of finite duration, T_0 , has just reached the free surface at point A. The length of the wave train in space is $L_0 = T_0\beta$. The reflected wave will travel down along path AC at the same time that the trailing edge of the wave train is approaching the free surface along path BC. There will be a critical depth, Y_c , at which the reflected wave and the end of incident train arrive at point C at the same time. From Figure 28, $AC = BC = L_c = Y_c / \cos \theta$, and $L_0 = L_c(1 + \cos 2\theta)$. But $L_0 = \beta T_0$, so that the critical depth is given by

$$Y_c = \frac{\beta T_0 \cos \theta}{(1 + \cos 2\theta)} = \frac{\beta T_0}{2 \cos \theta} \quad (29)$$

Beyond this critical depth, no interference is possible; therefore, the ratio of the peak amplitude at depth to the peak amplitude at the surface will be one-half for all $x_2 > Y_c$. In general this ratio is greater than one-half for depths above the critical depth (that is, for $x_2 < Y_c$). However, if large peaks of comparable magnitudes but opposite signs exist in the incident and



NOTE: $AC = L_c = Y_c / \cos \theta$

Figure 28. Critical depth for interference of incident and reflected wave trains.

reflection waves, it is possible to have occasional isolated depths above the critical depth where, for a particular earthquake record, the amplitude ratio is less than one-half due to destructive interference. Thus, the precise behavior of the amplitude ratio above the critical depth is a function of the detailed nature of the incident time history.

Parametric Studies of Depth Dependence

A computer program has been written that will input a displacement time history for the surface ground motion and then calculate the corresponding displacement and strain at any point at depth. The program considers only plane SH-waves in a homogeneous, isotropic half-space. The origin of coordinates is taken at the surface recording point, with x_1 being the horizontal axis and x_2 the vertical (depth) axis. The program will handle arbitrary angle of incidence of the wave front (i.e., $\theta = 0^\circ$, vertical incidence, to $\theta = 90^\circ$, horizontal incidence). The main input parameters are the shear wave velocity in the medium, the depth of the observation point, the distance off the vertical axis of the observation point, the angle of incidence of the plane wave, and the time history of the ground motion (at the origin).

The program is structured to allow expansion of its capabilities at some time in the future. The next step would be to include layering in the media as well as three-dimensional body wave input (i.e., P, SV, and SH), with the resultant three-dimensional response. Material damping, which involves the use of a complex material modulus, may be easily incorporated into the program. This can be readily accomplished by adding an imaginary part to the shear wave velocity in evaluating the transfer function given by Equation (25).

Study Using a Simple Pulse. To investigate the variation of seismic wave motion with depth, a simple parametric study was conducted considering a horizontally polarized, plane shear wave traveling in a half-space with shear wave velocity, β , and incident to the free surface at an arbitrary angle, θ (see Figure 27).

So as not to obscure the information contained in the parameter variation, a simple wave form of finite duration was chosen as the surface control motion.

The wave is represented by

$$f(t) = \begin{cases} \frac{8\sqrt{3}}{9} \sin\left(\frac{2\pi t}{T_0}\right) \sin^2\left(\frac{\pi t}{T_0}\right) & \text{for } 0 \leq t \leq T_0 \\ 0 & \text{otherwise} \end{cases} \quad (30)$$

The derivatives and integrals of $f(t)$ exist and are well behaved; that is, there are no discontinuities or residuals to make calculations difficult to interpret. The motion at the surface is then specified as

$$u_3(x_1, 0, t) = u_3^{0p} f(t) \quad (31)$$

where $u_3^{0p} = [u_3(0, 0, t)]_{\text{peak}}$, the peak value of the motion at the control point (0, 0).

Two parameters were varied, the depth of the observation point and the angle of incidence of the incoming wave. For this study, the wave form was discretized into 30 equally spaced time intervals of 0.02 sec, resulting in a wave train of 0.60-sec duration (T_0). A constant shear wave velocity of 2,000 fps (609.6 m/sec) was assigned to the medium. Using these values of wave train duration and shear wave velocity, we obtain a critical depth of 600 ft (182.9 m) for a vertically incident wave ($\theta = 0^\circ$) and a critical depth of 693 ft (211.2 m) for a wave incident at $\theta = 30^\circ$.

To observe the variation with depth of the input wave motion, the displacement and strain time histories were computed at five separate depths, $x_2 = 100, 200, 400, 600,$ and $1,000$ ft (30.5, 61.0, 121.9, 182.9, and 304.8 m), and for two angles of incidence, $\theta = 0^\circ$ and 30° . The depths were chosen to bracket the critical depth in order to observe the effect of the interference of the incident and reflected wave trains.

The first case considered is that of a vertically incident wave ($\theta = 0^\circ$). The time histories of the displacement, u_3 , and of the strain component*, ϵ_{32} , have been computed for each of the designated depths and are presented in Figures 29 and 30, respectively. The displacement time histories (Figure 29) clearly show

*The strain component ϵ_{ij} is the shear strain between the x_i and x_j directions, $i \neq j$.

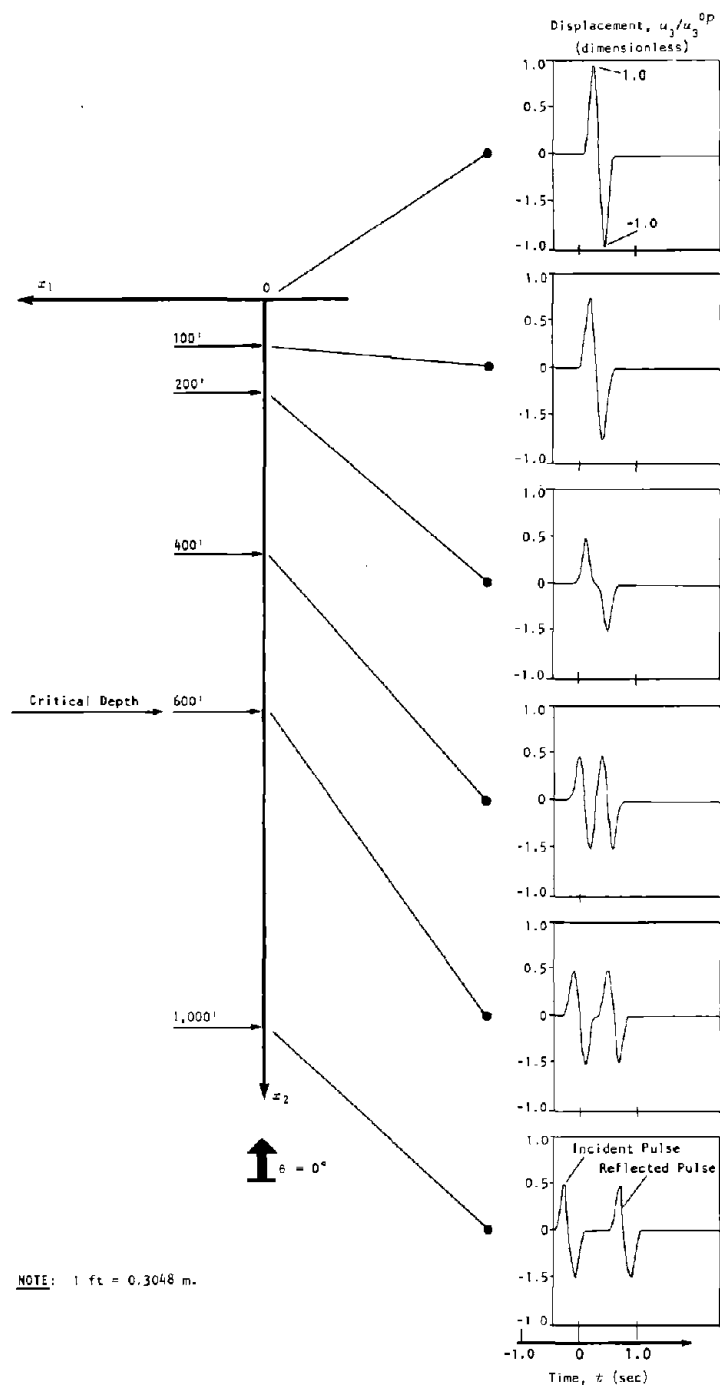


Figure 29. Displacement time histories at depth for vertically incident wave ($\theta = 0^\circ$).

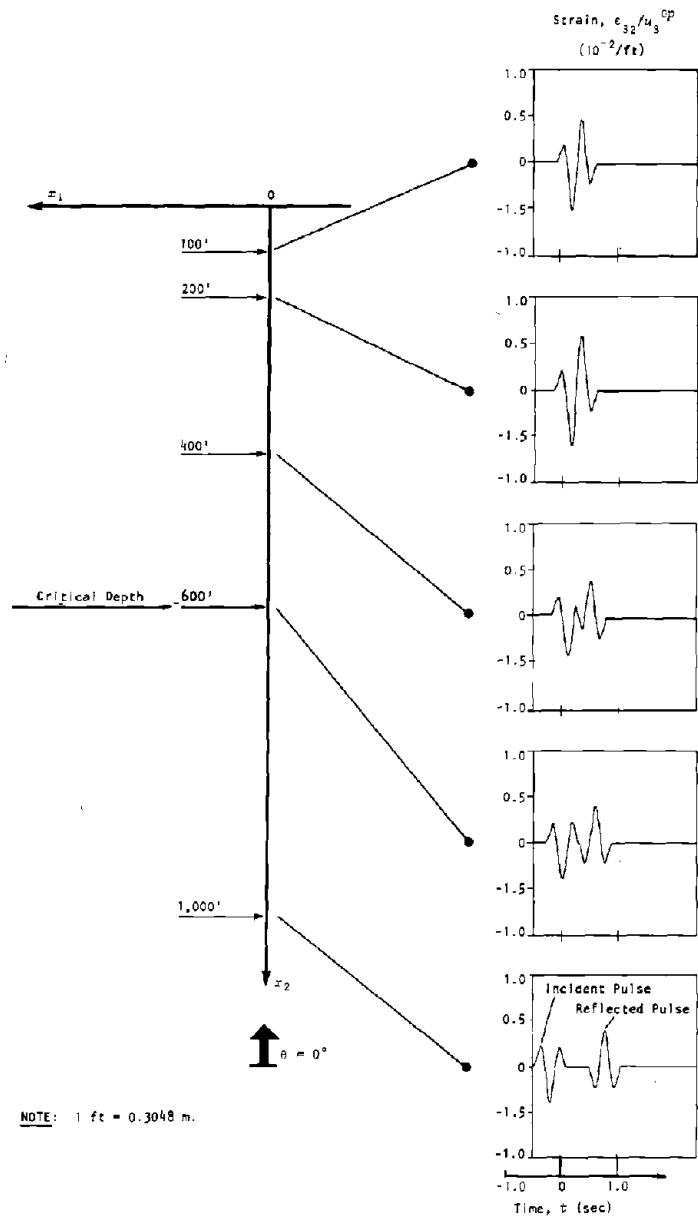


Figure 30. Strain component, ϵ_{32} , time histories at depth for vertically incident wave ($\theta = 0^\circ$).

the effects of depth. The incident and reflected wave trains are completely separated below the critical depth, resulting in the wave amplitude always being one-half the surface amplitude depth. For the chosen wave form, the ratio of the amplitude at depth to the surface amplitude gradually reduces from a value of one at the surface to a value of one-half upon reaching the critical depth.

The strain component ϵ_{32} time histories monitored at the same depths are displayed in Figure 30. (Note: $\epsilon_{32} = 0$ at the surface due to the stress-free boundary condition, and $\epsilon_{31} = 0$ at all points because $\theta = 0^\circ$.) Again, the separation between the incident and reflected wave trains below the critical depth is clearly observed. This figure illustrates the nonuniformity of the reduction of amplitude with depth. Here the amplitude of the ϵ_{32} strain component at the 200-ft (61-m) monitor point is clearly larger than the amplitude at the 100-ft (30.5-m) monitor point. Note also the sign change in the ϵ_{32} strain component between the incident θ and reflected wave trains.

The wave form incident to the free surface at $\theta = 30^\circ$ is shown in Figure 31. The displacement time history at the surface is assumed to be the same as that for the vertically incident wave. The displacement time history at depth is similar to that for the vertically incident wave, except that the amplitude reduction near the surface is less for the wave incident at $\theta = 30^\circ$. At $x_2 = 100$ ft (30.5 m) there is a 26% reduction in amplitude from the surface amplitude for $\theta = 0^\circ$ incidence and a 20% reduction for $\theta = 30^\circ$. Figure 32 displays both components of strain ϵ_{31} and ϵ_{32} for a wave incident at $\theta = 30^\circ$.* Here both the ϵ_{31} and ϵ_{32} strain components do not exhibit a uniform reduction of amplitude with depth. The amplitude of the ϵ_{31} component at the 400-ft (121.9-m) monitor point is 100% larger than the amplitude at the 200-ft (61-m) monitor point. Similarly, the amplitude of the ϵ_{32} component at the 200-ft (61-m) monitor point is 30% greater than that at the 100-ft (30.5-m) monitor point.

The variation of displacement and strain with angle of incidence is shown in Figures 33 and 34. The monitoring point was taken off axis at $x_1 = -100$ ft

* $\epsilon_{32} = 0$ at the surface. $\epsilon_{31} \neq 0$ at the surface and is double the incident strain pulse.

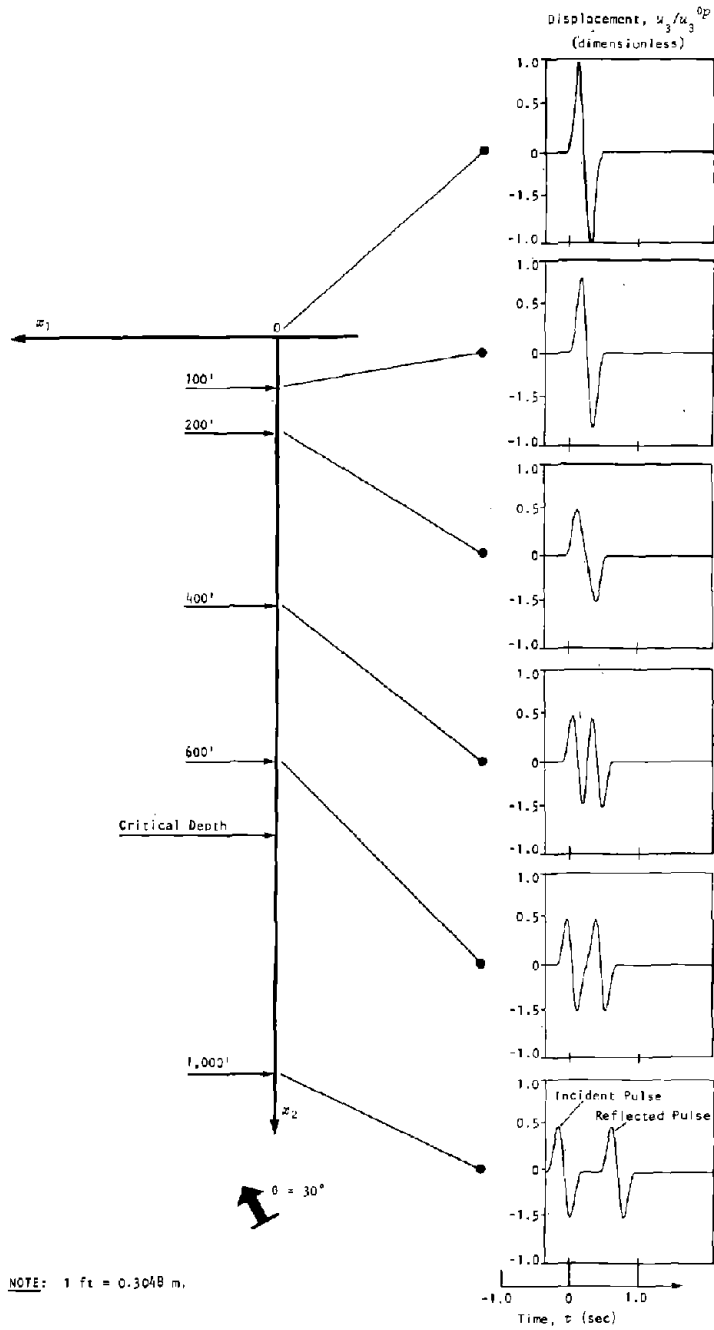


Figure 31. Displacement time histories at depth for wave incident at $\theta = 30^\circ$.

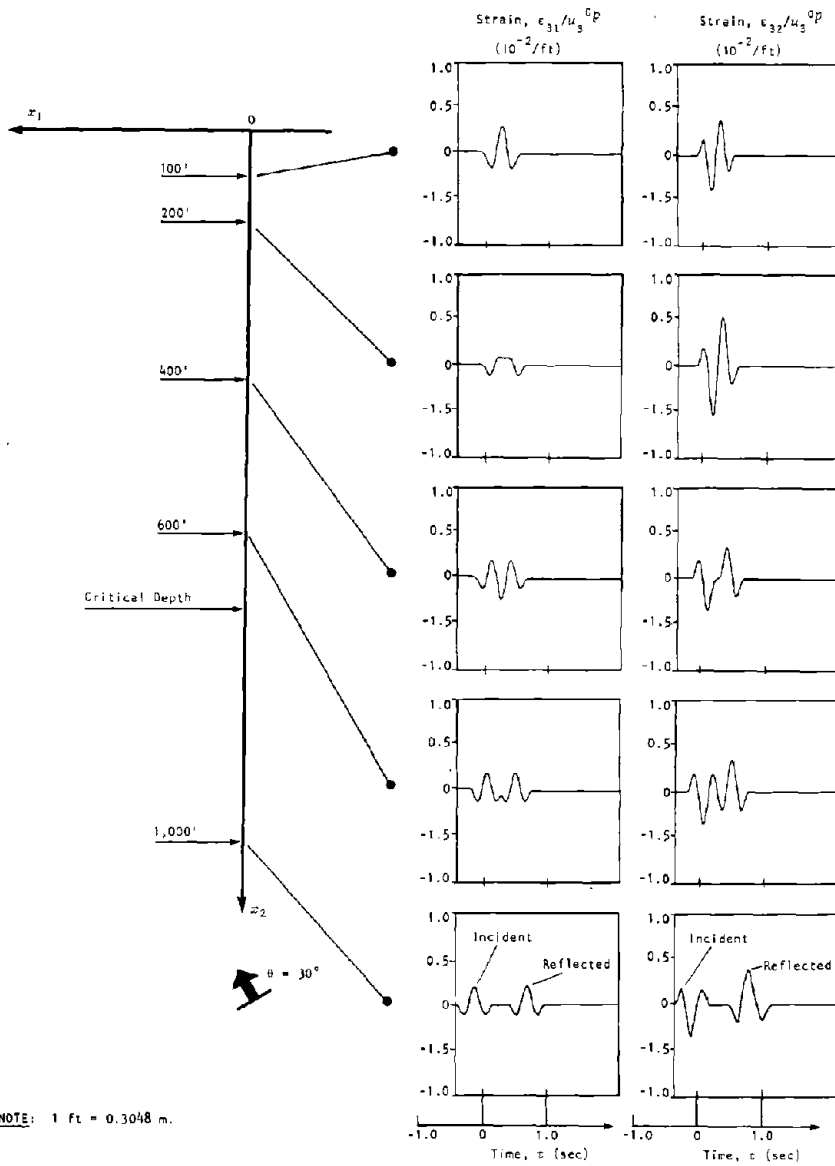


Figure 32. Strain components, ϵ_{31} and ϵ_{32} , time histories for angle of incidence $\theta = 30^\circ$.

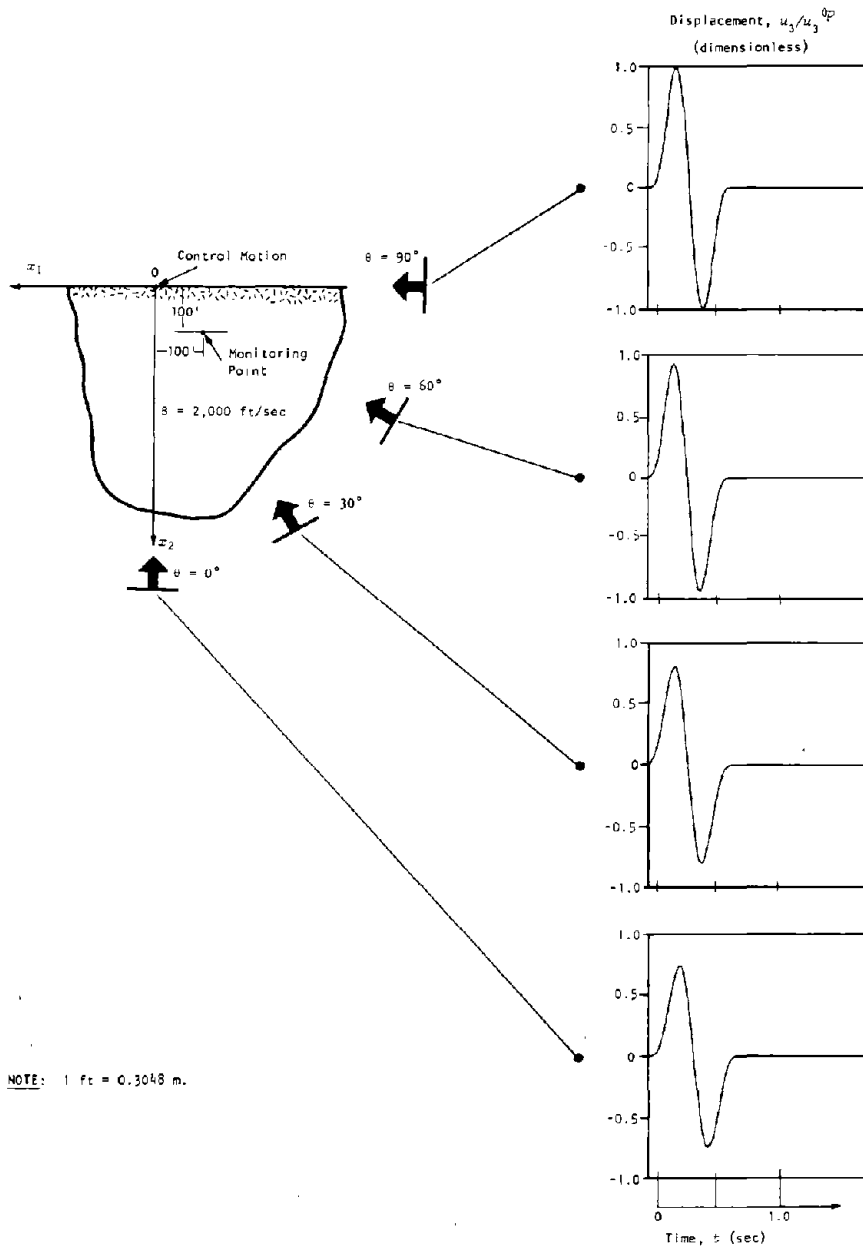
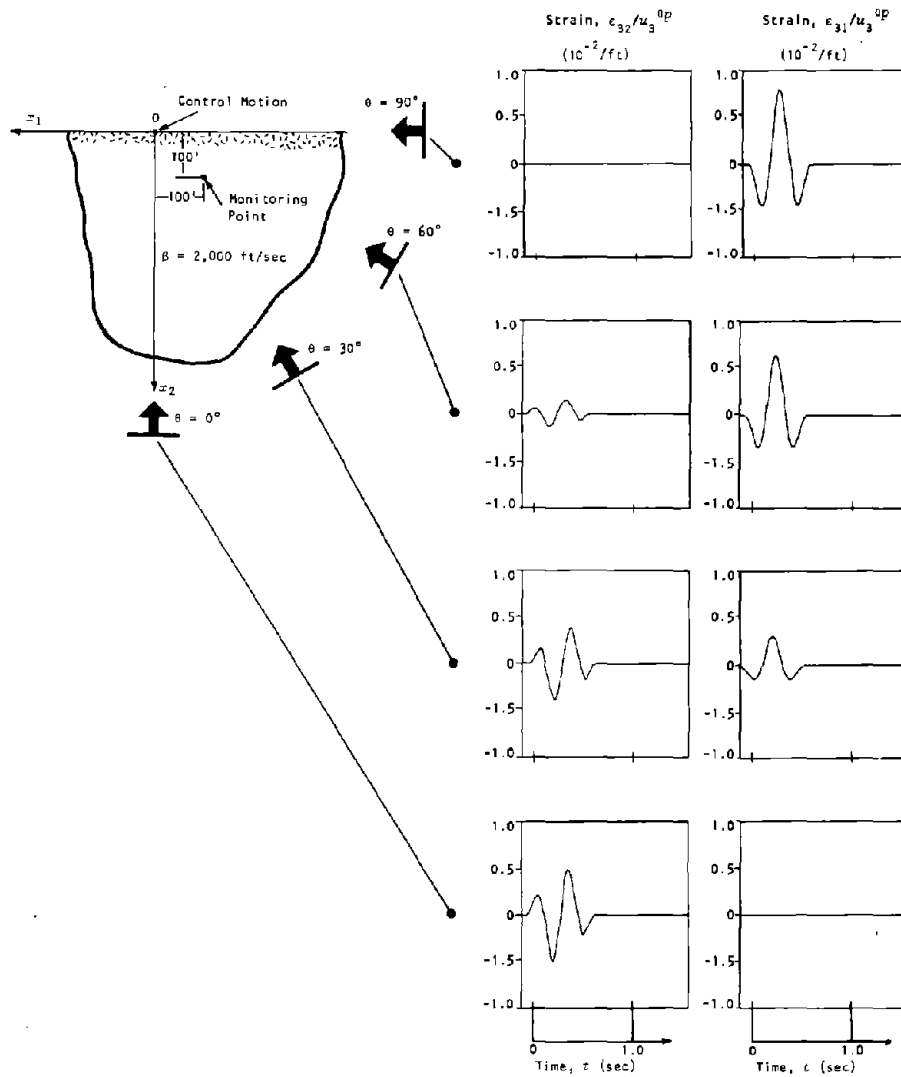


Figure 33. Displacement time histories at the same monitoring point for variable angle of incidence of incoming wave.



NOTE: 1 Ft = 0.3048 m.

Figure 34. Strain components, ϵ_{31} and ϵ_{32} , time histories at the same monitoring point for variable angle of incidence of incoming wave.

(-30.5 m) and at $x_2 = 100$ ft (30.5 m), and the displacement and strain time histories were calculated for angles of incidence of $\theta = 0^\circ, 30^\circ, 60^\circ,$ and 90° . The displacement time history (Figure 33) for $\theta = 90^\circ$ shows no reduction in amplitude because there is no reflection off the free surface and consequently no interference of incident and reflected wave trains. There is a reduction in amplitude as the wave front approaches the vertical angle of incidence, where it is reduced to approximately 80% of its surface value.

Study Using an Earthquake Time History. To observe depth effects with an actual earthquake time history, the Tumbler N65W record of the 1966 Parkfield earthquake was chosen as the surface control motion. The record was of particular interest due to several factors: it was a free-field rock site recording at a hypocentral distance of 9.9 miles (16 km), it had a relatively high horizontal peak acceleration of 0.27g for a magnitude 5.6 event, and it displayed approximately 1.5 sec of ground acceleration equal to or greater than one-half the peak ground acceleration. The raw acceleration was fitted with a parabolic baseline connection and integrated twice to obtain the ground displacement. The first 22.72 sec of record were analyzed, and the displacement time history calculated for the depths is given in Figure 35, assuming $\theta = 0^\circ$ and $\beta = 2,000$ fps (609.6 m/sec).

The interference between the incident and reflected wave trains can be observed in Figure 35. The two wave trains are completely superimposed on each other at the ground surface, resulting in a doubling of displacement amplitudes at the surface. Another way to view this is to observe that the two wave trains separate with depth so that below the critical depth the amplitudes are one-half those at the surface. However, the peak displacement amplitudes do not reduce uniformly with depth. In this example, the peak amplitude is reduced by 5% at a depth of 1,000 ft (305 m) and by 34% at 4,000 ft (1,219 m). At 8,000 ft (2,438 m) it is still only reduced by 34%. At 12,000 ft (3,658 m) it is reduced to 50%, but at 16,000 ft (4,877 m) it is increased, with only a 31% reduction from the surface value. This nonuniformity in the reduction of amplitudes with depth is due to the interference between different peaks in the incident and reflected waves. Clearly, then, the spatial arrangement of the peaks within the time histories have an important influence on the reduction of amplitudes with depth.

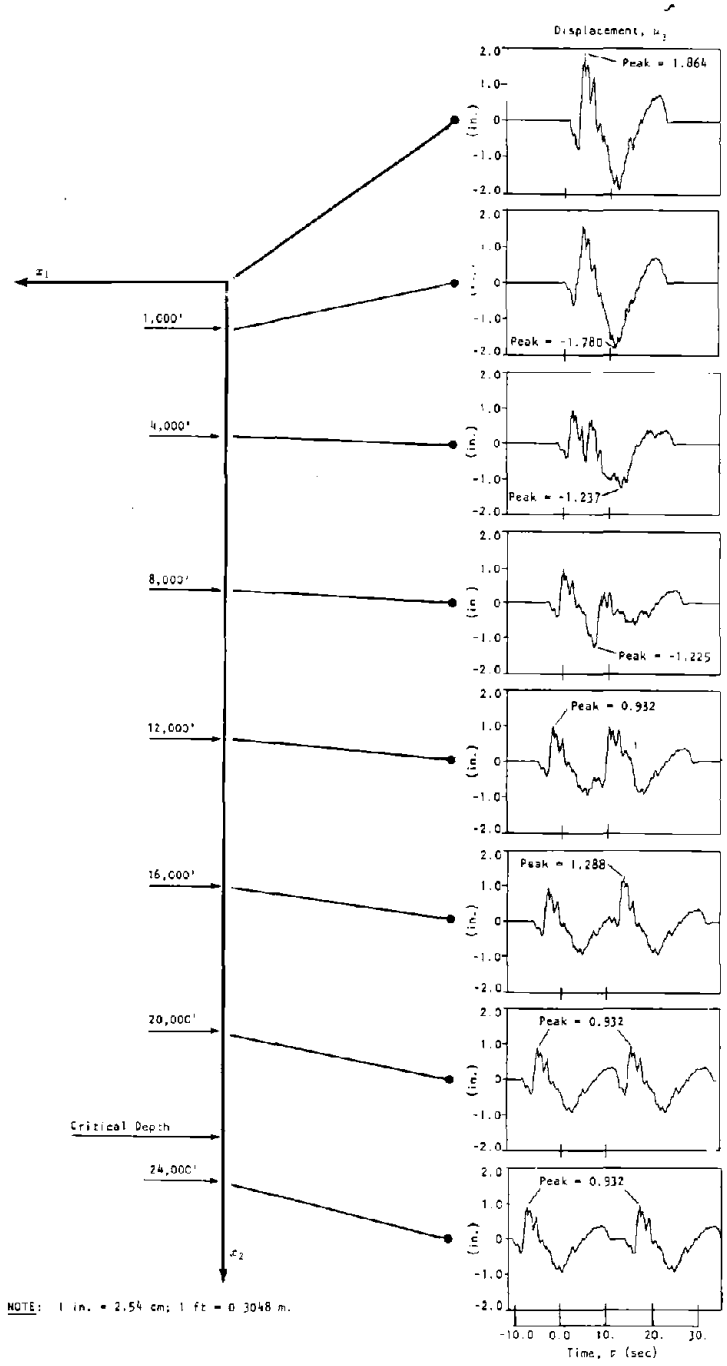
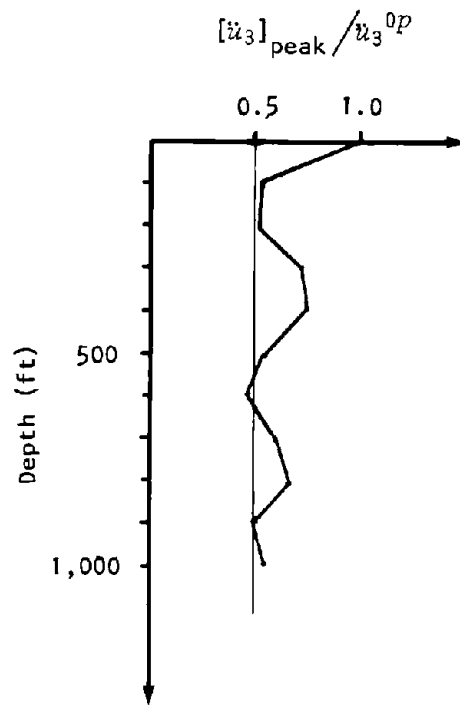
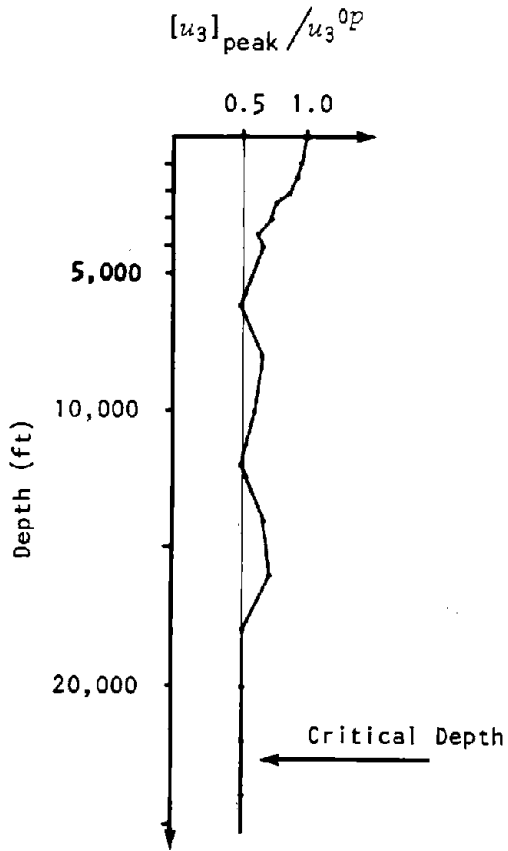


Figure 35. Displacement record of the 1966 Parkfield (California) earthquake monitored to below the critical depth.

Nonuniformity in the reduction with depth is very clearly observed by the plot of peak displacement with depth in Figure 36. For purposes of comparison, the acceleration time history for the Temblor N65W record was also analyzed, and the variations of peak acceleration with depth are plotted to a depth of 1,000 ft (305 m). Although the peak acceleration drops to nearly one-half the surface value at a depth of 100 ft (30.5 m), it increases again substantially at 400 ft (121.9 m). For this particular record, where almost all the high peaks in the acceleration time history occur within a 2-sec interval, the peak accelerations below 1,000 ft (305 m) remain approximately one-half the surface value. However, for acceleration time histories with major peaks over an interval of many seconds, a much slower trend in reduction with depth is found.

This parametric study shows that it is not possible to make a general statement about the amount of reduction that occurs with depth. There is some point, called the critical depth in this report, below which the incident and reflected body waves will not interfere. In the case of a homogeneous, elastic half-space the peak motions below the critical depth will be one-half the peak motions at the surface. The critical depth depends upon the duration of the strong motion, T_0 , the wave velocity, and the angle of incidence, θ . For SH-waves, the critical depth is given by Equation (29). When considering a realistic earthquake record at the surface, such as the Temblor record for the 1966 Parkfield earthquake, this study showed that peak motions may decrease with depth at first and then increase again before finally reducing to one-half at the critical depth. Furthermore, the critical depth might be extremely deep -- in this example, 22,720 ft (6.93 km) for a duration of 22.72 sec. The variation of the maximum amplitude with depth (between the surface and the critical depth) and the complexity of the wave form will greatly depend upon the character of the surface record used in this type of study.

When considering shallow depths -- say within 300 ft (100 m) of the surface -- in homogeneous materials, this study shows little reduction. This finding agrees with the data reported by Iwasaki et al.¹²⁰ for a Tokyo Bay site (Kannonzaki) which consists of fairly homogeneous rock layers from the surface to the deepest monitoring point. Thus, when considering a site that is fairly homogeneous with



b. Ratio of peak acceleration at depth to peak acceleration at the surface

a. Ratio of peak displacement at depth to peak displacement at the surface

NOTE: 1 ft = 0.3048 m.

Figure 36. Variation of peak displacement and peak acceleration with depth for the 1966 Parkfield (California) earthquake.

depth, the reduction in amplitude with depth is expected to be very small for body waves.

This parametric study did not consider the effect of surface layers on ground motion. Soil layers, particularly soft soils overlying hard rock, are responsible for large reductions in peak motion with depth. Actually, the inverse statement better describes the situation. Soil layers amplify the incoming incident wave as it propagates upward from the bedrock, resulting in very large amplifications of peak motion at the ground surface as compared with those in the bedrock. It is well known that the peak surface motions for soil sites are associated with the frequencies in the wave that correspond to the natural frequencies of the soil system. Most reductions in peak ground motion recorded at depth are undoubtedly due to near-surface geology, such as layering.

DYNAMIC RESPONSE OF UNDERGROUND CAVITIES

This section deals with the dynamic response of a two-dimensional cavity in an elastic half-space. The cavity is circular in cross section. Its axis lies at a finite distance from and parallel to the free surface of the half-space. The seismic excitation is represented by a plane, SH-wave of arbitrary angle of incidence. Its displacement component is parallel to the infinite dimension of the cavity and, of course, parallel to the free surface. This is schematically shown in Figure 37.

There is a loss in generalization by considering only SH-waves and ignoring SV-waves and P-waves. It is justified for this study because it permits the easy evaluation of cavity response in a half-space without the complications introduced by coupled waves.

The integral equation method was chosen to evaluate the response of the two-dimensional cavity. The integral equation was formulated by the use of the appropriate form of the Green's function for the half-space, thereby satisfying the stress-free conditions on both the free surface of the half-space and on the surface of the cavity. The integral equation was discretized, casting it in a matrix form of a system of linear equations with complex coefficients.

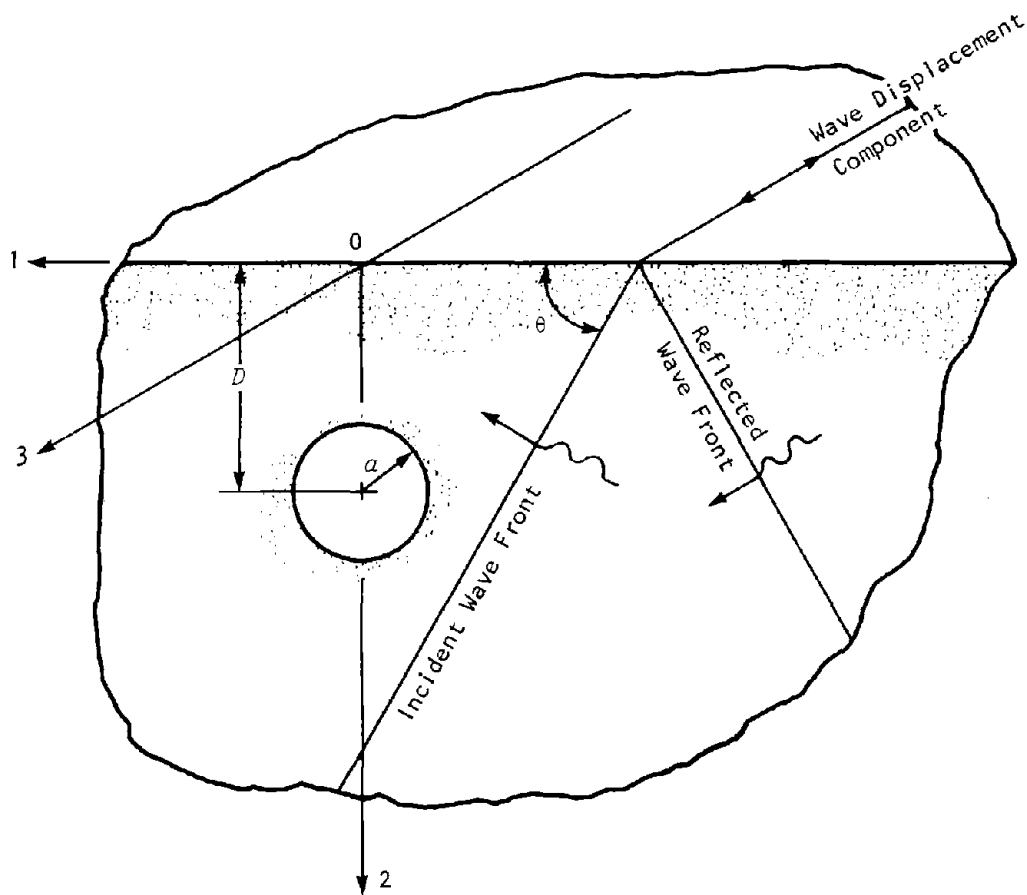


Figure 37. The cavity, coordinates, and excitation.

The system was solved for impinging plane waves of several angles of incidence.

There are basically two approaches to predicting the response of a cavity in a half-space: discrete model methods, such as finite difference and finite element, and integral equation methods. The advantages and disadvantages of the discrete models have been discussed previously (Chapter 4). However, it is worth noting that there are several drawbacks to using finite-element and finite-difference codes to study cavity response in a half-space. One drawback is that a cavity at great depth would require a fine mesh to obtain high resolution of the response, thus necessitating a prohibitively large storage capacity in the computing machine. Also, radiations from the boundaries of the modeled region other than the free surface will contaminate the response. Although there are special absorbing boundaries to control this effect, the problem cannot be entirely eliminated. Another disadvantage of the finite-element and finite-difference methods is that a generalized seismic input with an arbitrary angle of incidence to the free surface cannot be used.

The integral equation method offers several unique advantages. Because there are no artificial boundaries in the model, spurious reflections do not exist. Thus, the radiation of the scattered wave field is correctly incorporated in the solution through the use of the Green's function. Furthermore, a cavity at great depth does not require a large storage capacity in the computing machine. Another advantage of the integral equation method is that through steady-state formulation the earth material can readily be made viscoelastic. Although this was not done for this study, it can be easily achieved by the addition of a frequency-dependent imaginary part to the material modulus. At present, the integral equation method has not been developed sufficiently to account for spatial variations in material properties.

Literature Review

A large number of excellent papers treating the scattering of plane seismic waves by cylindrical holes and rigid inclusions have been published; however, no studies have been reported on the scattering of seismic waves by cavities in a half-space. The scattering of compressional waves by a rigid cylinder in a

full space was studied by Gilbert and Knopoff.¹³³ They obtained the exact solution in integral form, which they evaluated asymptotically for an estimate of first motions. Gilbert¹³⁴ presented the scattering of P-, SV-, and SH-waves by a cavity of circular cross section in a full space, similarly looking at first motions. Banaugh and Goldsmith,¹³⁵ using an integral equation formulation, studied the scattering of plane steady-state acoustic waves by cavities of arbitrary shape embedded in a full space. The transient response of an elastically lined circular cylinder in a full space excited by a plane compressional wave was given by Garnet and Crouzet-Pascal.¹³⁶ In a very thorough study, Mow and Pao⁶⁵ treated both transient and steady-state diffraction problems of all wave types by various scattered configurations. Their work also contains an excellent bibliographic review of previously published studies.

Other studies worthy of mention include a very recent paper by Niwa et al.,¹³⁷ who used the integral equation method to study the transient stresses around a tunnel, lined or unlined. They obtained a good comparison with the results of Garnet and Crouzet-Pascal.¹³⁶ Niwa et al.¹³⁷ also dealt with the full space problem, as did all the authors of the previously cited works. Glass⁶¹ summarized previous closed-form solutions for lined circular cavities and used the finite-element method to extend these analyses to adjacent unlined cavities. Studies have also been performed by Yoshihara et al. at the University of Illinois at Urbana.¹³⁸ The above-mentioned publications are not a complete bibliographic review, but they serve to highlight the background for this study.

Theoretical Formulation of Cavity Response

Consider the displacement field in the half-space as excited by a plane, horizontally polarized shear wave of angle of incidence θ measured between the normal to the wave front and the outward normal to the free surface at $x_2 = 0$. The exciting wave is propagating to the left in the positive sense of x_1 , as illustrated in Figure 37. The total displacement in the half-space in the absence of the cavity is due to this wave and the reflected wave from the free surface. The Fourier transform of this displacement was given by Equation (25):

$$U_3(x_1, x_2, \omega) = U_3^0(\omega) \cos\left(\frac{\omega}{\beta} x_2 \cos \theta\right) e^{-i \frac{\omega}{\beta} x_1 \sin \theta}$$

where $U_3^0(\omega) = U_3(0,0,\omega)$, the Fourier transform of the displacement time history in the absence of the cavity as observed at point 0.

The cavity, of radius a , is located with its center at depth $x_2 = D$ from the free surface. Notice that the cavity center is directly beneath point 0.

Introducing a cylindrical polar coordinate system whose origin is at the cavity center, the relation to the original Cartesian system is given by

$$x_1 = r \sin \psi \quad (32)$$

$$x_2 = D + r \cos \psi \quad (33)$$

in which the polar angle ψ is measured clockwise starting from the x_2 -axis as shown in Figure 38, and r is the polar distance given by

$$r = \sqrt{x_1^2 + (x_2 - D)^2} \quad (34)$$

Using these new coordinates, we can alternatively express the incident wave field given in Equation (25) as

$$U_3(r, \psi; \omega) = U_3^0(\omega) \cos \left(\frac{\omega}{\beta} \cos \theta (D + r \cos \psi) \right) e^{-i \frac{\omega}{\beta} r \sin \psi \sin \theta} \quad (35)$$

Introducing the appropriate form of the Green's function for this problem, it is given in the Cartesian coordinates by

$$G_{33}(x_1, x_2, \xi_1, \xi_2, \omega) = \frac{-i}{4\mu} \left[H_0^{(2)} \left(\frac{\omega}{\beta} \sqrt{(x_1 - \xi_1)^2 + (x_2 - \xi_2)^2} \right) + H_0^{(2)} \left(\frac{\omega}{\beta} \sqrt{(x_1 - \xi_1)^2 + (x_2 + \xi_2)^2} \right) \right] \quad (36)$$

where μ is the shear modulus of the half-space, ξ_1 and ξ_2 are the coordinates of the source point, and $H_0^{(2)}(Z)$ is the Hankel function of the second kind of order zero of argument Z . Specifically, Equation (36) gives the displacement component in the direction 3 at point (x_1, x_2) due to a line force acting in direction 3 at (ξ_1, ξ_2) for the harmonic component of frequency ω . Notice that the second Hankel function in Equation (36) gives the contribution from an image

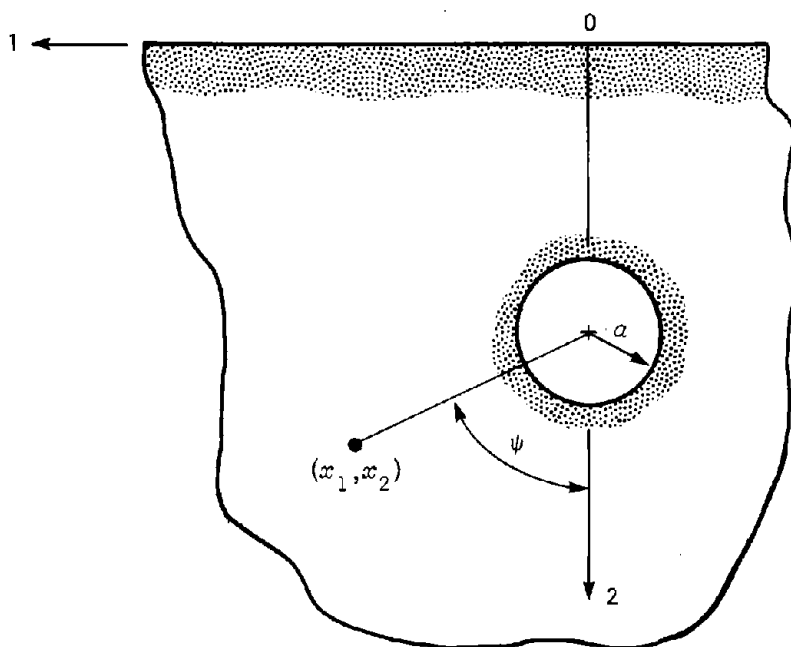


Figure 38. Relation between Cartesian coordinates and cylindrical polar coordinates.

source representing the effect of the free surface at $x_2 = 0$. Appendix E gives the derivation of this Green's function.

Using the new polar coordinates, we can rewrite the Green's function given in Equation (36) as

$$G_{33}(r, \psi, \zeta, \eta; \omega) = \frac{-i}{4\mu} \left[H_0^{(2)}\left(\frac{\omega}{\beta} R\right) + H_0^{(2)}\left(\frac{\omega}{\beta} R^*\right) \right] \quad (37)$$

in which the source-observation point distance is

$$R = \sqrt{r^2 + \zeta^2 - 2r\zeta \cos(\psi - \eta)} \quad (38)$$

and the image source-observation point distance is

$$R^* = \left[r^2 + \zeta^2 + 2r\zeta \cos(\psi + \eta) + 4r^2 \left(1 + \frac{D}{r} \cos \psi + \frac{D\zeta}{r^2} \cos \eta \right) \right]^{1/2} \quad (39)$$

The coordinates ζ and η are the source point cylindrical polar radial distance and angle, respectively, analogous to r and ψ of the observation point.

The problem of determining the response of the cavity surface due to any impinging wave can be found in the solution to the following integral equation:⁶⁵

$$U_3(a, \psi) = \frac{1}{2} U_3^e(a, \psi) - \mu \int_A U_3^e(a, \eta) \frac{\partial}{\partial n} G_{33}(a, \psi, \zeta = a, \eta) dA(\eta) \quad (40)$$

where A denotes the perimeter of the cavity, and n is the outward normal to the cavity surface. In Equation (40), the frequency ω in the function arguments has been omitted for convenience. The solution of Equation (40), $U_3^e(a, \eta)$, then, is the desired displacement response of the cavity perimeter due to the incident wave $U_3(a, \psi)$. Equation (40) can be discretized as

$$U_3(a, \psi_j) = \frac{1}{2} U_3^e(a, \psi_j) + \mu a \Delta \eta \sum_{m=1}^N U_3^e(a, \eta_m) \frac{\partial}{\partial \zeta} G_{33}(a, \psi_j, a, \eta_m) \quad (41)$$

in which the sum on m replaces the integral, and the incremental circumferential length becomes

$$dA(\eta) = a\Delta\eta = a \frac{2\pi}{N} \quad (42)$$

The normal derivative is given by the negative of the radial derivative. This last term can be determined from Equation (37) for $m \neq j$ as

$$\begin{aligned} & \mu \frac{\partial}{\partial \zeta} G_{33}(a, \psi_j, a, \eta_m) \\ &= \frac{i\omega}{4\beta} \left\{ \sqrt{\frac{1 - \cos(\psi_j - \eta_m)}{2}} H_1^{(2)} \left(\frac{\sqrt{2} \omega a}{\beta} \sqrt{1 - \cos(\psi_j - \eta_m)} \right) \right. \\ &+ H_1^{(2)} \frac{\sqrt{2} \omega a}{\beta} \sqrt{1 + \cos(\psi_j + \eta_m) + 2 \left(\frac{D^2}{a^2} + \frac{D}{a} \cos \psi_j + \frac{D}{a} \cos \eta_m \right)} \\ &\left. \left[1 + \cos(\psi_j + \eta_m) + 2 \frac{D}{a} \cos \eta_m \right] / \right. \\ &\left. \left[\sqrt{2} \sqrt{1 + \cos(\psi_j + \eta_m) + 2 \left(\frac{D^2}{a^2} + \frac{D}{a} \cos \psi_j + \frac{D}{a} \cos \eta_m \right)} \right] \right\} \quad (43) \end{aligned}$$

and for $m = j$ after using the appropriate asymptotic form for the Hankel function

$$\begin{aligned} & \mu \frac{\partial}{\partial \zeta} G_{33}(a, \psi_j, a, \eta_j) \\ &= \frac{i\omega}{4\beta} \left\{ \frac{i\omega}{\pi\omega a} + H_1^{(2)} \left(\sqrt{2} \frac{\omega a}{\beta} \sqrt{1 + \cos 2\eta_j + 2 \left(\frac{D^2}{a^2} + 2 \frac{D}{a} \cos \eta_j \right)} \right) \right. \\ &\left. \left[1 + \cos 2\eta_j + 2 \frac{D}{a} \cos \eta_j \right] / \right. \\ &\left. \left[\sqrt{2} \sqrt{1 + \cos 2\eta_j + 2 \left(\frac{D^2}{a^2} + 2 \frac{D}{a} \cos \eta_j \right)} \right] \right\} \quad (44) \end{aligned}$$

The incident wave expression of Equation (35) can also be evaluated at the same discretization points. This yields

$$U_3(a, \psi_j) = U_3^0(\omega) \cos \left(\frac{\omega}{\beta} \cos \theta (D + a \cos \psi_j) \right) e^{-i \frac{\omega}{\beta} a \sin \psi_j \sin \theta} \quad (45)$$

Substitution of Equations (43), (44), and (45) into Equation (41) leads to an $N \times N$ system of linear equations in $U_3^c(\alpha, \psi_j)$ with complex coefficients.

The response of the cavity $U_3^c(\alpha, \psi_j)$, as defined by Equation (41), is put into dimensionless form before solution. Dividing it by the Fourier transform of the surface motion $U_3^0(\omega)$ leads to a system of equations in the ratios of the cavity response at the discretization points on the circumference to the motion above on the free surface. This division conveniently removes the dimensionality of Equation (41). Thus, the solution has been generalized for any arbitrary time dependence associated with the incident wave. A spectral multiplication of the response ratio for the point on the cavity surface with the Fourier transform of the time history to be assigned to the surface motion results in the Fourier transform of the response of that point. A Fourier inversion yields the corresponding response time history at that point.

Numerical Study of Cavity Response

For convenience, the frequency was expressed in a dimensionless form as

$$\Omega = \omega a / \beta \quad (46)$$

and is identical to Ω defined by Equation (12). For most applications, the dimensionless frequency range $0 \leq \Omega \leq 1.0$ should be adequate. The significant frequencies in damaging earthquakes should range from 0.1 to 15.0 Hz. Shear wave velocities should range from 1,000 fps (305 m/sec) for a stiff soil to 10,000 fps (3,050 m/sec) for granite. For tunnels of radius 10 ft (3 m), the range of interest in the dimensionless frequency would be $0.006 \leq \Omega \leq 0.942$ for a stiff soil and $0.0006 \leq \Omega \leq 0.094$ for granite. Only in the case of a very large tunnel -- that is, a tunnel with a radius much greater than 10 ft (3 m) -- in stiff soils will the range of the dimensionless frequency extend beyond 1.0.

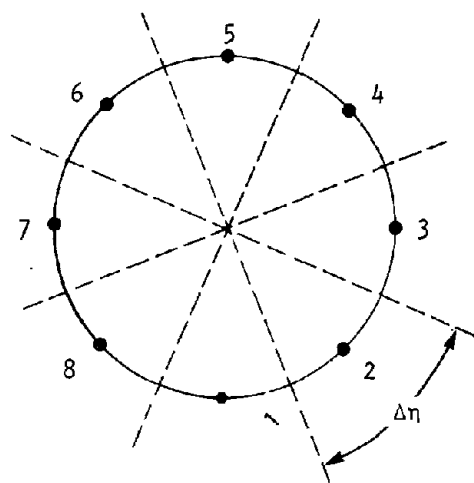
The number of discretization points used varied with the frequency of the wave motion. For values of Ω between zero and 0.4, 16 points were used in the discretization. In the interval 0.4 to 0.6, 32 points were used. Finally from 0.6 to 1.0, 64 points were used. This scheme was selected to assure a sufficient number of points per wavelength, especially for the higher frequency

range. Figure 39 graphically depicts the discretization scheme for $N = 8$. The accuracy of the discretization technique used here was not studied. This consideration has been reported elsewhere.^{65,135}

The solution of the set of equations described above was performed using a complex Gaussian elimination procedure, which was verified to have an accuracy of 5×10^{-13} compared with 1.0.

Results of Numerical Study. The response ratios obtained in the solution of the discretized integral equation are for a particular value of the frequency. As an example of the kind of results obtained therein, Figure 40 shows the response ratio values around the circumference of the circle for four different angles of incidence of the impinging wave. Both the real and imaginary parts are displayed, inward towards the circle center being a positive value. The frequency for the response depicted in Figure 40 has the value 0.4. The depth-to-radius ratio, D/a , is 6. Notice that for 0° angle of incidence the cavity response is symmetric about the vertical centerline, as should be expected. As the angle of incidence increases to that of a horizontally impinging wave, the response becomes more symmetric about the horizontal centerline, although it never achieves symmetry because of the influence of the reflected wave from the free surface. For the horizontally propagating wave (angle of incidence equal to 90°), the real part appears fairly symmetric across the horizontal centerline, whereas the zero crossing of the imaginary part is clearly shifted from the vertical line passing through the circle's center. Figure 40 also shows the completeness of the solution obtained from the integral equation method used in this work. The response of all points around the circumference of the cavity is obtained as the system of equations is solved. This is a very desirable feature of the method since the response point of interest may depend on the particulars of the application.

Figure 41 presents the response ratio for the point on the cavity bottom versus the dimensionless frequency Ω . A single plot was created by repeatedly reconstructing the system of equations and solving for a number of different frequency values to permit a reasonably smooth response curve. Three depth-to-radius ratios are shown: 6, 20, and 100. These represent a moderate-sized tunnel at shallow depth, intermediate depth, and great depth. The results for



$$N = 8$$

$$\Delta\eta = \frac{2\pi}{N} = \frac{\pi}{4}$$

Figure 39. Discretization scheme for eight points.

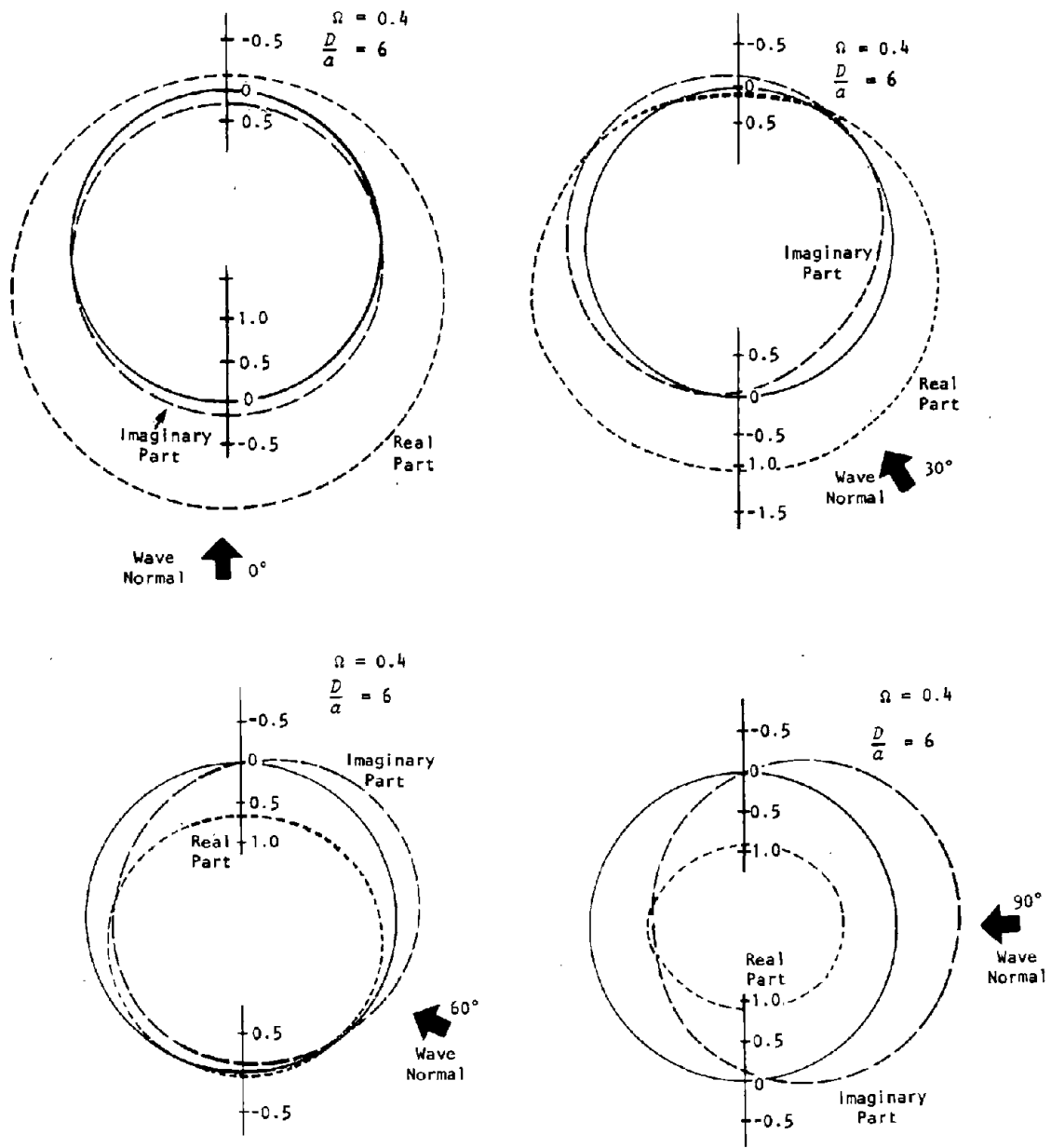
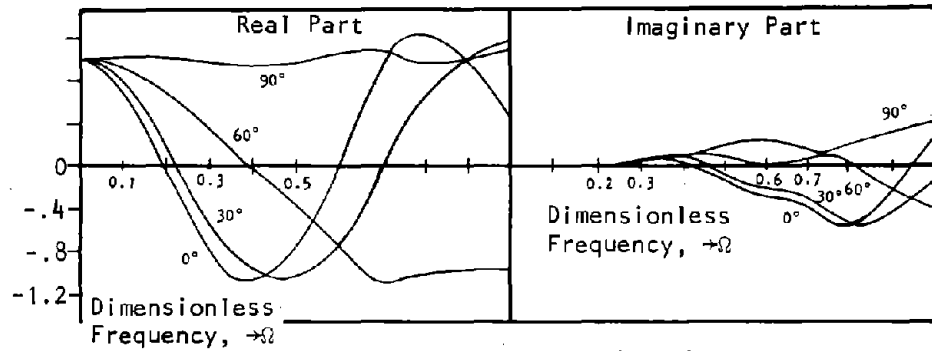
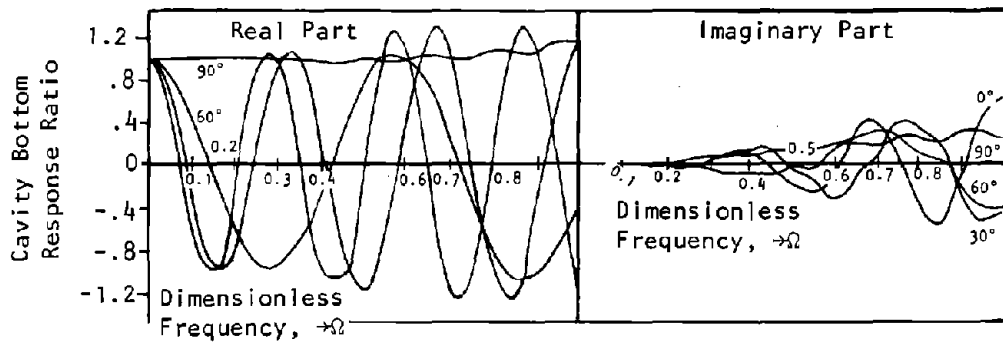


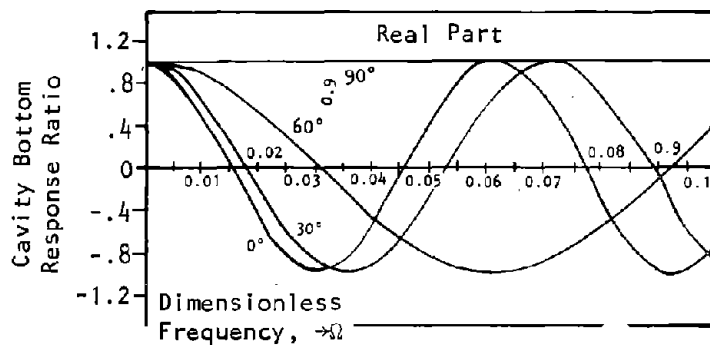
Figure 40. Effect of angle of incidence on cavity response ratio around the circumference.



a. Shallow depth, $D/a = 6$



b. Intermediate depth, $D/a = 20$



c. Great depth, $D/a = 100$

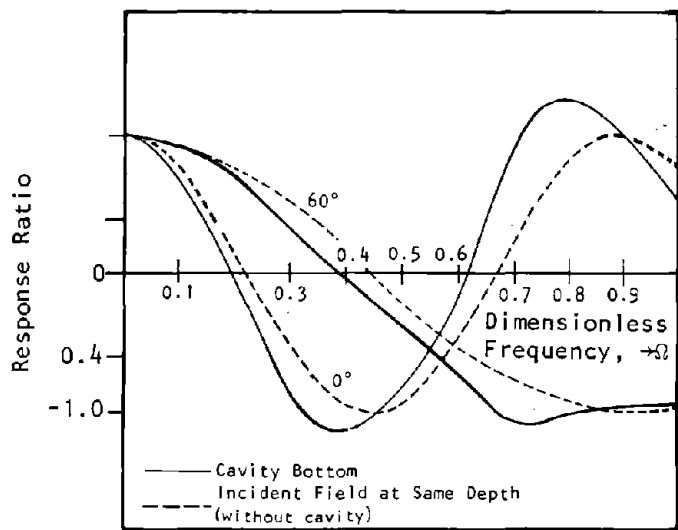
NOTE: Imaginary part for $D/a = 100$ is less than 0.01 for $0 \leq \omega \leq 0.1$.

Figure 41. Ratio of steady-state cavity bottom response to free-surface response versus frequency for various depths and various angles of inclination.

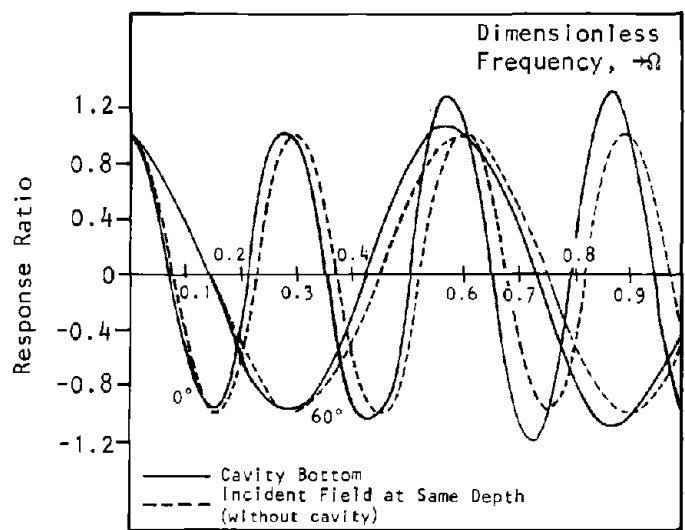
four angles of incidence, 0° , 30° , 60° , and 90° , are plotted. The range of dimensionless frequency for which the ratios have been displayed is between zero and 1.0 for the depth-to-radius ratios of 6 and 20. For the depth-to-radius ratio of 100, the dimensionless frequency range is between zero and 0.1. This different range in the latter case was chosen because, at the same scale, the curves would be very difficult to distinguish due to their many oscillations. The behavior of the curves is clearly seen as plotted. The amplitude of the imaginary part increases slowly from negligibly small values near zero frequency to significant values in the vicinity of $\Omega = 1$. The imaginary part is negligible for the range of Ω between zero and 0.1. Because the response of the deep cavity, $D/a = 100$, is only plotted over that range, the imaginary part was not plotted.

Examination of the diffraction of the SH-wave around the cavity is also of interest in this study. Thus, a comparison is made between the response at the bottom of the cavity and the motion at that same point in the absence of the cavity. This undiffracted field is given by Equation (25) in which $x_1 = 0$ and $x_2 = D + a$. Of course, as in the previous treatment, Equation (25) is first normalized by dividing by the quantity $U_3^0(\omega)$. This represents both the incident plane wave front and the front reflected from the free surface.

Figure 42 gives the comparison between the response of the cavity bottom and that of the incident field at the same depth as the cavity bottom (in the absence of the cavity) versus the dimensionless frequency Ω . Two angles of incidence, 0° and 60° , are shown for two depth-to-radius ratios of 6 and 20. In all cases, at low frequencies the response of the incident field is very close to the response of the cavity bottom. The curves slowly diverge as the frequency increases. Even as the frequency approaches 1.0, the curves of the incident field are fairly close to those that include scattering. The difference shown here between these curves is due to the effect of scattering. It should be noted that the imaginary part of the incident field is identically zero. Thus, a comparison between it and the imaginary part of the response ratios in Figure 41 has not been made. The same comparison for the deep cavity with a depth-to-radius ratio of 100 was made; however, these results were not shown on this figure because the difference between the incident and scattered fields was so slight that they could not be distinguished in a plot. For practical



a. Shallow depth, $D/a = 6$



b. Intermediate depth, $D/a = 20$

Figure 42. Motion at cavity bottom and incident wave field in absence of cavity.

purposes, it can be concluded that in the frequency range $0 \leq \Omega \leq 0.1$ the incident field and the cavity responses are the same at great depth.

Other response quantities in this problem that are of interest are the shear stresses and strains in the medium around the cavity. These have not explicitly been obtained in this study. They can be found by using, for example, a finite-difference scheme from the discretized response that has been evaluated.

Conclusions from Numerical Study. The comparison in Figure 42 suggests that the cavity response can be estimated by the incident wave in the low-frequency range. How far out on the frequency scale this estimate can be used will depend on the acceptable error. The difference between these curves in Figure 42, then, is a measure of error. Scanning the curves and deciding the frequency beyond which the difference is unacceptable will define the acceptable low-frequency approximation range. Using the incident field will, however, never yield an imaginary part.

In general, the motion of a shallow cavity in most geologic media will be significantly different from the incident wave field (or free-field) motion. For a cavity at shallow depth, say $D/a = 6$, the incident field would provide an approximation of the cavity response only for very low frequencies, say $0 < \Omega < 0.1$. If the cavity is 10 ft (3 m) or less in radius and located in a competent granite, that frequency range is exactly the one of interest. In this case, the incident wave field should approximately, but not exactly, represent the cavity response. However, in less competent rock or in softer rock with lower wave speeds, the frequency range for an earthquake will extend beyond $\Omega = 0.1$ and may even extend to $\Omega = 1.0$. In such rock, the incident wave field will be a very poor approximation of the cavity response. This suggests that the seismic motion of a shallow cavity strongly interacts with the free surface, particularly in stiff soils or soft rocks.

The motion of a cavity at intermediate depth, say $D/a = 20$, may also be approximated by the incident field for very low frequencies. However, at this depth, the range $0 < \Omega < 0.1$ provides a much better approximation than it affords for the shallow cavity, and the range could probably be extended to 0.2 without serious consequences. Thus, the seismic motion of an intermediately deep cavity also interacts with the free surface, but less strongly than that of a shallow

cavity. This interaction is less noticeable for cavities in hard, competent rock than for cavities in stiff soil.

The response of a cavity at great depth, say $D/\alpha \geq 100$, is essentially identical to the response of the incident field for the frequency range $0 < \Omega < 0.1$, and an excellent approximation is to be expected over a much longer range, say $0 < \Omega < 0.5$. Because low wave velocities corresponding to stiff soils and very soft rocks are not, in general, expected at great depths, that frequency range should adequately represent most earthquakes. Thus, in general, the seismic motion of a deep cavity will not interact or will interact very weakly with the free surface so that the cavity response is essentially the same as the incident field response at that depth.

These general statements may be extended to layering of geologic materials. The behavior of a cavity near a high-impedance boundary (such as the interface between bedrock and an alluvial layer) should be very similar to that of a cavity near the free surface. If the cavity is within a distance of 20α from the high-impedance surface, significant variations in the cavity behavior with respect to the incident field should be expected. Of course, the variations will be greater for a cavity located in soft rock than for one located in hard rock.

This discussion has been in reference to the study undertaken with SH-waves only. However, the same general conclusions with respect to proximity of the cavity to the free surface and type of geologic medium should apply for P- and SV-waves.

In summary, the problem of a circular cavity in a half-space subjected to horizontally polarized shear waves of arbitrary angle of incidence has been studied. The steady-state response of the cavity expressed in terms of the free-surface motion has been evaluated for a shallow, an intermediate, and a deep cavity. Four angles of incidence have been considered for the excitation, giving the effect of the full variation of this parameter. Comparisons between the response of the cavity and the incident wave field have been presented. These comparisons suggest that for low frequencies the diffraction effects are small and cavity response can be estimated by the incident, unscattered motion. This applies most to deep cavities and hard rock sites.

Future research in this field should include examination of damping in the earth medium, lining on the cavity, and an arbitrary shape for the cavity cross section. Also, the problems of compressional and in-plane shear wave excitation of arbitrary angles of incidence, and Rayleigh waves, should be investigated.

6. Current Practice in Seismic Design

Seismic design is a part of the overall design process of an underground structure, just as it is for a surface structure. The overall design process might be schematically represented by the chart in Figure 43. The design process is illustrated on the left side of the figure, and the five components of seismic design are illustrated on the right side. Construction is included as part of the design process because design modifications are usually carried out during construction, particularly in the case of excavation within rock.

It should be noted that the word *design* has two different meanings. The most common meaning refers only to the proportioning of structural components to resist the loads without exceeding the failure criteria. This meaning is exemplified by many textbooks in the field of structural engineering whose titles refer to the design of steel or reinforced concrete structures. The other meaning of design refers to the overall process that begins with a statement of need for a particular structure and culminates in the detailed specification of the structure. In this chapter, seismic design is used in this broader sense and includes all those components illustrated on the right side of Figure 43.

The more narrow sense of seismic design is embodied in the strengthening or hardening* of the ground supports. The reader is cautioned not to regard strengthening or hardening to mean decreasing flexibility, but instead to mean modifying the structure for satisfactory performance under dynamic loads. In some circumstances, it might be more appropriate to modify the underground structure by increasing rather than decreasing its flexibility because a more rigid structure attracts load to it.

Current practice in the seismic design of underground structures is primarily defined by papers presented at conferences, by journals, and by design criteria documents prepared for specific projects. This literature has been reviewed and is summarized in this chapter. Some information has also been

*Hardening is a term more common to the design of protective structures for defense applications.

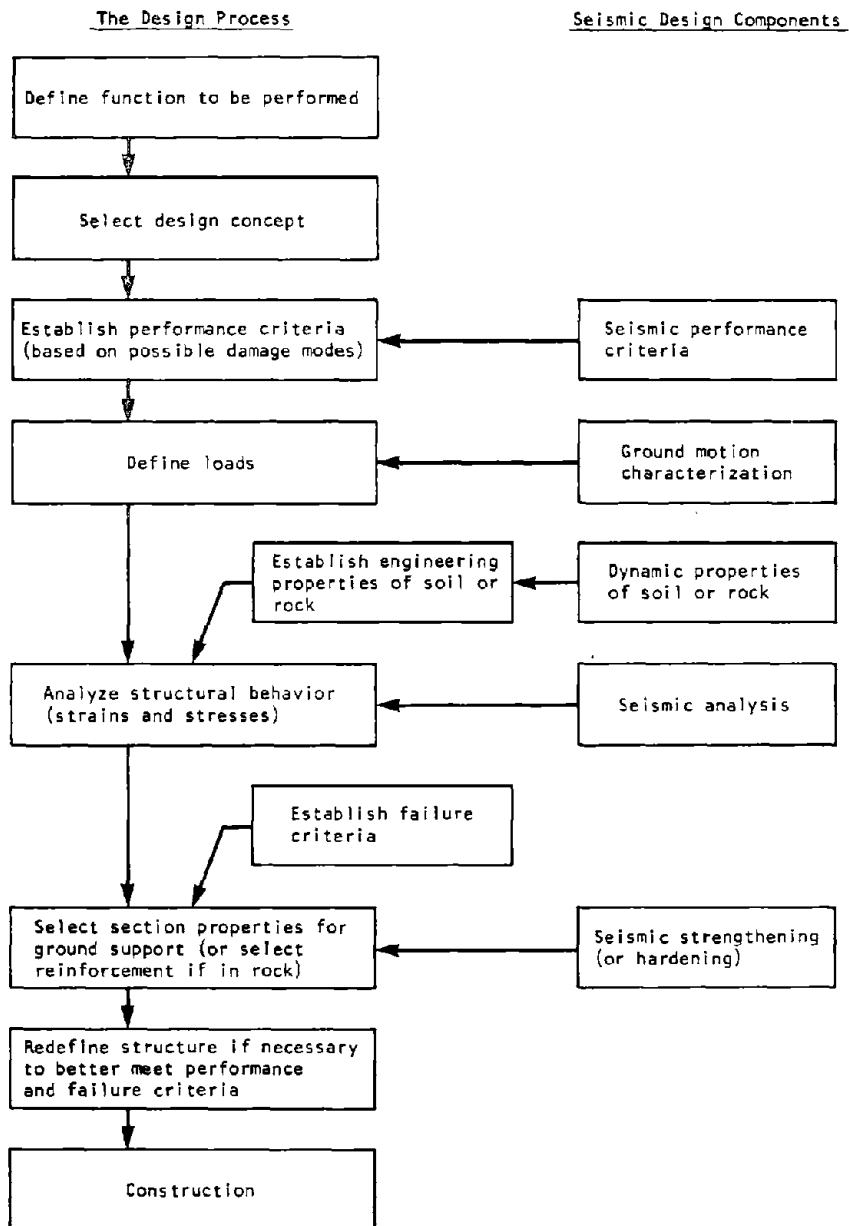


Figure 43. The overall design process for underground structures.

collected through discussions with design engineers of several government agencies and engineering firms (see Appendix A).

Major codes that address the seismic design of surface structures in the United States^{9,139-141} contain no provisions for underground structures. In Japan, however, the large number of submerged tunnels constructed since World War II have prompted the Japan Society of Civil Engineers to propose a rational seismic design method titled *Specifications for Earthquake Resistant Design of Submerged Tunnels*.¹⁴² To the best of our knowledge, this is the only example of an effort to codify the seismic design of any type of underground structure.

Earthquake engineering of underground structures addresses the mitigation of possible damage from two principal sources: ground shaking and fault rupture. Because the design approach to ground shaking is rather dependent upon the type of structure and the medium in which the structure is to be built, the discussion that follows is divided into sections on submerged tunnels, underground structures in soil, and underground structures in rock. If an underground structure crosses a fault that slips, damage is inevitable, and nothing can be done to prevent it; however, certain practices may help reduce the damaging effects of fault movement. These practices are described in a separate section at the end of the chapter.

SUBMERGED TUNNELS

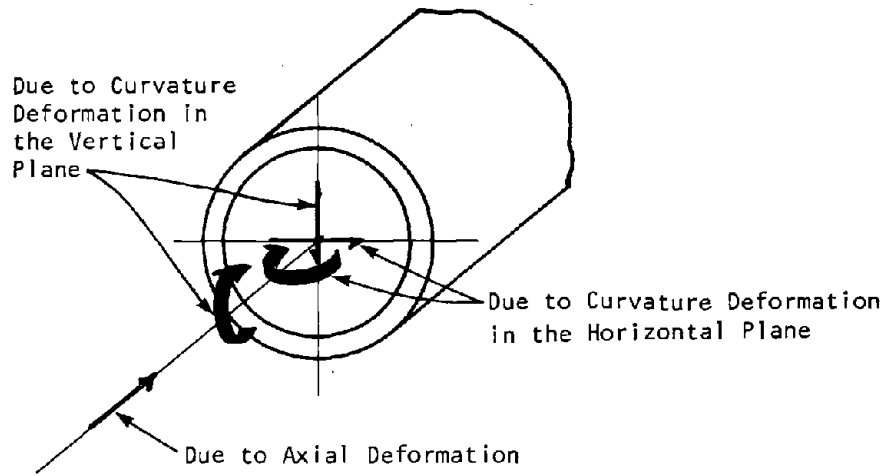
The development of design methodologies for submerged tunnels has been more concerned with quantifying the dynamic response of the tube than with selecting appropriate properties for the cross section and connections. A description of tube behavior requires an understanding of how the ground deforms, how the tube conforms to this deformation, the extent of interaction between the structure and the soil, and the forces imposed on the structure. There are various degrees of sophistication of modeling and assumptions that go into these analyses. In contrast, the procedures for strengthening (designing in the narrow sense) are standard for structural engineering and are governed by codes on the design of steel and reinforced concrete structures.

In the late 1950s the San Francisco Bay Area Rapid Transit (SFBART) District was involved in the design of a subaqueous tube, approximately 3.6 miles (5.8 km) long, between San Francisco and Oakland. The tube was to be constructed by placing precast tube segments in a dredged trench, a method that had been successfully used for a number of submerged tunnels in the United States and Japan, as well as in other countries. However, the seismic environment of the Bay Area presented a new design condition that had never before been considered for such a structure. No information was available at that time on the effects of seismic motion upon subaqueous tunnels, and analytical methods for estimating seismic stresses did not yet exist. Consequently, SFBART engineers developed their own method for analyzing the tunnel, as published in the *Trans-Bay Tube, Technical Supplement to the Engineering Report*.¹⁴

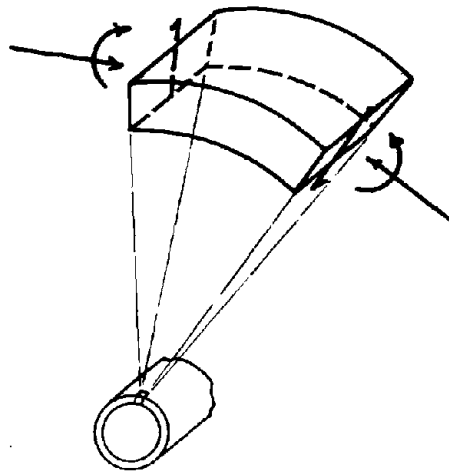
The SFBART engineers identified the effects of an earthquake on a submerged tube as four different types of behavior:¹⁴

- Curvature deformation in both the horizontal and vertical planes, imposing bending moments and shear forces on the cross section of the tube (Figure 44a)
- Axial deformation, imposing axial forces on the cross section of the tube (Figure 44a)
- Dynamic soil pressure, imposing circumferential bending moments, radial shear forces, and thrusts in the tube walls (Figure 44b)
- Transverse acceleration forces due to the mass of the tube, also inducing circumferential bending moments, radial shear forces, and thrusts in the tube walls (Figure 44b)

The method developed by SFBART twenty years ago to analyze these four types of behavior was based upon readily available solutions in the mechanics of solids and the theory of elasticity. The development of the SFBART method predated the availability of computer codes for dynamic structural analysis. Today, the analytical method of SFBART could be largely replaced by more sophisticated computer methods. However, the SFBART procedures are of more than historical interest because their conceptualization of tube behavior during an earthquake is still at the state of the art. Furthermore, the simplicity of the SFBART method makes it very useful today for preliminary design studies. This method is summarized below under the heading SFBART Approach to Submerged Tunnels.



a. Sectional forces due to curvature and axial deformations.



b. Circumferential forces due to dynamic soil pressure and inertial forces.

Figure 44. Identification of sectional and circumferential forces.

Kuribayashi et al.⁶⁰ reviewed the SFBART approach approximately ten years after it was developed and proposed some procedural changes, most notably in the specification of the ground motion. That work became the basis of the proposed code by the Japan Society of Civil Engineers for the design of submerged tunnels.^{142,143} The procedures are summarized under the heading Japanese Approach to Submerged Tunnels.

The forces developed in a subaqueous tunnel during seismic motion may also be investigated by modern computer techniques. These methods are briefly discussed and illustrated under the heading Dynamic Analysis of Submerged Tunnels.

The dynamic behavior of a subaqueous tunnel may be expressed in terms of internal forces (or stresses). However, the engineering designer should realize that ground shaking imposes a deformation on the structure that is largely unaffected by the strength of the structure. Thus, the strengthening of an overstressed section might not result in reduced stresses. It might be more prudent under such circumstances to provide sufficient ductility to the structure or to articulate the structure by means of seismic joints. In this manner, the structure will be able to conform to the seismic deformation without losing its capacity to resist static forces.⁵⁹ Details of the seismic joint used in the SFBART tunnel are described under the heading Special Design Consideration: Seismic Joint.

SFBART Approach to Submerged Tunnels

Sectional Forces due to Curvature Deformation. Consider first the curvature deformation in the horizontal plane, referred to in Reference 14 as transverse-horizontal deformation. This deformation can result from the passage of any type of plane seismic wave at some oblique angle to the longitudinal axis of the tube, although the largest deformations might be caused by a horizontally propagating SH-wave. Assume a sinusoidal S-wave with amplitude A and wavelength L . The wave geometry is given in Figure 45. This figure represents either an SH-wave propagating in a horizontal plane or an SV-wave propagating in the vertical plane of the tunnel. Propagation along the structure axis, $\phi = 0$, would result in the worst situation.

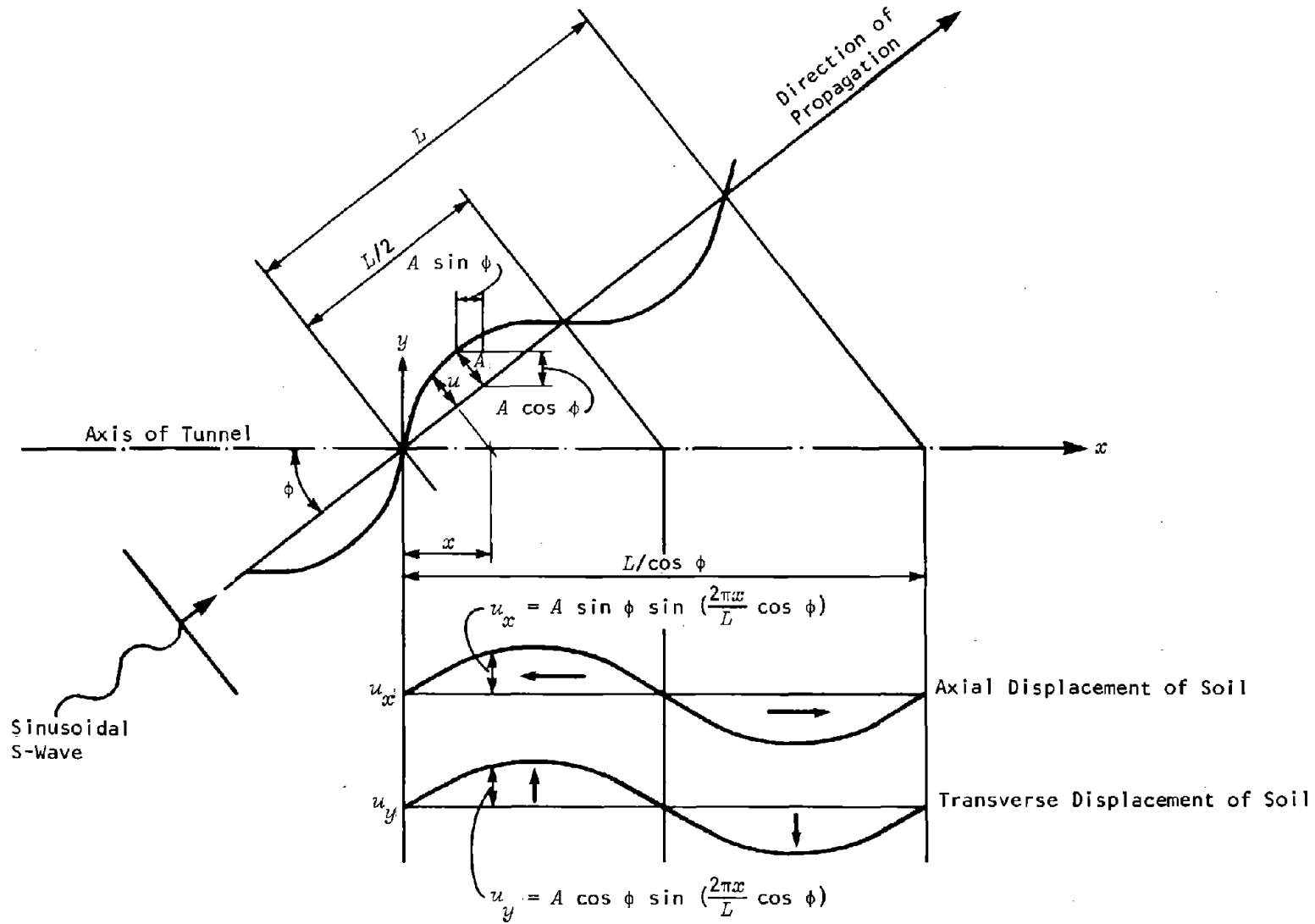


Figure 45. Geometry of sinusoidal shear wave oblique to axis of tunnel.

Because the tube is stiffer than the surrounding soil, it will distort less than the soil in the absence of the tube, creating zones of tension, compression, and shear in the soil around the tube (see Figure 46). By representing the tube and soil interaction as an elastic beam on an elastic foundation and neglecting longitudinal shearing stresses between the soil and the tube, we can derive expressions for the bending moment and shear force along the tunnel. The largest value of the shear would be given by

$$V = \frac{KL/2\pi}{1 + (K/E_t I)(L/2\pi)^4} A \quad (47)$$

and the bending moment by

$$M = \frac{K(L/2\pi)^2}{1 + (K/E_t I)(L/2\pi)^4} A \quad (48)$$

where:

- K = transverse stiffness modulus of the soil per unit length of the tube (in force per unit area)
- E_t = modulus of elasticity of the tube
- I = moment of inertia of the tube section
- A = free-field displacement amplitude of a sinusoidal S-wave
- L = wavelength of a sinusoidal S-wave

In the SFBART model, the soil stiffness K is defined as

$$K = K_t + K_c + K_s \quad (49)$$

where the subscripts t , c , and s designate tension, compression, and shear, respectively. In reality, the tension zone is realized as a reduction in the static compression; therefore, $K_t = K_c$. The compression stiffness K_c is determined by using the Boussinesq theory for a load on an elastic half-space, assuming that the tube produces a strip load that is alternately positive and negative due to the sinusoidal seismic wave.¹⁴ The expression for K_c thus determined is

$$K_c = E_s L^{-0.3} / 0.233 \quad (50)$$

where E_s is the modulus of elasticity of the soil at the level of the tube.

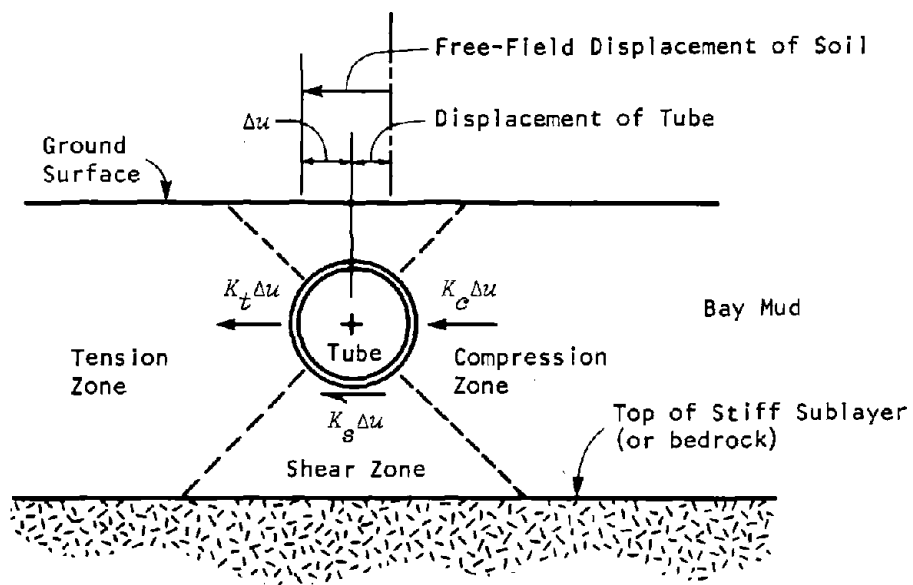


Figure 46. Interaction between tube and soil due to difference between free-field and tube displacements in SFBART approach.

The shear stiffness K_s is determined by assuming that the trapezoidal soil prism between the tube and the stiff sublayer resists horizontal deformation by uniform shear stresses across the horizontal planes. The geometry of the trapezoid is described by the height h of the tube above the bottom of the mud layer, the outside diameter d_o of the tube, and some angle T as defined in Figure 47 (Reference 14 assumes $T = 52.5^\circ$). Assuming that the shear modulus of the soil varies linearly with depth, the expression for K_s is

$$K_s = \frac{2G_o \tan T}{\ln \left[\frac{G_t(1 + h/h_o)}{G_b} \right]} \quad (51)$$

where:

$$h_o = d_o/2 \tan T$$

$$G_o, G_t, G_b = \text{shear modulus of the soil at a distance } x_1 \text{ above the tube, at the level of the tube, and at the bottom of the mud layer, respectively}$$

$$h = \text{thickness of soil layer between tube axis and stiff sublayer}$$

Note that, given the width of the tube and an assumed value for T , the value of K_s varies only with the vertical location of the tube within the mud layer. The value of K_s does not vary with wavelength as do the values of K_o and K_t .

The design amplitude A is obtained from the ground displacement spectrum, prepared by Housner.¹⁴ This design spectrum is intended for use in the muds of San Francisco Bay, where the shear wave velocity is between 200 and 600 fps (61 and 183 m/sec), and for a magnitude 8.2 earthquake on the San Andreas fault. The spectrum is represented by a power law

$$A = CL^n \quad (52)$$

where:

$$C = 4.9 \times 10^{-6}$$

$$n = 1.4$$

The units of L and A are in feet.

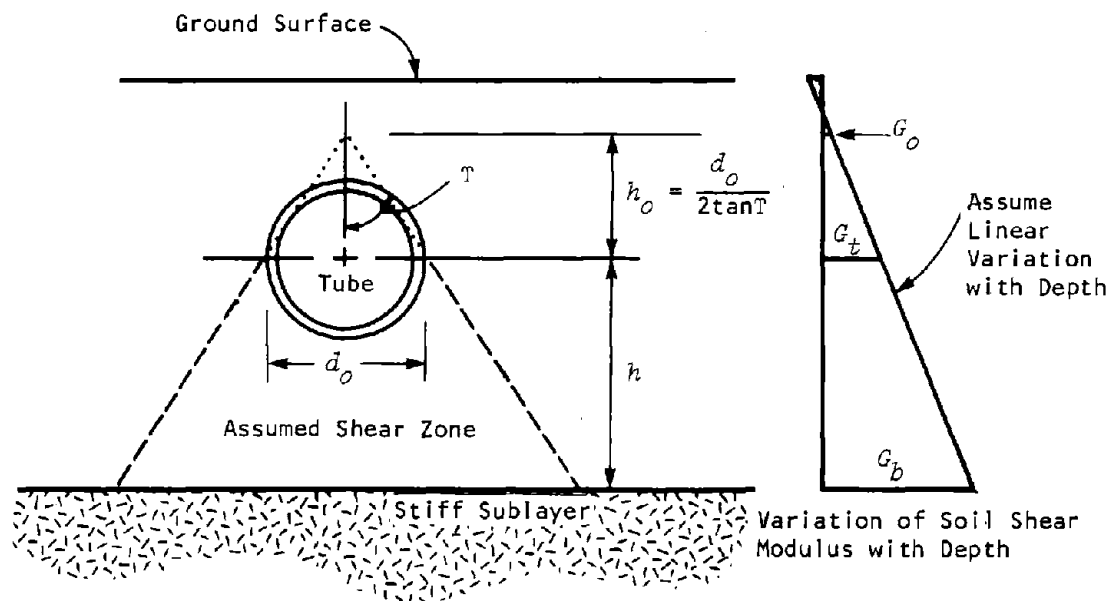


Figure 47. Assumed geometry for determination of K_b in SFBART approach.

The values of L that will maximize the values of shear and bending moment within the tube are determined by differentiating Equations (47) and (48) with respect to L and setting the results at zero. Since A varies with wavelength, Equation (52) is substituted into Equations (47) and (48) prior to differentiation. Although K also varies with wavelength, it does so gradually and is therefore assumed constant. This procedure yields the value of the wavelength, L_v , which maximizes the shear

$$L_v = 2\pi \left[\frac{E_t I}{K} \frac{n+1}{3-n} \right]^{1/4} \quad (53)$$

and the value of the wavelength, L_m , which maximizes the bending moment

$$L_m = 2\pi \left[\frac{E_t I}{K} \frac{n+2}{2-n} \right]^{1/4} \quad (54)$$

Note that these expressions depend upon the value of K , which, conversely, depends upon the wavelength. Consequently, a pair of values for K and L must be obtained by the simultaneous solution of Equations (49) and (53) to maximize shear and of Equations (49) and (54) to maximize bending moment.

Next, consider the curvature deformation in the vertical plane, which is referred to as transverse-vertical deformation in Reference 14. This deformation can also result from the passage of any type of plane wave at some oblique angle to the tube; however, the principal effect is probably due to an SV-wave propagating in the vertical plane of the tube. The maximum values for the shear and bending moments within the tube are determined by the same formulas that are used for determining the curvature in the horizontal plane, that is, Equations (47) and (48), with maximizing wavelengths given by Equations (53) and (54). However, some changes in A and K are required, as described below.

Inspection of recordings of past California earthquakes reveals that vertical motions are about one-half to two-thirds as great as horizontal motions. Consequently, the design amplitude A for vertical motion is computed as two-thirds of the value given by Equation (52).

The soil stiffness modulus, identified for vertical motion as K_v , cannot be determined by Equations (49) through (51). Because rigid vertical geologic

structures do not exist parallel to the tube, significant shear zones are not developed on each side of the tube. Furthermore, because the soil above the tube is not very thick, no compression (or tension) zone is created in that region. Thus K_v is determined only by the compressive resistance of the soil between the tube and the stiff sublayer to a strip loading that is alternately positive and negative and that corresponds to the assumed sinusoidal form of the seismic wave. Reference 14 utilizes published charts on influence coefficients for a soft soil layer over a stiff one to obtain values for K_v . This procedure does not lend itself to a simple representation that could be summarized here. For this study, it is sufficient to note that K_v does vary with L , but not significantly.

The design values for bending moment and shear force on the tube cross section can now be determined for the seismic condition. Maximum bending moments are determined separately for horizontal displacement and for vertical displacement, as described above. Then the two values are combined by the square-root-of-the-sum-of-the-squares method, yielding the design seismic moment. Similarly, the design seismic shear is obtained. In a preliminary study assuming a circular tube 35 ft (10.7 m) in diameter, buried at a depth of 60 ft (18.3 m) in a 100-ft (30.5-m) layer of San Francisco Bay mud, Reference 14 computes the design moment to be 92,800 kip-ft (125.8×10^6 N-m). The moment of inertia for the preliminary concrete configuration of the tube is 37,300 ft⁴ (322 m⁴). This results in a longitudinal seismic stress in the concrete of approximately 300 psi (2.1 MPa).

Sectional Forces due to Axial Deformation. Having considered curvature deformation, we will now focus on axial deformation. Reference 14 reasons that longitudinal strains produced in the tube by a P-wave propagating in the direction of the tube would be smaller than those produced in the underlying rock. Consequently, there is no question about the ability of the tube to withstand axial strains due to a P-wave. However, a shear wave propagating obliquely to the tube can also create axial strain within the tube. As shown in Figure 45, the free-field displacement in the soil parallel to the tube axis is

$$u_x = A \sin \phi \sin \left(\frac{2\pi x}{L} \cos \phi \right) \quad (55)$$

where x is measured along the tunnel axis. Because $\sin \phi \cos \phi$ is maximum for $\phi = 45^\circ$, the worst case for the free-field soil strain parallel to the tube is

$$\epsilon = \frac{\pi A}{L} \cos\left(\frac{2\pi x}{\sqrt{2}L}\right) \quad (56)$$

Reference 14 assumes that the tube is more rigid than the soil in the axial direction and that therefore the tube restrains the soil in its vicinity from experiencing this strain. Thus the axial force created in the tube is equal to the force necessary to prevent this strain in the soil. Only the layer of soil between the horizontal plane of the tube and the stiff soil sublayer (bedrock) is considered. Taking a rectangular block of the soil layer below the tube, the force needed to be mobilized over one-quarter of the apparent wavelength ($\sqrt{2}L/4$) is derived in Reference 14 to be

$$F_{\alpha} = d_o G_{av} A \left(\frac{\pi h}{L} + \frac{L}{2\pi h} \right) \quad (57)$$

where G_{av} = average shear modulus of the soil.

Then, assuming that the rest of the soil layer -- that is, the soil to each side of the tube -- has an effect equal to the rectangular block of soil below the tube, the maximum axial force is twice F_{α} or

$$F = 2d_o G_{av} A \left(\frac{\pi h}{L} + \frac{L}{2\pi h} \right) \quad (58)$$

An estimate of the axial force is provided in Reference 14, assuming a circular tube 35 ft (10.7 m) in diameter, buried at a depth of 60 ft (18.3 m) in a 100-ft (30.5-m) layer of mud in San Francisco Bay. The design wavelength is 500 ft (152 m), following the recommendations of Housner.¹⁴ The design axial force is computed to be 7,917 kips (35.22 MN). Assuming a gross concrete area of 286 ft² (26.6 m²), this yields a longitudinal seismic stress in the concrete of approximate 190 psi (1.3 MPa).

Circumferential Forces due to Dynamic Soil Pressure. So far this discussion of the SFBART approach has dealt with the development of bending moments and shear forces on the cross section. Now the discussion shifts to circumferential bending and the development of circumferential bending moments, radial shear forces, and normal thrusts in the wall of the tube by dynamic soil pressure and inertial forces of the tube mass.

During curvature bending, a pressure develops between the tube and the soil because the tube does not displace as much as the free-field soil. This soil pressure, derived in the same manner as Equations (47) and (48), is given by

$$p = \frac{K}{1 + (K/E_t I) (L/2\pi)^4} A \quad (59)$$

As discussed earlier, if the curvature is in the horizontal plane, then $K = 2K_c + K_g$; if the curvature is in the vertical plane, $K = K_v$. The maximum value of p is realized for a wavelength

$$L_p = 2\pi \left[\frac{EI}{K} \frac{n}{4-n} \right]^{1/4} \quad (60)$$

As an approximate model for circumferential bending, the tube is taken to be a circular ring loaded by horizontal and vertical pressure as shown in Figure 48. The pressures p_h and p_v are due to horizontal and vertical displacement, respectively, and are computed from Equation (59) with appropriate values for K , L , and A . From sample calculations in Reference 14, the maximum circumferential stress due to dynamic soil pressure is estimated to be about 240 psi (1.7 MPa).

Circumferential Forces due to Inertial Forces. Assuming that the peak horizontal acceleration of 0.66g, corresponding to the design earthquake, is experienced by the tube, the horizontal inertial force is $0.66W$, where W is the total weight of the tube (including roadway) per unit length. As an approximate model for circumferential bending, the tube is taken to be a circular ring with the inertial force distributed around the circumference and the reactive soil pressure divided between compression on one side and tension (reduced compression) on the other (see Figure 49). Assuming the weight of the tube to be only slightly heavier than the water it displaces and assuming a 35-ft (10.7-m) diameter and a 2.83-ft (0.86-m) thick wall, the maximum circumferential stress is approximately 32 psi (0.2 MPa). On this basis, circumferential bending due to inertial forces may be ignored in more detailed analyses of tube behavior.¹⁴

Static-Plus-Seismic Forces. The above discussion summarizes the SFBART approach for the determination of stresses induced in the transbay tube by the design earthquake. Of course, a subaqueous tube is always designed to resist static

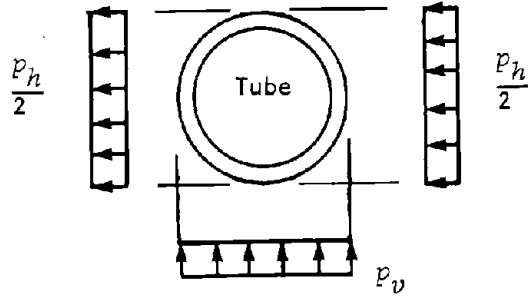


Figure 48. Simple model for the analysis of circumferential bending due to dynamic soil pressure in SFBART approach.

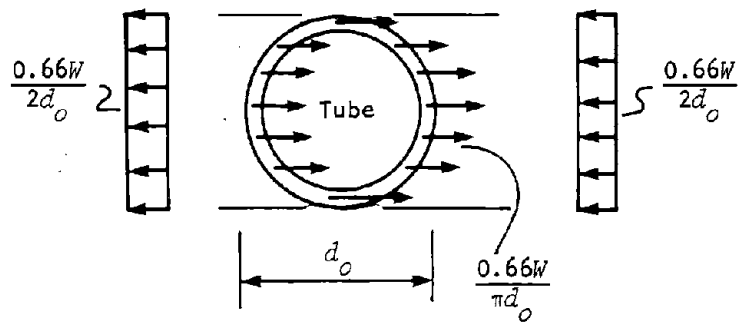


Figure 49. Simple model for the analysis of circumferential bending due to inertial forces in SFBART approach.

stress due to dead load, water pressure, static soil pressure, and temporary construction loads. It should be noted that an analysis of permanent static load does not predict longitudinal bending; however, a minimum amount of longitudinal reinforcement is required, even without seismic considerations. Analysis of the earthquake load did predict longitudinal stresses for the SFBART tube, although the values were relatively small. Because standard practice (in the United States) permits a 33% increase in the allowable stresses for the static-plus-dynamic condition, little additional reinforcement was needed for the combined static and earthquake loads on the SFBART tube.^{14,144}

Japanese Approach to Submerged Tunnels

The Public Works Research Institute (PWRI) of the Ministry of Construction, Japan, began research and investigations into the seismic behavior and design of submerged tunnels in 1968. In 1971, the Japan Society of Civil Engineers (JSCE), in close cooperation with the PWRI, organized a committee to establish a rational earthquake-resistant design method. The committee's work resulted in the 1975 publication of the *Specifications for Earthquake Resistant Design of Submerged Tunnels*.¹⁴² Further elaboration of the specifications and a numerical example are provided by the JSCE document, *Earthquake Resistant Design Features of Submerged Tunnels in Japan*.¹⁴³ Many of the developments in support of those two documents, as well as continuing research, are reported in various papers and reports by personnel of the PWRI.^{60,145-149}

The JSCE specifications cover the complete range of concerns in the design of the submerged tunnel. They require site investigations into seismicity, geology, and soil conditions and specify the data to be collected. The procedures outlined for seismic design not only cover the precast tubular portion but also ventilation towers, approaches, and stability of subsoils. There is even a section on the safety equipment and special operating procedures that are needed immediately following an earthquake. In the summary below, the emphasis is placed on the submerged tube.*

*Although the major emphasis will be on the precast tube portion of the subaqueous tunnel, other portions also should be investigated, including the ventilation towers, the approaches, and the soil fills. The Japanese specifications provide a very detailed checklist of all the various considerations for design.^{142,143}

Sectional Forces due to Axial and Curvature Deformation. In the Japanese approach, the sectional forces (bending moment, shear and axial forces) are determined by the seismic deformation method, which closely parallels the SFBART approach for curvature bending. The method is derived by assuming that a shear wave propagates with an angle ϕ to the axis of the tunnel (see Figure 45).

The shear force and bending moment are derived with the same assumptions as the SFBART approach (wave propagating along axis, $\phi = 0$, and elastic beam on an elastic foundation). The resulting formulas are identical in form to Equations (47) and (48):

$$V = \frac{K_2 L / 2\pi}{1 + (K_2 / E_c I) (L / 2\pi)^4} A \quad (61)$$

$$M = \frac{K_2 (L / 2\pi)^2}{1 + (K_2 / E_c I) (L / 2\pi)^4} A \quad (62)$$

The previous designation for the soil stiffness in these two equations has been changed from K to K_2 because the Japanese use a different technique to determine soil stiffness.

The free-field displacement parallel to the tunnel axis, given by Equation (55), induces an apparent axial strain in the tunnel. This strain is maximized by $\phi = 45^\circ$, as in Equation (56). The SFBART approach assumes that the tube is rigid; the Japanese approach, however, assumes that the tube is an elastic rod embedded in an elastic foundation. Consequently, part of the free-field displacement creates a force in the tube, while the remainder creates an equilibrating force in the surrounding soil. Following these concepts and selecting the appropriate value for α , the largest value for the axial force is

$$P = \frac{K_1 L / 2\pi}{1 + (K_1 / E_c A_c) (\sqrt{2} L / 2\pi)^2} A \quad (63)$$

where:

K_1 = longitudinal stiffness modulus of the soil per unit length of the tube

A_c = cross-sectional area of the tube

K_1 and K_2 are estimated by considering the tunnel to be a rigid rectangular plate on the semi-infinite elastic body so that

$$K_1 = K_2 = G_{av} \quad (64)$$

where G_{av} is the average shear modulus of the soil. This is in contrast to the SFBART procedures for obtaining the soil stiffness represented by Equations (49), (50), and (51).

The values of wavelength L that will maximize Equations (61), (62), and (63) are determined by differentiating with respect to L and setting the results equal to zero. The fact that the wave amplitude varies with L is ignored in the Japanese approach so that the maximizing wavelengths can be obtained. The wavelengths for maximum values of shear force, bending moment, and axial force are, respectively,

$$L_v = 2\pi \left[\frac{E_t I}{3K_2} \right]^{1/4} \quad (65)$$

$$L_m = 2\pi \left[\frac{E_t I}{K_2} \right]^{1/4} \quad (66)$$

$$L_p = 2\pi \sqrt{\frac{E_t A e}{2K_1}} \quad (67)$$

Substituting Equations (65), (66), and (67) into Equations (61), (62), and (63), respectively, yields the design sectional forces

$$V_{\max} = \frac{4\sqrt{27}}{4} \sqrt[4]{K_2^3 E_t I} A \quad (68)$$

$$M_{\max} = \frac{1}{2} \sqrt{K_2 E_t I} A \quad (69)$$

$$P_{\max} = \frac{\sqrt{2}}{4} \sqrt{K_1 E_t A e} A \quad (70)$$

The design value for the ground displacement, A , is determined by using a response spectrum that is similar, but not identical, to that of the SFBART

approach. The horizontal ground displacement amplitude at the ground surface is obtained by the formula

$$A = \frac{2}{\pi^2} S_v \cdot T \cdot a_{br} \cdot f_I \quad (71)$$

where:

- S_v = relative response velocity per Gal of the maximum acceleration at the bedrock (1 Gal = 1 cm/sec² \cong 0.001g)
- T = fundamental natural period of the subsurface layer
- a_{br} = horizontal acceleration at the bedrock in Gal
- f_I = Importance factor

When the vertical displacement amplitude is needed, it is to be one-quarter to one-half of the horizontal values according to the Japanese specifications.

The relative response velocity can be obtained from the spectral curves shown in Figure 50, which were developed by the PWRI from seismic records measured on bedrock in Japan. Similar spectral curves were developed by the Port and Harbor Research Institute, Ministry of Transportation. The natural period of the soil layer may be obtained either by observation of microseismisms or from the formula

$$T = \frac{4H}{V_s} \quad (72)$$

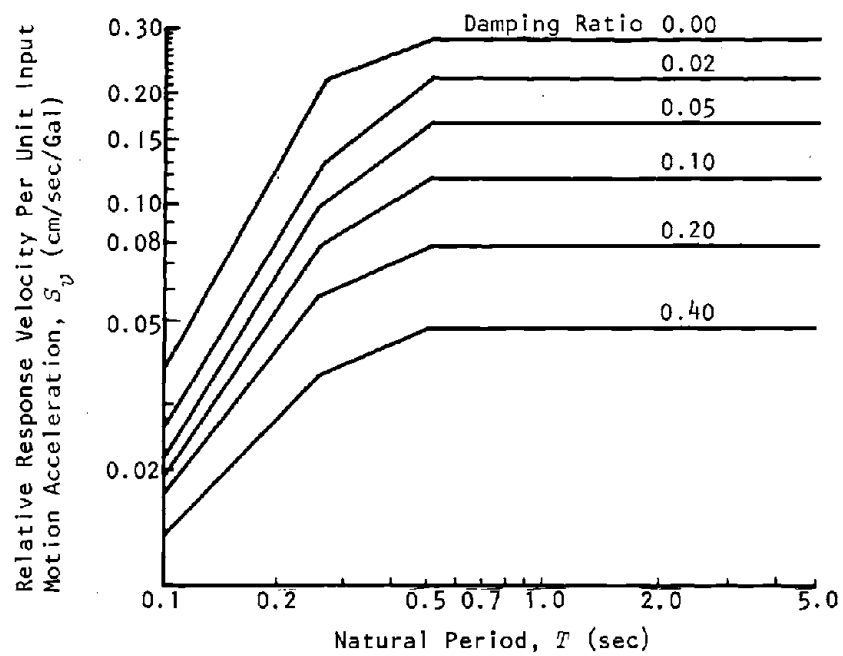
where H is the thickness of the layer and V_s is the shear wave velocity. The importance factor f_I is 1.0 for "tunnels serving higher public interests" and 0.8 for all other situations. Finally, the horizontal acceleration at the bedrock surface is stipulated as

$$a_{br} = f_z \cdot a_0 \quad (73)$$

where:

- f_z = seismic zone factor, equal to 1.0, 0.85, and 0.70, depending upon the location in Japan
- a_0 = standard horizontal acceleration at bedrock surface in Japan, taken as 100 to 150 Gal (0.102g to 0.153g)

The above procedures, which the Japanese refer to as the seismic deformation method, provide a rational approach to the computation of sectional forces along



Note: 1 cm/sec/Gal = 386 in./sec/g.

Figure 50. Relative response velocity per unit acceleration.
(Adapted from Reference 145.)

a submerged tunnel. This approach could be used in the design of a subaqueous tunnel project for any seismic region in the world, requiring only an appropriate site-dependent determination of S_v and α_{bz} .

Soil pressures during earthquakes are considered in the Japanese approach as they are in the SFBART approach; however, the methods for obtaining them differ. The Japanese specifications require that the horizontal earth pressures be determined by the Mononobe-Okabe earth pressure formula. A discussion of the Mononobe-Okabe approach is provided by Seed and Whitman.¹⁵⁰ The Mononobe-Okabe formula is presented later in this chapter in the section on tunnels in soil.

Circumferential Forces due to Dynamic Soil Pressure and Inertial Forces. The Japanese specifications also require the application of the seismic coefficient method to the design of the transverse section and the examination for sliding of the tunnel. In this method inertial forces arising from the weight of the structure itself, its contents, and the surrounding soil fill are applied as static equivalent forces. The horizontal seismic design coefficient k_h in Japan is to be obtained by the following formula:

$$k_h = f_z \cdot f_I \cdot f_s \cdot k_{oh} \quad (74)$$

where:

- f_z = seismic zone factor, as defined for Equation (73)
- f_I = importance factor, as defined for Equation (71)
- f_s = ground condition factor, ranging from 0.9 for bed-rock to 1.2 for very poor soil conditions
- k_{oh} = 0.2, standard seismic design coefficient

The vertical seismic design coefficient k_v is stipulated to be one-half of k_h . Both the SFBART and the Japanese approaches investigate circumferential bending of the transverse section; however, the SFBART approach is not concerned with sliding of the tunnel in the soft soils. A major difference between the two approaches is in the horizontal seismic coefficient: 0.66 for the SFBART procedure and approximately 0.20 for the Japanese procedure.

Dynamic Analysis of Submerged Tunnels

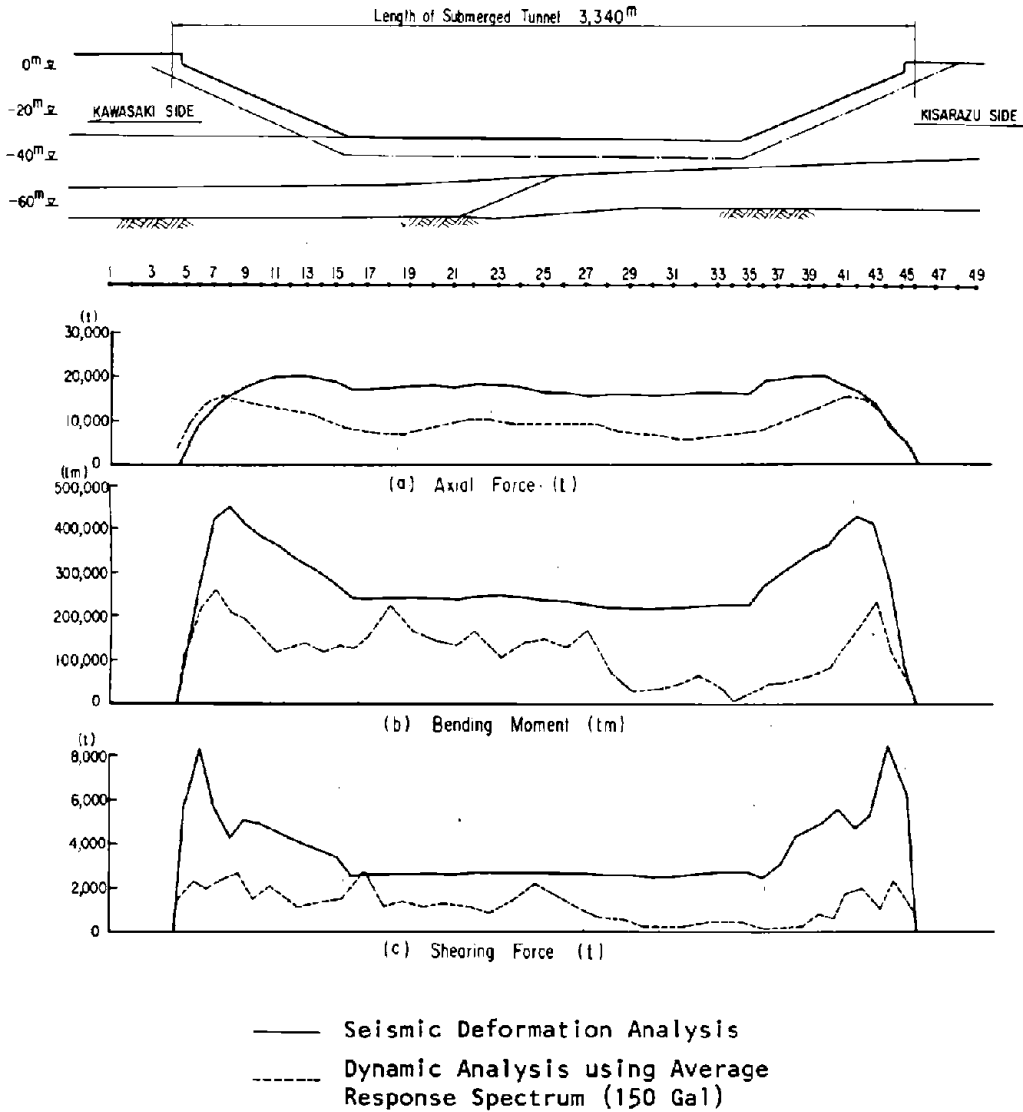
The bending moments and forces created in a submerged tunnel by an earthquake can also be determined by using the computer methods described in Chapter 4. Computer models permit more accurate descriptions of the physical systems and the input motions than do the seismic deformation and coefficient methods. However, this does not necessarily mean that the computer models should replace the seismic deformation and coefficient methods. In fact, the Japanese specifications¹⁴² require both:

Any part of the structural system shall be designed by the seismic deformation method and the seismic coefficient method. . . . Also the total structural system shall be designed according to the results of the dynamic response analysis, in which the influence of the surrounding topography and geology on the tunnel shall be considered.

An appropriate model for the determination of sectional forces uses beam elements to represent the tunnel segments and a lumped-parameter system to represent the soil.^{95,96} The input motion for this model is represented either by a response spectrum or by a time history at the bedrock. Kuribayashi et al. present the results of a computer model analysis of the proposed highway tunnel crossing Tokyo Bay between Kawasaki and Kisaraza.^{60,145} In Figure 51, the results of this analysis (which uses an averaged response spectrum with a maximum acceleration of 150 Gal) are compared with the results of the seismic deformation analysis. The model is also analyzed for four earthquake time histories; the results are shown in Figure 52, with the peak accelerations given in parentheses after the name of each earthquake.

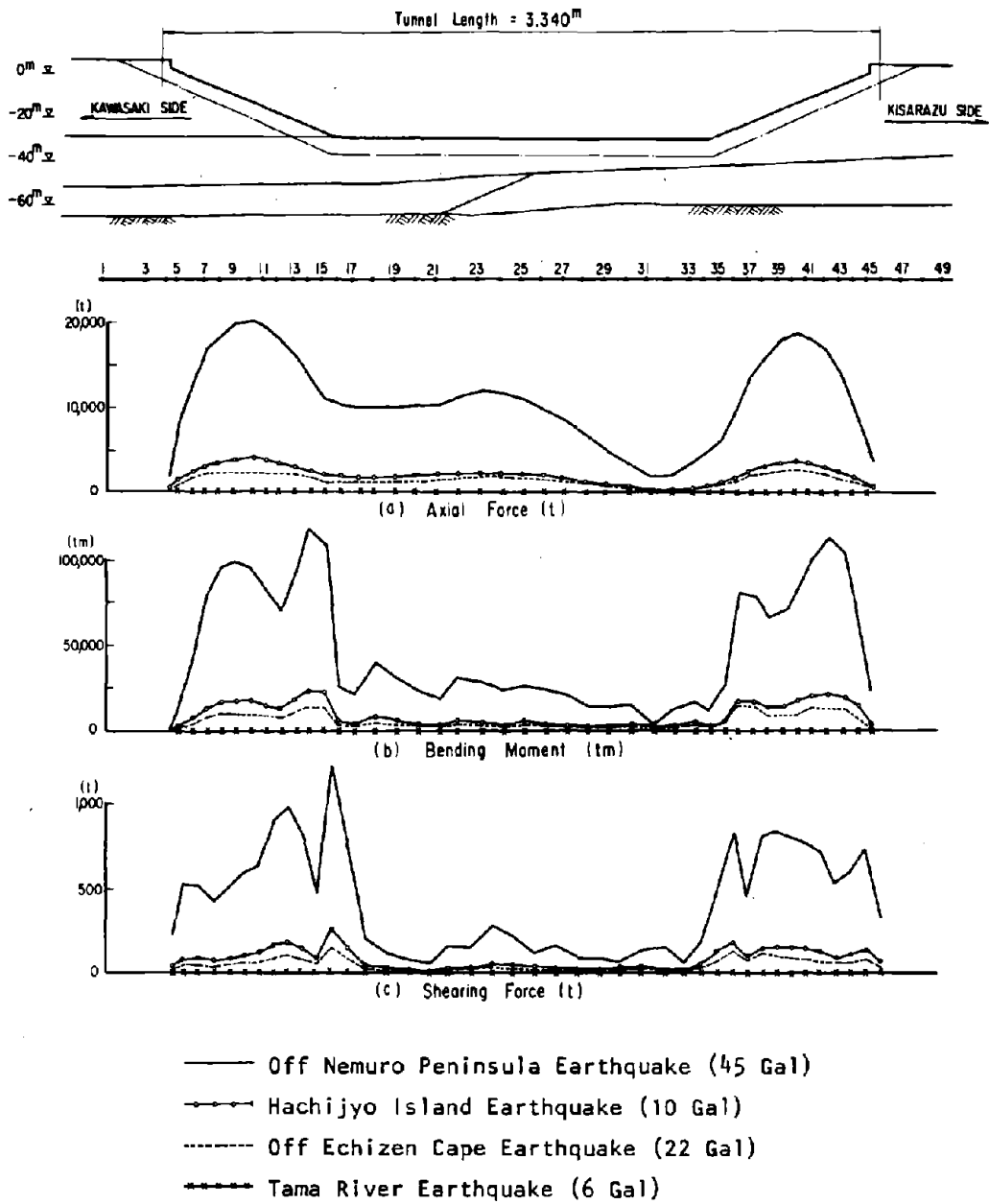
Circumferential bending due to seismic earth pressures and inertial forces can be investigated by a two-dimensional finite-element model of the tube cross section and a portion of the surrounding soil. If sufficient details of the concrete cross section and circumferential reinforcement are modeled in the finite-element scheme, the details in the cracking of the concrete can be readily studied.¹⁴⁶

Japanese investigators have also studied other aspects of dynamic analysis of submerged structures. For example, the literature includes references to response spectra,¹⁵¹ motion recorded in submerged tunnels,^{95,96,152} and physical models.^{95,96,153}



NOTE: 1 m = 3.28 ft; 1 t = 2,205 lb;
1 tm = 7,233 ft-lb; 1 Gal ≈ 0.001g.

Figure 51. Distribution of sectional forces by seismic deformation analysis and dynamic analysis.
(Source: Reference 145.)



NOTE: 1 m = 3.28 ft; 1 t = 2,205 lb;
 1 tm = 7,233 ft-lb; 1 Gal = 0.001g.

Figure 52. Distribution of sectional forces by dynamic analysis using four different earthquake waves.

(Source: Reference 145.)

Special Design Consideration: Seismic Joint

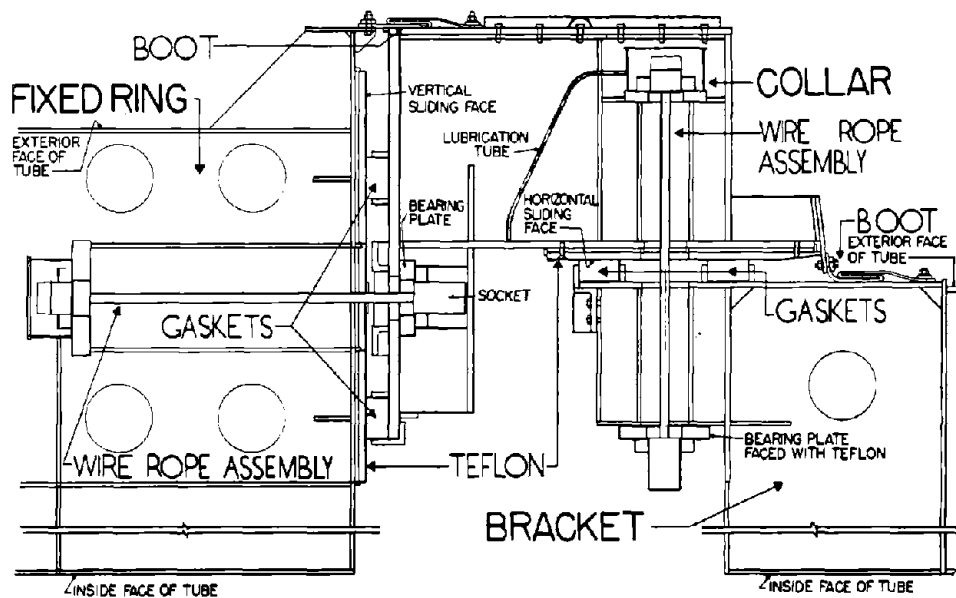
An important design consideration for submerged tunnels is the possibility of differential motion between the ends of the tube and its approaches. In general, a tube lies in the soft muds below the waterway, while the tunnel approaches pass through firmer soil. During earthquake vibrations the two soil masses will respond differently, producing differential displacements between the precast tube and the tunnel approaches.

The San Francisco approach of the SFBART transbay tube consists of two shield-driven, steel-ring tunnels with a transition to the tube at a ventilation structure founded 400 ft (122 m) offshore in the San Francisco Bay mud. The Oakland approach, a cut-and-cover tunnel, is connected to the tube by an onshore ventilation structure. The transbay tube itself, consisting of 57 prefabricated tube segments placed in a dredged trench, spans a distance of approximately 3.6 miles (5.8 km) between ventilation structures.

Theoretical analyses and tests of scale models indicated that there would be differential movements between the SFBART tube and the ventilation structures during ground shaking. Thus, a seismic joint was incorporated into the tube segments at each end to permit calculated movements during an earthquake of 1-1/2 in. (3.8 cm) in either direction axial to the tube and 4 in. (10.2 cm) in any direction transverse to the tube (i.e., in the vertical plane between the tube and the ventilation building). An additional 2 in. (5.1 cm) was permitted in the vertical plane to allow for the possibility of differential settlement. A sliding joint was devised to accommodate these movements as well as the earth and water pressure.

The details of the sliding joint are illustrated in Figure 53. The joint consists of six major elements, as described below by Douglas and Warshaw:¹⁵⁴

1. Bracket - The bracket is rigidly attached to the tunnel section, and around the periphery of the bracket are two elastic gaskets that act in a manner very similar to a piston ring.
2. Collar - The collar is a ring section that is designed to slip over the gaskets of the bracket in a manner similar to a cylinder of an automobile over a piston. The inside face of the collar is designed to permit it



Reprinted by permission of the publisher.

Figure 53. Details of seismic joint for the SFBART subaqueous tube.
(Source: Reference 154.)

to slide along the bracket gaskets. The dimensions of the sliding surface are such that when the collar is placed over the bracket the collar will compress the bracket gaskets to form a watertight seal. Two elastic gaskets are placed on the vertical face of the collar.

3. Fixed Ring - The fixed ring is a tunnel-shaped section rigidly attached to the building. When the collar is assembled to the fixed ring these gaskets are compressed on the vertical face of the fixed ring in such a way that they provide a watertight seal. The vertical face of the fixed ring is designed to permit gaskets on the collar to slide along this face.
4. Wire Ropes - In order to compress the collar gaskets to the face of the fixed ring, wire ropes are placed between the collar and the fixed ring and tensioned, thereby compressing the gaskets. The wire ropes are flexible and are designed so that they can safely carry the increased stress in them because of the sliding movement of the joint. Wire ropes are also used to compress the bracket gaskets to the collar as well as to transmit any unbalanced loads on the collar to the bracket.
5. Gaskets - These elements are made of a rubber compound and are attached to the collar and the bracket and provide the watertight seal between components.
6. Teflon Surfaces - In order for the sliding joint to be effective, it has to be able to move under a small force which will not damage the tunnels or the buildings. The only restraint to the motions in the sliding joint is the frictional force which will develop between the gaskets and the faces on which they are in contact. The coefficient of friction between rubber on steel is high and, if the rubber gaskets were directly in contact with steel, the force to overcome the friction of the rubber against the steel face would be such that the stresses produced in the tunnel and building would be too high. Therefore, all surfaces in contact with the rubber gaskets were faced with Teflon in order to reduce the restraining frictional force to a value that will minimize the stresses in the structures.

UNDERGROUND STRUCTURES IN SOIL

Most underground structures in soil are tunnels for the conveyance of motor vehicles, trains, fresh water, or wastewater. Such structures are distinguished by being very long compared with their cross-sectional dimensions because their purpose is to connect places together, not to provide volume. Other underground

structures, such as convention halls, parking garages, office areas, or water reservoirs, provide volume or enclose spaces. (The basement portion of surface structures is not included in this definition of underground structures.) Seismic design concerns for tunnels and for volume structures in soil are similar. However, the specific procedures and formulas for curvature and axial deformations presented below are developed for tunnels and are not directly applicable to volume structures.

SFBART Approach to Structures in Soil

The method of analysis for curvature and axial deformation of a lined tunnel in soil is similar to that for a subaqueous tube. Assuming an elastic beam embedded in an elastic medium, the formulas for sectional forces would be Equations (61), (62), and (63).

Kuesel, in setting forth the seismic design criteria used for the SFBART subways, describes a departure from that approach.⁵⁹ Instead of assuming interaction between the soil and the structure, Kuesel makes the more conservative assumption that the structure conforms to the shear wave deformation shown in Figure 45. The strain due to axial displacements is

$$\epsilon_a = \frac{\partial u_x}{\partial x} = \frac{2\pi A}{L} \sin \phi \cos \phi \cos \left(\frac{2\pi}{L} x \cos \phi \right) \quad (75)$$

From the theory of bending for an elastic beam, the extreme fiber strain is

$$\epsilon_b = \frac{B/2}{R_c} \quad (76)$$

where:

B = width of the tunnel structure in the plane of bending

R_c = radius of curvature of bending

The radius of curvature is derived by

$$\frac{1}{R_c} = \frac{\partial^2 u_y}{\partial x^2} = -\left(\frac{2\pi}{L}\right)^2 A \cos^3 \phi \sin \left(\frac{2\pi}{L} x \cos \phi \right) \quad (77)$$

Neglecting the fact that Equations (75) and (77) are maximized by different values of x , Kuesel gives the combined axial and bending strain as

$$\epsilon = \frac{\pi A}{L} \left[2 \sin \phi \cos \phi + \frac{2\pi B}{L} \cos^3 \phi \right] \quad (78)$$

Clearly this is maximized by minimizing the value of L . Because Equation (76) is valid as long as the beam-span-to-depth ratio does not become much less than 3,¹⁵⁵ Kuesel assumes $L/\cos \phi = 6B$. Substituting this assumption into Equation (78) yields

$$\epsilon = \frac{\pi A}{L} \left[2 \sin \phi \cos \phi + \frac{\pi}{3} \cos^2 \phi \right] \quad (79)$$

The function in brackets has a maximum value of 1.67 for $\phi = 32^\circ$; therefore,

$$\epsilon_{\max} = 1.67 \frac{\pi A}{L} \cong 5.2 \frac{A}{L} \quad (80)$$

in which L is taken as $6B$ (this should be $6B \cos 32^\circ$, but $\cos 32^\circ$ is dropped for convenience). The value of A is determined from Equation (52), the design displacement spectrum for SFBART, as

$$A = CL^n$$

where $C = 1.0 \times 10^{-7}$ for loose sand and soft clay or 1.1×10^{-8} for dense sand and stiff clay and where $n = 1.86$ for loose sand and soft clay or 1.95 for dense sand and stiff clay. The units of A and L are in feet.

Box structures in soils are subject to racking by shear distortions in the soil, as illustrated in Figure 54. The amount of racking Γ imposed on the structure is estimated from the assumed distortions in the soil. Assuming $\Gamma = u_y/h$ (see Figure 54), Kuesel uses a parametric study to determine an approximate relation for the racking in terms of the depth of the soil layer and the shear wave velocity of the soil. Because that approximate relation is only applicable to the soil conditions in the locations of the SFBART subway structures, it is not presented here. Regardless of how the shear distortion is determined, the capacity of the reinforced concrete box structure to withstand the racking within accepted limits of elastic and plastic distortion must be investigated. When the imposed shear distortion creates plastic rotation of joints, such joints should be detailed in accordance with design practice for reinforced concrete structures.

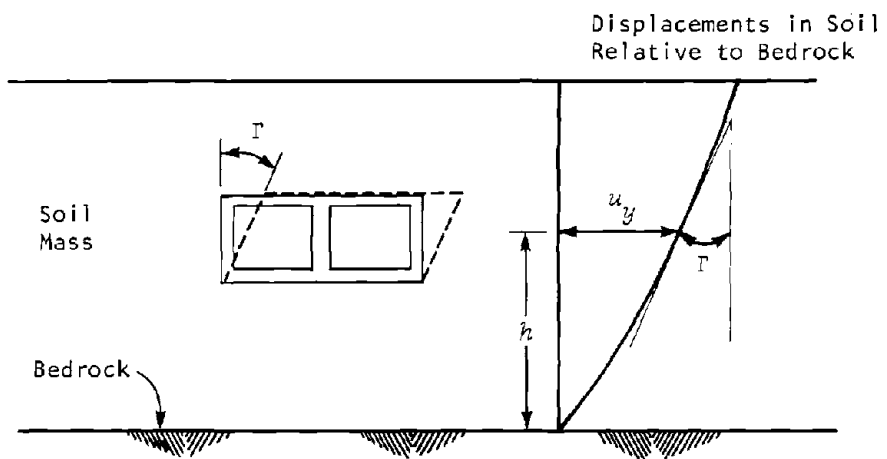


Figure 54. Racking due to shear distortion of the soil.

Mononobe-Okabe Theory of Dynamic Soil Pressure

Lateral earth pressures on earth-retaining structures increase during earthquakes. Although most codes do not recognize this fact,^{9,139-141} the need to consider increases in the lateral earth pressure on underground structures is recognized in several documents, namely the Japanese *Specification for Earthquake Resistant Design of Submerged Tunnels*,¹⁴² the SFBART procedures,¹⁴ and the seismic design requirements of the East Bay Municipal Utility District.¹⁵⁶ The accepted theory for determining the increase in lateral earth pressure is the Mononobe-Okabe theory, which is described by Seed and Whitman.¹⁵⁰

Using the Coulomb theory, Mononobe and Okabe compute the active earth pressure P_{AE} during an earthquake to be¹⁵⁰

$$P_{AE} = \frac{1}{2} \gamma_s H_w^2 (1 - k_v) \cdot K_{AE} \quad (81)$$

where:

$$K_{AE} = \frac{\cos^2 (\phi - \xi - \psi_w)}{\cos \xi \cos^2 \psi_w \cos (\delta + \psi_w + \xi) \Xi^2}$$

$$\xi = \tan^{-1} \frac{k_h}{1 - k_v}$$

$$\Xi = 1 + \left\{ \frac{\sin (\phi + \delta) \sin (\phi - \xi - \psi_g)}{\cos (\delta + \psi_w + \xi) \cos (\psi_g - \psi_w)} \right\}^{1/2}$$

γ_s = unit weight of soil

H_w = height of retaining wall

ϕ = angle of friction of soil

δ = angle of wall friction

ψ_g = slope of ground surface behind wall

ψ_w = slope of back of wall to vertical

k_h = horizontal design ground acceleration (in g)

k_v = vertical design ground acceleration (in g)

Seed proposes that the increment of dynamic pressure ΔP_{AE} above the static pressure can be approximated by¹⁵⁰

$$\Delta P_{AE} \cong \frac{1}{2} \gamma_s H_w^2 \cdot \frac{3}{4} k_h \quad (82)$$

For the underground box structure with shallow cover, H_w is the vertical dimension of the structure. Mononobe and Okabe considered that the total pressure computed by Equation (81) would act on the wall at the height of $H_w/3$ above the base. However, in the underground structure, vertical walls are restrained at the top as well as at the bottom. Consequently, it is more appropriate to apply the additional seismic earth pressure at midheight, so as to distribute it uniformly over the depth of the structure.

It should be noted that the static-plus-seismic earth pressure will usually not create a more severe design situation than the static-only earth pressure. During dynamic loading, allowable stresses may be increased by one-third. A study of the seismic earth pressure, Equation (82), reveals that the static design can probably withstand accelerations up to about 0.2g or 0.25g.¹⁵⁰

Computer Methods for Structures in Soil

Structures in soil can be analyzed using modern computer techniques much as subaqueous tunnels can. For example, a two-dimensional finite-element model, subjected to an input seismic motion, can be used to calculate stresses in the walls of the structure. Sectional forces can be evaluated using computer models of elastic beams for the structure and lumped masses and springs for the surrounding soil.

Two-dimensional computer models of cross sections of long tunnels are neither practical nor necessary along the entire length of the tunnel. Such models are impractical because they would require a prohibitively expensive exploration program to determine soil properties along the entire length. The dynamic behavior can be adequately evaluated by modeling several sections that bound the extremes of the problem. When the structure serves a critical function, more extensive computer modeling may be required. If the linear extent of the critical structure is confined, then an extensive exploration program to support the modeling effort will not be as costly as it would be for a long tunnel. Examples of critical structures for which more extensive modeling may be both necessary and practical are water reservoirs and subaqueous tunnel approaches.

Special Considerations in Design

Rock Intrusions. Rock zones within a soil mass may provide a hard bearing point for the underground structure during seismic activity. At transitions from soil to rock and at locations where bedrock juts into the excavation region, the structure should not be cast directly against the rock. Kuesel suggests at least a 2-ft (0.6-m) over-excavation filled with soil or aggregate backfill.⁵⁹

Abrupt Changes in Cross Section. Discontinuities in the underground structure itself may also present problems. The designers of SFBART recognized that the junction of a tunnel structure with a larger station structure will be subjected to differential rotation and translation due to the difference in stiffnesses of the two structures. It is better to design the joints at these junctions to accommodate the differential deformations than to provide rigid connections.⁵⁹ This principle should be followed wherever abrupt changes in the underground structure occur.

Corner Reinforcement. In the static design of a box-type cut-and-cover structure, the vertical reinforcing steel on the inside face of the earth-retaining walls is only needed in the midheight regions of the walls. To simplify placement of reinforcement, this steel is usually extended to the top and the bottom of the wall. However, during racking, the inside face of the corners will experience tension. Therefore, for seismic considerations, the steel should be further extended into the top and bottom slabs and hooked at the far face, as illustrated in Figure 55. This detail was included in the design of the reinforced concrete tunnel structure of the Stanford Linear Accelerator.¹⁵⁷

Abrupt Soil-Rock Interface. If a tunnel must be excavated through an abrupt interface between large soil and rock masses, a seismic joint may be required. For example, the North Point tunnel (North Shore Outfalls Consolidation, Contract N-2) of the current construction program in the San Francisco Wastewater System will pass through an abrupt soil-rock interface. An evaluation of the relative motion between the tunnel in rock and the tunnel in soil was conducted by Dames & Moore, one of the geotechnical consultants to the wastewater program. They recommended design for a relative tunnel displacement of 12 in. (30.5 cm) in any direction over a distance of approximately 50 ft

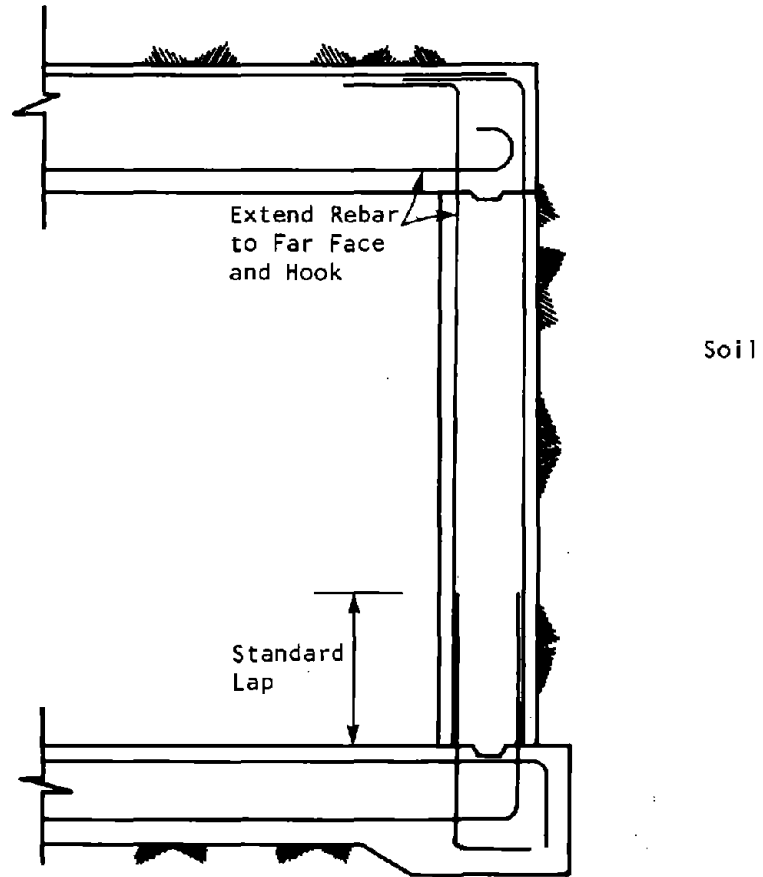


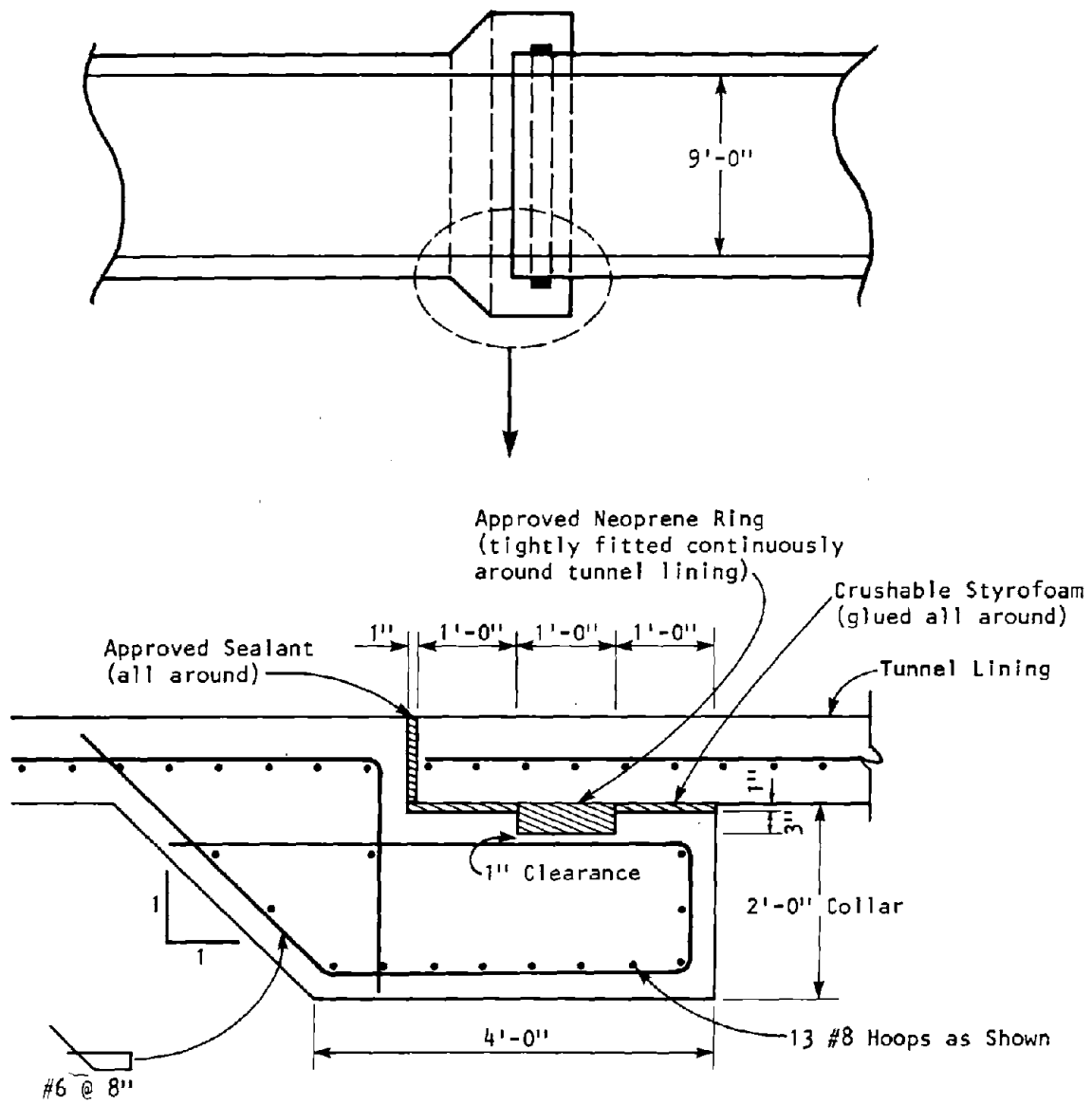
Figure 55. Corner details for seismic design.

(15.2 m) where the tunnel passes abruptly from rock to soft soil.¹⁵⁸ Thus the wastewater program has specified the construction of a seismic joint at the rock-soil interface and another seismic joint 50 ft (15.2 m) from the interface in the soil.¹⁵⁹ Details of the seismic joint are illustrated in Figure 56, which is based upon construction drawings.¹⁶⁰ The 1-in. (2.54-cm) thickness of crushable styrofoam in the joint will allow the joint to articulate sufficiently to conform to the predicted displacements. This detail would be very difficult to construct in a tunneling operation, especially if wet, running soils are encountered. However, the detail is feasible for cut-and-cover construction.

Excess Pore Pressure. Excess pore pressure due to seismic motion may create a potential for uplift on a box structure; one possible solution to this problem has been adopted for the San Francisco Wastewater System. The large sewer box structure under Marina Boulevard (North Shore Outfalls Consolidation, Contract N-4) will pass through soil with a high potential for liquefaction during an earthquake. One possible consequence of liquefaction is uplift of the box structure due to excess pore pressure acting on the underside of the structure. To mitigate this effect, Dames & Moore recommended gravel drains beneath the structure and gravel drains along the sides extending above the water table.¹⁶¹ This will permit excess pore pressure to dissipate, thereby reducing uplift. The bottom drain must be continuous, which can be easily achieved by over-excavation and backfilling with gravel. Because longitudinally continuous side drains introduce construction difficulties, vertical gravel drains can be developed by using alternate cells of steel sheet piling. Details of the gravel drains are illustrated in Figures 57 and 58, which are based upon construction drawings.¹⁶⁰

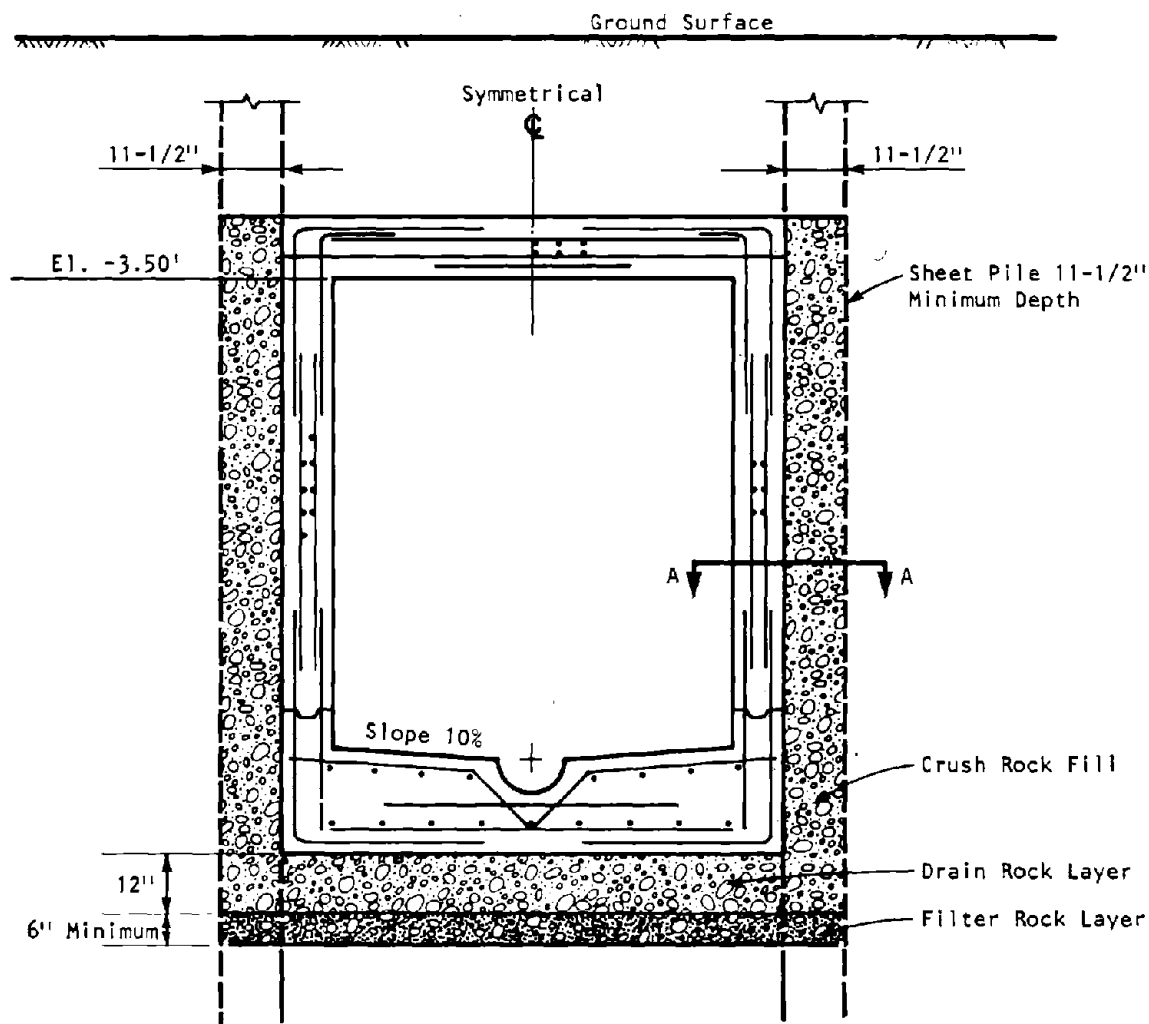
UNDERGROUND STRUCTURES IN ROCK

The distinction between the supports for tunnels in rock and those in soil may be blurred because of the large range of conditions that exists in both rock and soil. However, openings in competent rock are often quite different from those in soil. Competent rock in general permits larger spans and may require little or no support for static stabilization. If support is needed, it may consist of rock bolts and/or a thin layer of shotcrete. When considering the dynamic behavior of such underground structures, it is readily apparent that the lining, if it exists, is so flexible that it cannot be thought of as an elastic



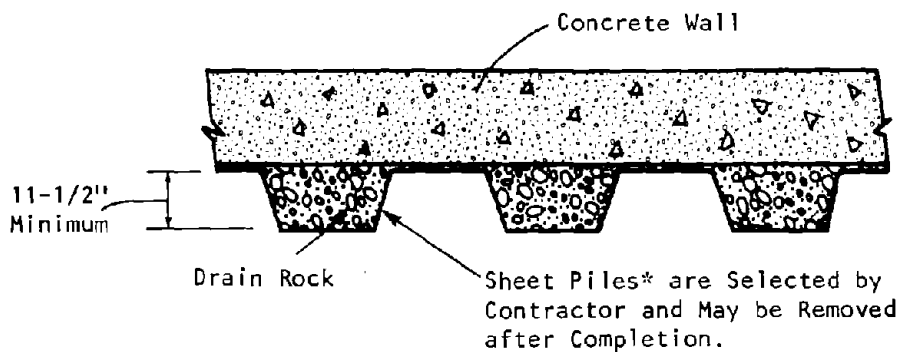
NOTE: 1 in. = 2.54 cm; 1 ft = 0.3048 m.

Figure 56. Seismic joint for North Point tunnel.
(Adapted from Reference 160.)



NOTE: 1 in. = 2.54 cm; 1 ft = 0.3048 m.

Figure 57. Cross-sectional details of drain for Marina Boulevard box. (Adapted from Reference 160.)



Section A-A

NOTE: 1 in. = 2.54 cm.

*If sheet piling is not used, equivalent vertical drain passage shall be provided with the approval of the engineer. Continuity between vertical drains and bottom drain rock layer must be provided.

Figure 58. Detail of vertical drain for Marina Boulevard box.

(Adapted from Reference 160.)

beam embedded in an elastic medium as is the case for many structures in soil. Steel sets with lagging, often used in poor rock, also cannot be viewed in this way. Reinforced shotcrete liners for poor rock or the thick concrete liner often required in highway tunnels or water conveyances (for reasons other than static stability) may be considered embedded beams, although the moduli of the liner material and the rock are approximately the same. Consequently, many of the simplifying assumptions employed in modeling the dynamic behavior of structures in soil cannot be used for structures in rock. For this reason, and because of the popular assumption that openings in rock are not vulnerable to earthquake motion, the current practice of earthquake engineering is poorly developed for structures in rock.

Perhaps another reason for this retarded development is that the static design in rock is largely dominated by empirical procedures. The development of sophisticated dynamic design methods is not encouraged because of the lack of compatibility with prevalent static design methods. However, this situation may be changing. In recent years there have been many studies evaluating static ground-liner interaction and design procedures.¹⁶²⁻¹⁶⁷ It may be that these activities will lead to significant gains in the state of the art within static design. Thus, at this time, very little can be discussed about seismic design procedures other than to point out what has been tried to date and some of the potential developments.

Design Based on Geologic Engineering Principles

A simple approach to earthquake engineering of rock tunnels was developed and applied to a conceptual design study of a proposed nuclear waste repository.^{63,168} With this approach, dynamic stresses are calculated using a simplified model for determining free-field stresses within the rock mass and assuming a plane compressive or shear wave propagating in a homogeneous full-space. This method is explained in Chapter 4 and is based upon Equations (6) and (10):

$$\sigma_{\max} = \pm \rho V_p |v_{\text{peak}}|$$

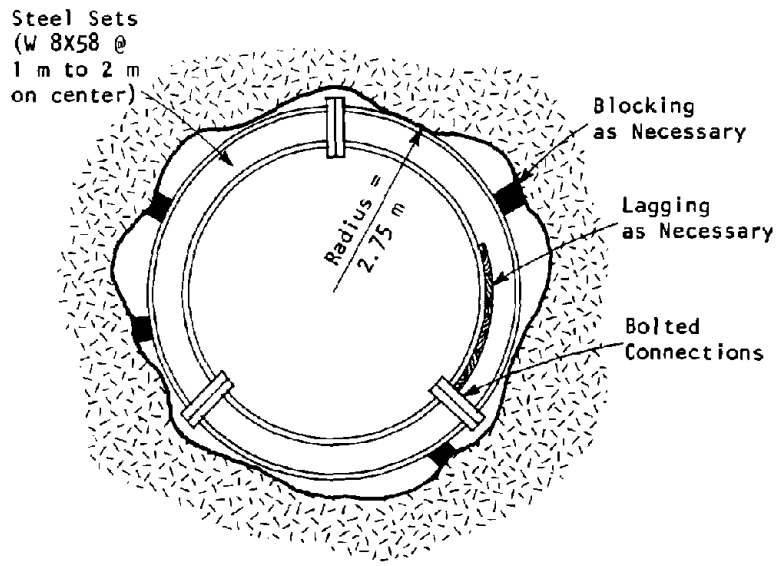
$$\tau_{\max} = \pm \rho V_s |v_{n,\text{peak}}|$$

The approach ignores the nonhomogeneities and discontinuities in the rock, the refraction of wave energy around the opening, and the complicated

superposition of incident and reflective waves from the free ground surface. However, such computations seem to be acceptable within the largely empirical framework of current underground static design. Dynamic stresses determined by this procedure are compared with the estimated in situ stresses. If the subtraction of a tensile seismic stress pulse from the compressive in situ stresses results in tensile stresses in the rock, seams may open and permit rock blocks in the tunnel to loosen (and perhaps even to fall) as the tensile pulse passes. Thus, an approximate evaluation of the dynamic stability of a tunnel is provided.

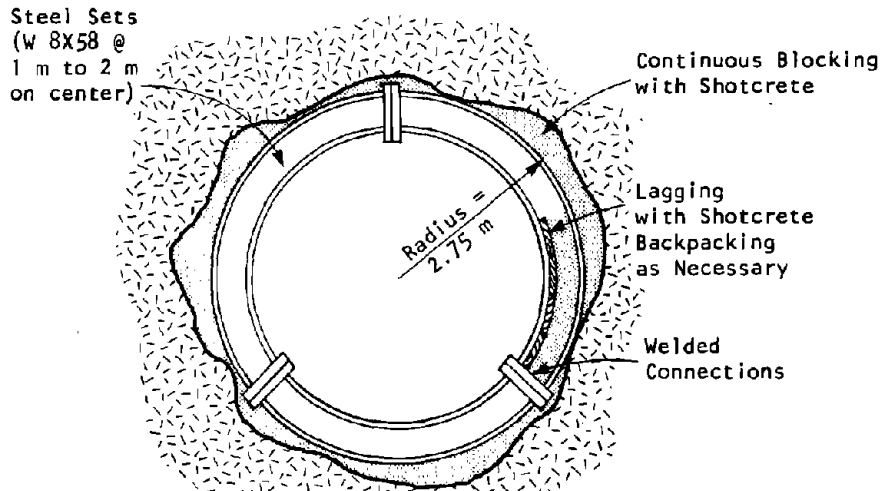
In addition to a rough determination of seismic stresses, Reference 168 suggests a further evaluation of the dynamic response of the cavity by reviewing the reported experience from tunnels exposed to dynamic loads and by qualitatively considering the interaction between supports and surrounding rock. Two very different stabilization systems are considered, one using steel sets, as shown in Figure 59a, for a shale that is likely to behave as squeezing ground at great depth, and the other using rock bolts, as shown in Figure 60a, for a highly competent granite. The following design concepts, which represent a conservative approach for resisting peak accelerations of 1.0g, were established:¹⁶⁸

- It is not advantageous to harden these two systems in terms of stiffening them. An approach of maintaining flexibility is the better one. The incremental effort associated with dynamic loads should be focused on the quality of the details of the support and reinforcement systems selected for static loads and on the prevention of possible spalling or popping of rock blocks. In principle, a carefully executed, flexible stabilization system is preferable to a relatively stiff system of stabilization. Hence, attention is given to improving construction details to achieve a more coherent medium-tunnel system.
- Consider first the steel support system selected for the tunnels in shale. Inherently, this system carries a substantial reserve, or resilience. Both the assessment of static load and the assessment of the capacity of the system, derived from the squeezing-ground load condition, are rather conservative. A steel set seldom fails because the ultimate strength of a given, continuous member of the steel set is exhausted. Rather, it is the failure of connections between the different parts of the set, or a situation of unbalanced loading, that results in failure of the set. Consequently, the



a. For static load

(scale is distorted to emphasize details)

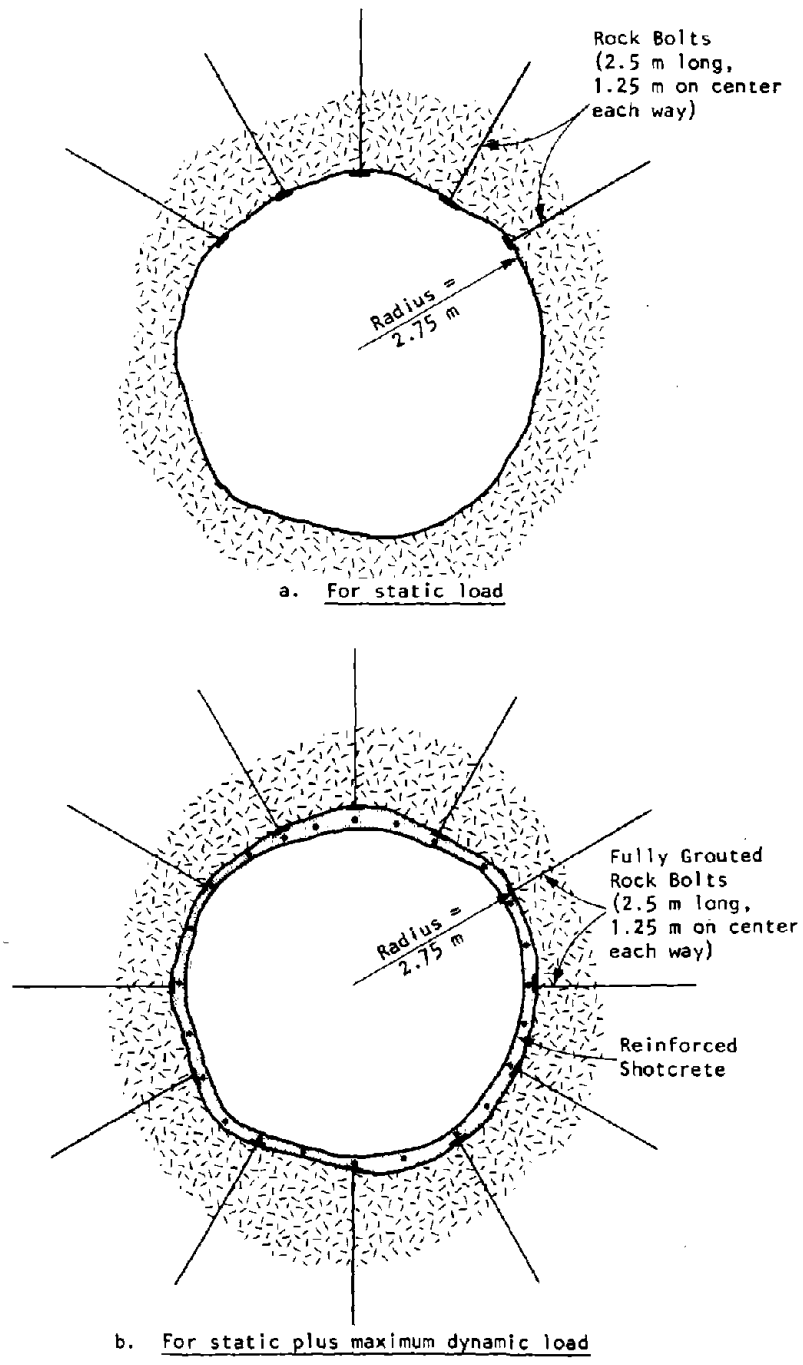


b. For static plus maximum dynamic load

NOTE: 1 m = 3.28 ft.

Reprinted by permission of the publisher.

Figure 59. Tunnel stabilization system using steel sets.
(Source: Reference 168.)



Reprinted by permission of the publisher.

Figure 60. Tunnel stabilization system using rock bolts.
(Source: Reference 168.)

incremental support requires greater attention to construction detail and workmanship than normally would be required if only the static loads were considered. It is better to weld rather than simply to bolt together the different pieces of a steel set in order to establish continuity. Steel sets should be securely tied together in the longitudinal direction.

It is imperative that the ground and the support be continuously coupled under dynamic loads. Thus, continuous blocking is much preferable to spot blocking. This can be attained by using continuous shotcrete blocking of the steel set and, if needed, back-packed lagging or reinforced shotcrete between the sets.

- Similar considerations are applicable for the rock-reinforcement systems selected for the granite. Rock-bolt details are improved by grouting the full length of the bolt. It is [preferable] to increase the amount of rock reinforcement by bringing it around the full circumferential area of the opening rather than springline to springline, as dictated by static conditions. The spalling of rock blocks between the fully grouted bolts can be prevented by the use of reinforced shotcrete.

As stated above, the design procedure presented in Reference 168 was originally applied to a conceptual design study for a nuclear waste repository.⁶³ The critical nature of such an underground structure and the shortness of time and money for the study encouraged the somewhat arbitrary application of the full improvement program to the 1.0g level, as shown in Figures 59b and 60b, with various reductions for decreasing g-levels. The application of the full improvement program to the 1.0g level is probably quite conservative. However, more information is needed to quantitatively relate the requirements for additional stabilization to increases in expected peak acceleration.

Design Based on Stress Calculations

In the above method,¹⁶⁸ the simple stress calculations do not account for the presence of the tunnel. Dynamic stress calculations should consider two general situations: one in which a plane seismic wave propagates normal to the tunnel axis and another in which it propagates parallel to the tunnel axis. The first situation has received considerable interest because it results in dynamic stress concentrations in the circumferential stresses around the cavity. Furthermore, this situation can be modeled as a two-dimensional plane strain

problem that can be treated by classical methods for circular cavities and by finite-element or finite-difference schemes for noncircular cavities.

The situation in which the seismic wave propagates parallel to the tunnel axis has not received any attention, perhaps because there are no stress concentrations associated with longitudinal stresses. However, as was pointed out in Chapter 4, waves propagating parallel to the tunnel result in axial and curvature deformation. This may cause opening of seams and joints, possibly leading to rock fall. However, a numerical evaluation of stresses due to curvature bending cannot be modeled by a beam and would require a three-dimensional model. The extreme computational difficulties and high costs involved with three-dimensional models are very real deterrents to stress computations for this situation.

Homogeneous Media. As described in Chapter 4, circumferential stresses due to plane waves propagating normal to the tunnel axis can be calculated by several procedures. A simple procedure presented by Chen, Deng, and Birkmyer⁶⁴ for circular cylindrical tunnels uses the free-field stresses as given by Equations (6) and (10) multiplied by appropriate stress-concentration factors depending on whether the wave is a P-wave or an S-wave and on whether the tunnel is lined or unlined. Many of the dynamic stress-concentration factors used in Reference 64 were computed by Mow and Pao⁶⁵ and are shown in Figures 20, 21, 23, and 24.

The advantage of the analytical method presented in Reference 64 is its simplicity in calculating the maximum possible circumferential stresses for circular tunnels. These stresses may be used to evaluate the strength of the lining or, if the tunnel is unlined, of the rock itself. The procedure is based upon elastic behavior and does not consider joint properties or plastic response of the rock mass. Lew⁶⁸ presents a very detailed outline for the design of liners for circular openings in rock. The procedure was developed for the hardening of a deep underground structure subjected to an extreme shock load created by a nuclear blast at the ground surface. The load is visualized as a large vertical pressure induced by a compressional wave propagating downward. Conceptually this has similarities to the earthquake load, except that the imposed pressure from a nuclear blast will be many times

(probably many orders of magnitude) greater than the pressure from an earthquake. The design steps itemized by Lew follow very logically from acquisition of specific material and load data, to determination of liner forces, and finally to determination of liner thickness. Procedures are detailed for both steel plate and reinforced concrete liners. Because the steps are very straightforward, they will not be reviewed here; however, a few comments are in order.

The circumferential forces, such as springline thrust and springline bending movement, are determined by Lew from rock-liner interaction curves for given values of the medium Poisson's ratio, the medium-to-line modular ratio, and the liner radius-to-thickness ratio. However, the curves are not derived using a dynamic wave loading but rather using a static pressure equivalent to the peak dynamic pressure. In Chapter 4 it was noted that maximum stress concentration, for the unlined cavity, is about 10% to 15% greater in the dynamic case than in the static case and that this corresponds to long wavelengths approximately 25 times the cavity radius. Thus, the rock-liner interaction curves contain an unknown amount of nonconservatism for long wavelengths.

Lew discusses the basic concepts by which a steel or reinforced concrete liner maintains the stability of an opening in rock under shock loading. For steel liners used in protective structures, Lew has these comments:⁶⁸

These liners are usually grouted into place with a cement mortar. The cement mortar acts as a filler, filling in the space between the liner and rock and providing essentially continuous contact between the liner and the rock. The continuous contact reduces the circumferential bending moments induced in the liner by the rock. Irregular contact between the liner and adjacent rock causes high, localized circumferential bending moments in the liner. Moreover, these high bending moments may cause the liner to buckle locally and collapse.

Note the great similarity in these concepts with those propounded by Owen, Scholl, and Brekke.¹⁶⁸ Furthermore, Lew added these comments on reinforced concrete liners:⁶⁸

A reinforced concrete liner does not tend to attract forces in the rock mass unless it is exceptionally thick and over-reinforced because its modulus is about the same order of magnitude as that for most competent rock masses: Within

certain limits, the bending strength of a R/C liner can be increased, as required, by increasing the amount of steel reinforcement.

Although these comments are made in the context of design for extreme shock loading, they are conceptually applicable to earthquake loadings.

Nonhomogeneous Media. When important discontinuities exist in the rock mass around the cavity or when the cavity is noncircular in cross section, the above-mentioned models can provide only very approximate values for the seismic stresses. In these situations, two-dimensional finite-element or finite-difference models become very useful tools for evaluating seismic stresses around cavities. Examples of finite-element and finite-difference codes and examples of their applications are given in Chapter 4. The use of these methods to model elastic and elastic-plastic behavior of continua is very common. However, models that incorporate various important rock mass properties, such as joint slip, strain softening, dilatancy, and tensile cracking, are still being developed (as noted in Chapter 4) and are not generally available for analysis of rock cavities.

The accuracy of the stress computation is not only limited by the ability of the model to accurately represent the behavior of the rock mass but also by the uncertainties in the geology. The rock mass is such a variable material that data collected at a few discrete points cannot possibly provide an accurate description for the entire rock mass under consideration. Consequently, a probabilistic description of the geology would be a desirable approach to rock tunneling. Such an approach has been suggested for evaluating alternative strategies for construction of rock tunnels.¹⁶⁹ In the area of seismic evaluation of rock cavities, Dendrou introduced uncertainty analysis into a finite-element calculation.¹⁷⁰ Dendrou expressed uncertainty in the geology by statistical variations in the modulus of elasticity, the Poisson's ratio, and mass density. Uncertainty was introduced into the dynamic behavior of the finite-element model by perturbing the natural frequencies of the model. Dendrou demonstrated that the application of uncertainty analysis and decision theory for seismic evaluation of rock tunnels is feasible. However, the experience

with this approach is so limited to date that there is little to guide the designer.

Special Design Considerations

Portals. The review of the effects of shaking on rock tunnels in Chapter 3 indicates that portals are vulnerable to damage. Although the literature does not contain any references to seismic design considerations for portals, there are certain obvious procedures a designer might follow. Some portals have been damaged by rock or soil slides; therefore, a careful evaluation of the seismic stability of the rock or soil slopes above and adjacent to the portal should be undertaken. Since rock tunnels sometimes emerge at the ground surface through surficial soil deposits, the portal structures may actually be serving as soil-retaining walls. In such cases, the retaining structures should be designed by the Mononobe-Okabe theory.¹⁵⁰

Caverns. Large caverns, such as those required for underground power plants or oil reservoirs, are generally excavated from hard competent rock that can be reinforced with rock bolts and/or shotcrete if needed. In general, the same concerns and design procedures described above for rock tunnels also apply to caverns. A potential concern in large caverns would be the movement of large rock blocks into the opening during seismic motion because the dimensions of the opening will exceed the spacing between joints in major sets of discontinuities. A thorough geologic survey of the joint systems is required. Attention should be given to improving the details of the rock reinforcement to achieve a more coherent medium-cavern system.

Finite-element and finite-difference models can be very effectively applied to caverns, perhaps more so than to tunnels. Because caverns are usually shorter than tunnels and house critical facilities, extensive explorations of cavern sites are justified. A computer model for a cavern can usually be more detailed than one for a tunnel because more geologic information is available. Furthermore, a single model is much more representative of a cavern than a long tunnel. An example of a seismic evaluation of a rock cavern using a computer model is presented by Yamahara et al.⁷⁴

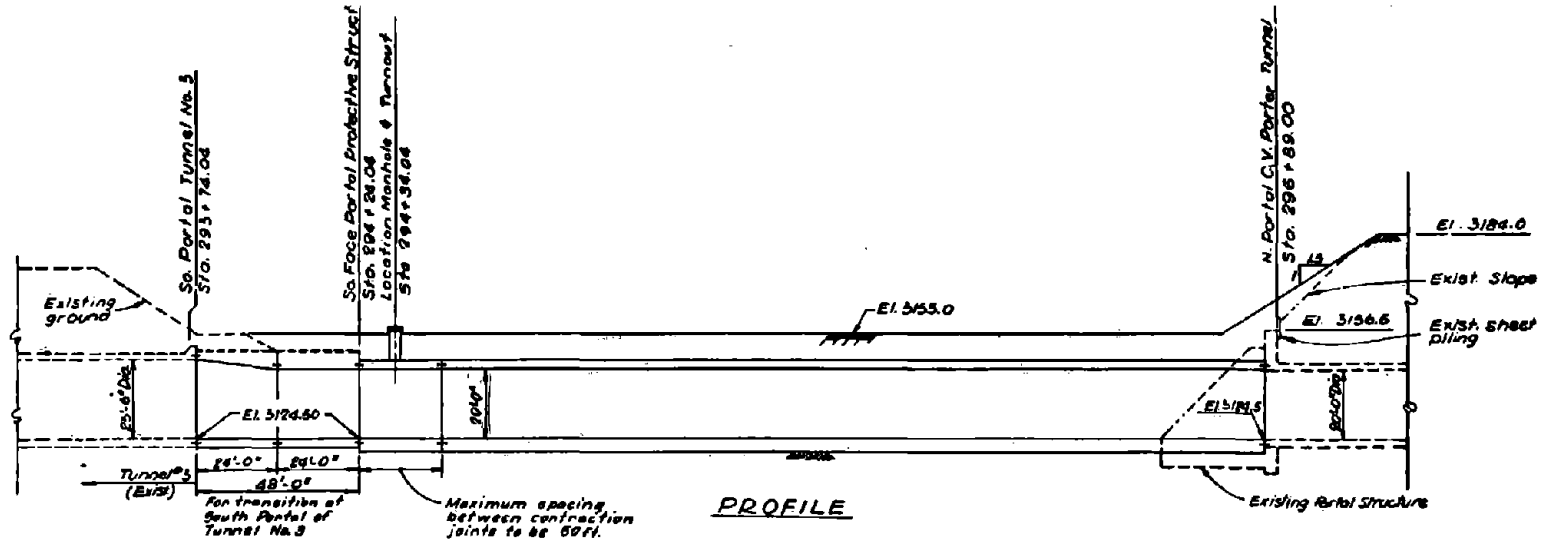
UNDERGROUND STRUCTURES INTERSECTING ACTIVE FAULTS

When a tunnel crosses an active fault, it is not possible to design the tunnel to withstand a potential offset in that fault. However, special design features can be incorporated to facilitate postearthquake repairs and reduce the extent of the damage. Examples of such design features are given below for three projects. In addition, special design features recommended for box conduits are presented.

Case Studies of Special Design Features

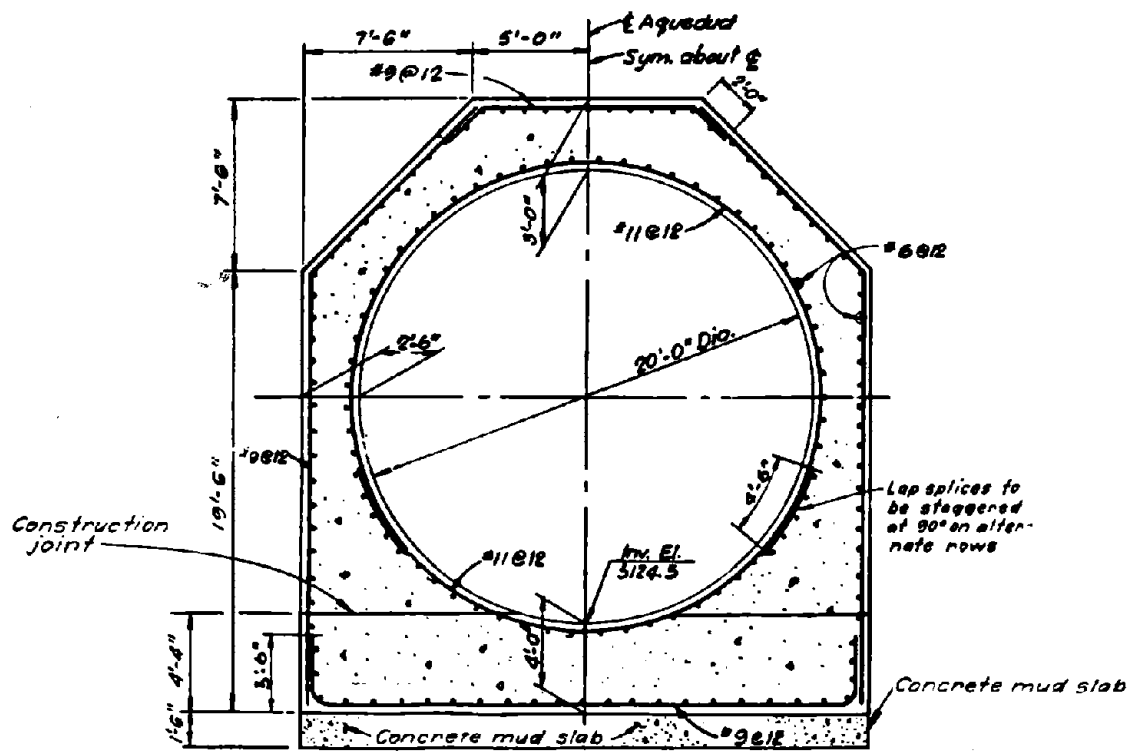
California State Water Project. The design philosophy in the California State Water Project was to cross major active faults either at the ground surface or at very shallow depths.^{171,172} This would facilitate repair in case of damage resulting from movement along a fault. The philosophy played an important role in determining the alignment of the California Aqueduct through the Tehachapi Mountains. Two basic alignments were originally considered for crossing these mountains: a low-level alignment, which would allow a relatively low pump lift at the southern end of the San Joaquin Valley, and a high-level alignment, which would allow a series of relatively short tunnels. The low-level alignment would have resulted in a long tunnel penetrating several major faults at great depth and would have resulted in adverse tunneling conditions and high construction costs. But the major reasons for not adopting this alignment were the extreme difficulty and high cost of repairing damage to the tunnel due to movement along one of the major faults. In spite of the high cost of lifting the water, the high-level alignment was chosen so that faults could be crossed at or near the surface. This also resulted in shorter tunnels and more favorable tunneling conditions.

In the final selection of the high-level alignment, only the Garlock fault was crossed underground. The south branch of the Garlock fault at Beartrap Canyon is crossed by the Beartrap access structure. This structure is a buried reinforced concrete conduit, 20 ft (6.1 m) in diameter and 315 ft (96.0 m) long, providing the connection between Tunnel No. 3 and the Carley V. Porter Tunnel. Details of this structure are provided by the profile and plan in Figure 61 and the typical cross section in Figure 62. The information given in these



NOTE: 1 in. = 2.54 cm; 1 ft = 0.3048 m.

Figure 61. Profile for Beartrap access structure. (Source: Reference 173.)



Scale 1/4" = 1'

NOTE: 1 in. = 2.54 cm; 1 ft = 0.3048 m.

Figure 62. Typical section of Beartrap access structure.
(Source: Reference 173.)

figures is derived from Reference 173. The north branch of the Garlock fault is also crossed, but on the ground surface. This crossing, known as the Pastoria Siphon, consists of a 0.5-mile (0.8-km) long steel conduit with an inside diameter of 16 ft (4.9 m).

SFBART. When a rock tunnel must cross an active fault, the tunnel might be made oversized through the fault zone. This approach was taken by SFBART where the train system crossed the Hayward fault in the Berkeley Hills between Oakland and Orinda. "The tunnel was made slightly oversized and was lined with closely spaced steel rib sections, to permit absorption of tectonic deformations and promote rapid repair and realignment of track in the event of any major shift along the fault."¹⁷⁴

East Bay Municipal Utility District. A rock tunnel used for the conveyance of water presents special problems if it crosses a fault that undergoes a major offset. Apart from having to drain the tunnel, rapid repairs to the tunnel may have to be made following an earthquake. The East Bay Municipal Utility District (EBMUD) of Oakland, California, has made extensive preparations for a major earthquake.¹⁷⁵ EBMUD's 10-ft (3-m) horseshoe-shaped Claremont tunnel crosses the Hayward fault in the Berkeley Hills. To facilitate repairs in the event of future slip along that fault, EBMUD modified the access structures at each end of the tunnel in 1967. Furthermore, steel sets and other materials essential to the rapid repair of this tunnel (and other facilities as well) have been stock-piled.¹⁷⁶

Recommendations for Special Design Features of Box Conduits

Some special construction features may be useful in mitigating the damage to a reinforced concrete tunnel in soil. Hradilek studied the damage to two underground box conduits, the Wilson Canyon and Mansfield Street boxes, due to the San Fernando earthquake of February 9, 1971.^{29,177} The Wilson Canyon box is intersected by the Sylmar segment of the San Fernando fault zone, which at that point experienced a left-lateral slip of about 4 ft (1.2 m) and a reverse dip slip of almost 8 ft (2.4 m). The Wilson Canyon box was severely damaged for a length of about 300 ft (91 m) by this thrusting and shearing. In addition, about another 200 ft (61 m) of the box to the north of this zone suffered major

cracks and separation because the soil in that region experienced a permanent extension. The damage to the Mansfield Street box was confined to a short length of 50 ft (15 m) adjacent to its confluence with the Wilson Canyon box due to compressive shortening of about 7 in. (18 cm). Although there were no surface expressions of faulting in that area, the damage was attributed to fault movement. The alignment of the two boxes is colinear; however, the Wilson Canyon box has a short branch off to one side that connects to an upstream open channel just at the point of confluence. Hradilek suggests that this jog offered resistance to longitudinal movements in the Mansfield Street conduit resulting in a local manifestation of compression crushing at that point.

From these observations, Hradilek offers several useful suggestions for the design of reinforced concrete conduits crossing a known active fault zone:¹⁷⁷

- Seismic joints should be closely spaced. Spacings of 30 ft (9 m) or less are suggested, but Hradilek notes that this is based on very limited data. The seismic joints provide weak bands around the box but maintain minimum strength during normal static conditions. During fault slip the seismic joints absorb the movements by separating or crushing. The seismic joint is formed by providing a void or crush-space with a wood form or friable masonry blocks as shown in Figure 63.
- Construction joints and seismic joints in the invert, walls, and soffit should all occur in the same vertical plane. The shear resistance R_j of the joint and the length L_j between the joints should be such that $2R_j \leq qL_j$, where q is the least transverse design load per unit length of the box. The use of shear keys in vertical joints is discouraged.
- If large displacements are anticipated, the conduit should be oversized.
- Changes in the geometry or properties of the cross section, sudden changes of direction, and confluence should be avoided in an active fault zone.

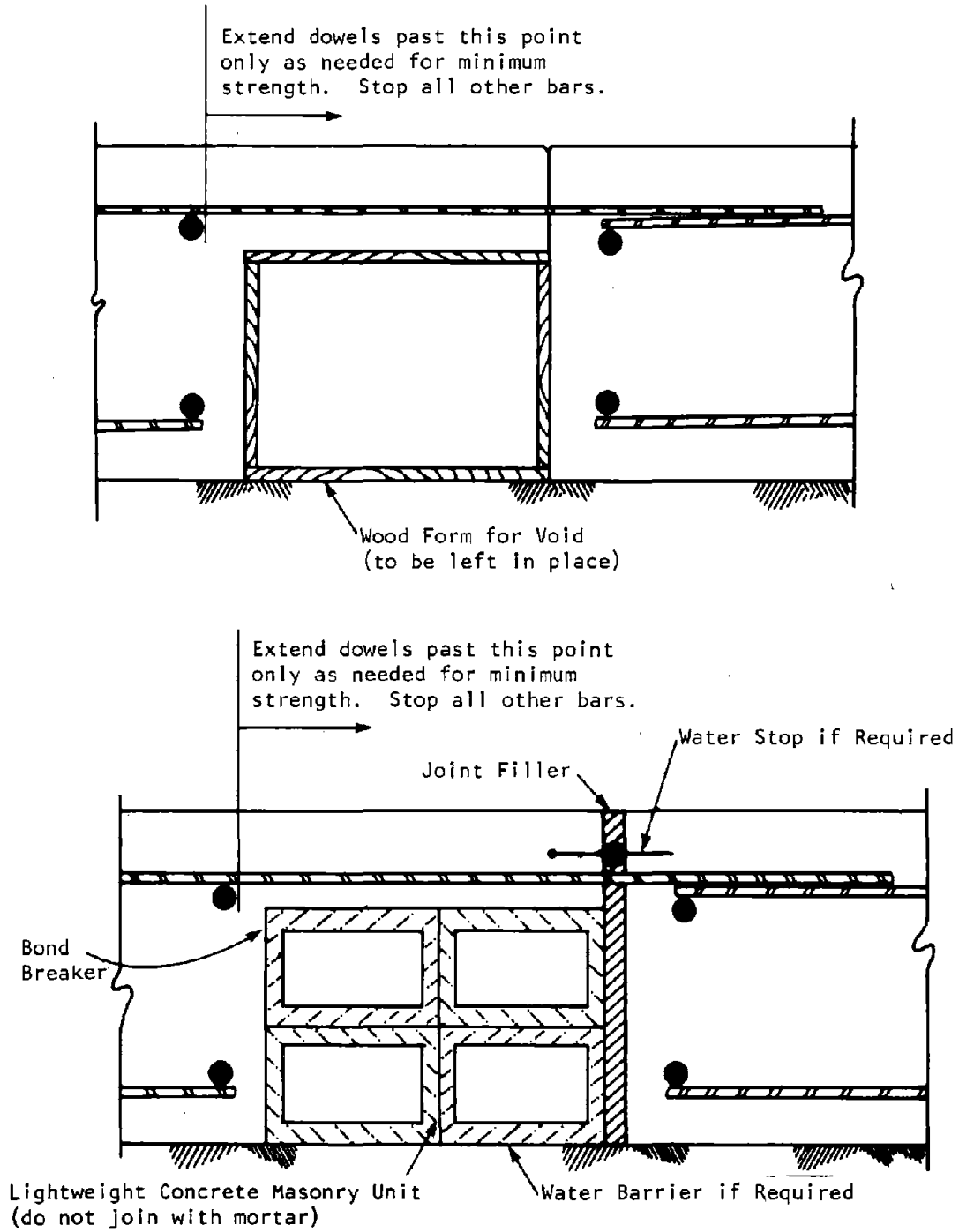


Figure 63. Proposed seismic joint for reinforced concrete conduit.

(Source: Reference 29.)

7. Critique of the State of the Art

The previous chapters discussed in considerable detail what is known about seismic damage to underground structures, the nature of underground motion, and the available technologies for analysis and design. The information presented constitutes the state of the art of earthquake engineering for underground structures. In this chapter, we shall indicate the areas where data and techniques are generally adequate and those where they are not.

EFFECTS OF EARTHQUAKES ON UNDERGROUND STRUCTURES

More data on the response of underground structures to earthquake shaking have been collected for this study than have been collected for any other single report. The data expands our understanding of the seismic vulnerability of various types of underground structures in different geologic settings. In general, the reported damage to underground structures is less severe than damage to surface structures at the same location. Damage to underground structures from shaking is generally minor, although major damage, meaning a large cave-in or closure, sometimes occurs.

This study has indicated that the type of data available is not sufficient to determine the relative importance of various parameters for predicting damage or lack of damage. The important parameters that influence the earthquake behavior of underground structures are identified in Chapter 3. These parameters are cross-sectional dimensions, depth below ground surface, strength and other characteristics of the rock or soil, support and lining systems, and severity of the shaking. The ground shaking at the site can be characterized by peak ground motion parameters, duration, frequency content, and intensity. At this time, it is not clear whether damage should be correlated with peak acceleration or with peak particle velocity; however, intuition suggests that correlation with peak acceleration is better for massive concrete structures in soil and that correlation with peak particle velocity is better for hard rock openings. Duration of the shaking is believed to be an important factor in that longer duration is expected to correlate with greater damage, particularly for buried concrete structures. Frequency content of the vibration may

also be important because some researchers suspect that damage to openings in rock is associated with wavelengths on the order of twice the cavity dimensions. These parameters have not been sufficiently studied in previous studies of observed effects, and it has not been possible in the confines of this study to collect information on all the parameters for the 127 cases cited in Appendix C.

The historical data base on the response of underground structures to earthquakes, while significantly larger than any reported elsewhere, is really a very small base from which to draw hard conclusions. The small size of the data base is in extreme contrast to the volumes of data recorded about the performance of surface structures during earthquakes. One of the reasons for this is that there are fewer tunnels, underground caverns, and other large underground structures than surface structures in the epicentral regions of most major earthquakes. Probably an even more important reason is the apparent lack of systematic surveys of underground facilities following major earthquakes. In general, damage to surface structures is more dramatic than damage to underground structures and is, of course, much more visible. As a consequence, reconnaissance teams sent to survey damage after major earthquakes are usually composed of engineers primarily interested in surface structures. This situation needs to be changed by establishing teams to survey underground structures following major earthquakes.

UNDERGROUND SEISMIC MOTION

Information on seismic motion recorded at depth (in boreholes, tunnels, mines, etc.) has been thoroughly reviewed in this study. These data indicate a general trend in the reduction of peak acceleration with depth, although records exist of peak amplitudes at depth that were greater than those at the surface. The records from layered soil deposits indicate amplitude amplification at the ground surface with respect to base rock for selective frequencies associated with the natural frequencies of the soil layers. This phenomenon seems to be well understood and can be modeled fairly well mathematically. However, the variation of amplitudes within rock at great depth seems to be poorly understood. For many decades, data were sparsely collected; only within the past several years have data been collected in a systematic way. Clearly many more records will have

to be obtained at depth before better descriptions can emerge as to variation of motion amplitudes and frequency content with depth.

Mathematical models could perform a useful function in helping us to understand the basic nature of underground motion. By using a very simple wave propagation model (SH-waves in an elastic half-space) in this study, we found that the variations of peak amplitudes with depth are strongly dependent upon the characteristics of the time history (in particular the temporal dispersion of peaks of approximately the same amplitude) and the duration of the motion. Much greater understanding could be obtained by employing more sophisticated models in conjunction with the further collection of recorded motion.

The importance of a good collection of data concerning the characteristics of underground motion and concerning the behavior of underground structures to seismic motion cannot be overstated. The development of earthquake engineering technologies for underground structures will only make significant advances when our understanding of underground motion and its effects on underground structures is adequately founded on observation. An analogy may be drawn with earthquake engineering of surface structures, which did not begin to approach the general level of present-day sophistication until after the recording and analysis of many time histories of strong surface motion and the detailed observation of buildings damaged by earthquakes. The state of the art of earthquake engineering of underground structures may be where the state of the art of earthquake engineering of surface structures was 20 to 25 years ago.

CURRENT PRACTICE IN SEISMIC DESIGN OF UNDERGROUND STRUCTURES

Seismic Design of Subaqueous Tunnels

In Chapter 6, the various methods currently used for the analysis and design of underground structures are reviewed in terms of subaqueous tunnels, structures in soil, and structures in rock. Of the three, the current methods for the analysis and design of subaqueous tunnels are the most sophisticated. This is because the submerged tube is constructed from highly predictable materials, such as reinforced concrete and steel, and does not depend upon the highly variable geologic medium to maintain the strength and stability of the opening.

In this way, the subaqueous tube is similar to surface structures. Consequently, the seismic design methodologies have been drawn from contemporary analytical technologies and up-to-date procedures for the design of steel and reinforced concrete surface structures.

Seismic Design of Underground Structures in Rock

Structures in rock differ from subaqueous tunnels in that the geologic medium is a major component of the structure. In fact, in cases where the rock does not require support or reinforcement, the geologic medium is the structure. The technologies for analyzing the seismic stability of an opening in rock and for determining hardening procedures are poorly developed. One reason for this retarded development is that there are very few reports of major damage to openings in rock from earthquakes, and therefore designers usually ignore this potential failure mode.

Perhaps the most significant reason that earthquake engineering technologies are so poorly developed for rock openings is that the state of the art in static design of such openings is itself still in its infancy. The relationship between the static and seismic design methods can be best understood by referring to Table 5 and Figure 64.

The available technologies for static and seismic design take sharply different approaches depending upon whether the rock mass is assumed to be homogeneous and elastic or is assumed to be nonhomogeneous and inelastic. If the rock is assumed to be homogeneous and elastic, compatible procedures exist for the analysis of both static and seismic stresses. The Kirsch's solution is used to determine the stresses in homogeneous, elastic rock around circular openings due to the in situ stress field. Terzaghi and Richart used the Kirsch's solution to compute the distribution of stresses around a circular tunnel for a case in which the horizontal in situ stress was 0.25 times the vertical in situ stress, which corresponded to a Poisson's ratio of 0.20.¹⁷⁸ (Terzaghi and Richart also presented solutions for elliptical tunnels and spheroidal cavities.) Mow and Pao have determined the dynamic stress-concentration factor for the circumferential stress in homogeneous, elastic rock around a circular tunnel due to steady-state harmonic waves.⁶⁵ In an analysis for earthquake motion, the maximum stress around the opening can be estimated by multiplying the peak seismic stress in

Table 5. Compatibility of earthquake design methods with static design methods for openings in rock.

Description of Geologic Medium	Static Design Method	Earthquake Design Method
Homogeneous and elastic	Two-dimensional stress analysis solutions available (For circular and elliptic tunnels, see Reference 178.)	Two-dimensional stress analysis solutions available (For circular tunnels, see Reference 65.)
Nonhomogeneous; various degrees of rock fracturing, joint inclination, etc.	Empirical methods	Some initial development ¹⁶⁸
	Simple analytical methods	?
	Rigorous analytical methods (i.e., finite element and finite difference)	Some initial development (finite element and finite difference)

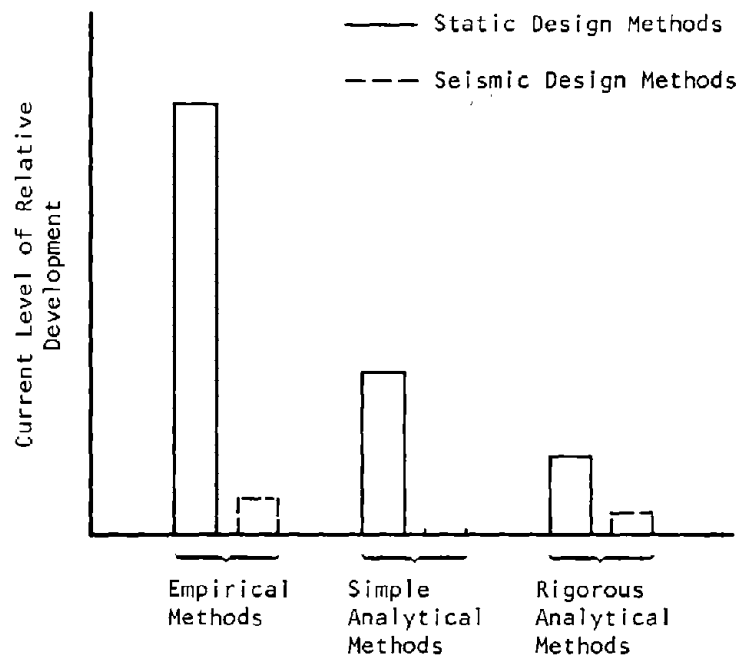


Figure 64. Comparison of current level of development between the various design methods.

the free field (determined from the peak particle velocity of the earthquake) by the Mow and Pao dynamic stress-concentration factor as described in Chapter 4. Thus, for circular tunnels in homogeneous, elastic rock, the methods for the analysis of static and seismic stresses are quite compatible, and the design can be evaluated by comparing the sum of the static and seismic stresses to the rock strength.

Even for noncircular openings, compatible static and seismic design technologies exist for homogeneous, elastic rock. Static stresses around such an opening can be computed by various contemporary approaches, such as finite-element, finite-difference, or boundary-element methods. Seismic stresses can also be computed using propagation of the earthquake motion with some of these same methods.

Real rock masses are not homogeneous and do not behave in an elastic manner. A number of empirical and analytical methods are available for the static design of tunnel supports in real rock masses. The empirical methods include Terzaghi's rock load approach,¹⁷⁹ the new Austrian tunneling method of Rabcewicz,¹⁸⁰ and the methods by Barton et al.,¹⁸¹ Bieniawski,¹⁸² and Wickham et al.,¹⁸³ which use a number of parameters to quantify the geology. These and other empirical methods have been reviewed in a recent paper by Einstein et al.¹⁸⁴ Sophisticated analytical methods, such as finite-element analysis, have been applied to both two-dimensional and three-dimensional analyses of tunnels in jointed rock (for example, References 184 and 185). While the application of rigorous analyses requires accurate and detailed information on the geology and the development of appropriate constitutive models, the application of empirical methods, which are based on actual observations of prototype openings, does not require such detailed quantification of the geologic information. In the design of an underground opening, the information on the geology is usually very limited prior to excavation, thus favoring empirical methods. During construction, although the information about the geology has greatly increased, decisions regarding the initial support must be made rather quickly, which also favors the use of empirical methods over analytical procedures. Consequently, there is a much greater dependence upon empirical methods and with that a much greater development of empirical methods. A third type of method -- a simplified analysis -- has been developed for circular tunnels. This method uses limited quantitative

data on the geology in conjunction with a simple but rational analytical model to determine support requirements.¹⁶⁴ Conceptually, the simplified analysis falls between the empirical and rigorous analytical methods. It should be noted that this discussion of static design of openings in rock is not intended to be complete, but only to indicate the general nature of the design methods.

In the design of supports for openings in real rock conditions, few seismic methods exist that are compatible with the existing empirical and analytical methods in static design. The only seismic design method that is compatible with the empirical methods for static design is the one proposed by Owen, Scholl, and Brekke,¹⁶⁸ which is based upon a qualitative assessment of rock-support interaction and upon the empirical relationship between damage to rock tunnels and peak ground motion parameters of earthquakes. Seismic methods compatible with rigorous analyses for static stresses are based on the same procedures as the static methods (for example, finite-element and finite-difference methods), but at this time rigorous analyses for seismic stresses for openings in rock have not progressed beyond preliminary developmental stages.

Clearly seismic design technology is poorly developed for openings in rock. The significance of this poor development is relative to the function and location of the structure and the condition of the rock. While most rock openings probably will not need to be evaluated for seismic stability, structures located in areas with moderate to high seismic hazard should be evaluated. The need for a seismic evaluation becomes more emphatic if collapse of the opening could lead to major loss of life or could severely disrupt lifelines. Structures that perform very critical functions -- for example underground nuclear power plants and nuclear waste repositories -- require seismic evaluations regardless of the degree of seismic hazard.

Seismic Design of Underground Structures in Soil

A distinction must be made between cut-and-cover structures and soil tunnels that are excavated by tunneling methods. Cut-and-cover structures are generally reinforced concrete structures at shallow depths. Static loads are determined by conventional soil mechanics, and static designs follow the same well-established procedures that are used for reinforced concrete structures on the surface. Thus, the earthquake design procedures presented in Chapter 6

to design soil structures for deformation and increased soil pressure are compatible with static design practice for cut-and-cover structures.

The static design of soil tunnels is very different from that of cut-and-cover structures, partly because soil tunnels are usually deeper and often below the water table but more importantly because of the different construction methods used for soil tunnels. Tunnels excavated through stiff soils can be initially supported by steel ribs and lagging, with permanent concrete liners installed later. In contrast, tunnels in poor soils might require excavation with the aid of a shield and immediate lining with concrete or steel liner segments. The final static loads on the supports for a soil tunnel are determined by the principles of soil mechanics;^{186,187} however, the static design of liner segments for shield-driven tunnels is often governed by the forces required to jack the shield forward. Sometimes the hydrostatic water pressure on the final tunnel may be a much larger concern than the loads due to the soil. These brief comments on the static design of tunnel supports in soils are presented only for a general frame of reference and not for completeness.

Design of soil tunnels is very similar to that of rock tunnels. Because information on the soil prior to excavation is sparse and the time in which to make design decisions about support during construction is limited, there is a heavy reliance upon past experience with prototype structures. In this respect, the relationship between earthquake design methods and static design methods for soil tunnels is similar to that for rock tunnels; the methods are not entirely compatible and are very poorly developed at this time.

8. Recommended Research Activities

This assessment of the state of the art of earthquake engineering of large underground structures has led to the identification of several major research needs. These needs are summarized below, and specific research activities are suggested in answer to these needs.

The research activities will provide information essential to the design of critical underground structures. The design of repositories for the disposal of nuclear waste and toxic chemicals will require seismic evaluations regardless of the level of seismic hazard. Transportation tunnels, aqueducts, and other underground structures whose failure during an earthquake could seriously imperil public health and safety must be designed for earthquakes in regions of high seismicity.

The research activity with the highest priority is the collection of data on the effects of earthquakes on underground structures. These data will help to identify the conditions that lead to damage and to predict the types of damage that are likely to occur. Research activities directed toward the development of rigorous analytical and design methodologies are not as high a priority as those activities directed toward obtaining observational data. The development of these methods could wait until a design project arises that demands the application of rigorous procedures, although such postponement will not be particularly cost effective.

OBSERVED EFFECTS OF EARTHQUAKES ON UNDERGROUND STRUCTURES

It has been noted in the previous chapter that the data about the effects of earthquakes on underground structures form too small a data base from which to draw hard conclusions. In addition, the data needed for a definitive evaluation of the influence of various factors on damage to underground structures are not readily obtainable for past earthquakes. The parameters that are believed to influence the response of underground structures and about which information should be collected are as follows:

- Cross-sectional dimensions of the opening
- Depth of the structure below the ground surface
- Type of rock or soil, including strength and deformability characteristics
- Type and condition of the support and lining system
- Shaking severity, characterized by peak ground motion parameters, duration, frequency content, and intensity

Another situation that affects the usefulness of damage reports is the general lack of inspections of structures before an earthquake. Sometimes it is difficult to determine whether minor cracks in concrete lining or movements of steel sets resulted from the earthquake motion or were due to other events and existed prior to the earthquake.

It is often very difficult to obtain all the needed information indicated above, even for fairly recent events. Because some of the most useful information can be obtained from technical and lay persons close to the scene (perhaps more than from reports that have been prepared by outside reconnaissance teams), the more time that has elapsed since an earthquake, the less information can be obtained. Thus, efforts would best be spent on studying only very recent earthquakes (say, within the last ten years) and on preparing plans to conduct more thorough surveys of underground structures in future earthquakes. It is from this viewpoint that three experimental research activities are recommended.

Research Activity 1: Comprehensive Survey of Earthquake Effects on Underground Structures

A systematic study of all underground structures in the epicentral regions of recent destructive earthquakes should be undertaken on a worldwide scale. Detailed information should be collected on the earthquake and the underground structure (the ground and the support) so that comprehensive entries can be made in all columns of a table such as Appendix C. To provide the best opportunity for obtaining definite conclusions, the study should be limited to earthquakes that have occurred within the past ten years. The objectives of the study would be to initiate the establishment of a detailed data base and to formulate more definitive conclusions about how the various parameters affect damage or lack of damage.

Research Activity 2: Postearthquake Reconnaissance of Underground Structures

In the future, when a destructive earthquake occurs, special reconnaissance teams should be sent to the affected region to survey underground structures. It is recommended that the reconnaissance teams convened and dispatched to earthquake-devastated regions by such agencies as the U.S. National Science Foundation or the Earthquake Engineering Research Institute include among their members several people specifically delegated for surveying underground structures. Underground structures that should be surveyed include highway tunnels; railroad tunnels; fresh water tunnels (although if the tunnels are still operational, visual inspection will be impossible); tunnels and conduits that serve as major collectors for storm water and wastewater; subways; buried water reservoirs and water treatment facilities; powerhouse caverns; and storage facilities. Some of these structures are important components of lifeline systems and should be surveyed anyway. Data should be collected in as much detail as possible and with the intent to complete a table with headings similar to those given in Appendix C. It is important that all underground structures be included in the survey, not just those that are damaged. Thus the survey will provide a data base from which meaningful and definitive conclusions can later be formulated about the relationships of the various parameters and the extent or lack of damage.

Research Activity 3: Observations of Selected Tunnels Before and After Earthquakes

It is recommended that preearthquake observations be conducted in a number of tunnels so that it will be possible to distinguish between cracks, movements, and other damage due to nonearthquake sources and those due to an earthquake, should one occur. Of course, sites in regions of high seismic activity should be selected to increase the likelihood of being able to observe the results of a major earthquake within several decades.

A program of this type was proposed in a report by Brekke and Korbin to promote early installment of relatively simple instrumentation in a few selected tunnels in California.¹⁸⁸ The report suggested four levels of instrumentation with increasing sophistication. The basic level concerned the kinds of preearthquake observation envisioned here. (The other three levels involved the installation

of triaxial accelerometers.) Brekke and Korbin suggested that the following basic observations and measurements be conducted for a length of approximately 100 ft (30 m) along a tunnel:¹⁸⁸

- All defects in the support/lining system that can be observed at present should be carefully mapped either through sketches and/or through photographs. The orientation, length, and offset of cracks should be documented. Plaster can be placed occasionally over cracks to serve as an indicator of subsequent displacement.
- Measuring points for tape extensometer readings should be installed [at appropriate locations around the tunnel perimeter]. The points can be balls, rings, or pins, depending on the type of tape extensometer that is employed. After installation, careful extensometer readings shall be made, and repeated as part of the maintenance program (i.e., at least once a year) to check for possible deformations that are not earthquake induced.

Brekke and Korbin proposed three candidate tunnels in California for instrumentation: the Loleta Railroad Tunnel No. 40 in Humboldt County, the Caldecott Tunnel in Alameda County, and the San Fernando Railroad Tunnel No. 25 in Los Angeles County. At this time, these basic observations and measurements are being conducted in only the Caldecott Tunnel (along with the installation of some triaxial accelerometers).

UNDERGROUND SEISMIC MOTION

This study has thoroughly reviewed the available information on seismic motion at depth and concluded that the characteristics of underground seismic motion are poorly understood, except for motion in horizontal soil layers near the ground surface. Until recently researchers have obtained very few underground records, and most of those have been obtained in Japan. Additional strong motion instruments have been installed underground in recent years, mostly in Japan, where there is now a network of approximately 200 underground instruments; only a few installations exist in the United States and elsewhere. The published accounts of the records obtained to date indicate a general reduction of peak acceleration with depth, although there are instances where amplitudes at depth are greater than those at a more shallow depth or at the surface. At

this time, not enough data have been collected to provide a reliable predictive model or to address the anomalies of the variation of motion with depth.

Several other issues concerning underground seismic motion also remain poorly understood. The difference between the frequency content at depth in rock and at the surface and the role of frequency on depth dependence of motion amplitudes have been explored in the literature, but nothing definitive has been forthcoming. Some underground instruments have been placed in transportation tunnels, mines, and powerhouse caverns, but apparently only for the convenience of obtaining an underground site. There have been no attempts to compare the motions recorded in such structures with free-field motion in the nearby rock or soil at the same depth. Differences in motion between the underground structure and the free-field would indicate the manner in which the structure is responding to the motion.

It has already been noted (in Chapter 7) that mathematical models could perform a useful function in helping us understand the characteristics of underground motion. Unfortunately, it is difficult to represent the complexities of geology and wave types, and therefore only the simplest situations have been studied thus far.

The most obvious conclusion to draw from these observations is that a more aggressive program is needed in the United States for the recording of underground motions. Before recommending specific research activities for such a program, the general characteristics of instruments shall be discussed. In general, constraints on the fidelity of strong motion records are imposed by the type of transducer or seismometer rather than by the recorder.

Although velocity-sensitive transducers are desirable from the data processing viewpoint of ease of conversion to acceleration or displacement by either a single differentiation or integration, they have inherent low-frequency response limitations. A velocity-sensitive transducer must be physically large (and relatively expensive) to have a flat response much below 1 Hz. Nonlinear response at low frequencies can be corrected in the recording stage by electronic compensation or during data processing, but this complicates the system. Another constraint on velocity sensors is imposed by the mechanical limits of

coil-to-case motion in the transducer itself. A reasonably priced sensor (approximately \$1,000 in 1979) that has a natural frequency of 1 Hz and that is 0.7 critically damped will reach its limit at a displacement of only about 0.24 in. (0.6 cm), zero to peak. This constraint is a serious one if the seismic environment suggests a reasonable probability of exceeding this level of ground displacement. For example, a moderate-size earthquake will probably generate considerable motion in a frequency band from 1 to 5 Hz; for a peak particle velocity of approximately 4 in./sec (10 cm/sec), the displacements will range from 0.12 to 0.63 in. (0.3 to 1.6 cm).

Accelerometers do not have a limit on the amount of displacement they can tolerate. Force-balance (or servo) accelerometers will respond down to DC and can easily handle the anticipated levels of strong ground motion. Dynamic stress-concentration factors for circular cavities (discussed in Chapter 4) are highest for the low frequencies between DC and about 10 to 15 Hz, the upper value depending upon the wave speed and the cavity radius. Higher frequencies, corresponding to wavelengths on the order of two times the cavity dimension, may also be important to cavity behavior. Thus, it is desirable for the instrument to be able to respond from DC to about 100 Hz, which is within the capabilities of current accelerometers.

Accelerometers require a very stable power supply in contrast to the typical velocity-sensitive transducer, which is self-generating and requires no external source of power. Although the use of accelerometers would sacrifice some of the simplicity of data acquisition and processing provided by velocity-sensitive transducers, the broad dynamic range of accelerometers makes them the preferred type.

There are several digital recorders on the market that are specifically designed and admirably suited for the proposed task. All of them have the capability of continuously accepting motion data but recording only motions that exceed a predetermined threshold; all the data, including data for the quiescent period prior to the onset of motion, are preserved by means of introducing delay buffers between the incoming signal and the output to the recording mechanism.

The cost of a triaxial seismometer package consisting of three accelerometers, three amplifiers, and a three-channel recorder is approximately \$7,000 (in 1979 dollars).

Research Activity 4: Recording of Seismic Motion in Deep Boreholes

It is recommended that a program be undertaken to record and evaluate underground motions in boreholes down to depths of approximately 3,000 ft (approximately 1,000 m). Although shallow depths of just several hundred feet are of interest for shallow structures and for interaction between soil and surface structures, greater depths are important for understanding the nature of the motion arriving at deep tunnels and powerhouse caverns. A suite of four or five triaxial instruments distributed from the surface to the bottom of a deep borehole can provide an excellent source of data for studying the variation of motion with depth. The study should evaluate variations of peak values of acceleration, particle velocity, and displacement; the variations in frequency content; and the uphole-downhole spectral ratio. The ideal location for such boreholes would be in an area of active faulting, such as certain sections of the San Andreas fault, where a fair amount of data can be collected within a period of a few months to a year.

Research Activity 5: Recording of Seismic Motion in Underground Openings

To address the issues regarding the differences between the motion of an underground structure and the free-field motion at the same depth, an instrumentation program similar to that proposed by Brekke and Korbin¹⁸⁸ should be conducted. We recommend that several additional rock tunnels be selected in regions of high seismicity. (An actual number is not recommended, but two seems to be a minimum.) These tunnels, in conjunction with the already-instrumented Caldecott Tunnel in Alameda County, California, would begin to provide very useful comparative results after several years of observation. In selecting the rock tunnels, it would be useful to get different maximum covers. Because the Caldecott Tunnel has a maximum cover of about 500 ft (152 m), it would be advantageous to have one additional tunnel at a shallower depth and, if possible, the other deeper.

Additional structures other than rock tunnels should be considered for the program. A large rock cavern would be an excellent choice because the geometry and size of the opening is quite different from a tunnel. Another candidate structure would be a very shallow structure in soil, such as a cut-and-cover subway tunnel.

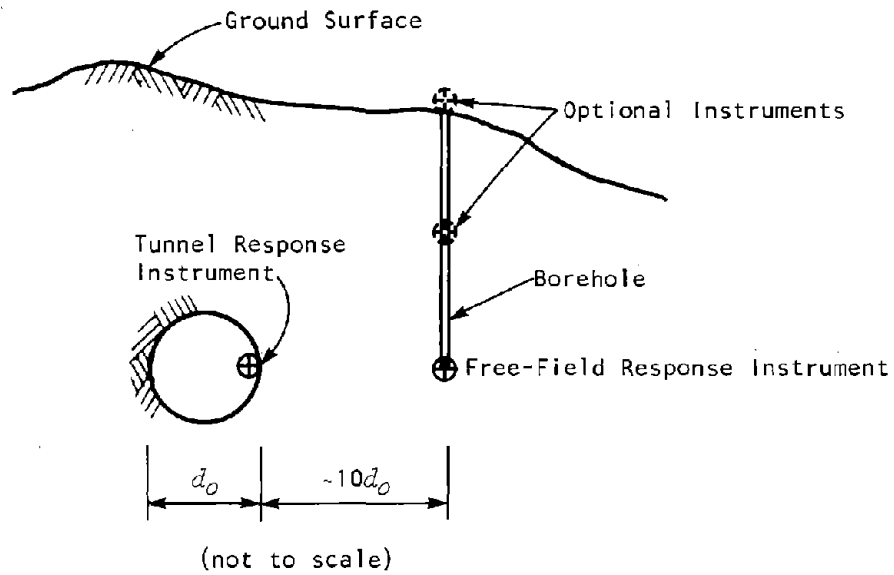
The type of instrumentation to be installed should be the triaxial accelerometer and recorder package described above. In keeping with the recommendation of Brekke and Korbin,¹⁸⁸ the minimum number of triaxial accelerometers for a rock tunnel would be three, located as follows (see Figure 65):

- One in the tunnel, well away from the portal region and, if possible, in the region of maximum cover, to measure the response
- Another located in the rock mass at the same elevation as the tunnel instrument, to measure the free-field motion
- Another located at one of the portals, to measure the portal response

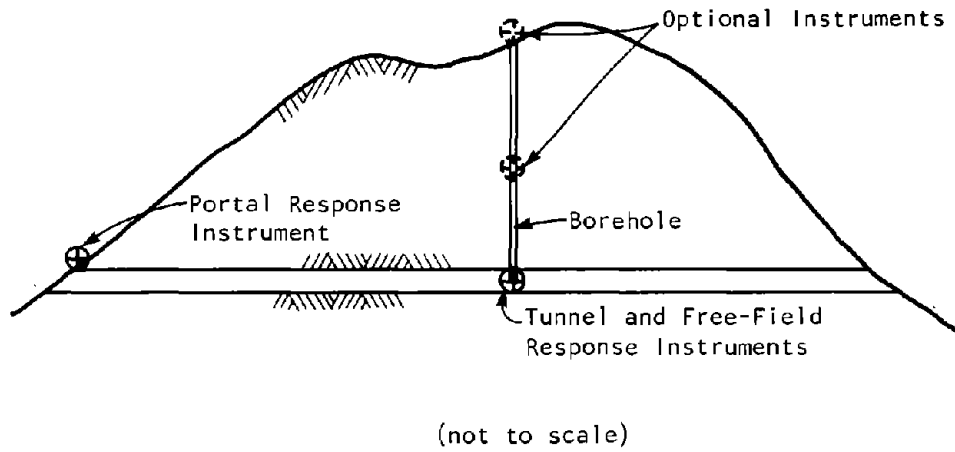
The free-field instrument must be located sufficiently far from the tunnel so that waves reflected from the tunnel will be attenuated to negligible values by the time they arrive at the free-field instrument. Brekke and Korbin suggest a distance of at least ten tunnel diameters;¹⁸⁸ this seems like a very conservative but practical suggestion.

Instrumentation of a portal is recommended because the portal is the part of the tunnel most susceptible to damage. Motions recorded there can be compared with the free-field motion and with the tunnel responses to see if there are important differences in the motions that might contribute to the greater susceptibility to damage.

The recording of free-field motion at the ground surface above the tunnel is not recommended for this program. Motion at the surface would be a poor basis for comparing tunnel response because of the reflection of wave energy at the free surface and the multiple reflection within the soil layers near the surface. However, because a borehole will probably have to be drilled to install the subsurface free-field instrument, certain elements of Research



a. Section through tunnel



b. Profile of tunnel

Figure 65. Proposed locations of triaxial accelerometers for a tunnel.

Activity 4 could be incorporated. By installing triaxial accelerometers at the surface of the borehole and perhaps another at middepth, a collection of data could be obtained to study the variation of motion with depth.

The locations of the instruments within a large rock cavern are more specialized than for a tunnel. Whereas a tunnel is long and connects to the ground at the portal, a cavern has large cross-sectional dimensions and is limited in length. Because we are mainly interested in the possible differences in motion around the perimeter of the cavern section, there should be four instruments located around the perimeter (away from the ends of the cavern) on the invert, the crown, and the sidewalls, in addition to the free-field instrument at the cavern elevation (see Figure 66).

It should be noted that the basic preearthquake observations and measurements proposed in Research Activity 3 should be carried out at the instrument stations recommended above.

Research Activity 6: Development of Analytical Models for Predicting Seismic Motion at Depth

Simple parametric studies such as those begun in this report should be continued as part of a program to develop analytical models for predicting seismic motion at depth. These efforts should be parallel to experimental efforts to understand the effects of depth upon underground motion from downhole records (see Research Activity 4).

This report considered only SH-waves in an elastic half-space. Models should be developed by slowly increasing their ability to represent the complexities of the geology and the waves. Premature development of a grandiose model that includes many complexities will be costly and may actually obscure the basic behaviors of underground motion. Thus, models should be improved in a small incremental fashion. A first step would be to include the propagation of P-waves and SV-waves in an elastic half-space; later steps would involve improving the model with horizontal layers over a half-space. The theoretical basis for these later steps is provided by Thomson¹⁸⁹ and Haskell.¹⁹⁰ What is now needed is the application of those techniques to actual geologic conditions

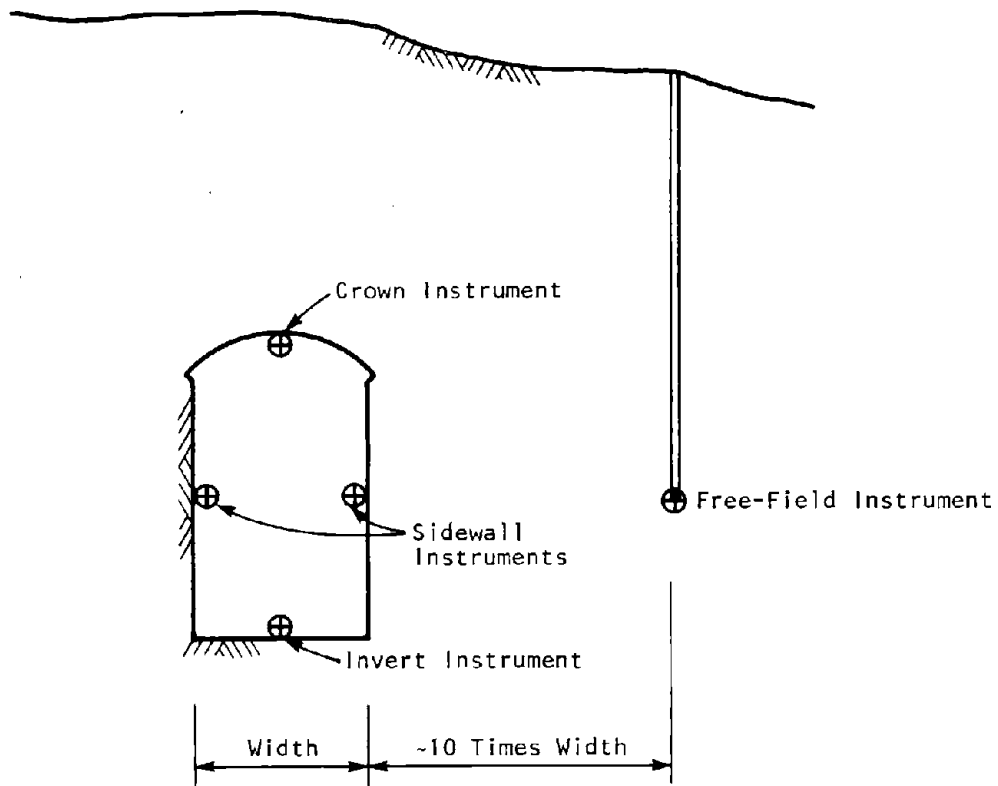


Figure 66. Proposed location of triaxial accelerometers for a large cavern.

and comparisons of predicted motion at depth with experimental values. Some work in this direction has already been started by O'Brien and Saunier,¹³⁰ who developed transfer functions for P-waves and SV-waves propagating through a single layer over a half-space. O'Brien and Saunier applied the model to an actual site and compared theoretical predictions of motion at depth with experimental values. Another step leading to improvement in the model would be to include nonlinear material properties.

Once these improvements to the model have been made, other improvements might be desirable. However, at this time it is not useful to speculate on what further improvements would be the most beneficial. The purpose of the improved models is really to mathematically determine what happens as seismic motion, partitioned into various combinations of P-, SV-, and SH-waves, approaches the ground surface at various angles of incidence. By comparing the results of such parametric studies to actual observed motion, it should be possible to begin to develop a better understanding of how and why motion varies with depth. In addition, the development of improved models would contribute to the construction of a definitive predictive model suitable for all situations.

SEISMIC ANALYSIS AND DESIGN OF UNDERGROUND STRUCTURES

This study indicates that there is a lack of appropriate analytical techniques for the determination of seismic stresses around tunnels and other large underground structures of arbitrary shape and for real geologic media. Existing dynamic codes are limited in their ability to model such important rock mass properties as joint slip, strain, softening, and dilatation. They are also somewhat limited in their ability to consider simultaneous propagation of different types of body waves (e.g., P-waves and SV-waves) with arbitrary angles of incidence. The importance of having such analytical techniques lies mostly in being able to conduct parametric studies of alternative locations and shapes of an opening for increased stability during seismic motion. Once such models are perfected, they will be useful in decisions regarding details of the support for specific designs.

At this time, the development of analytical techniques to predict shaking damage to underground openings in rock is probably more important to the design of large

caverns than to the design of transportation or water tunnels. Little is known about the seismic stability of large caverns because there have been so few observations of large caverns during strong ground motion. In contrast, observations of tunnels during earthquakes have been much more frequent and generally indicate the excellent stability of tunnels in hard, competent rock. Analytical techniques would be useful in resolving the uncertainty about cavern stability. In particular, analytical techniques would assist in assessing the effect of rock block sizes on the seismic stability of caverns. The sizes of rock blocks are generally more important to cavern stability than to tunnel stability because the block sizes are usually small compared with the cavern dimensions whereas they are large compared with the typical tunnel dimensions. A program to develop computer codes for stability evaluations for openings in rock, particularly for large caverns, is recommended below (Research Activity 7).

This study also indicates that there is a general lack of procedures upon which to base design decisions regarding additional support requirements for soil and rock tunnels and for rock caverns (see Chapter 7). There is a need to further develop the empirical seismic design method so that it can be used in conjunction with the fairly well-developed empirical methods for static design. At this time, there is no clear correlation between incremental increases in the severity of the earthquake shaking and corresponding incremental increases in the support requirements. Two programs (Research Activities 8 and 9) are recommended to begin to clarify this correlation.

Research Activity 7: Development of Computer Codes for Stability Evaluation of Openings in Rock

The development of computer codes for the analysis of the stability of openings in rock with particular application to large caverns should be encouraged. The code might build upon the existing works in finite-element, finite-difference, discrete-element, and boundary-element methods. In particular, the development should focus on incorporating better models of the rock mass and its properties, such as joint slip, strain softening, and dilatation. Advances in the codes for dynamic analysis should be compatible with developments of these codes for static and thermal analysis.

Research Activity 8: Development of Empirical Procedures for Seismic Design

The data base collected from studies of past and future earthquakes (Research Activities 1, 2, and 3) together with the records gathered from instrumented tunnels (Research Activity 5) should be carefully evaluated to develop empirical procedures for seismic design decisions. Tunnels might be grouped by different types and conditions of rock or soil so that variations in the support system for given ground conditions can be investigated. Then, by analyzing correlations between level of damage (or lack of damage) and various parameters representing the severity of the ground motion, it should be possible to draw conclusions about the additional needs for support for different ground conditions. The success of this proposed investigation requires a much larger and detailed data base than is presently available and is, therefore, dependent upon the careful execution of Research Activities 1, 2, 3, and 5.

Research Activity 9: Analytical Parametric Study of Seismic Stability of Openings in Rock

In conjunction with the development of a strictly empirical approach to seismic design decisions as described above, an analytical parametric study would be very useful in understanding those features of the rock mass and the support system that most affect the stability of an opening. An analytical parametric study could investigate the optimal use of rock bolts, shotcrete, steel sets, and various details of the support to stabilize openings in rock with different material properties, joint spacings, and joint orientations and under different magnitudes of in situ stress. The earthquake motion should be represented by two components of motion, which would be a much more realistic characterization than a single component of motion.

The success of Research Activity 9 will depend upon the further development of analytical technologies as suggested in Research Activity 8. Verification of its findings will depend upon the detailed collection of data from past and future earthquakes (Research Activities 1, 2, and 3).

Appendix A

Persons Contacted About Seismic Design of Underground Structures

A number of persons in both private firms and government agencies were contacted and asked to voice their concerns about the seismic stability of underground structures and to outline their approaches to seismic design. A list of these persons is provided below.

<u>Agency or Firm</u>	<u>Person(s)</u>
Fenix & Scisson, Inc. Tulsa, Oklahoma	R. S. Mayfield
Acres American Inc. Buffalo, New York	Dougal R. McCreath
McCarthy Engineering/ Construction, Inc. Tulsa, Oklahoma	D. F. McCarthy
RE/SPEC Inc. Rapid City, South Dakota	Paul Gnirk
Bureau of Reclamation Denver, Colorado	Jim Warden J. S. Dodd
Harza Engineering Chicago, Illinois	Kolden Zerneke William Shieh
California State Department of Water Resources Sacramento, California	Jack Marlette
Foundation Sciences Portland, Oregon	Larry Wilkenson Ken Dodds
Parsons Brinckerhoff Quade & Douglas New York, New York, and San Francisco, California	T. R. Kuesel Elwyn King George Murphy
U.S. Army Corps of Engineers, Los Angeles District Los Angeles, California	Peter J. Hradilek
U.S. Department of Defense, Nevada Test Site Mercury, Nevada	Joe LaComb

<u>Agency or Firm</u>	<u>Person(s)</u>
U.S. Navy Public Works Center Great Lakes, Illinois	Lloyd C. Jones (now at Purdue University)
J. Barry Cooke Inc. San Rafael, California	J. Barry Cooke
University of Illinois Urbana, Illinois	William J. Hall
University of California, Berkeley Berkeley, California	Tor L. Brekke Richard Goodman
Merritt Cases Redlands, California	J. L. Merritt
TeraTek Salt Lake City, Utah	Howard R. Pratt
Agbajian Associates El Segundo, California	George Young Bob Ewing
Jacobs Associates San Francisco, California	J. Donovan Jacobs A. M. (Pete) Petrofsky
Northwestern University Evanston, Illinois	Theodore Belytschko
Massachusetts Institute of Technology Cambridge, Massachusetts	Herbert Einstein
San Francisco Department of Public Works San Francisco, California	Frank Moss W. J. Scruggs Stephen Soo
San Francisco Water Department San Francisco, California	Paul Matsumura
East Bay Municipal Utility District Oakland, California	Walter Anton
National Science Foundation Washington, D.C.	William W. Hakala
Federal Highway Administration Washington, D.C.	James D. Cooper

<u>Agency or Firm</u>	<u>Person(s)</u>
Marin Historical Society San Rafael, California	L. Mazzini
University of Arizona Tucson, Arizona	Charles E. Glass
Southern Pacific Transportation Co. San Francisco, California	Tom L. Fuller Lynn Farrar
Ontario Hydro Toronto, Ontario	R. C. Oberth
Golder Associates Vancouver, British Columbia	Evert Hoek
Norwegian Geotechnical Institute Oslo, Norway	Nicholas Barton
Hagconsult AB Stockholm, Sweden	C. O. Morfeldt
The Royal Institute of Technology Stockholm, Sweden	Bengt B. Broms
Norwegian Institute of Technology Trondheim, Norway	Einar Broch
VBB Engineers Stockholm, Sweden	Rainer Massarsch
Basler & Hofmann Zurich, Switzerland	R. Sagesser
Electric Power Development Company Tokyo, Japan	Y. Ichikawa
Muto Institute of Structural Mechanics, Inc. Tokyo, Japan	K. Muto K. Uchida
Japan Railway Construction Public Corporation Tokyo, Japan	T. Ohira T. Tottori K. Aoki

<u>Agency or Firm</u>	<u>Person(s)</u>
Research Laboratory, Shimizu Construction Co. Tokyo, Japan	K. Yamahara K. Fukumitsu
Public Works Research Institute Tsukuba, Japan	E. Kuribayashi T. Iwasaki T. Tazaki T. Konda K. Kawashima

Appendix B

Abridged Modified Mercalli Intensity Scale

Descriptions of intensity values I through XII of the abridged Modified Mercalli Intensity scale² are given below.

- I. Not felt except by a very few under especially favorable circumstances. (I Rossi-Forel scale.)
- II. Felt only by a few persons at rest, especially on upper floors of buildings. Delicately suspended objects may swing. (I to II Rossi-Forel scale.)
- III. Felt quite noticeably indoors, especially on upper floors of buildings, but many people do not recognize it as an earthquake. Standing motorcars may rock slightly. Vibration like passing of truck. Duration estimated. (III Rossi-Forel scale.)
- IV. During the day felt indoors by many, outdoors by few. At night, some awakened. Dishes, windows, doors disturbed; walls make creaking sound. Sensation like heavy truck striking building. Standing motorcars rocked noticeably. (IV to V Rossi-Forel scale.)
- V. Felt by nearly everyone, many awakened. Some dishes, windows, and so on broken; cracked plaster in a few places; unstable objects overturned. Disturbances of trees, poles, and other tall objects sometimes noticed. Pendulum clocks may stop. (V to VI Rossi-Forel scale.)
- VI. Felt by all, many frightened and run outdoors. Some heavy furniture moved; a few instances of fallen plaster and damaged chimneys. Damage slight. (VI to VII Rossi-Forel scale.)
- VII. Everybody runs outdoors. Damage negligible in buildings of good design and construction; slight to moderate in well-built ordinary structures; considerable in poorly built or badly designed structures; some chimneys broken. Noticed by persons driving cars. (VIII Rossi-Forel scale.)
- VIII. Damage slight in specially designed structures; considerable in ordinary substantial buildings, with partial collapse; great in poorly built structures. Panel walls thrown out of frame structures. Fall of chimneys, factory stacks, columns, monuments, walls. Heavy furniture overturned. Sand and mud ejected in small amounts. Changes in well water. Persons driving cars disturbed. (VIII+ to IX Rossi-Forel scale.)

- IX. Damage considerable in specially designed structures; well-designed frame structures thrown out of plumb; great in substantial buildings, with partial collapse. Buildings shifted off foundations. Ground cracked conspicuously. Underground pipes broken. (IX+ Rossi-Forel scale.)
- X. Some well-built wooden structures destroyed; most masonry and frame structures destroyed with foundations; ground badly cracked. Rails bent. Landslides considerable from river banks and steep slopes. Shifted sand and mud. Water splashed, slopped over banks. (X Rossi-Forel scale.)
- XI. Few, if any, (masonry) structures remain standing. Bridges destroyed. Broad fissures in ground. Underground pipelines completely out of service. Earth slumps and land slips in soft ground. Rails bent greatly.
- XII. Damage total. Waves seen on ground surface. Lines of sight and level distorted. Objects thrown into the air.

Appendix C

Summary of Damage to Underground Structures from Earthquake Shaking

Information concerning damage to underground structures from earthquake shaking is summarized in tabular form in the pages that follow. One hundred and twenty-seven cases are cited. Each case has been assigned a number, which is shown in Column 1. The remaining columns (2 through 15) provide the following information, when available:

Source of Data: Column 2 identifies the reference(s) from which the information in the following columns is obtained.

Earthquake Data: Column 3 provides general information about the earthquake, such as location or name, date of occurrence, magnitude (M), and duration (D).

Underground Structure: Column 4 identifies the underground structure by name or describes the type of structure if a name is not available. The distance of the structure from the earthquake epicenter (R) is also given.

Underground Structure Data: Columns 5 through 8 provide information about the underground structure. The cross-sectional dimensions and depth of the structure are given in Columns 5 and 6, respectively. Column 7 describes the ground conditions, and Column 8 indicates the type of support or lining used for the structure.

Surface Shaking Data: Columns 9 through 12 provide information about the ground motion at the surface near the underground structure. The effects of the earthquake on surface structures, etc., are given in Column 9. Column 10 lists the ground motion parameters -- acceleration (a), velocity (v), and displacement (d). Personal perceptions of surface ground motion are noted in Column 11, and the intensity of the earthquake at the surface, estimated according to the Modified Mercalli Intensity (MMI) scale or the Rossi-Forel scale, is given in Column 12.

Subsurface Shaking Data: Columns 13, 14, and 15 provide information about the subsurface ground motion. The effects of the earthquake on the underground structure are given in Column 13. Personal perceptions of subsurface ground motion are noted in Column 14. Column 15 gives the intensity of the earthquake (MMI or Rossi-Forel) below the ground surface.

SUMMARY OF DAMAGE TO UNDERGROUND STRUCTURES
FROM EARTHQUAKE SHAKING

Number (1)	Source of Data (2)	Earthquake Data (3)	Underground Structure (4)	Underground Structure Data			
				Cross Section (5)	Depth (6)	Ground Conditions (7)	Support, Lining (8)
1	15, 17, 19, 24	San Francisco, California 1906 M = 8.3, D = 40 sec	Wright Tunnel #2 near Los Gatos R = 135.8 km	4.0 m wide	206 m	sandstone, jasper	timber sets
2	15, 17, 19, 24	"	Wright Tunnel #1 R = 135 km	4.0 m wide	214 m	shale, serpentine, soapstone	timber sets
3	15, 17, 24	Kwanto (Kanto) Region, 1923, or Great Tokyo, 1923 M = 8.16, D = 38 sec	Terao R = 31.6 km				bricks
4	15, 17, 24	"	Hichigama R = 36.4 km				
5	15, 17, 24	"	Taura R = 31.6 km		15 m	loose surface rock	
6	15, 17, 24	"	Numama R = 46.0 km				
7	15, 17, 24	"	Nokogiri- Yama R = 70.7 km				concrete
8	15, 17, 24	"	Kanome- Yama R = 26.9 km			boulders in slope	
9	15, 17, 24	"	Ajo R = 25.0 km				

Surface Shaking Data				Subsurface Shaking Data		
Surface Effects (9)	Ground Motion Parameters (10)	Personal Perceptions (11)	Intensity (12)	Underground Effects (13)	Personal Perceptions (14)	Estimated Intensity (15)
80% of chimneys damaged, nearly all brick fronts cracked, a dozen upheavals of sidewalks (in Los Gatos)	a = 0.13g v = 26.8 cm/sec d = 41.9 cm		IX to X Rossi-Forel	timbers broken, roof caved		
"	a = 0.13g v = 26.9 cm/sec d = 42.1 cm		"	timbers broken, roof caved, (also damage due to faulting)		
	a = 0.47g v = 82.5 cm/sec d = 91.8 cm			cracked brick portal, no interior damage		
	a = 0.42g v = 74.8 cm/sec d = 99.1 cm			no damage		
	a = 0.47g v = 82.5 cm/sec d = 91.8 cm			no damage		
	a = 0.35g v = 62.8 cm/sec d = 75.1 cm			cracked brick portal, no interior damage		
	a = 0.24g v = 43.9 cm/sec d = 57.7 cm			concrete walls slightly fractured, some spalling of concrete		
	a = 0.52g v = 91.6 cm/sec d = 117.1 cm			no interior damage (masonry portal damaged by landslide)		
	a = 0.55g v = 95.8 cm/sec d = 112.5 cm			"		

(continued)

SUMMARY OF DAMAGE TO UNDERGROUND STRUCTURES
FROM EARTHQUAKE SHAKING (Continued)

Number (1)	Source of Data (2)	Earthquake Data (3)	Underground Structure (4)	Underground Structure Data			
				Cross Section (5)	Depth (6)	Ground Conditions (7)	Support, Lining (8)
10	15, 17, 24	Kwanto (Kanto) Region, 1923, or Great Tokyo, 1923 M = 8.16, D = 35 sec	Ippamatzu R = 25.0 km				masonry
11	15, 17, 24	"	Nagoye R = 24.0 km		30 m		
12	15, 17, 24	"	Komine R = 26.9 km		1.5-6 m		rein- forced concrete
13	15, 17, 24	"	Fudu San R = 24.0 km		18 m	thin, loose material on hillside	
14	15, 17, 24	"	Meno- Kamijama = 32.0 km		16.5 m	loose rock	masonry
15	15, 17, 24	"	Yonegami- Yama R = 32.0 km		50 m		masonry
16	15, 17, 24	"	Shimomaki- Matsu R = 36.5 km		29 m		masonry
17	15, 17, 24	"	Happon-Matzu R = 20.0 km		20 m	loose material on steep slope	
18	15, 17, 24	"	Nagasaha- Yama R = 20.0 km		90 m		brick and concrete
19	15, 17, 24	"	Hakone No. 1 R = 15.6 km		61 m		
20	15, 17, 24	"	Hakone No. 2 R = 15.6 km				

Surface Shaking Data				Subsurface Shaking Data		
Surface Effects (9)	Ground Motion Parameters (10)	Personal Perceptions (11)	Intensity (12)	Underground Effects (13)	Personal Perceptions (14)	Estimated Intensity (15)
	a = 0.55g v = 95.8 cm/sec d = 112.5 cm			masonry dis-lodged near floor		
	a = 0.50g v = 98.1 cm/sec d = 107.4 cm			interior cracked		
	a = 0.52g v = 91.6 cm/sec d = 99.1 cm			destroyed, ceiling slabs caved in, formed section cracked		
	a = 0.50g v = 98.1 cm/sec d = 107.4 cm			cracked masonry portal, no interior damage		
	a = 0.46g v = 81.8 cm/sec d = 91.2 cm			partial collapse		
	a = 0.46g v = 81.8 cm/sec d = 91.2 cm			minor interior masonry damage, cracks near portal		
	a = 0.42g v = 74.7 cm/sec d = 85.3 cm			deformed interior masonry		
	a = 0.63g v = 108.7 cm/sec d = 112.5 cm			badly cracked interior		
	a = 0.59g v = 102.1 cm/sec d = 107.4 cm			some interior fractures in bricks and concrete		
	a = 0.72g v = 123.0 cm/sec d = 123.2 cm			interior cracks		
	a = 0.72g v = 123.1 cm/sec d = 123.2 cm			no damage		

(continued)

SUMMARY OF DAMAGE TO UNDERGROUND STRUCTURES
FROM EARTHQUAKE SHAKING (Continued)

Number (1)	Source of Data (2)	Earthquake Data (3)	Underground Structure (4)	Underground Structure Data			
				Cross Section (5)	Depth (6)	Ground Conditions (7)	Support, Lining (8)
21	15, 17, 24	Kwanto (Kanto) Region, 1923, or Great Tokyo, 1923 M = 8.16, D = 35 sec	Hakone No. 3 R = 17.2 km		46 m		
22	15, 17, 24	"	Hakone No. 4 R = 19.7 km		49 m		
23	15, 17, 24	"	Hakone No. 7 R = 22.4 km		31 m	fissured, faulted, weathered rock	
24	15, 17, 24	"	Yose R = 26.9 km		20 m	soft, fine- grain rock	
25	15, 17, 24	"	Doki R = 61.0 km		very shallow		brick
26	15, 17, 24	"	Namuya R = 63.0 km		75 m		brick and concrete
27	15, 17, 24	"	Mineoka- Yama R = 65.0 km			some basalt, de- formed rock	masonry
28	15, 17, 24	Idu Peninsula 1930 M = 7.0 D = 15 sec	Tanna R = 0.0 km		150 m	agglomerate and andesite	concrete
29	15, 17, 24	Fukui 1948	Kumasaka R = 25.0 km				brick

Surface Shaking Data				Subsurface Shaking Data		
Surface Effects (9)	Ground Motion Parameters (10)	Personal Perceptions (11)	Intensity (12)	Underground Effects (13)	Personal Perceptions (14)	Estimated Intensity (15)
over tunnel, 55% of dwellings destroyed, surface fault displacements for 15 km	a = 0.69g v = 117.4 cm/sec d = 119.0 cm			interior cracks, ceiling collapse near portal, some damage to masonry portal		
	a = 0.64g v = 109.6 cm/sec d = 113.1 cm			collapse of loose material		
	a = 0.59g v = 102.1 cm/sec d = 107.4 cm			interior collapse		
	a = 0.52g v = 91.6 cm/sec d = 99.1 cm			shallow portions collapsed and daylighted		
	a = 0.27g v = 49.9 cm/sec d = 63.4 cm			collapsed at shallow parts		
	a = 0.26g v = 48.5 cm/sec d = 62.1 cm			cave-in, cracks with 25-cm displacement, possibly due to landsliding		
	a = 0.26g v = 47.3 cm/sec d = 60.9 cm			cracks in bulges in masonry from local earth pressure		
	a = 0.30g v = 39.5 cm/sec d = 39.3 cm			few cracks in walls (major damage due to faulting)		
				no interior damage, brick arches of portal partially fractured		

(continued)

SUMMARY OF DAMAGE TO UNDERGROUND STRUCTURES
FROM EARTHQUAKE SHAKING (Continued)

Number (1)	Source of Data (2)	Earthquake Data (3)	Underground Structure (4)	Underground Structure Data			
				Cross Section (5)	Depth (6)	Ground Conditions (7)	Support, Lining (8)
30	15, 17, 24	Hokkaido (off Tokachi) 1952 M = 8.0 D = 30-35 sec					concrete brick
31	15, 17, 21, 22, 24	Kern County 1952 M = 7.7	S. Pacific R.R. Tunnel #3 R = 46.0 km		46 m	decomposed diorite (granite)	timber and 30-53 cm concrete
32	15, 17, 21, 22, 24	"	S.P.R.R. #4 R = 46.0 km		38 m	decomposed diorite, many sur- face cracks	"
33	15, 17, 21, 22, 24	"	S.P.R.R. #5 R = 46.5 km		76 m	"	"
34	15, 17, 21, 22, 24	"	S.P.R.R. #6 R = 46.5 km		15 m	decomposed diorite	"
35	17, 24	Kita Mino 1961 M = 7.2 D = 15-20 sec	Powerhouse R = 32.0 km	77 m long, 22 m wide, 43 m high		jointed, igneous rock	
36	17, 24	"	Aqueduct			soft ground	
37	17, 24	Niigata, 1964 M = 7.5 D = 20-25 sec	Nezugaseki				
38	17, 24	"	Terasaka				

Surface Shaking Data				Subsurface Shaking Data		
Surface Effects (9)	Ground Motion Parameters (10)	Personal Perceptions (11)	Intensity (12)	Underground Effects (13)	Personal Perceptions (14)	Estimated Intensity (15)
			IV to V MMI	minor cracking in both brick and concrete linings		
	a = 0.24g v = 37.5 cm/sec d = 42.9 cm		XI MMI	no interior damage due to shaking reported (severely damaged by faulting)		
	a = 0.24g v = 37.5 cm/sec d = 42.9 cm			"		
	a = 0.24g v = 37.2 cm/sec d = 42.7 cm			"		
	a = 0.24g v = 37.2 cm/sec d = 42.7 cm			no interior damage due to shaking reported (fractured due to fault movement)		
	a = 0.25g v = 33.7 cm/sec d = 39.3 cm			no damage		
	"			cracking		
				spalling of concrete at crown, cracking at portal		
				spalling of concrete at crown, crushing of invert at bottom of side-walls		

(continued)

SUMMARY OF DAMAGE TO UNDERGROUND STRUCTURES
FROM EARTHQUAKE SHAKING (Continued)

Number (1)	Source of Data (2)	Earthquake Data (3)	Underground Structure (4)	Underground Structure Data			
				Cross Section (5)	Depth (6)	Ground Conditions (7)	Support, Lining (8)
39	17, 23, 24	Great Alaska 1964 M = 8.4 D = 45 sec	Whittier 1 R = 75.0 km			greywacke	unlined, except for wooden shoring at portals
40	17, 23, 24	"	Whittier 2 R = 75.0 km				"
41	17, 23, 24	"	Seward 1 R = 85.0 km				"
42	17, 23, 24	"	Seward 2 R = 85.0 km				"
43	17, 23, 24	"	Seward 3 R = 100 km				"
44	17, 23, 24	"	Seward 4 R = 100 km				"
45	17, 23, 24	"	Seward 5 R = 110 km				"
46	17, 23, 24	"	Seward 6 R = 115 km				"
47	17, 24, 27	San Fernando 1971 M = 6.4 D = 15 sec	Balboa Inlet R = 16.0 km	4.3 m diameter	shallow, under canyon		rein- forced concrete
48	17, 24, 27	"	San Fernando R = 16.0 km	5.5 m diameter	approx. 46 m	alluvium- soft, satu- rated silt, sand, and gravel	rein- forced concrete, under construc- tion
49	17, 24, 27	"	Maclay R = 16.0 km	2.0 m high, horseshoe shaped			concrete
50	17, 24, 27, 28	"	Chatsworth R = 20.0 km	2.0 m diameter			concrete

Surface Shaking Data				Subsurface Shaking Data		
Surface Effects (9)	Ground Motion Parameters (10)	Personal Perceptions (11)	Intensity (12)	Underground Effects (13)	Personal Perceptions (14)	Estimated Intensity (15)
	a = 0.26g v = 52.0 cm/sec d = 79.4 cm		IX to XI MMI	overhead raveling of material which fell on track		
	a = 0.26g v = 52.0 cm/sec d = 79.4 cm		"	no damage		
	a = 0.23g v = 46.3 cm/sec d = 64.8 cm		"	no damage		
	a = 0.23g v = 46.3 cm/sec d = 64.8 cm		"	no damage		
	a = 0.19g v = 39.7 cm/sec d = 60.9 cm		"	no damage		
	"		"	no damage		
	a = 0.19g v = 36.2 cm/sec d = 56.7 cm		"	no damage		
	a = 0.17g v = 34.7 cm/sec d = 56.7 cm		"	no damage		
	a = 0.23g v = 23.9 cm/sec d = 21.0 cm		X MMI	severe spalling, steel bars deformed, severity attributed to canyon		
	"		X MMI	no damage due to shaking reported (damage due to faulting)		
	"		X MMI	wide, long cracks, but liner did not fall into tunnel		
	a = 0.20g v = 21.4 cm/sec d = 19.4 cm		VIII MMI	slight damage		

(continued)

SUMMARY OF DAMAGE TO UNDERGROUND STRUCTURES
FROM EARTHQUAKE SHAKING (Continued)

Number (1)	Source of Data (2)	Earthquake Data (3)	Underground Structure (4)	Underground Structure Data			
				Gross Section (5)	Depth (6)	Ground Conditions (7)	Support, Lining (8)
51	17, 24, 27	San Fernando 1971 M = 6.4 D = 15 sec	Tehachapi 1 R = 70.0 km	7.2 m diameter			
52	17, 24, 27	"	Van Norman Inlet R = 33.0 km				
53	17, 24, 27	"	Tehachapi 2 R = 73.0 km	7.2 m diameter			
54	17, 24, 27	"	Tehachapi 3 R = 73.0 km	7.2 m diameter			
55	17, 24, 27	"	Carley Porter R = 65.0 km	6.1 m diameter			
56	17, 24, 27	"	Van Morrison North (first Los Angeles aqueduct) R = 23.0 km	2.9 m x 3.2 m			unrein- forced concrete
57	17, 24	"	Saugus R = 23.0 km				
58	17, 24	"	San Francisquito R = 24.5 km				
59	17, 24	"	Elizabeth R = 27.3 km				
60	17, 24	"	Antelope R = 37.5 km				
61	17, 24	Inyo-Kern 1946 M = 6.3 D = ?	Jawbone 1 R = 26.0 km				
62	17, 24	"	Jawbone 2 R = 28.0 km				

Surface Shaking Data				Subsurface Shaking Data		
Surface Effects (9)	Ground Motion Parameters (10)	Personal Perceptions (11)	Intensity (12)	Underground Effects (13)	Personal Perceptions (14)	Estimated Intensity (15)
	a = 0.07g v = 8.7 cm/sec d = 10.0 cm		V MMI	no damage		
	a = 0.15g v = 15.8 cm/sec d = 15.5 cm			no damage		
	a = 0.07g v = 8.4 cm/sec d = 9.7 cm		V MMI	no damage		
	"		V MMI	no damage		
	a = 0.08g v = 9.3 cm/sec d = 10.5 cm		V MMI	no damage		
	a = 0.19g v = 19.8 cm/sec d = 18.3 cm		VIII to X MMI	hundreds of new fractures in concrete lining, up to 6 mm, no structural damage, fractures primarily circumferential, also longitudinal and diagonal		
	"			no damage		
	a = 0.18g v = 19.1 cm/sec d = 17.8 cm			no damage		
	a = 0.17g v = 17.9 cm/sec d = 17.0 cm			no damage		
	a = 0.13g v = 14.4 cm/sec d = 14.5 cm			no damage		
	a = 0.16g v = 16.8 cm/sec d = 15.7 cm			no damage		
	a = 0.16g v = 16.0 cm/sec d = 15.2 cm			no damage		

(continued)

SUMMARY OF DAMAGE TO UNDERGROUND STRUCTURES
FROM EARTHQUAKE SHAKING (Continued)

Number (1)	Source of Data (2)	Earthquake Data (3)	Underground Structure (4)	Underground Structure Data			
				Cross Section (5)	Depth (6)	Ground Conditions (7)	Support, Lining (8)
63	17, 24	Inyo-Kern 1946 M = 6.3 D = ?	Jawbone 3 R = 31.0 km				
64	17, 24	"	Freeman R = 22.0 km				
65	17, 24	Arvin Tehachapi 1952 M = 7.7 D = ?	Saugus R = 90.0 km				
66	17, 24	"	San Francisquito R = 75.0 km				
67	17, 24	"	Elizabeth R = 70.0 km				
68	17, 24	"	Antelope R = 48.0 km				
69	17, 24	"	Jawbone R = 90.0 km				
70	17, 24	Cholame, 1922 M = 6.1	Jawbone R = 52.0 km				
71	17, 24	"	Freeman R = 52.0 km				
72	15, 16	Kern County 1952 Aftershock M = 5.6 or 6.1 D = ?	Crystal Cave				
73	16	Chile, 1960	coal mines under ocean				
74	15	Montana June 27, 1925	mines under Butte, Barker		76 m		

Surface Shaking Data				Subsurface Shaking Data		
Surface Effects (9)	Ground Motion Parameters (10)	Personal Perceptions (11)	Intensity (12)	Underground Effects (13)	Personal Perceptions (14)	Estimated Intensity (15)
	a = 0.14g v = 15.0 cm/sec d = 14.4 cm			no damage		
	a = 0.18g v = 18.5 cm/sec d = 16.9 cm			no damage		
	a = 0.14g v = 23.0 cm/sec d = 31.0 cm			no damage		
	a = 0.17g v = 27.2 cm/sec d = 35.0 cm			no damage		
	a = 0.18g v = 29.0 cm/sec d = 36.7 cm			no damage		
	a = 0.25g v = 39.7 cm/sec d = 46.3 cm			no damage		
	a = 0.14g v = 23.0 cm/sec d = 31.0 cm			no damage		
	a = 0.08g v = 8.5 cm/sec d = 8.9 cm			no damage		
	"			no damage		
		generally, quake was sharply felt		no damage	not noticed in cave	
		generally noticed at surface		no damage	miners heard strange noises	
					generally unaware of earthquake	

(continued)

SUMMARY OF DAMAGE TO UNDERGROUND STRUCTURES
FROM EARTHQUAKE SHAKING (Continued)

Number (1)	Source of Data (2)	Earthquake Data (3)	Underground Structure (4)	Underground Structure Data			
				Cross Section (5)	Depth (6)	Ground Conditions (7)	Support, Lining (8)
75	15, 16	Sonora, Mexico May 3, 1887	mines at Tombstone and Bisbee, Arizona		46 m	limestone and other rocks	some timber- ing
		"	"		152 m	hard limestone	"
		"	"		152 m	soft limestone	"
76	16	Cedar Mt., Nevada December 21, 1932 M = 7.3	various mines				
77	16	Excelsior Mts., Nevada January 1, 1930 M = 6.3	mine tunnel near Marietta				
78	16	"	Silver Dike Mine				
79	16	"	Quailey Mine				
80	16	Idaho May 9, 1944	Morning Mine at Mullan		1,350 m		
81	16	Calif.-Nev., Inyo-Mono counties August 24, 1945	Lone Pine Mine				

Surface Shaking Data				Subsurface Shaking Data		
Surface Effects (9)	Ground Motion Parameters (10)	Personal Perceptions (11)	Intensity (12)	Underground Effects (13)	Personal Perceptions (14)	Estimated Intensity (15)
<p>falling plaster, chimneys, disarranged foundations, resetting of engines</p> <p>"</p> <p>"</p> <p>a stone cabin demolished, a mine mill damaged considerably</p>		<p>people at surface heard more noise and were frightened</p> <p>accutely perceptible</p> <p>felt by many</p>	<p>IV to VI MMI</p> <p>VI MMI near Burke and Mullan towns</p>	<p>minor damage, rock fell from roof, making loud noises</p> <p>some sloughing underground in various mines</p> <p>considerable damage</p> <p>timbers broken, a heading knocked out, staging fell, flying rock as timbers broke</p>	<p>heavy roaring noise, vibration culminating with a jolt</p> <p>miners frightened, lost equilibrium</p> <p>miners did not notice anything unusual</p> <p>miners lost balance, heard less noise and were less frightened than people on the surface</p> <p>scarcely noticed</p> <p>officials heard roar which drowned out blasting</p>	
windows rattled, no surface damage						

(continued)

SUMMARY OF DAMAGE TO UNDERGROUND STRUCTURES
FROM EARTHQUAKE SHAKING (Continued)

Number (1)	Source of Data (2)	Earthquake Data (3)	Underground Structure (4)	Underground Structure Data			
				Cross Section (5)	Depth (6)	Ground Conditions (7)	Support, Lining (8)
82	16	Inyo County, California, Owens Valley March 26, 1872	Cerro Gordo and Eclipse Mine				
83	16	Sonora, Mexico May 3, 1887 D = 20 sec	mine at Tombstone, Arizona	46 m and 49 m	46 m and 183 m		
84	16	Reno, Nevada April 28, 1888 D = 10 sec	Orleans Mine				
85	16	"	Idaho Mine		488 m		
86	16	Central California May 19, 1889	Mayflower Mine in Forest Hill		183 m and 244 m		
87	16	Juab and Utah counties, Utah July 31, 1900	Tintic Mine, Juab County				

Surface Shaking Data				Subsurface Shaking Data		
Surface Effects (9)	Ground Motion Parameters (10)	Personal Perceptions (11)	Intensity (12)	Underground Effects (13)	Personal Perceptions (14)	Estimated Intensity (15)
<p>at Geyer Gulch, 70 or 80 km from Independence, Inyo County, miners' cabins collapsed</p> <p>no building of any stability damaged, no one injured, RR track 11.5 cm out of line for 91 m (see no. 75)</p> <p>at Goshen, Utah County, dishes were broken, plaster fell from walls, and a chimney was broken, at Santaquin, Utah County, an adobe house was split in two and people thrown from beds</p>		<p>load detonations, tremors for 1 minute</p> <p>washbowl rattled against a pitcher over mine</p>	VII MMI in Grass Valley	mine flooded	<p>rock motion observed, especially in timbering, miners went to surface but soon returned to work</p> <p>miners at 183 m felt shock severely and some became sick, miners at 46 m noticed shock less</p> <p>felt by miners</p> <p>not felt by miners</p> <p>miners came to the surface frightened</p>	

(continued)

SUMMARY OF DAMAGE TO UNDERGROUND STRUCTURES
FROM EARTHQUAKE SHAKING (Continued)

Number (1)	Source of Data (2)	Earthquake Data (3)	Underground Structure (4)	Underground Structure Data			
				Cross Section (5)	Depth (6)	Ground Conditions (7)	Support, Lining (8)
88	16	Juab and Utah counties, Utah July 31, 1900	Mammoth Mine				
89	16	Kern County, California July 9, 1871	Joe Walker Mine				
90	16	Humboldt County, California October 28, 1909 D = 30 sec	Bully Hill Mine at Delamar, Shasta County				
91	16	Bishop, Inyo County, California March 21, 1917	LAQWP Tunnel under con- struction				

Surface Shaking Data				Subsurface Shaking Data		
Surface Effects (9)	Ground Motion Parameters (10)	Personal Perceptions (11)	Intensity (12)	Underground Effects (13)	Personal Perceptions (14)	Estimated Intensity (15)
<p>at Goshen, Utah County, dishes were broken, plaster fell from walls, and a chimney was broken, at Santaquin, Utah County, an adobe house was split in two and people thrown from beds</p> <p>in Redding, clock in courthouse stopped, all chimneys and concrete structures destroyed at Rohnerville, at Upper Mattole, chimneys were destroyed and cemetery monuments were thrown down</p> <p>rock slides</p>		<p>3 sharp shocks felt, in Redding, persons occupying upper floors of brick buildings rushed into streets</p> <p>rapid trembling N-S for 25 sec felt by many in Bishop area, felt at Crooked Creek Camp at the L.A. Power Bureau 39 km NW of Bishop for 30 sec</p>	IV MMI (at Bishop)	<p>the deep shaft was so twisted that the cage could not be lowered to the bottom</p> <p>mine almost instantly filled with water</p>	<p>severe shock felt underground</p> <p>miners badly frightened by rumbling and shaking, came to surface</p> <p>shocks felt by workers</p>	

(continued)

SUMMARY OF DAMAGE TO UNDERGROUND STRUCTURES
FROM EARTHQUAKE SHAKING (Continued)

Number (1)	Source of Data (2)	Earthquake Data (3)	Underground Structure (4)	Underground Structure Data			
				Cross Section (5)	Depth (6)	Ground Conditions (7)	Support, Lining (8)
92	16	Owens Valley, Inyo County, California September 4, 1917	Reward Gold Mine				
93	16	Grass Valley, California November 7, 1939	mine		1,372 m		
94	16	Calumet, Michigan July 26, 1905 (could have been induced seismicity)	mine				
95	16	Pleasant Valley, Nevada October 2, 1915 M = 7.75	mine				
96	16	Idaho near Rathdrum November 27, 1926	Hecla Mine		305 m and 610 m		

Surface Shaking Data				Subsurface Shaking Data		
Surface Effects (9)	Ground Motion Parameters (10)	Personal Perceptions (11)	Intensity (12)	Underground Effects (13)	Personal Perceptions (14)	Estimated Intensity (15)
<p>doors flew open, dishes fell off shelves, and bricks fell off chimneys in Grass Valley</p> <p>chimneys fell and plate glass windows broke</p> <p>at Lovelock, large water tanks were collapsed and cracks in road, great increase in water flow - new water rights filed, new rift formed - vertical scarp 1.5 to 4.5 m high, 35 km long</p> <p>slight damage at Kellogg</p>		<p>slight shock felt</p> <p>noise like an explosion</p> <p>felt all over Keweenaw Peninsula, Michigan, felt heaviest at Calumet, sound perceived as a loud explosion</p> <p>at Kennedy, there was a great roar and people were thrown from their beds and others were thrown to the floor</p> <p>strongly felt at Wallace, vertical jar noted, two distinct shocks felt at Rathdrum</p>	<p>II MMI</p> <p>X MMI (at epicenter) V MMI (at Reno)</p>	<p>at Kennedy, concrete mine foundations cracked and mine tunnels caved in</p>	<p>slight shock felt by one at rest</p> <p>felt underground</p> <p>sound like an explosion heard far down in the mine</p> <p>felt at 305 m but not at 610 m</p>	

(continued)

SUMMARY OF DAMAGE TO UNDERGROUND STRUCTURES
 FROM EARTHQUAKE SHAKING (Continued)

Number (1)	Source of Data (2)	Earthquake Data (3)	Underground Structure (4)	Underground Structure Data			
				Cross Section (5)	Depth (6)	Ground Conditions (7)	Support, Lining (8)
97	16	Wallace, Idaho December 18, 1957	Galena Silver Mine		1,036 m		
98	16	Eastern Kentucky July 13, 1969	Zinc Mine at Jefferson City				
99	30	Near Izu- Ohshima, Japan January 14, 1970 M = 7.0	Tomoro Tunnel				concrete lining
100	30	"	Izu-Kitagawa Tunnel				assumed to be concrete lined
101	30	"	Izu-Atagawa Tunnel				"
102	30	"	Izu-Inatori	horseshoe shaped, other sec- tions are circular			steel sets encased in concrete
103	30	"	Kawazu				"

Surface Shaking Data				Subsurface Shaking Data		
Surface Effects (9)	Ground Motion Parameters (10)	Personal Perceptions (11)	Intensity (12)	Underground Effects (13)	Personal Perceptions (14)	Estimated Intensity (15)
<p>at Jefferson City, Tennessee, a few bricks loosened on chimneys, at Knoxville, plaster and concrete cracked, houses shook strongly, and furniture jumped up and down, plaster cracked at Seymour and small objects fell from shelves</p> <p>surface fault displacement of 46 cm, landslides, minor damage to buildings</p>		<p>awakened all and frightened many at Wallace, also felt at Osburn and Mullan</p>		<p>extensive damage, timber fell and walls caved in</p> <p>some rocks fell in zinc mine</p> <p>pieces of lining in crown and sidewall fractured and fell out</p> <p>spalling of lining</p> <p>lining damaged, cause unknown to authors</p> <p>no damage due to shaking reported (extensive damage due to faulting)</p> <p>lining damaged, probably due to landsliding</p>	<p>frightened miners 1,036 m underground</p>	

(continued)

SUMMARY OF DAMAGE TO UNDERGROUND STRUCTURES
FROM EARTHQUAKE SHAKING (Continued)

Number (1)	Source of Data (2)	Earthquake Data (3)	Underground Structure (4)	Underground Structure Data			
				Cross Section (5)	Depth (6)	Ground Conditions (7)	Support Lining (8)
104	30	Near Izu- Ohshima, Japan January 14, 1978 M = 7.0	Shirata Tunnel			rhyolite	unrein- forced concrete lining, some sections unlined
105	191	Tangshan, China July 28, 1978 M = 8+	Tangshan Coal Mine	shaft - 12 m diameter	40.5 m		
106	191	"	Lailuan Coal Mine	several shafts	700 m		

Surface Shaking Data				Subsurface Shaking Data		
Surface Effects (9)	Ground Motion Parameters (10)	Personal Perceptions (11)	Intensity (12)	Underground Effects (13)	Personal Perceptions (14)	Estimated Intensity (15)
road surfaces fractured, subsidence, cracking, sliding, and differential settling of road beds "			XI MMI	many cracks throughout the lining, large landslide above the tunnel, a 30.5-m lined section collapsed - probably due to the landslide cross section fractured in lower portion, shaft tilted 6°25', mine flooded		
			XI MMI	ring fractures around the cylinder walls in upper 20 m of several shafts, degree of shaft damage closely correlated to soil conditions, serious damage where shaft passed through liquefied soil layer, 1.7 to 5 times greater water flows into mines		

(continued)

SUMMARY OF DAMAGE TO UNDERGROUND STRUCTURES
FROM EARTHQUAKE SHAKING (Continued)

Number (1)	Source of Data (2)	Earthquake Data (3)	Underground Structure (4)	Underground Structure Data			
				Cross Section (5)	Depth (6)	Ground Conditions (7)	Support, Lining (8)
107	32	Bishop, California October 4, 1978 M = 5.8	Pine Creek Tungsten Mine about 13 km from epicenter	3-m x 3-m drifts, large rooms up to 24 m x 6 m x 6 m, 240 to 320 km of tunnels	152 m to more than 914 m	hard, strong, competent granite, quartzite, and marble, local pock- ets of de- composed, soft ground	mostly unsup- ported, some areas sup- ported with steel sets, timber, or rock bolts with wire mesh, shafts all sta- bilized with rock bolts and wire mesh
108	192	"	Helms Pumped Power Plant under construction R = 61 km	large room under con- struction	305 m	granite	rock bolts, spill- ing, shot- crete
109	193	Gemoa-Friuli May 6, 1976 M = 6.5 D = 55 sec	San Simeone highway tunnels (2), under construction in immediate epicentral region	semi- circular or horseshoe, height = 7.6 m		limestone	general- ly not lined

Surface Shaking Data				Subsurface Shaking Data		
Surface Effects (9)	Ground Motion Parameters (10)	Personal Perceptions (11)	Intensity (12)	Underground Effects (13)	Personal Perceptions (14)	Estimated Intensity (15)
cracks in masonry at foundations of small houses, contents of some closets disarranged, objects like vases fell over, light fixtures swung, numerous rock falls were reported on the slopes and cliffs in the area, cracks reported in fills	a = 0.26g at Crowley Lake Dam, about 8 km from epicenter and 20 km from mine a = 0.21g at LADWP Lower Gorge Power House, about 16 km from epicenter and 16 km from mine	people had difficulty standing, some became sick, loud rumbling, booming, and crackling noises heard, people became frightened and ran outside	V or VI MMI	no damage reported, nothing fell off shelves, light fixtures swung a couple of inches, one miner noticed that the clear water turned milky colored for 3 or 4 hours after quake, no increase in flow rates could be discerned	the motion was felt underground at all depths, but nobody experienced difficulty standing or became sick or frightened, various levels of noise were reported	III to IV MMI
woodpile collapsed, rock falls on slopes		felt indoors by nearly everyone and outdoors by most, many people ran outside, sensation of a heavy body striking a building, windows and doors rattled and building frame creaked	IV to V MMI	no damage	one or two impulses felt by those away from working headings, estimated duration of one or two sec	II to III MMI
severe damage to or destruction of many buildings	a = 0.34g ~15 km from epicenter v = 42 cm/sec		IX to X MMI	no damage reported	workers felt the quake, abandoned their machinery and fled	VI MMI

(continued)

SUMMARY OF DAMAGE TO UNDERGROUND STRUCTURES
FROM EARTHQUAKE SHAKING (Continued)

Number (1)	Source of Data (2)	Earthquake Data (3)	Underground Structure (4)	Underground Structure Data			
				Cross Section (5)	Depth (6)	Ground Conditions (7)	Support, Lining (8)
110	194	Gemoa-Friuli May 6, 1976 M = 6.5 D = 55 sec	Foos Caves				
111	31	Miyagi- Ken-oki, Japan June 12, 1978 M = 7.4 D = 30 sec	Hamadu Tunnel (near Matsushima) R = 160 km	horseshoe shaped, 6 m wide		tuff	steel sets at portals, unrein- forced concrete lining in inter- rior
112	31	"	Matsushima Tunnel (near Matsushima) R = 160 km	horseshoe shaped, 6 m wide		"	unrein- forced concrete lined
113	31	"	3 other highway tunnels near Matsushima	*	*	*	*
114	20	San Francisco, California 1906 M = 8.3, D = 40 sec	S.P.R.R. San Francisco #1 R = 45 km	horseshoe shaped, 9 m wide	24 m	Franciscan shale, weak, highly fractured	under construc- tion, 6-course brick lining
115	20	"	S.P.R.R. San Francisco #2 R = 45 km	two barrels, each approx. 6 m wide	1.2-m cover	loose soil	6-course brick lining, cut-and- cover construc- tion
116	20	"	S.P.R.R. San Francisco #3 R = 46 km	horseshoe shaped, 9 m wide	46 m	Franciscan shale, weak, highly fractured	under construc- tion, weak, 6-course brick lining
117	20	"	S.P.R.R. San Francisco #4 R = 47 km	"	38 m	"	"

*Data similar to data for Nos. 111 and 112.

Surface Effects (9)	Surface Shaking Data			Subsurface Shaking Data		
	Ground Motion Parameters (10)	Personal Perceptions (11)	Intensity (12)	Underground Effects (13)	Personal Perceptions (14)	Estimated Intensity (15)
severe damage to or destruction of many buildings	a = 0.34g ~15 km from epicenter v = 42 cm/sec		IX to X MMI	no damage reported		
landslides, buildings damaged in the vicinity				no damage		
"				no damage		
"				no damage		
			VII Rossi- Forel	no damage		
			VIII Rossi- Forel	both barrels collapsed		
			VII Rossi- Forel	no damage		
			VII Rossi- Forel	"		

(continued)

SUMMARY OF DAMAGE TO UNDERGROUND STRUCTURES
FROM EARTHQUAKE SHAKING (Continued)

Number (1)	Source of Data (2)	Earthquake Data (3)	Underground Structure (4)	Underground Structure Data			
				Cross Section (5)	Depth (6)	Ground Conditions (7)	Support, Lining (8)
118	20	San Francisco, California 1906 M = 8.3, D = 40 sec	S.P.R.R. San Francisco #5 R = 50 km	horseshoe shaped, 9 m wide		Franciscan shale, weak, highly fractured	under construc- tion, 6-course brick lining
119	195	"	North Pacific Coast R.R., Bothin tunnel R = 11 km				
120	195	"	North Pacific Coast R.R., Corte Madera tunnel R = 22 km				
121	27, 28	San Fernando 1971 M = 6.4 D = 15 sec	Maclay (Covered Conduit) R = 10.0 km	1.5 m high, 1.8 m wide	top probably at grade	alluvium	plain concrete sides and bottom, top slab rein- forced
122	27, 28	"	Chatsworth (Covered Conduit) R = 20 km	"	"	alluvium	"
123	27, 28, 29	"	Wilson Canyon Channel (Covered Box) R = 11 km	3.7 m high, 5.5 m wide, typical	approx. 1.5-m cover		rein- forced concrete
124	27, 28, 29	"	Mansfield Street Channel (Covered Box) R = 11 km	2.4 m high, 2.4 m wide, typical	approx. 1.5-m cover		rein- forced concrete

Surface Shaking Data				Subsurface Shaking Data		
Surface Effects (9)	Ground Motion Parameters (10)	Personal Perceptions (11)	Intensity (12)	Underground Effects (13)	Personal Perceptions (14)	Estimated Intensity (15)
			VII to VIII Rossi-Forel	minor damage reported		
			IX to X Rossi-Forel	no report of damage		
			IX Rossi-Forel	"		
	(see No. 49; however, calculations used R = 16 km instead of 10 km)		X MMI	heavy spalling and long, wide cracks in sides		
	(see No. 50)		VIII MMI	some cracking and spalling		
	estimated horizontal acceleration 0.3-0.5g		X MMI	damage not attributed to shaking, but probably aggravated by cycling (severe damage due to faulting)		
	"		X MMI	"		

(continued)

**SUMMARY OF DAMAGE TO UNDERGROUND STRUCTURES
FROM EARTHQUAKE SHAKING (Continued)**

Number (1)	Source of Data (2)	Earthquake Data (3)	Underground Structure (4)	Underground Structure Data			
				Cross Section (5)	Depth (6)	Ground Conditions (7)	Support, Lining (8)
125	27	San Fernando 1971 M = 6.4 D = 15 sec	Bee Canyon Storm Drain R = 15 km	triple-box, each 2.1 m high, 3.0 m wide		layers of sandy silt and silty sand	rein- forced concrete
126	27, 28	"	Jensen Filtration Plant, Box Culvert R = 15 km	4-barrel box culvert, each 2.6 m high, 3.7 m wide		fill	rein- forced concrete
127	26, 27, 28	"	Jensen Filtration Plant, Buried Reservoir R = 15 km	158 m x 152 m plan, 11.4 m high	2-m cover	alluvium	rein- forced concrete

NOTE: 1 mm = 0.04 in.; 1 cm = 0.39 in.; 1 m = 3.28 ft; 1 km = 0.62 mile.

Surface Shaking Data				Subsurface Shaking Data		
Surface Effects (9)	Ground Motion Parameters (10)	Personal Perceptions (11)	Intensity (12)	Underground Effects (13)	Personal Perceptions (14)	Estimated Intensity (15)
	estimated horizontal acceleration 0.4g		VIII to X MMI	concrete spalled and longitudinal steel ruptured or sheared at transverse construction joints		
	"		"	spalling at top of walls due to lateral racking		
	estimated horizontal acceleration 0.4g		"	severe damage to roof, columns, and walls, west wall pushed in about a meter at bottom construction joint, many columns damaged at top and bottom		

Appendix D

A Short Review of Seismological Terms

In the real earth, seismic waves emanating from the earthquake source appear in a number of forms and travel along a number of paths (see Figure 67). The ground motion recorded by a seismograph reflects the passage of waves that have traveled along many different paths, all of which compose the motion at the location of the recording instrument. The path taken by each wave (or phase) depends upon the internal structure of the earth; for example, some waves are reflected from the earth's core, and some are reflected from the boundary between the earth's crust and underlying mantle. Some wave types owe their existence to the fact that the earth has internal structure. If the earth's interior were perfectly homogeneous (all properties of the medium independent of position) and isotropic (all properties of the medium independent of direction), the surface waves recognized by seismologists would not exist at all except for the Rayleigh wave. The number of body wave phases recognized on seismograms would also be greatly reduced in a homogeneous, isotropic earth. One way we can see how these various wave types arise is to begin with a very simplified model of the earth and see what kinds of waves it can have. Then, by complicating its structure by stages, we can see what waves can be added, until we see some of the complexity in the real earth.

We begin with the most uncomplicated earth possible: a homogeneous, isotropic, flat earth. We can then build a mathematical model equivalent to this flat earth. This model is called a homogeneous, isotropic half-space. It is called a half-space because there is a boundary ($x_2 = 0$) below which the homogeneous, isotropic medium (in which the waves may propagate) extends to infinity (i.e., $-\infty < x_1 < \infty$, $-\infty < x_3 < \infty$, $0 < x_2 < \infty$) and above which there is nothing (see Figure 67). The surface of the half-space is called a free surface because nothing exists above it to place any dynamic constraints upon it; thus it is free to move under the influence of waves approaching from below. A full space would be one in which the medium exists everywhere.

It is known that there are two wave types that can exist in an isotropic solid: compression (P) and shear (S) waves (proof of this statement would

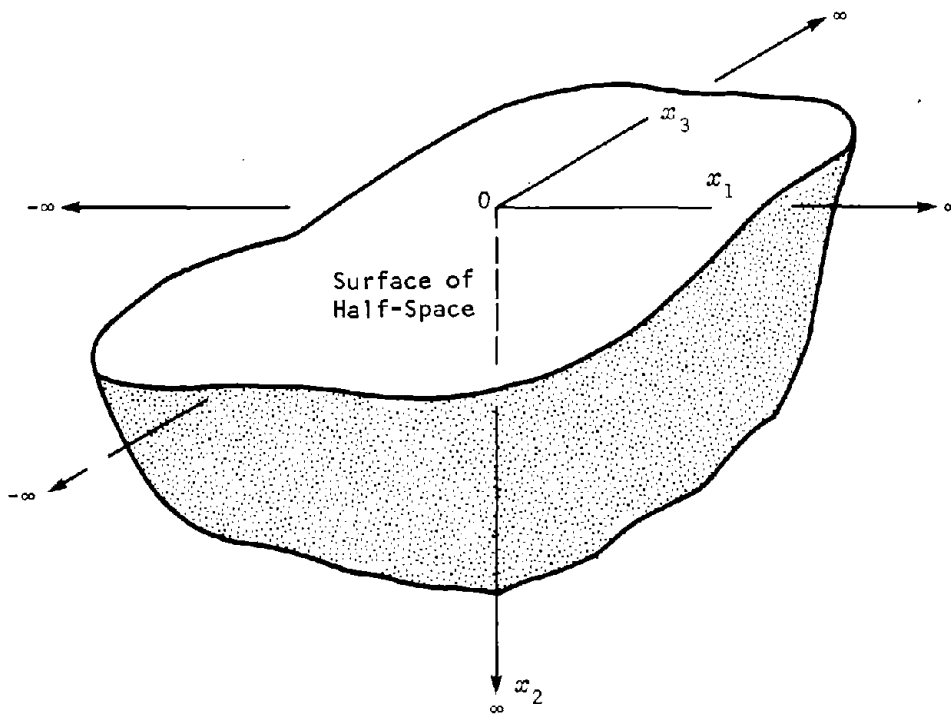
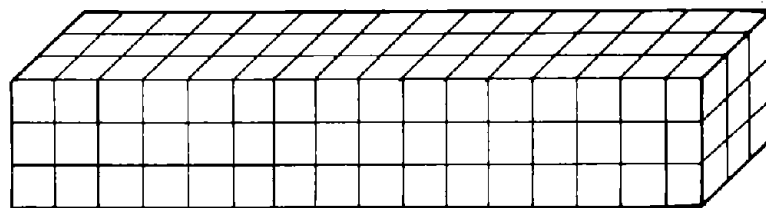


Figure 67. Representation of half-space model and associated coordinate system.

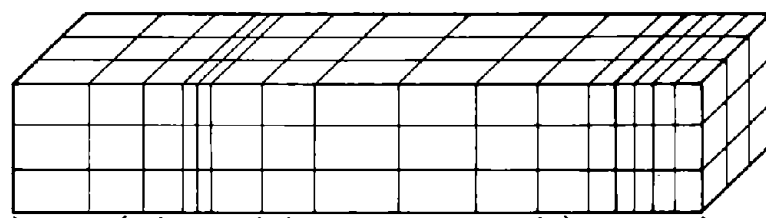
require a more detailed mathematical treatment appropriate to an introductory seismology course and is beyond the intended scope of this appendix). The P-waves are characterized by the fact that they excite motion in the particles constituting the medium, which is parallel to the direction of propagation of the wave. Thus P-waves are actually acoustic or sound waves (see Figure 68). S-waves, on the other hand, excite particle motion that is perpendicular, or transverse, to their direction of propagation. Because this transverse motion can be polarized relative to the path of the wave, S-waves are often identified in terms of their vertical (SV) and horizontal (SH) particle motions. Thus, there are three types of body waves: P-, SV-, and SH-waves.

If we now imagine body waves approaching the surface of the half-space from below and examine their reflection from the free surface, we find that a fourth wave type is possible. This fourth wave type consists of both P and SV motion, and its amplitudes decrease exponentially with increasing depth. It is a wave that travels parallel to the free surface, and it is called a Rayleigh wave. In this stark geometry, it is the only surface wave possible. It is the fundamental Rayleigh mode and corresponds to the lowest harmonic at which our hypothetical earth's surface may vibrate. A Rayleigh wave consists of displacements in a vertical plane, with the horizontal components being parallel to the direction of propagation. Shape functions for the components are illustrated in Figure 69. The Rayleigh particle motion is basically elliptic and, in the classical solution for the elastic half-space, is retrograde at the surface. The velocity V_R of the Rayleigh wave is given approximately by $V_R \approx 0.9 V_S$ (for Poisson's ratio approximately equal to 0.25), where V_S is the velocity of the shear waves in the same material.

We may also note in passing that a body wave approaching the free surface from below will be reflected, generating a downward-traveling wave. If the upward-traveling wave has some duration, then part of the disturbance will still be approaching the free surface, while the reflected part is moving away. The actual particle motion in the overlapping region will be the sum of motions contributed by the incident and reflected parts and will, in general, vary with both time and position below the surface.



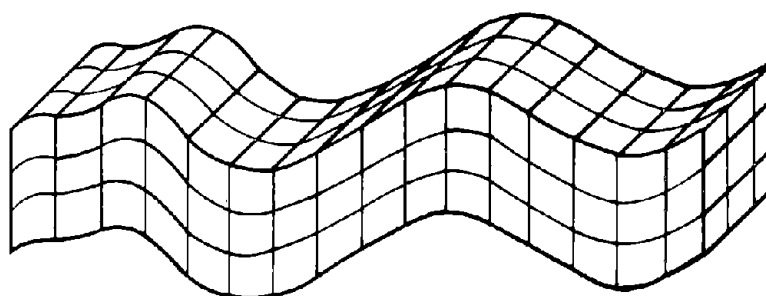
a. Undeformed ground



Tension Compression Tension Compression

Direction of Propagation →

b. Axial deformation due to P-wave



Direction of Propagation →

c. Shear deformation due to S-wave

Figure 68. Deformation due to body waves.

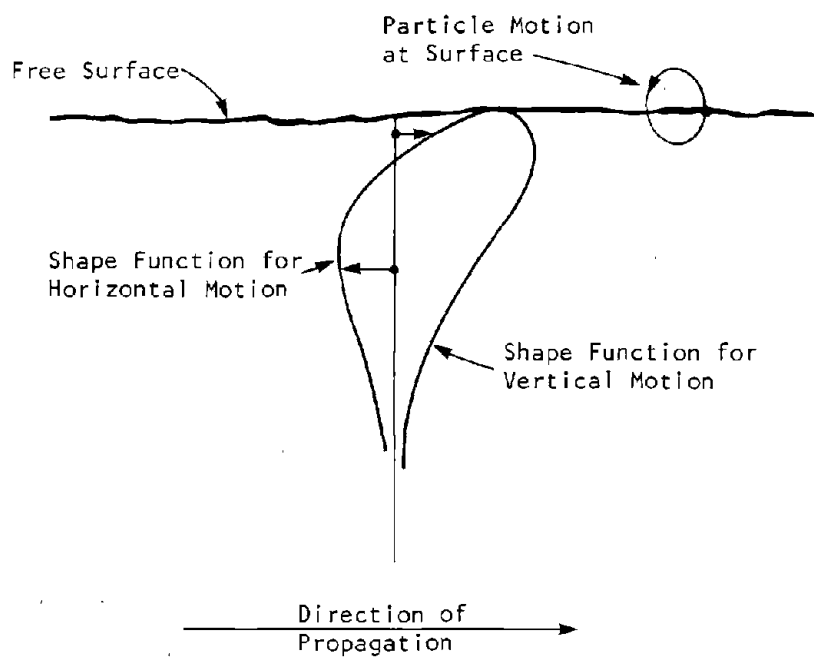


Figure 69. Motion due to Rayleigh waves.

Thus, in the homogeneous, isotropic half-space, the particle motion at some point below the free surface could be composed of that due to incident and reflected body waves plus that due to passage of the fundamental-mode Rayleigh wave.

Consider now the next order of complication in structure, the layer over a half-space (see Figure 70). In this geometry, a large number of possibilities exist. The most striking addition is to the family of surface waves. To begin with, there are now higher mode Rayleigh waves in addition to the fundamental mode. These higher order modes are analogous to the harmonic overtones of a vibrating string. As the order of the mode is increased by one, so are the number of nodal depths (depths at which the particle motion is always zero). The amplitudes of the particle motions associated with these waves decrease with increasing depth.

In addition to the higher mode Rayleigh waves, with their P-SV particle motion, the presence of the layer over half-space geometry now allows the full range of surface waves with SH particle motion, beginning with the fundamental mode and including all the higher modes. These waves, called Love waves, do not exist in the classical elastic half-space as do the Rayleigh waves. Love waves arise only when one or more layers of soil or rock of different composition exist over the base rock.

The presence of a layer allows the surface waves to exist in all their modes and with the entire range of particle motions (P, SV, SH). The presence of additional layers beyond the first complicates the behavior of the surface waves, but only in degree, not in kind.

If the velocity of seismic waves in the layer is less than in the half-space below it, another interesting thing happens. The reflection and refraction of seismic waves at a plane interface is controlled by Snell's law:

$$\frac{\sin \theta_1}{V_1} = \frac{\sin \theta_2}{V_2} = \text{constant}$$

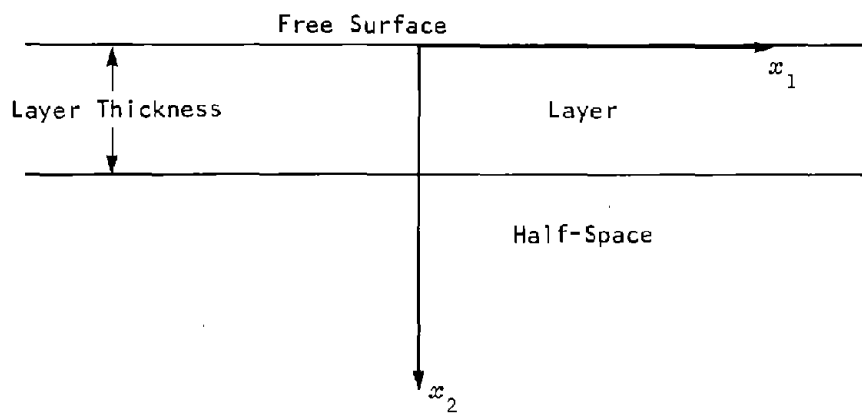


Figure 70. Plane layer over a half-space.

where:

θ_1, θ_2 = angle of ray paths with vertical, as shown in Figure 71

V_1, V_2 = wave velocities in medium 1 and medium 2, respectively

If medium 1 is the layer and medium 2 is the half-space, and if $V_2 > V_1$, then there are values of θ_1 for which $\sin \theta_2 > 1$, which is not mathematically permitted. What does happen is total reflection, which occurs for an angle of incidence, θ_1 , larger than the critical angle, θ_c . The critical angle is defined by

$$(\sin \theta_c)^{-1} = \frac{V_1}{V_2}$$

Thus, a body wave that approaches the bottom of the layer with an incident angle equal to θ_c is refracted along the base of the layer. It will travel along the interface of the layer and half-space with speed V_2 but will radiate energy back toward the free surface with a reflected angle θ_c and a velocity V_1 . It is called a head wave and is a common phenomenon.

There are many other complications introduced by layering, but discussion of these is beyond the scope of this appendix. For more details, the interested reader is referred to References 4, 114, 196, 197, and 198.

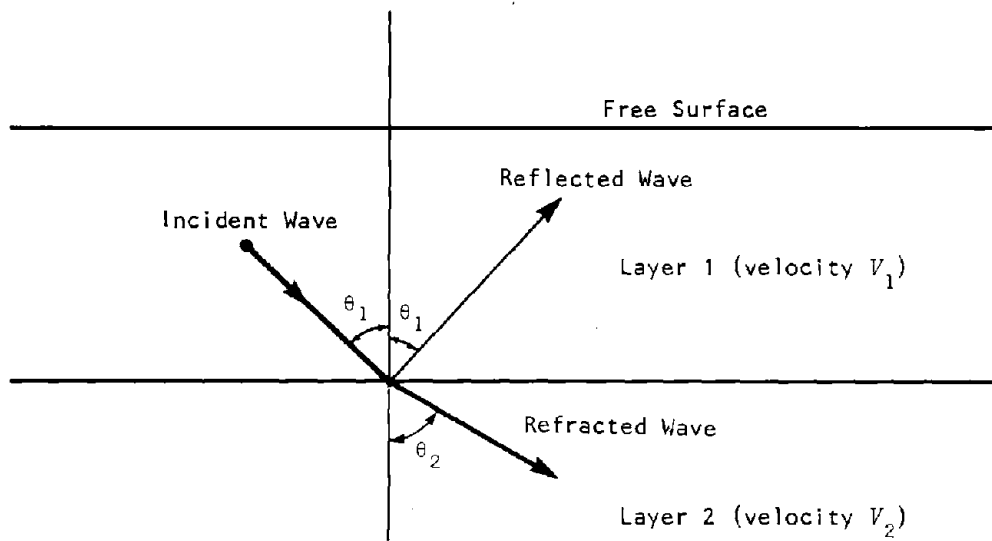


Figure 71. Reflection and refraction of body waves.

Appendix E

Derivation of the Green's Function for Two-Dimensional SH Motion in a Half-Space

The Green's function in an infinite elastic medium is given by

$$G_{ij}^0(\vec{x}, \vec{\xi}) = \frac{1}{4\pi\rho\omega^2} \left[k_2^2 \delta_{ij} \frac{e^{-ik_2 R}}{R} - \frac{\partial^2}{\partial x_i \partial x_j} \left(\frac{e^{-ik_1 R} - e^{-ik_2 R}}{R} \right) \right] \quad (83)$$

where:

- ρ = the mass density of the medium
- ω = the circular frequency
- $k_1 = \omega/\alpha$ = the compression wave number
- $k_2 = \omega/\beta$ = the shear wave number
- $R = \sqrt{(x_1 - \xi_1)^2 + (x_2 - \xi_2)^2 + (x_3 - \xi_3)^2}$
= the source to observation point distance
- $\vec{x} = (x_1, x_2, x_3)$ = the Cartesian coordinates of the observation point
- $\vec{\xi} = (\xi_1, \xi_2, \xi_3)$ = the Cartesian coordinates of the source point
- α = the compression wave velocity
- β = the shear wave velocity

Specifically, $G_{ij}^0(\vec{x}, \vec{\xi})$ gives the displacement component in the direction i at point \vec{x} due to a "unit" point force acting in the direction j at $\vec{\xi}$ for the harmonic component of frequency ω . The time dependence used herein is $e^{i\omega t}$.

First consider constructing the displacement field for a line force acting parallel to the 3 direction

$$G_{ij}^*(\vec{x}, \vec{\xi}) = \int_{-\infty}^{\infty} G_{ij}^0(\vec{x}, \vec{\xi}) d\xi_3 \quad (84)$$

Introducing the cylindrical, radial distance r in the 1-2 plane, defined as

$$r = \sqrt{(x_1 - \xi_1)^2 + (x_2 - \xi_2)^2} \quad (85)$$

the integral of Equation (84) can be reduced to the evaluation of

$$\int_{-\infty}^{\infty} \frac{e^{-ik_2 R}}{R} d\xi_3 = \frac{1}{r} \int_{-\infty}^{\infty} \frac{e^{-ik_2 \sqrt{r^2 + (x_3 - \xi_3)^2}}}{\sqrt{r^2 + (x_3 - \xi_3)^2}} d\xi_3 \quad (86)$$

Then, using the substitution

$$\sinh(\tau) = \frac{x_3 - \xi_3}{r} \quad (87)$$

and recognizing the even and odd behavior of the resulting sine and cosine terms, Equation (86) can be expressed as

$$\begin{aligned} \int_{-\infty}^{\infty} \frac{e^{-ik_2 R}}{R} d\xi_3 &= 2 \int_0^{\infty} \cos[k_2 r \cosh(\tau)] d\tau \\ &\quad - 2i \int_0^{\infty} \sin[k_2 r \cosh(\tau)] d\tau \end{aligned} \quad (88)$$

These two integrals on the right side of Equation (88) are easily recognized as integral representations for the Bessel and Neumann functions,

$$\int_{-\infty}^{\infty} \frac{e^{-ik_2 R}}{R} d\xi_3 = 2 \left[-\frac{\pi}{2} Y_0(k_2 r) \right] - 2i \left[\frac{\pi}{2} J_0(k_2 r) \right] \quad (89)$$

or, alternatively, this can be written in terms of the Hankel function of the second kind of order zero as

$$\int_{-\infty}^{\infty} \frac{e^{-ik_2 R}}{R} d\xi_3 = -i\pi H_0^{(2)}(k_2 r) \quad (90)$$

Using this result to find Equation (84), it should be noted that $i = j = 3$. Substitution of Equation (90) and its equivalent form for terms involving k_1 yields

$$\begin{aligned} G_{33}^*(\vec{x}, \vec{\xi}) &= \frac{1}{4\pi\rho\omega^2} \left[k_2^2 \left\{ -i\pi H_0^{(2)}(k_2 r) \right\} \right. \\ &\quad \left. - \frac{\partial^2}{\partial x_3^2} \left\{ -i\pi H_0^{(2)}(k_1 r) + i\pi H_0^{(2)}(k_2 r) \right\} \right] \end{aligned} \quad (91)$$

Because the second part, involving the derivative with respect to x_3 , is independent of x_3 , it vanishes. This leads to the result

$$G_{33}^*(\vec{x}, \vec{\xi}) = \frac{-i}{4\mu} H_0^{(2)}(k_2 r) \quad (92)$$

where $\mu = \rho\beta^2$ is the shear modulus of the medium. This result is the Green's function for antiplane motion in an infinite medium.

Now consider finding the Green's function for the semi-infinite medium with a traction-free surface at $x_2 = 0$. The method of images can be effectively used for this purpose. Place an image source at $\xi_3 = -\xi_3$ (see Figure 72). The Green's function for the half-space is thus given by

$$G_{33}(x_1, x_2; \xi_1, \xi_2) = \frac{-i}{4\mu} \left[H_0^{(2)}(k_2 r) + H_0^{(2)}(k_2 r^*) \right] \quad (93)$$

in which the distance between the image source and observation point is denoted by

$$r^* = \sqrt{(x_1 - \xi_1)^2 + (x_2 + \xi_2)^2} \quad (94)$$

One check of these results is to verify whether Equation (93) satisfies the stress-free boundary condition on $x_2 = 0$. For this, it is required that

$$\left. \frac{\partial G_{33}}{\partial x_2} \right|_{x_2 = 0} = 0 \quad (95)$$

This derivative is

$$\frac{\partial G_{33}}{\partial x_2} = \frac{i}{4\mu} \left[H_1^{(2)}(k_2 r) \frac{x_2 - \xi_2}{r} + H_1^{(2)}(k_2 r^*) \frac{x_2 + \xi_2}{r^*} \right] \quad (96)$$

On the free surface $x_2 = 0$

$$r = \sqrt{(x_1 - \xi_1)^2 + \xi_2^2} \quad (97)$$

which is identical to the value for r^* . Thus,

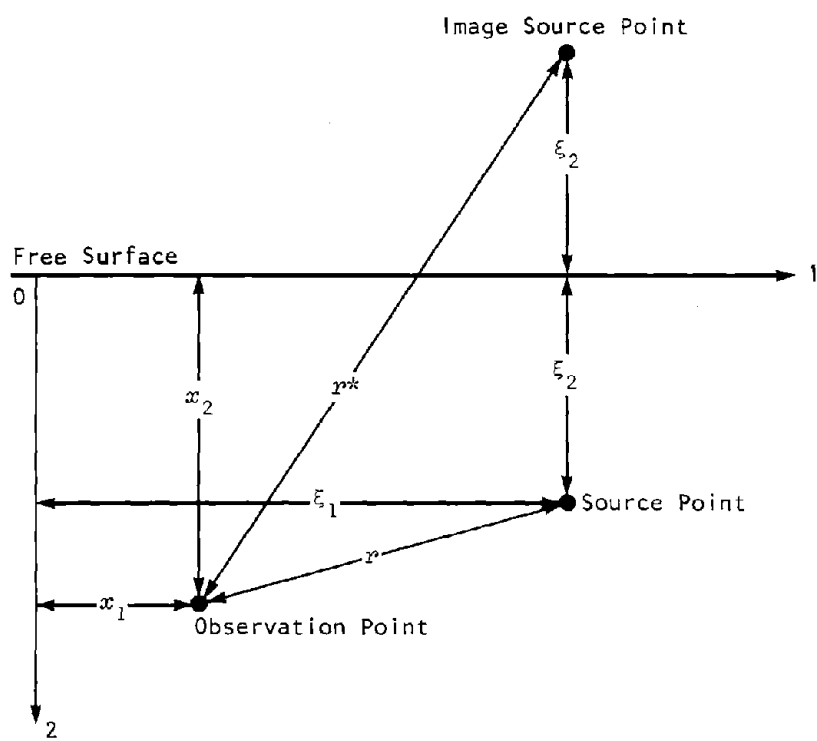


Figure 72. Image source location.

$$\left. \frac{\partial G_{33}}{\partial x_2} \right|_{x_2 = 0} = \frac{i \xi_2}{4\mu} \left[- \frac{H_1^{(2)} \left(k_2 \sqrt{(x_1 - \xi_1)^2 + \xi_2^2} \right)}{\sqrt{(x_1 - \xi_1)^2 + \xi_2^2}} + \frac{H_1^{(2)} \left(k_2 \sqrt{(x_1 - \xi_1)^2 + \xi_2^2} \right)}{\sqrt{(x_1 - \xi_1)^2 + \xi_2^2}} \right] = 0 \quad (98)$$

Hence, this boundary condition is satisfied.

References

1. Peck, R. B., A. J. Hendron, Jr., and B. Mohraz, "State of the Art of Soft Ground Tunneling," *Proceedings of the First Rapid Excavation and Tunneling Conference*, Vol. 1, American Institute of Mining, Metallurgical, and Petroleum Engineers, Inc., New York, New York, 1972, pp. 259-286.
2. Bolt, B. A., *Earthquakes: A Primer*, W. H. Freeman and Company, San Francisco, California, 1978, p. 14 (Fig. 4).
3. Gutenberg, B., and C. F. Richter, *Seismicity of the Earth and Associated Phenomena*, Hafner Publishing Company, New York, New York, 1965.
4. Richter, C. F., *Elementary Seismology*, W. H. Freeman and Company, San Francisco, California, 1958.
5. Bath, M., *Introduction to Seismology*, Birkhauser Verlag, Basel, Switzerland, and Stuttgart, Germany, 1973.
6. Sykes, L., "Intraplate Seismicity, Reactivation of Preexisting Zones of Weakness, Alkaline Magnetism, and Other Tectonism Post-Dating Continental Fragmentation," *Reviews of Geophysics and Space Physics*, Vol. 16, No. 4, 1978, pp. 621-688.
7. Bollinger, G. A., "The Seismic Regime in a Minor Earthquake Zone," *Numerical Methods in Geomechanics*, C. S. Desai, ed., Vol. 2, American Society of Civil Engineers, New York, New York, 1976, pp. 917-937.
8. Ambraseys, N. N., "Value of Historical Record of Earthquakes," *Nature*, Vol. 232, 1971, pp. 375-379.
9. International Conference of Building Officials, *Uniform Building Code*, Whittier, California, 1979, p. 145 (Fig. 1).
10. Applied Technology Council, *Tentative Provisions for the Development of Seismic Regulations for Buildings*, NBS Special Publication 510 (also

ATC 3-06 or NSF 78-8), National Bureau of Standards, Washington, D.C., June 1978.

11. Schnabel, P. B., and H. B. Seed, "Accelerations in Rock for Earthquakes in the Western United States," *Bulletin of the Seismological Society of America*, Vol. 63, No. 2, April 1973, pp. 501-516.
12. Idriss, I. M., "Characteristics of Earthquake Ground Motions," *Earthquake Engineering and Soil Dynamics*, Proceedings of the Specialty Conference on Earthquake Engineering and Soil Dynamics, Pasadena, California, June 19-21, 1978, Vol. 3, American Society of Civil Engineers, New York, New York, 1979.
13. Blume, J. A., "The SAM Procedures for the Site-Acceleration-Magnitude Relationships," *Proceedings of the Sixth World Conference on Earthquake Engineering*, Vol. 2, New Delhi, India, 1977, pp. 87-92.
14. Parsons-Brinckerhoff-Tudor-Bechtel, *Trans-Bay Tube, Technical Supplement to the Engineering Report*, San Francisco, California, prepared for San Francisco Bay Area Rapid Transit District, Oakland, California, July 1960.
15. Duke, C. M., and D. J. Leeds, *Effects of Earthquakes on Tunnels*, P-1762, The RAND Corporation, Santa Monica, California, July 28, 1959.
16. Stevens, P. R., *A Review of the Effects of Earthquakes on Underground Mines*, Open-File Report 77-313, U.S. Department of the Interior, Geological Survey, Reston, Virginia, April 1977.
17. Dowding, C. H., and A. Rozen, "Damage to Rock Tunnels from Earthquake Shaking," *Journal of the Geotechnical Engineering Division*, American Society of Civil Engineers, Vol. 104, No. GT2, February 1978, pp. 178-179 (Figs. 3, 4).
18. Pratt, H. R., W. A. Hustrulid, and D. E. Stephenson, *Earthquake Damage to Underground Facilities*, DP-1513, Savannah River Laboratory, Aiken, South Carolina, November 1978.

19. Carnegie Institution, *The California Earthquake of April 18, 1906*, Report of the State Earthquake Investigation Commission, A. C. Lawson, Chairman, Washington, D.C., 1908.
20. Personal communication from L. Farrar, Southern Pacific Transportation Company, San Francisco, California, to G. N. Owen, URS/John A. Blume & Associates, Engineers, San Francisco, California, Job File No. 7821, June 1979.
21. Steinbrugge, K. V., and D. F. Moran, "An Engineering Study of the Southern California Earthquake of July 21, 1952, and its Aftershocks," *Bulletin of the Seismological Society of America*, Vol. 44, No. 2B, April 1954.
22. Kupfer, D. H., S. Muessig, G. I. Smith, and G. N. White, "Arvin-Tehachapi Earthquake Damage Along the Southern Pacific Railroad Near Bealville, California," *Earthquakes in Kern County, California, During 1952*, G. B. Oakeshott, ed., California Division of Mines, Bulletin 171, November 1955.
23. National Research Council, *The Great Alaska Earthquake of 1964, Engineering*, U.S. National Academy of Sciences, Washington, D.C., 1973.
24. Rozen, A., "Response of Rock Tunnels to Earthquake Shaking," Masters Thesis, presented to the Massachusetts Institute of Technology, Cambridge, Massachusetts, September 1976.
25. Dowding, C. H., "Seismic Stability of Underground Openings," *Proceedings of the Rockstore Conference*, Stockholm, Sweden, September 1977.
26. Jennings, P. C., ed., *Engineering Features of the San Fernando Earthquake, February 9, 1971*, EERL 71-02, California Institute of Technology, Pasadena, California, June 1971.
27. Benfer, N. A., J. L. Coffman, and L. T. Dees, eds., *San Fernando, California, Earthquake of February 9, 1971*, Vols. 2 and 3, National Oceanic and Atmospheric Administration, Washington, D.C., 1973.
28. American Society of Civil Engineers, *Earthquake Damage Evaluation and Design Considerations for Underground Structures*, Los Angeles Section, February 1974.

29. Hradilek, P. J., *Behavior of Underground Box Conduits in the San Fernando Earthquake of 9 February 1971*, Technical Report E-72-1, U.S. Army Corps of Engineers, Los Angeles District, California, January 1972.
30. Nakazawa, K., et al., "Damage Features of Engineering Structures Due to the Near Izu-Oshima Earthquake of January 14, 1978," presented at the 10th Joint Meeting, *U.S.-Japan Panel on Wind and Seismic Effects*, Washington, D.C., May 23-26, 1978.
31. Yanev, P. I., ed., *Miyagi-Ken-Okii, Japan, Earthquake, June 12, 1978*, Earthquake Engineering Research Institute, Berkeley, California, December 1978.
32. URS/John A. Blume & Associates, Engineers, "Reconnaissance Report of the October 4, 1978, Earthquake Near Bishop, California," San Francisco, California, unpublished report.
33. Okamoto, S., *Introduction to Earthquake Engineering*, John Wiley & Sons, New York, New York, 1973.
34. Woodward-Clyde Consultants, *Offshore Alaska Seismic Exposure Study*, San Francisco, California, prepared for Alaska Subarctic Operators' Committee, March 1978.
35. McGuire, R. K., "Seismic Ground Motion Parameter Relations," presented at the Annual Meeting of the American Society of Civil Engineers, San Francisco, California, October 1977.
36. Duke, C. M., K. E. Johnsen, L. E. Larson, and D. C. Engman, *Effects of Site Classification and Distance on Instrumental Indices in the San Fernando Earthquake*, Report No. UCLA-ENG-7247, School of Engineering and Applied Sciences, University of California, Los Angeles, California, 1972.
37. Langefors, U., and B. Kihlstrom, *The Modern Technique of Rock Blasting*, John Wiley & Sons, New York, New York, and Almquist & Wiksell, Stockholm, Sweden, 1963.

38. Bauer, A., and P. N. Calder, "The Influence and Evaluation of Blasting on Stability," *Proceedings of the 1st International Conference on Stability in Open Pit Mining*, Vancouver, B.C., Canada, 1970, pp. 83-95.
39. Engineering Research Associates, *Underground Explosion Test Program, Final Report, Rock*, Vol. 2, U.S. Army Corps of Engineers, Sacramento District, California, April 1953.
40. Hendron, A. J., Jr., "Engineering of Rock Blasting on Civil Projects," *Structural and Geotechnical Mechanics*, W. J. Hall, ed., Prentice-Hall, Englewood Cliffs, New Jersey, 1977, p. 256 (Fig. 7).
41. Holmes, R. S., L. T. Kwan, E. H. Skinner, and E. Y. Wong, *Loading, Response, and Evaluation of Tunnels and Tunnel Liners in Granite (U)*, POR-1801, Operation Nougat, Shot Hard Hat, Holmes & Narver, Inc., Los Angeles, California, April 1963.
42. Desai, C. S., ed., *Numerical Methods in Geomechanics*, Vols. 1-3, American Society of Civil Engineers, New York, New York, 1976.
43. Desai, C. S., and J. T. Christian, eds., *Numerical Methods in Geotechnical Engineering*, McGraw-Hill, New York, New York, 1977.
44. Newmark, N. M., "Problems in Wave Propagation in Soil and Rock," *Proceedings, International Symposium on Wave Propagation and Dynamic Properties of Earth Materials*, University of New Mexico Press, Albuquerque, New Mexico, August 23-25, 1968.
45. Schnabel, P. B., J. Lysmer, and H. B. Seed, *SHAKE - A Computer Program for Earthquake Response Analysis of Horizontally Layered Sites*, Report No. EERC 72-12, Earthquake Engineering Research Center, University of California, Berkeley, California, December 1972.
46. Jones, T. J., and J. M. Roesset, *Soil Amplification of SV and P Waves*, Research Report No. R70-3, Massachusetts Institute of Technology, Cambridge, Massachusetts, January 1970.

47. Seed, H. B., and I. M. Idriss, "The Influence of Soil Conditions on Ground Motions During Earthquakes," *Journal of the Soil Mechanics and Foundations Division*, American Society of Civil Engineers, Vol. 15, No. SM1, 1961.
48. Idriss, I. M., and H. B. Seed, "Seismic Response of Horizontal Soil Layers," *Journal of the Soil Mechanics and Foundations Division*, American Society of Civil Engineers, Vol. 96, No. SM4, 1968.
49. Seed, H. B., and I. M. Idriss, "Influence of Soil Conditions on Ground Motions During Earthquakes," *Journal of the Soil Mechanics and Foundations Division*, American Society of Civil Engineers, Vol. 94, No. SM1, January 1969.
50. Lysmer, J., T. Udaka, C. F. Tsai, and H. B. Seed, *FLUSH - A Computer Program for Approximate 3-D Analysis of Soil-Structure Interaction Problems*, Report No. EERC 75-30, Earthquake Engineering Research Center, University of California, Berkeley, California, November 1975.
51. Lysmer, J., and R. L. Kuhlemeyer, "A Finite Dynamic Model for Infinite Media," *Journal of the Engineering Mechanics Division*, American Society of Civil Engineers, Vol. 95, No. EM4, August 1969, pp. 859-877.
52. Martin, P. P., and H. B. Seed, *MASH - Computer Program for the Non-Linear Analysis of Vertically Propagating Shear Waves in Horizontally Layered Deposits*, Report No. EERC 78-23, Earthquake Engineering Research Center, University of California, Berkeley, California, October 1978.
53. Streeter, B. L., B. B. Wylie, and F. E. Richart, Jr., "Soil Motion Computations by Characteristics Methods," *Journal of the Geotechnical Engineering Division*, American Society of Civil Engineers, Vol. 100, No. GT3, March 1974.
54. Cundall, P. A., *QUAKE - A Computer Program to Model Shear Wave Propagation in a Hysteretic Layered Site*, Dames & Moore, Los Angeles, California, April 1975.

55. Banister, J. R., D. M. Ellett, C. R. Mehl, and F. F. Dean, "Stress and Strains Developed by the Reflection of Seismic Waves at a Free Surface," Draft Report No. SAND77-0673, Sandia Laboratories, Albuquerque, New Mexico, February 1978.
56. Nair, G. P., and J. J. Emery, "Spatial Variations in Seismic Motions," *Canadian Journal of Civil Engineering*, National Research Council of Canada, Vol. 3, No. 1, 1976.
57. URS/John A. Blume & Associates, Engineers, "The Use of the Explicit Finite-Difference Method for Linear Elastic Soil-Structure Interaction Analyses," *Applications in Soil-Structure Interaction*, EPRI NP-1091, Vol. 1, Electric Power Research Institute, Palo Alto, California, June 1979.
58. Science Applications, Inc., *STEALTH - A Lagrange Explicit Finite-Difference Code for Solids, Structural, and Thermohydraulic Analysis*, EPRI NP-176, Electric Power Research Institute, Palo Alto, California, June 1976.
59. Kuesel, T. R., "Earthquake Design Criteria for Subways," *Journal of the Structural Division*, American Society of Civil Engineers, Vol. 95, No. ST6, June 1969, pp. 1213-1231.
60. Kuribayashi, E., T. Iwasaki, and K. Kawashima, "Dynamic Behavior of a Subsurface Tubular Structure," *Bulletin of the New Zealand National Society for Earthquake Engineering*, Vol. 7, No. 4, December 1974, pp. 200-209.
61. Glass, C. E., "Seismic Considerations in Siting Large Underground Openings in Rock," Ph.D. Thesis, University of California, Berkeley, California, 1976.
62. Campbell, R. B., and J. S. Dodd, "Estimated Rock Stresses at Morrow Point Underground Power Plant from Earthquakes and Underground Nuclear Blasts," *Status of Practiced Rock Mechanics -- Ninth Symposium on Rock Mechanics*, Colorado School of Mines, Golden, Colorado, April 1967, published by the Society of Mining Engineers of the American Institute of Mining, Metallurgical, and Petroleum Engineers, Inc., New York, New York, 1972.

63. Yanev, P. I., and G. N. Owen, *Facility Hardening Studies; Design Cost Scoping Studies*, JAB-99-123, URS/John A. Blume & Associates, Engineers, San Francisco, California, prepared for the U.S. Department of Energy, Nevada Operations Office, Nevada Nuclear Waste Storage Investigations, Las Vegas, Nevada, April 1978.
64. Chen, P. C., D. Z. F. Deng, and A. J. Birkmyer, "Considerations of Dynamic Stress Concentrations in the Seismic Analysis of Buried Structures," *Proceedings of the 2nd U.S. National Conference on Earthquake Engineering*, Stanford University, Stanford, California, August 22-24, 1979.
65. Mow, C. C., and Y. H. Pao, *The Diffraction of Elastic Waves and Dynamic Stress Concentrations*, R-482-PR, Report for the U.S. Air Force Project Rand, April 1971, pp. 252, 274, 302, 304 (Figs. 3.7, 3.15, 3.16, 4.9a, 4.10a).
66. Mente, L. J., and F. W. French, "Response of Elastic Cylinder to Plant Shear Waves," *Journal of the Engineering Mechanics Division, Proceedings of ASCE*, American Society of Civil Engineers, No. EM5, October 1964.
67. Lew, T. K., *Soil/Structure Interaction: Horizontal Cylinders*, AD/A-200 216, Civil Engineering Laboratory, Port Hueneme, prepared for the Defense Nuclear Agency, Washington, D.C., October 1974.
68. Lew, T. K., *Deep-Underground, Lined, Horizontal, Circular Openings in Rock*, AD/A-021 867, Civil Engineering Laboratory, Port Hueneme, prepared for the Defense Nuclear Agency, Washington, D.C., February 1976.
69. Bathe, K.-J., E. L. Wilson, and F. E. Peterson, *SAP IV, A Structural Analysis Program for Static and Dynamic Response of Linear Systems*, Report No. EERC 73-11, Earthquake Engineering Research Center, University of California, Berkeley, California, 1974.
70. Bathe, K.-J., E. L. Wilson, and R. H. Iding, *NONSAP--A Structural Analysis Program for Static and Dynamic Response of Nonlinear Systems*, Report No. UC SESM74-3, Department of Civil Engineering, University of California, Berkeley, California, February 1974.

71. Swanson Analysis Systems Inc., *ANSYS--Engineering Analysis System User's Manual*, Huston, Pennsylvania, July 1975.
72. Cundall, P. A., R. Kunar, J. Marti, and P. Carpenter, "Solution of Infinite Dynamic Problems by Finite Modeling in the Time Domain," *Proceedings of the 2nd International Conference on Applied Numerical Modeling*, Spain, 1978.
73. John A. Blume & Associates, Engineers, *Engineering Study of Remedial Measures for Tunnel No. 1*, San Francisco, California, prepared for Southern Pacific Company, San Francisco, California, August 1968.
74. Yamahara, H., Y. Hisatomi, and T. Morie, "A Study on the Earthquake Safety of Rock Cavern," *Proceedings of the Rockstore Conference*, Stockholm, Sweden, September 1977.
75. Murtha, R. N., *Dynamic Response of a Horizontally Buried Cylinder Above a Soil/Rock Interface--Results of a Finite Element Analysis*, AD/A-024 052, Civil Engineering Laboratory, Port Hueneme, prepared for the Defense Nuclear Agency, Washington, D.C., March 1976.
76. Wahi, K. K., B. C. Trent, D. E. Maxwell, R. M. Pyke, C. Young, and D. M. Ross Brown, "Numerical Simulation of Earthquake Effects on Tunnels for Generic Nuclear Waste Repositories," SAI-FR-126, Science Applications, Incorporated, Fort Collins, Colorado, July 1979, draft report, release pending review.
77. URS/John A. Blume & Associates, Engineers, *Comparative Structural Analysis of Type III Underground Waste Storage Tanks at the Savannah River Plant, Aiken, South Carolina*, San Francisco, California, prepared for E. I. du Pont de Nemours & Company, Wilmington, Delaware, December 1976.
78. Fukushima, D., M. Hamada, and T. Hanamura, "Earthquake-Resistant Design of Underground Tanks," *Proceedings of the Rockstore Conference*, Stockholm, Sweden, September 1977.

79. Goodman, R. E., R. L. Taylor, and T. L. Brekke, "A Model for the Mechanics of Jointed Rock," *Journal of the Soil Mechanics and Foundations Division, American Society of Civil Engineers*, Vol. 94, No. SM3, May 1968, pp. 637-659.
80. Roberds, W. J., and H. H. Einstein, "Comprehensive Model for Rock Discontinuities," *Journal of the Geotechnical Engineering Division, American Society of Civil Engineers*, May 1978.
81. Agbabian Associates, *Analytic Modeling of Rock Structure Interaction*, R-7215-2701, 3 Vols., El Segundo, California, April 1973.
82. Karwoski, W. J., and D. E. Van Dillen, "Applications of BMINES Three Dimensional Finite Element Computer Code to Large Mine Structural Problems," *Proceedings of 19th U.S. Rock Mechanics Symposium*, Mackey School of Mines, University of Nevada, May 1978, published by Conferences and Institutes, Extended Programs and Continuing Education, University of Nevada, Reno, Nevada, 1978.
83. Cundall, P. A., "A Computer Model for Simulating Progressive, Large Scale Movements in Blocky Rock Systems," *Symposium of the International Rock Mechanics Society*, Nancy, France, 1971.
84. Cundall, P. A., *Rational Design of Tunnel Supports*, Technical Report MRD-2-74, U.S. Army Corps of Engineers, Missouri River Division, 1974.
85. Maini, T., P. Cundall, J. Marti, P. Beresford, N. Last, and M. Asgian, *Computer Modelling of Jointed Rock Masses*, Technical Report N-78-4, Dames & Moore, Los Angeles, California, prepared for the Defense Nuclear Agency, Washington, D.C., August 1978.
86. Personal communication from T. Belytschko, Northwestern University, Evanston, Illinois, to G. N. Owen, URS/John A. Blume & Associates, Engineers, San Francisco, California, Job File No. 7821, December 1979.

87. Brady, B. H. G., and J. W. Bray, "The Boundary Element Method for Determining Stresses and Displacements Around Long Openings in a Triaxial Stress Field," *International Journal of Rock Mechanics, Mineral Science, and Geomechanics Abstracts*, Vol. 15, 1978, pp. 21-28.
88. Brady, B. H. G., and J. W. Bray, "The Boundary Element Method for Elastic Analysis of Tabular Orebody Extraction, Assuming Complete Plane Strain," *International Journal of Rock Mechanics, Mineral Science, and Geomechanics Abstracts*, Vol. 15, 1978, pp. 29-37.
89. Brady, B. H. G., "A Boundary Element Method of Stress Analysis for Non-Homogeneous Media and Complete Plane Strain," *Proceedings of the 20th U.S. Symposium on Rock Mechanics*, Austin, Texas, June 4-5, 1979, pp. 243-250.
90. Cruse, T. A., and F. J. Rizzo, eds., *Boundary Integral Equation Method: Computational Application in Applied Mechanics*, American Society of Mechanical Engineers, New York, New York, 1975.
91. Brown, E. T., and G. Hocking, "The Use of the Three Dimensional Boundary Integral Equation Method for Determining Stresses at Tunnel Intersections," *Proceedings*, Second Australian Tunneling Conference, Melbourne, Australia, August 1976, pp. 55-64.
92. Alarcon, E., J. Dominguez, A. Martin, and F. Paris, "Boundary Methods in Soil-Structure Interaction," *Proceedings*, Second International Conference on Microzonation, San Francisco, California, November 26 to December 1, 1978, Vol. 2, pp. 921-932.
93. Barton, N., and H. Hansteen, *Large Underground Openings at Shallow Depth: Comparison of Deformation Magnitudes from Jointed Models and Linear Elastic F. E. Analysis*, Internal Report No. 54205-5, Norges Geotekniski Institute, Oslo, Norway, January 1979.
94. Daniel, I. M., "Viscoelastic Wave Interaction with Cylindrical Cavity," *Journal of the Engineering Mechanics Division*, American Society of Civil Engineers, Vol. 92, No. EM6, December 1966, pp. 25-42.

95. Okamoto, S., and C. Tamura, "Behavior of Subaqueous Tunnels during Earthquakes," *Earthquake Engineering and Structural Dynamics*, Vol. 1, 1973.
96. Okamoto, S., C. Tamura, K. Kato, and M. Hamada, "Behavior of Submerged Tunnels During Earthquakes," *Proceedings of the Fifth World Conference on Earthquake Engineering*, Rome, Italy, June 1973.
97. Wilson, S. D., F. D. Brown, Jr., and S. D. Schwarz, "In Situ Determination of Dynamic Soil Properties," *Dynamic Geotechnical Testing*, Publication STP 654, American Society of Testing and Materials, Philadelphia, Pennsylvania, 1978, pp. 295-317.
98. Kanamori, H., and D. L. Anderson, "Importance of Physical Dispersion in Surface Wave and Free Oscillation Problems," *Reviews of Geophysics and Space Physics*, Vol. 15, 1977, pp. 105-112.
99. Seed, H. B., and I. M. Idriss, *Soil Moduli and Damping Factors for Dynamic Response Analyses*, Report No. EERC 70-10, Earthquake Engineering Research Center, University of California, Berkeley, California, 1970.
100. Silver, M. L., and T. K. Park, "Testing Procedure Effects on Dynamic Soil Behavior," *Journal of the Geotechnical Engineering Division*, American Society of Civil Engineers, Vol. 101, No. GT10, 1975, pp. 1061-1083.
101. Halmson, B. C., "Effect of Cyclic Loading on Rock," *Dynamic Geotechnical Testing*, Publication STP 654, American Society of Testing and Materials, 1978, pp. 228-245.
102. Drnevich, V. P., B. O. Hardin, and D. J. Shippy, "Modulus and Damping of Soils by Resonant Column Method," *Dynamic Geotechnical Testing*, Publication STP 654, American Society of Testing and Materials, Philadelphia, Pennsylvania, 1978, pp. 91-125.
103. Hendron, A. J., Jr., "Mechanical Properties of Rock," *Rock Mechanics in Engineering Practice*, K. G. Stagg and O. C. Zienkiewicz, eds., John Wiley & Sons, New York, New York, 1968, pp. 21-53.

104. Silver, V. A., S. P. Clemence, and R. W. Stephenson, "Predicting Deformations in the Fort Union Formation," *Rock Engineering for Foundations and Slopes*, Vol. 1, American Society of Civil Engineers, New York, New York, 1968, pp. 13-33.
105. McDonal, F. J., et al., "Attenuation of Shear and Compressional Waves in Pierre Shale," *Geophysics*, Vol. 23, 1958, pp. 421-439.
106. Joyner, W. B., R. E. Warrick, and A. A. Oliver, III, "Analysis of Seismograms from a Downhole Array in Sediments Near San Francisco Bay," *Bulletin of the Seismological Society of America*, Vol. 66, No. 3, June 1976, pp. 937-958.
107. Reiter, L., and M. E. Monfort, "Variations in Initial Pulse Width as a Function of Anelastic Properties and Surface Geology in Central California," *Bulletin of the Seismological Society of America*, Vol. 67, 1977, pp. 1319-1338.
108. Stagg, K. G., "In Situ Tests on the Rock Mass," *Rock Mechanics in Engineering Practice*, K. G. Stagg and O. C. Zienkiewicz, eds., John Wiley & Sons, New York, New York, 1968, pp. 125-156.
109. Brown, E. T., and J. A. Hudson, "Fatigue Failure Characteristics of Some Models of Jointed Rock," *Earthquake Engineering and Structural Dynamics*, Vol. 2, 1974, pp. 379-386.
110. Richart, F. E., Jr., D. G. Anderson, and K. H. Stokoe, II, "Predicting In Situ Strain-Dependent Shear Moduli of Soil," *Proceedings of the Sixth World Conference on Earthquake Engineering*, New Delhi, India, 1977, pp. 2310-2315.
111. Hardin, B. O., and V. P. Drnevich, "Shear Modulus and Damping: Measurement and Parameter Effects," *Journal of the Soil Mechanics and Foundations Division*, American Society of Civil Engineers, Vol. 98, No. SM6, 1972, pp. 603-624.

112. Miller, R. P., J. H. Troncoso, and R. R. Brown, Jr., "In Situ Impulse Test for Dynamic Shear Modulus of Soils," *Proceedings of the Conference on In Situ Measurement of Soil Properties*, Raleigh, North Carolina, Vol. 1, American Society of Civil Engineers, New York, New York, 1975, pp. 319-335.
113. Baecher, G. B., N. A. Lanney, and H. H. Einstein, "Statistical Description of Rock Properties and Sampling," *Proceedings of the 18th U.S. Symposium on Rock Mechanics*, Keystone, Colorado, 1977, pp. 5C1-1 to 5C1-8.
114. Richart, F. E., J. R. Hall, and R. D. Woods, *Vibrations of Soils and Foundations*, Prentice-Hall, Englewood Cliffs, New Jersey, 1970, p. 89 (Fig. 3-14).
115. Nasu, N., "Comparative Studies of Earthquake Motions Above-Ground and in a Tunnel (Part 1)," *Bulletin of the Earthquake Research Institute*, Vol. 9, Part 4, December 1931, pp. 454-472.
116. Inouye, W., "Comparison of Earth Shaking Above Ground and Underground," *Bulletin of the Earthquake Research Institute*, Vol. 12, 1934, pp. 712-741 (in Japanese).
117. Kanai, K., and T. Tanaka, "Observations of the Earthquake-Motion at the Different Depths of the Earth I," *Bulletin of the Earthquake Research Institute*, Vol. 29, 1951, pp. 107-113.
118. Kanai, K., K. Osada, and S. Yoshizawa, "Observations Study of Earthquake Motion in the Depth of the Ground IV (Relation between the Amplitude at Ground Surface and the Period)," *Bulletin of the Earthquake Research Institute*, Vol. 31, 1953, pp. 228-234.
119. Kanai, K., K. Osada, and S. Yoshizawa, "Observational Study of Earthquake Motion in the Depths of the Ground V (The Problem of the Ripple of Earthquake Motion)," *Bulletin of the Earthquake Research Institute*, Vol. 32, 1954, pp. 361-370.

120. Iwasaki, T., S. Wakabayashi, and F. Tatsuoka, "Characteristics of Under-ground Seismic Motions at Four Sites Around Tokyo Bay," *Wind and Seismic Effects*, H. S. Lew, ed., U.S. Department of Commerce, Washington, D.C., May 1977.
121. Shima, E., "Modifications of Seismic Waves in Superficial Soil Layers as Verified by Comparative Observations on and Beneath the Surface," *Bulletin of the Earthquake Research Institute*, Vol. 40, 1962, pp. 187-259.
122. Kanai, K., T. Tanaka, S. Yoshizawa, T. Morishita, K. Osada, and T. Suzuki, "Comparative Studies of Earthquake Motions on the Ground and Underground II," *Bulletin of the Earthquake Research Institute*, Vol. 44, 1966, pp. 609-643.
123. Seed, H. B., and I. M. Idriss, "Analysis of Ground Motions at Union Bay, Seattle, During Earthquakes and Distant Nuclear Blasts," *Bulletin of the Seismological Society of America*, Vol. 60, 1970, pp. 125-136.
124. Tsai, N. C., and G. W. Housner, "Calculation of Surface Motions of a Layered Half-Space," *Bulletin of the Seismological Society of America*, Vol. 60, 1970, pp. 1625-1651.
125. Dobry, R., R. V. Whitman, and J. M. Roesset, *Soil Properties and the One-Dimensional Theory of Earthquake Amplification*, Research Report No. R71-18, Department of Civil Engineering, Massachusetts Institute of Technology, Cambridge, Massachusetts, 1971..
126. Joyner, W. B., R. E. Warrick, and A. A. Oliver, III, "Analysis of Seismo-grams from a Downhole Array in Sediments Near San Francisco Bay," *Bulletin of the Seismological Society of America*, Vol. 66, No. 3, June 1976, pp. 937-958.
127. Blume, J. A., *Surface and Subsurface Ground Motion*, Engineering Foundation Conference on Earthquake Protection of Underground Utility Structure, Asilomar, California, September 1972.

128. Berardi, R., F. Capozza, and L. Zonetti, "Analysis of Rock Motion Accelerograms Recorded at Surface and Underground During the 1976 Friuli Seismic Period," *The 1976 Friuli Earthquake and the Antiseismic Design of Nuclear Installations*, Rome, Italy, October 1977.
129. Personal communication from Y. Ichikawa, Electric Power Development Company, Ltd., Tokyo, Japan, to G. N. Owen, URS/John A. Blume & Associates, Engineers, San Francisco, California, Job File No. 7821, October 1979.
130. Personal communication from T. Iwasaki, Public Works Research Institute, Tsukuba, Japan, to G. N. Owen, URS/John A. Blume & Associates, Engineers, San Francisco, California, Job File No. 7821, June 1978.
131. Nakano K., and Y. Kitagawa, "Earthquake Observation System In and Around Structures in Japan," presented at the 11th Joint Meeting, U.S.-Japan Panel on Wind and Seismic Effects, Tokyo, Japan, September 4-7, 1979.
132. O'Brien, L. J., and J. Saunier, "Comparison of Predicted and Observed Subsurface-Surface Seismic Spectral Ratios," NVO-624-2, prepared for Nevada Operations Office, U.S. Department of Energy, Las Vegas, Nevada, March 1980.
133. Gilbert, F., and L. Knopoff, "Scattering of Impulsive Elastic Waves by a Rigid Cylinder," *Journal of the Acoustical Society of America*, Vol. 31, No. 9, September 1959, pp. 1169-1175.
134. Gilbert, F., "Scattering of Impulsive Elastic Waves by a Smooth Convex Cylinder," *Journal of the Acoustical Society of America*, Vol. 32, No. 7, July 1960, pp. 841-857.
135. Banaugh, R. P., and W. Goldsmith, "Diffraction of Steady Acoustic Waves by Surfaces of Arbitrary Shape," *Journal of the Acoustical Society of America*, Vol. 35, No. 10, October 1963, pp. 1590-1601.

136. Garnet, H., and J. Crouzet-Pascal, "Transient Response of a Circular Cylinder of Arbitrary Thickness, in an Elastic Medium, to a Plane Dilatational Wave," *Journal of Applied Mechanics*, American Society of Mechanical Engineers, Vol. 33, September 1966, pp. 521-531.
137. Niwa, Y., S. Kobayashi, and T. Fukui, "Applications of Integral Equation Method to Some Geomechanical Problems," *Numerical Methods in Geomechanics*, C. S. Desai, ed., Vol. 1, American Society of Civil Engineers, New York, New York, 1976, pp. 120-131.
138. Yoshihara, T., A. R. Robinson, and J. L. Merritt, *Interaction of Plane Elastic Waves with an Elastic Cylindrical Shell*, Technical Report No. SRS 261, Department of Civil Engineering, University of Illinois, Champaign, Illinois, January 1963.
139. American Association of State Highway and Transportation Officials, *Standard Specifications for Highway Bridges*, 11th edition, Washington, D.C., 1973.
140. Department of General Services, *State of California Administrative Code*, Title 24 (Building Standards), Office of Administrative Hearing, Sacramento, California, 1979.
141. Structural Engineers Association of California, *Recommended Lateral Force Requirements and Commentary*, San Francisco, California, 1976.
142. Japan Society of Civil Engineers, *Specifications for Earthquake Resistant Design of Submerged Tunnels*, Tokyo, Japan, March 1975.
143. Japan Society of Civil Engineers, *Earthquake Resistant Design Features of Submerged Tunnels in Japan*, Tokyo, Japan, 1977.
144. Personal communication from G. J. Murphy, Parsons, Brinckerhoff, Quade & Douglas, San Francisco, California, to G. N. Owen, URS/John A. Blume & Associates, Engineers, San Francisco, California, Job File No. 7821, January 1980.

145. Kuribayashi, E., and K. Kawashima, *Earthquake Resistant Design of Submerged Tunnels and an Example of Its Application*, PWRI Technical Memorandum No. 1169, Public Works Research Institute, Tsukuba, Japan, November 1976.
146. Kuribayashi, E., T. Iwasaki, and K. Kawashima, "Earthquake Resistance of Subsurface Tubular Structure," *Proceedings of the Sixth World Conference on Earthquake Engineering*, New Delhi, India, January 1977.
147. Kuribayashi, E., K. Kawashima, and Shibata, *Sectional Forces in a Submerged Tunnel by the Seismic Deformation Method*, PWRI Technical Memorandum No. 1193, Public Works Research Institute, Tsukuba, Japan, March 1977 (in Japanese).
148. Kuribayashi, E., K. Kawashima, Shibata, and Miyata, *A Study of Ultimate Strength of a Submerged Tunnel Using the Seismic Deformation Method*, PWRI Technical Memorandum No. 1253, Public Works Research Institute, Tsukuba, Japan, April 1977 (in Japanese).
149. Kuribayashi, E., K. Kawashima, and Shibata, *The Influence of a Flexible Connection on the Sectional Forces in a Submerged Tunnel*, PWRI Technical Memorandum No. 1272, Public Works Research Institute, Tsukuba, Japan, February 1978 (in Japanese).
150. Seed, H. B., and R. V. Whitman, "Design of Earth Retaining Structures for Dynamic Loads," *Lateral Stresses in the Ground and Design of Earth-Retaining Structures*, American Society of Civil Engineers, New York, New York, 1970.
151. Aoki, Y., and S. Hayashi, "Spectra for Earthquake-Resistive Design of Underground Long Structures," *Proceedings of the Fifth World Conference on Earthquake Engineering*, Rome, Italy, June 1973.
152. Hamada, M., T. Akimoto, and H. Izumi, "Dynamic Stress of a Submerged Tunnel During Earthquakes," *Proceedings of the Fifth World Conference on Earthquake Engineering*, Rome, Italy, June 1973.

153. Goto, Y., J. Ota, and T. Sato, "On Earthquake Response of Submerged Tunnels," *Proceedings of the Fifth World Conference on Earthquake Engineering*, Rome, Italy, June 1973.
154. Douglas, W. S., and R. Warshaw, "Design of Seismic Joint for San Francisco Bay Tunnel," *Journal of the Structural Division*, American Society of Civil Engineers, Vol. 97, No. ST4, April 1971, pp. 1129-1141 (p. 1131, Fig. 2).
155. Roark, R. J., and W. C. Young, *Formulas for Stress and Strain*, 5th edition, McGraw-Hill, New York, New York, 1975.
156. East Bay Municipal Utility District, *Seismic Design Requirements*, Oakland, California, May 1973.
157. Personal communication from J. M. Keith, Vice President, URS/John A. Blume & Associates, Engineers, San Francisco, California, to G. N. Owen, URS/John A. Blume & Associates, Engineers, San Francisco, California, Job File No. 7821, January 1980.
158. Dames & Moore, *Interpretive Report--Engineering Recommendations*, NSOC-N-2, Los Angeles, California, prepared for the San Francisco Wastewater Program, Department of Public Works, San Francisco, California, March 1979.
159. Personal communication from F. Moss, Department of Public Works, San Francisco, California, to G. N. Owen, URS/John A. Blume & Associates, Engineers, San Francisco, California, Job File No. 7821, December 28, 1979.
160. Personal communication from D. J. Birrer, Department of Public Works, San Francisco, California, to G. N. Owen, URS/John A. Blume & Associates, Engineers, San Francisco, California, Job File No. 7821, January 17, 1980.
161. Dames & Moore, *Supplementary Soils Report*, NSOC-N-4 (Marina Boulevard), Los Angeles, California, prepared for the San Francisco Wastewater Program, Department of Public Works, San Francisco, California, November 1979.

162. Ranken, R. E., and J. Ghaboussi, *Tunnel Design Considerations: Analysis of Stresses and Deformations Around Advancing Tunnels*, FRS-OR&D 75-84, Federal Railroad Administration, U.S. Department of Transportation, Washington, D.C., August 1975.
163. Ranken, R. E., J. Ghaboussi, and A. J. Hendron, Jr., *Analysis of Ground-Liner Interaction for Tunnels*, UMTA-IL-06-0043-78-3, Urban Mass Transportation Administration, U.S. Department of Transportation, Washington, D.C., October 1978.
164. Einstein, H. H., and C. W. Schwartz, "Simplified Analysis for Tunnel Supports," *Journal of the Geotechnical Engineering Division*, American Society of Civil Engineers, Vol. 105, No. GT4, April 1979, pp. 499-518.
165. Schwartz, C. W., and H. H. Einstein, *Simplified Analysis for Ground-Structure Interaction in Tunneling*, R79-27, Department of Civil Engineering, Massachusetts Institute of Technology, Cambridge, Massachusetts, June 1979.
166. Schwartz, C. W., A. S. Azzouz, and H. H. Einstein, *Aspects of Yielding in Ground-Structure Interaction*, R79-28, Department of Civil Engineering, Massachusetts Institute of Technology, Cambridge, Massachusetts, June 1979.
167. Einstein, H. H., W. Steiner, and G. B. Baecher, "Assessment of Empirical Design Methods for Tunnels in Rock," *Proceedings of the 1979 Rapid Excavation and Tunneling Conference*, Atlanta, Georgia, Vol. 1, American Institute of Mining, Metallurgical, and Petroleum Engineers, Inc., New York, New York, 1979, pp. 683-706.
168. Owen, G. N., R. E. Scholl, and T. L. Brekke, "Earthquake Engineering of Tunnels," *Proceedings of the 1979 Rapid Excavation and Tunneling Conference*, Atlanta, Georgia, Vol. 1, American Institute of Mining, Metallurgical, and Petroleum Engineers, Inc., New York, New York, 1979, pp. 709-721 (pp. 714-715, Figs. 4, 5).

169. Vick, S. G., *A Probabilistic Approach to Geology in Hard-Rock Tunneling*, R75-11, Department of Civil Engineering, Massachusetts Institute of Technology, Cambridge, Massachusetts, June 1974.
170. Dendrou, B., *Integrated Approach to Cavity System Seismic Evaluation*, FHWA-RD-78-159, Federal Highway Administration, U.S. Department of Transportation, Washington, D.C., October 1978.
171. Jansen, R. B., "Earthquake Protection of Water and Sewage Lifelines," *The Current State of Knowledge of Lifeline Earthquake Engineering*, American Society of Civil Engineers, New York, New York, 1977, pp. 136-149.
172. Department of Water Resources, *California State Water Project*, Vol. 2, Bulletin No. 200, Sacramento, California, November 1974.
173. Department of Water Resources, *California Aqueduct, Tehachapi Division, Beartrap Access Structure*, Drawing No. Q-12P1-1, Sacramento, California, Revised March 24, 1972.
174. Kuesel, T. R., "Structural Design of the Bay Area Rapid Transit System," *Civil Engineering*, American Society of Civil Engineers, New York, New York, April 1968, pp. 46-50.
175. Anton, W. F., "A Utility's Preparation for a Major Earthquake," *Journal of the American Water Works Association*, June 1978, pp. 311-314.
176. Personal communication from W. F. Anton, Director of Engineering, East Bay Municipal Utility District, Oakland, California, to G. N. Owen, URS/John A. Blume & Associates, Engineers, San Francisco, California, Job File No. 7821, December 1979.
177. Hradilek, P. J., "Behavior of Underground Box Conduit in the San Fernando Earthquake," *The Current State of Knowledge of Lifeline Earthquake Engineering*, American Society of Civil Engineers, New York, New York, 1977, pp. 308-319.

178. Terzaghi, K., and F. E. Richart, Jr., "Stresses in Rock About Cavities," *Geotechnique*, Vol. 3, 1952, pp. 57-90.
179. Terzaghi, K., "Rock Defects and Loads on Tunnel Supports," *Rock Tunneling with Steel Supports*, R. V. Proctor and T. L. White, eds., Commercial Sheaving and Stamping Company, Youngstown, Ohio, 1946, revised 1968.
180. Rabcewicz, L. V., "Principals of Dimensioning the Support System for the New Austrian Tunneling Method," *Water Power*, Vol. 25, No. 3, March 1973, pp. 88-93.
181. Barton, N. R., R. Lien, and J. Lunde, *Engineering Classification of Rock Masses for the Design of Tunnel Support*, Report No. 106, Norwegian Geotechnical Institute, Oslo, Norway, 1974.
182. Bieniawski, Z. T., "Rock Mass Classifications in Rock Engineering," *Proceedings of the Symposium on Exploration for Rock Engineering*, Johannesburg, South Africa, November 1976, pp. 97-106.
183. Wickham, G. E., H. R. Tiedemann, and E. H. Skinner, "Ground Support Prediction Model--RSR Concept," *Proceedings of the 1974 Rapid Excavation and Tunneling Conference*, American Institute of Mining, Metallurgical, and Petroleum Engineers, Inc., New York, New York, 1974, pp. 691-707.
184. Wittke, W., "Static Analysis for Underground Openings in Jointed Rock," *Numerical Methods in Geotechnical Engineering*, C. S. Desai and J. T. Christian, eds., McGraw-Hill, New York, New York, 1977, pp. 589-638.
185. Wittke, W., and B. Pierau, "3-D Stability Analysis of Tunnels in Jointed Rock," *Numerical Methods in Geomechanics*, C. S. Desai, ed., Vol. 3, American Society of Civil Engineers, New York, New York, 1976, pp. 1401-1418.
186. Proctor, R. V., and T. L. White, *Earth Tunneling with Steel Supports*, Commercial Sheaving, Inc., Youngstown, Ohio, 1977.

187. Terzaghi, K., *Theoretical Soil Mechanics*, John Wiley & Sons, New York, New York, 1943 (ninth printing, 1959).
188. Brekke, T. L., and G. E. Korbin, *Seismic Instrumentation of Transportation Tunnels in California*, Berkeley, California, prepared for the Federal Highway Administration, Office of Research, Structures and Applied Mechanics Division, Washington, D.C., August 1977.
189. Thomson, W. T., "Transmission of Elastic Waves Through a Stratified Solid Medium," *Journal of Applied Physics*, Vol. 21, 1950, pp. 89-93.
190. Haskell, N. A., "The Dispersion of Surface Waves on Multilayered Media," *Bulletin of the Seismological Society of America*, Vol. 43, 1953, pp. 17-44.
191. Chang Tsai-yung and Chen Da-sheng, *General Features of the Tangshan Earthquake*, Academia Sinica, Institute of Engineering Mechanics, Harbin, China, July 1978.
192. Steinhardt, O. W., and N. F. Sweeney, "Effects of October 4, 1978, Earthquake on Helms Pumped Storage Power Plant Site," *Earthquake Engineering Research Institute Newsletter*, Vol. 13, No. 1, January 1979.
193. Personal communication from P. I. Yanev, URS/John A. Blume & Associates, Engineers, San Francisco, California, to G. N. Owen, URS/John A. Blume & Associates, Engineers, San Francisco, California, Job File No. 7821, October 1979.
194. Ambraseys, N. N., "The Gemono-Friuli (Italy) Earthquake of 6 May 1976," *Proceedings*, CENTO Seminar on Recent Advances on Earthquake Hazard Minimization, Tehran, Iran, November 1976.
195. Personal communication from L. Mazzini, Marin Historical Society, San Rafael, California, to G. N. Owen, URS/John A. Blume & Associates, Engineers, San Francisco, California, Job File No. 7821, April 25, 1979.

196. Ewing, W. M., W. S. Jardetzky, and F. Press, *Elastic Waves in Layered Media*, McGraw-Hill, New York, New York, 1957.
197. Fung, Y. C., *Foundations of Solid Mechanics*, Prentice-Hall, Englewood Cliffs, New Jersey, 1965.
198. Kolsky, H., *Stress Waves in Solids*, Dover Publications, New York, New York, 1963.

